

# Radiolytic Stability of BTBP-, BTPPhen- and DGA-based Ligands for the Selective Actinide Separation by Solvent Extraction

Holger Schmidt

Energie & Umwelt / Energy & Environment

Band / Volume 617

ISBN 978-3-95806-723-3

**Radiolytic Stability of  
BTBP-, BTPPhen- and DGA-based Ligands  
for the Selective Actinide Separation by Solvent Extraction**

Von der Fakultät für Georessourcen und Materialtechnik der  
Rheinisch-Westfälischen Technischen Hochschule Aachen

zur Erlangung des akademischen Grades eines

**Doktors der Naturwissenschaften**

genehmigte Dissertation

vorgelegt von

**Holger Schmidt, M.Sc. RWTH**

**Berichter:** Univ. Prof. Dr. rer. nat. Dirk Bosbach  
Prof. Dr. Bengi Yagmurlu

Tag der mündlichen Prüfung: 14.08.2023

Diese Dissertation ist auf den Internetseiten der Universitätsbibliothek online verfügbar

Nukleonika 2015, 60 (4 (Pt. II)), 879-884.

DOI: 10.1515/nuka-2015-0156

Procedia Chem. 2016, 21, 32-37.

DOI: 10.1016/j.proche.2016.10.005

Procedia Chem. 2016, 21, 509-516.

DOI: 10.1016/j.proche.2016.10.071

Rad. Phys. Chem. 2019, 164, 108356.

DOI: 10.1016/j.radphyschem.2019.108356

Radiation Physics and Chemistry 2021, 189, 109696.

DOI: 10.1016/j.radphyschem.2021.109696

Dalton Trans. 2015, 44 (41), 18049-18056.

DOI: 10.1039/c5dt02484f

Solvent Extr. Ion Exch. 2015, 33 (5), 431-447.

DOI: 10.1080/07366299.2015.1012885

Solvent Extr. Ion Exch. 2016, 34 (5), 439-453.

DOI: 10.1080/07366299.2016.1212540

New J. Chem. 2017, 41, 13700-13711.

DOI: 10.1039/C7NJ02136D

Solvent Extr. Ion Exch. 2017, 35 (6), 396-407.

DOI: 10.1080/07366299.2017.1368901

D 82 (Diss. RWTH Aachen University, 2023)

Forschungszentrum Jülich GmbH  
Institut für Energie- und Klimaforschung (IEK)  
Nukleare Entsorgung (IEK-6)

# **Radiolytic Stability of BTBP-, BTPPhen- and DGA-based Ligands for the Selective Actinide Separation by Solvent Extraction**

Holger Schmidt

Schriften des Forschungszentrums Jülich  
Reihe Energie & Umwelt / Energy & Environment

Band / Volume 617

ISSN 1866-1793

ISBN 978-3-95806-723-3



Bibliografische Information der Deutschen Nationalbibliothek.  
Die Deutsche Nationalbibliothek verzeichnet diese Publikation in der  
Deutschen Nationalbibliografie; detaillierte Bibliografische Daten  
sind im Internet über <http://dnb.d-nb.de> abrufbar.

Herausgeber  
und Vertrieb:           Forschungszentrum Jülich GmbH  
                                Zentralbibliothek, Verlag  
                                52425 Jülich  
                                Tel.: +49 2461 61-5368  
                                Fax: +49 2461 61-6103  
                                **zb-publikation@fz-juelich.de**  
                                **[www.fz-juelich.de/zb](http://www.fz-juelich.de/zb)**

Umschlaggestaltung:   Grafische Medien, Forschungszentrum Jülich GmbH

Druck:                    Grafische Medien, Forschungszentrum Jülich GmbH

Copyright:             Forschungszentrum Jülich 2023

Schriften des Forschungszentrums Jülich  
Reihe Energie & Umwelt / Energy & Environment, Band / Volume 617

D 82 (Diss. RWTH Aachen University, 2023)

ISSN 1866-1793  
ISBN 978-3-95806-723-3

Vollständig frei verfügbar über das Publikationsportal des Forschungszentrums Jülich (JuSER)  
unter [www.fz-juelich.de/zb/openaccess](http://www.fz-juelich.de/zb/openaccess).



This is an Open Access publication distributed under the terms of the [Creative Commons Attribution License 4.0](https://creativecommons.org/licenses/by/4.0/),  
which permits unrestricted use, distribution, and reproduction in any medium, provided the original work is properly cited.

## Abstract

In the search for a deep geological repository for high-level radioactive waste, in particular for irradiated fuel from the operation of conventional power reactors, the thermal power of the waste to be emplaced and the long half-life of some nuclides (actinides and fission products) play a decisive role in addition to the waste quantity. In Germany, the direct disposal of nuclear waste in deep geological rock formations is being pursued. Internationally, however, the concept of partitioning and transmutation (P&T), i.e., the separation and irradiation and thus conversion of long-lived into short-lived radionuclides using fast reactor systems, is being researched as a supplement to and preparatory step for final disposal. Here, in addition to the PUREX (Plutonium-Uranium Reduction Extraction) process already used industrially for the elements uranium and plutonium, the separation of transplutonium and other repository-relevant elements (e.g.,  $^{129}\text{I}$ ,  $^{99}\text{Tc}$ ) is of high interest in research activities. In the long term (after decay of the short-lived fission products), these elements dominate in particular the thermal power of the waste, and thus the required size of the repository to be established.

In the present work, the two substance classes of diglycolamides (DGAs) and N-donor ligands of the BTBP/BTPhen type are investigated with respect to their stability against radiolytic degradation. DGA ligands cannot distinguish between trivalent actinides ( $\text{An(III)}$ ) and lanthanides ( $\text{Ln(III)}$ ), while selective separation of the trivalent actinides can be achieved by using N-donor ligands. The investigated compounds of the N-donor ligands differ by a modification of the molecular backbone, in which the bipyridine functionality of  $\text{CyMe}_4\text{BTBP}$  was replaced by a phenanthroline functionality in the  $\text{CyMe}_4\text{BTPhen}$  molecule. For DGA-type ligands, either the addition of one or two methyl-groups to the molecular backbone or modifications in the side chains of the molecule while retaining the molecular backbone were of interest. The influence of these modifications on radiolytic stability as well as the resulting radiolysis products were investigated. Since the studied solvent extraction processes are carried out in highly radioactive media with high acidity, radiolysis stability in addition to hydrolysis stability plays a decisive role for the feasibility of such separation processes. Radiolytic decomposition of the used extraction agents (ligand together with diluent) can lead to undesirable effects and reduced performance of the extraction systems.

In this work, the decrease in ligand concentration of DGA and N-donor ligands and the formation of radiolysis products as a function of absorbed dose is measured via mass spectrometric methods. The ability and performance of the irradiated ligand solutions to separate  $\text{An(III)}$  is elucidated by solvent extraction experiments. The radiolysis products were identified and, in the case of the N-donor ligands, addition products of the  $\alpha$ -hydroxyoctyl radical, originating from diluent radiolysis, were observed in particular. This leads to a remarkable preservation of the extraction properties of the irradiated ligand solutions, since the radiolysis products formed are similarly good extractants. The degradation mechanism was postulated for both classes of compounds, DGA-type as well as N-donor ligands, which was done from the interpretation of the obtained mass spectra.



## Kurzzusammenfassung

Bei der Suche nach einem tiefeingeologischen Endlager für hochradioaktive Abfälle, insbesondere für bestrahlte Brennelemente aus dem Betrieb konventioneller Leistungsreaktoren, spielt neben der Abfallmenge auch die Wärmeleistung des einzubringenden Abfalls und die lange Halbwertszeit einiger Nuklide (Actinide und Spaltprodukte) eine entscheidende Rolle. In Deutschland wird die direkte Endlagerung nuklearer Abfälle in tiefeingeologischen Gesteinsformationen angestrebt. International wird jedoch auch das Konzept der Abtrennung und Transmutation (Partitioning & Transmutation, P&T), also der Bestrahlung und damit Umwandlung langlebiger in kurzlebig Radionuklide in schnellen Reaktorsystemen als Ergänzung und vorbereitender Schritt zur Endlagerung erforscht. Dabei wird, zusätzlich zum bereits industriell eingesetzten PUREX (Plutonium-Uranium Reduction Extraction)-Prozess für die Elemente Uran und Plutonium, die Abtrennung von Transplutonium- und anderen endlagerrelevanten Elementen (z. B.  $^{129}\text{I}$ ,  $^{99}\text{Tc}$ ) erforscht. Diese Elemente dominieren bereits nach etwa 300 Jahren (nach Zerfall der kurzlebigen Spaltprodukte) insbesondere die Wärmeleistung der Abfälle und somit die erforderliche Größe des einzurichtenden Endlagers.

In der vorliegenden Arbeit werden die beiden Substanzklassen der Diglykolamide (DGAs) und N-Donor-Liganden vom BTBP/BTPhen-Typ in Bezug auf ihre Radiolysestabilität untersucht. DGAs extrahieren dreiwertige Actinide ( $\text{An(III)}$ ) und Lanthanide ( $\text{Ln(III)}$ ) zusammen, während durch die N-Donor-Liganden eine selektive Abtrennung der dreiwertigen Actinide erreicht werden kann. Die untersuchten Verbindungen der N-Donor-Liganden unterscheiden sich durch eine Modifikation des molekularen Grundgerüsts, indem die Bipyridin-Funktionalität des  $\text{CyMe}_4\text{BTBP}$ -Moleküls bei  $\text{CyMe}_4\text{BTPhen}$  durch eine Phenanthrolin-Funktionalität ersetzt wurde. Aus der Substanzklasse der DGAs wurden einerseits die Additionsprodukte von einer oder zwei Methylgruppen im molekularen Grundgerüst, oder, unter Beibehaltung des molekularen Grundgerüsts, Modifikationen in den Seitenketten des Moleküls und deren Einfluss auf die Radiolysestabilität sowie die entstehenden Radiolyse-Produkte untersucht. Da die hier untersuchten Prozesse zur flüssig-flüssig-Extraktion in hochradioaktiven Medien mit hoher Säurestärke durchgeführt werden, spielt neben der Hydrolysestabilität insbesondere die Radiolysestabilität eine entscheidende Rolle für die Realisierbarkeit solcher Abtrennprozesse. Durch radiolytische Zersetzung der eingesetzten Extraktionsmittel (Ligand zusammen mit dem Verdünnungsmittel) kann es zu ungewünschten Effekten und einer verringerten Leistungsfähigkeit der Extraktionssysteme kommen.

In dieser Arbeit wird die Abnahme der Ligandenkonzentration der DGA- und N-Donor-Liganden und Bildung von Radiolyseprodukten als Funktion der absorbierten Strahlungsdosen über massenspektrometrische Methoden gemessen. Die Fähigkeit der bestrahlten Ligandenlösungen zur  $\text{An(III)}$ -Abtrennung wird durch flüssig-flüssig Extraktionsversuche aufgeklärt. Die Radiolyseprodukte wurden identifiziert, wobei im Fall der N-Donor-Liganden insbesondere Additionsprodukte des, aus der Lösungsmittelradiolyse stammenden,  $\alpha$ -Hydroxyoktyl Radikals beobachtet wurden. Dies führt zu einer bemerkenswerten Erhaltung der Extraktionseigenschaften der bestrahlten Ligandenlösungen, da die gebildeten Radiolyseprodukte ähnlich gute Extraktionsmittel sind. Für beide Substanzklassen, DGAs und N-Donor Liganden, wurde der Degradationsmechanismus postuliert, welcher aus der Interpretation der erhaltenen Massenspektren erfolgte.



## Table of Contents

Abstract.....	I
Kurzzusammenfassung .....	III
List of Abbreviations .....	VII
1. Introduction.....	1
1.1. Back-end of the nuclear fuel cycle.....	2
1.2. Hydrometallurgical reprocessing: solvent extraction.....	4
2. Radiolysis in nuclear reprocessing.....	11
2.1. Radiolysis of the aqueous phase .....	11
2.2. Radiolysis of the organic phase .....	14
2.2.1. Radiolysis of alcohols .....	15
3. Ligands of interest for this work .....	17
3.1. Nitrogen donor ligands.....	17
3.1.1. Development and evolution of N-donor ligands.....	17
3.1.2. Radiolytic degradation of BTBP-type ligands .....	20
3.1.3. Pulse radiolysis of BT(B)Ps.....	21
3.2. Diglycolamides (DGA).....	22
3.2.1. Development and evolution of Diglycolamides.....	22
3.2.2. Radiolysis of Diglycolamides .....	23
4. Scope of the work and objectives .....	27
5. Materials and Methods.....	29
5.1. Experiments using N-donor extractants .....	29
5.2. Experiments using DGA extractants.....	31
6. Conclusions.....	33

6.1.	Summary of the work on CyMe <sub>4</sub> BTBP and CyMe <sub>4</sub> BTPPhen .....	33
6.2.	Summary of the work on DGA-type ligands .....	38
7.	List of Figures .....	43
8.	References .....	45
9.	Acknowledgements .....	59
10.	List of Papers .....	61

## List of Abbreviations

ACSEPT	<i>EU-project:</i> ACtinide recycling by SEParation and Transmutation
ADS	Accelerator Driven System
AFC	Advanced Fuel Cycles
APCI	Atmospheric-pressure chemical ionization
AtG	Atomgesetz
BT(B)P	2,6-bistriazinyl(bi)pyridines
BATP	annulated BTP
BGE	Bundesgesellschaft für Endlagerung mbH
BMUV	Bundesministerium für Umwelt, Naturschutz, nukleare Sicherheit und Verbraucherschutz
BMWK	Bundesministerium für Wirtschaft und Klimaschutz
BMWi	Bundesministerium für Wirtschaft und Energie
COEX	CO-EXtraction
CyMe <sub>4</sub> BTBP	6,6'-bis(5,5,8,8-tetremethyl-5,6,7,8-tetrahydro-benzo[1,2,4] triazine-3-yl)- [2,2']-bipyridine
CyMe <sub>4</sub> BTPhen	2,9-bis(1,2,4-triazin-3-yl)-1,10-phenantroline
<i>D</i>	Distribution ratio
D <sup>3</sup> DODGA	<i>N,N</i> -didodecyl- <i>N',N'</i> -dioctyldiglycolamide
DGA	diglycolamide
DIAMEX	DIAMide EXtraction
DMDOHEMA	<i>N,N'</i> -dimethyl- <i>N,N'</i> -dioctyl-2-(2-hexoxyethyl)malonamide
DOA	dioctylamine
DOAA	<i>N,N</i> -dioctylacetamide
DOFA	<i>N,N</i> -dioctylformamide
DOGA	<i>N,N</i> -dioctylglycolamide
DTPA	diethylen-etriamine pentaacetic acid
ESI-TOF-MS	electrospray-ionization time-of-flight mass spectrometry
EURATOM	Europäische Atomgemeinschaft
EXAm	EXtraction of Americium
EXAFS	Extended X-ray absorption fine structure
FTICR	Fourier-transform ion cyclotron resonance mass spectrometry
FT-IR	Fourier-transform infrared (spectroscopy)
GANEX	Grouped ActiNide EXtraction
GC	Gas chromatography



GENIORS	<i>EU-project:</i> GEN IV Integrated Oxide fuels Recycling Strategies
HLLW	High Level Liquid Waste
HPGe	High-purity Germanium detector
HPLC	High-performance liquid chromatography
IAEA	International Atomic Energy Agency
LC-DAD	Liquid chromatography coupled to diode array detection
LET	linear energy transfer
LUCA	Lanthaniden Und Curium Americium trennung
LWR	Light Water Reactor
MA	Minor Actinides
Me-TODGA	methyl tetraoctyldiglycolamide
Me <sub>2</sub> -TODGA	dimethyl tetraoctyldiglycolamide
MOX	Mixed U/Pu Oxide
NMR	Nuclear Magnetic Resonance
P&C	Partitioning and Conditioning
P&T	Partitioning and Transmutation
PUREX	Plutonium-Uranium Reduction Extraction
SACSESS	<i>EU-project:</i> Safety of ACTinide SEparation proceSSes
SANEX	Selective ActiNide EXtraction
i-SANEX	innovative Selective ActiNide EXtraction
r-SANEX	regular Selective ActiNide EXtraction
SF	Separation Factor
SNF	Spent Nuclear Fuel
StandAG	Standortauswahlgesetz
TBP	tributylphosphate
T(EH)DGA	<i>N,N,N',N'</i> -tetra-2-ethylhexyldiglycolamide
TODGA	<i>N,N,N',N'</i> -tetraoctyl diglycolamide
TPH	hydrogenated tetra propylene, a mixture of linear and branched C12 alkanes
TRLFS	Time-resolved fluorescence spectroscopy
TRU	TRansUranic
UHPLC	Ultra High-performance liquid chromatography
UV-VIS	ultraviolet-visible light (spectroscopy)
VAK	Versuchsatomkraftwerk Kahl

# 1. Introduction

The civil use of nuclear fission for energy production in Germany started in November 1960, when the VAK (Versuchsatomkraftwerk, test nuclear power plant) Kahl entered operation. In June 1961, first energy was fed into the grid. Since then, several nuclear power plants, mostly relying on pressurized water, some on boiling water technology, supplied about 5,490 billion kWh (gross) [12/2020] to the grid.<sup>[1]</sup>

Subsequent to the accident at the Japanese Nuclear Power Plant Fukushima Daiichi caused by an earthquake and tsunami, the German government decided in March 2011 to phase out the usage of nuclear fission for energy production until the end of 2022, which was recently shifted to April 2023 by the German government. Other countries act differently; numerous nations are still building new nuclear reactors (e.g., China, France, and Great Britain) or even step in the use of nuclear fission for energy production to avoid carbon dioxide emissions and therefore slow down climate change. Spent nuclear fuel (SNF) represents a harmful waste stream, independent on the current political decisions, since it contains fission products and long-lived transuranium elements (actinides) causing high radioactivity and radiotoxicity. Therefore, these wastes have to be treated carefully to avoid harmful effects of ionizing radiation to mankind and the environment.

In 1960, when the German Atomic Law (Atomgesetz, AtG)<sup>[2]</sup> entered into force, the preferred option for spent fuel treatment was the reprocessing allowing for the recovery of uranium (U) and plutonium (Pu) for future use in nuclear power plants. The remaining high level nuclear waste from reprocessing was vitrified and is foreseen for geological disposal. The spent fuel was therefore sent to the United Kingdom and France, where corresponding reprocessing plants are under operation. The vitrified wastes were sent back to Germany. In 1994, the law was adapted and from then both, direct geological disposal as well as reprocessing became legal options. Later, in 2002, the “Gesetz zur geordneten Beendigung der Kernenergienutzung zur gewerblichen Erzeugung von Elektrizität”,<sup>[3]</sup> “Act on the Orderly Termination of the Use of Nuclear Energy for the Commercial Generation of Electricity” prohibited reprocessing from 2005 on, which turned direct geological disposal into the only legal option in Germany. The European Union issued the directive 2011/70/EURATOM,<sup>[4]</sup> through which every country had to declare their plans for nuclear disposal. Internationally, Germany is engaged within the “Joint Convention on the Safety of Spent Fuel Management and on the Safety of Radioactive Waste Management”<sup>[5]</sup> of the International Atomic Energy Agency (IAEA). Under this convention, all participating countries report in a three-year interval on their national programs for spent fuel management.

The German “Kommission Lagerung hochradioaktiver Abfälle”, “Commission for the Storage of High-Level Radioactive Waste”, evaluated different approaches for the final disposal of SNF. Finally, the commission identified crystalline host rock, clay and salt as the most suitable options for the final disposal of SNF including vitrified high active wastes.<sup>[6]</sup>

In 2017, the German government enacted the “Gesetz zur Suche und Auswahl eines Standortes für Wärme entwickelnde radioaktive Abfälle und zur Änderung anderer Gesetze (Standortauswahlgesetz, StandAG)”<sup>[7]</sup>, “Site Selection Act”, which replaced the former national law and marked a re-start of the German disposal strategy. Under this law, the former project for nuclear disposal, “Erkundungsbergwerk Salzstock Gorleben”, “Gorleben salt dome exploratory mine” was terminated and a new process to identify the German final repository was started from a “white map”. Within three phases, a scientifically based

process shall find and decide on a site for Germany's final repository until 2031, the operational phase shall start in 2050. Recently the Bundesgesellschaft für Endlagerung mbH (BGE), the responsible authority for the search for a final repository, announced that a site will not be selected until 2046 and 2068.<sup>1</sup>

For Germany, a volume of about 28,000 cubic meters of high radioactive, heat generating waste is expected to be stored in such a repository for high-active wastes. Besides ~21,000 m<sup>3</sup> spent fuel, ~1,400 m<sup>3</sup> of vitrified high active waste from reprocessing and ~5,700 m<sup>3</sup> waste from research reactors and reactor demonstration projects are included.<sup>[8]</sup> Internationally, to date no final repository for SNF is under operation. But in Finland, where the world's first licensed final repository project is located, trial operation is foreseen to start in 2023, while commissioning is planned for the mid-2020s.

## **1.1. Back-end of the nuclear fuel cycle**

Nuclear power reactors of the so-called Gen. II and III, as they are used worldwide, only use a small fraction of the available fuel. The used nuclear fuel is not 'spent', even if this is the usual way of introducing fuel elements being removed after nuclear heat generation in fission reactors. In contrast, it still contains certain amounts of energy, since most of the fissile material (mostly <sup>235</sup>U in conventional light water reactors, modern Mixed OXide fuel (MOX) also contains <sup>239</sup>Pu in higher amounts) could still be used in fission reactors, although not as economically as 'fresh' fuel. New reactors of Gen. IV, which use different reactor concepts like molten salt, liquid metal or high temperature gas cooled technology, need different fuels like halide salts or uranium, plutonium, and minor actinides in carbidic or nitridic form. For most new reactor concepts, reprocessing of SNF is essential for their fuel concepts.

Nevertheless, the 'spent' nuclear fuel needs to be managed to protect environment and mankind from the harmful radioactive and chemotoxic effects of uranium, plutonium as well as its fission products and built up minor actinides (MA: Np, Am, Cm). In the European and International framework, different research programs like the European "7<sup>th</sup> Framework Programme for Research (FP7): Nuclear fission, safety and radiation protection" with its ACSEPT,<sup>[9]</sup> SACSESS<sup>[10-11]</sup> and GENIORS<sup>[12]</sup> programs, were launched. Besides the safety of nuclear power plants, nuclear reprocessing and partitioning were of high interest.

For SNF management, two approaches are available, depending on whether the remaining energy of the fuel is going to be used afterwards or sent to deep geological disposal: the open and the closed nuclear fuel cycle.

### **(a) The open fuel cycle**

By the term 'open fuel cycle', the one-time use of nuclear fuel in fission reactors is described. The natural uranium is enriched; fuel is fabricated, used in the fission reactor, and ultimately forwarded to final disposal. Germany currently applies this open fuel cycle, as described above.

---

<sup>1</sup> <https://www.base.bund.de/SharedDocs/Kurzmeldungen/BASE/DE/2022/zeitplan-endlagersuche.html>

### *(b) The closed fuel cycle*

In the ‘closed fuel cycle’, once irradiated nuclear fuel is not forwarded to direct disposal, but to reprocessing facilities, where uranium and plutonium are recovered by chemical processes. Therefore, the irradiated fuel is sent to reprocessing plants, where fuel rods are cut into pieces before the fuel matrix ( $\text{UO}_2$  and fission products) is dissolved in concentrated nitric acid. From this solution, uranium and plutonium are recovered to be used for the production of MOX fuel. The world’s largest reprocessing facilities are located in La Hague, France, and in Sellafield, UK. Here, uranium and plutonium are extracted from SNF solution *via* the hydrometallurgical PUREX process (see chapter 1.2(a)). The recovered uranium and plutonium are then sent back to enrichment- and fuel fabrication plants, where MOX fuel is manufactured for further use in nuclear fission reactors. The fission products and TRansUranic waste (TRU) remain at the reprocessing plant and are forwarded to vitrification and thereby immobilization of the nuclides within the glass-matrix for final disposal.

Traditionally, used LWR-fuel consists of uranium dioxide ( $\text{UO}_2$ ) with an  $^{235}\text{U}$  amount of up to 5 %w. During the fission processes in the reactor core, only these ~5 % are fissioned, while some of the bulk  $^{238}\text{U}$  is converted to higher actinides like Np, Pu, Am, and Cm *via* neutron capture. Only some of the built nuclides can participate in the fission process. The rest remains in the fuel until it is unloaded from the reactor core. Spent nuclear fuel still consists of about 93 % uranium. In a first step, this uranium is separated together with plutonium (chapter 1.2) from the spent fuel to minimize the waste volume. By using hydrometallurgical reprocessing, the volume of the German SNF was reduced to about 2,200 m<sup>3</sup>.<sup>[8]</sup> The separated uranium and plutonium were either fabricated to new MOX fuel or still need to be disposed separately. A further separation of the minor actinides Np, Am and Cm can reduce the long-term thermal power of the high-level wastes by one to two orders of magnitude.

After this separation (= partitioning) of uranium and plutonium, two complementary strategies were discussed: partitioning and conditioning (P&C) as well as partitioning and transmutation (P&T). In the first concept, which was also part of the BMBF project “Grundlegende Untersuchungen zur Immobilisierung Langlebiger Radionuklide mittels Einbau in Endlagerrelevante Keramiken (Conditioning)”<sup>[13]</sup>, separated radioactive nuclides are introduced into a stable matrix, which is suitable for deep geological disposal. It is important, that especially mobile long lived fission products like e.g.,  $^{14}\text{C}$ ,  $^{36}\text{Cl}$ ,  $^{99}\text{Tc}$  or  $^{129}\text{I}$  are immobilized. Due to their chemical durability and radiation resistance, glasses and ceramics are advantageous materials for the use in P&C.<sup>[14]</sup> This concept does not reduce radiotoxicity but can increase the long-term safety of final repositories.<sup>[15]</sup>

The P&T concept is not able to avoid the need of a final repository, but some of the associated risks, like criticality and proliferation can be eliminated when plutonium and uranium are separated from the spent fuel. Current research mainly deals with the separation of minor actinides (additionally to nowadays applied separation of U and Pu), which are responsible for heat generation especially after 150 years after removing spent fuel from the fission reactors. In transmutation facilities, which are mainly Gen. IV reactors with a fast neutron spectrum that need to be built, long lived radionuclides are transmuted via nuclear fission to short-lived or even stable radionuclides. Also, the nowadays little used  $^{238}\text{U}$  can be utilized in this kind of fast reactors. By this, on the one hand, the inventory of a final repository is optimized by removing fissile and fertile material and on the other hand, electricity is produced without generating greenhouse gases. However, since some mobile radionuclides cannot be transmuted efficiently, a final

repository is still needed. Based on several decades of research, development, and demonstration it is generally accepted at the technical and scientific level that disposal in mined deep geological repositories (i.e., at depths exceeding 500 m below ground level) is the safest and most sustainable option for the management of HLW, such as SNF – if considered as waste. The concept of P&T thereby can help to optimize the inventory of final repositories by developing a long-term nuclear energy program with a more efficient use of uranium in advanced reactors. By this, the need of uranium mining could be reduced since depleted uranium was collected for decades.

In Germany, reprocessing, more precisely the transport of SNF to reprocessing plants has no longer been allowed since July 2005 and a direct disposal of spent fuel is foreseen by law. Nevertheless, the German government, namely the Federal Ministry for the Environment, Nature Conservation, Nuclear Safety and Consumer Protection (BMUV, Bundesministerium für Umwelt, Naturschutz, Nukleare Sicherheit und Verbraucherschutz), is highly interested in knowledge preservation, education and research in the field of nuclear safety (e.g. 7<sup>th</sup> Energy Research Programme of the former BMWi, Bundesministerium für Wirtschaft und Energie, nowadays BMWK, Bundesministerium für Wirtschaft und Klimaschutz<sup>[16]</sup>). Besides, German research organizations like the Helmholtz Association actively participate in European Research Programs like ACSEPT (ACTinide recycling by SEPARation and Transmutation)<sup>2, [9]</sup> SACSESS (Safety of ACTinide SEparation proceSSes)<sup>3 [10-11]</sup> or GENIORS (GEN IV Integrated Oxide fuels Recycling Strategies)<sup>4 [12]</sup>. The work presented in this thesis was mainly realized under the scope and by funding of SACSESS.

In the next chapter, different approaches especially in hydrometallurgical reprocessing are presented and current developments and processes are described.

## **1.2. Hydrometallurgical reprocessing: solvent extraction**

In Figure 1-1, an overview of the European hydrometallurgical partitioning process strategy for homogeneous<sup>[17]</sup> (common separation of different radionuclides) and heterogeneous<sup>[18]</sup> (selective separation of specific radionuclides) recycling of TRU elements is shown.

---

<sup>2</sup> <https://cordis.europa.eu/project/id/211267>

<sup>3</sup> <http://www.sacsess.eu/>

<sup>4</sup> <https://www.geniors.eu/>

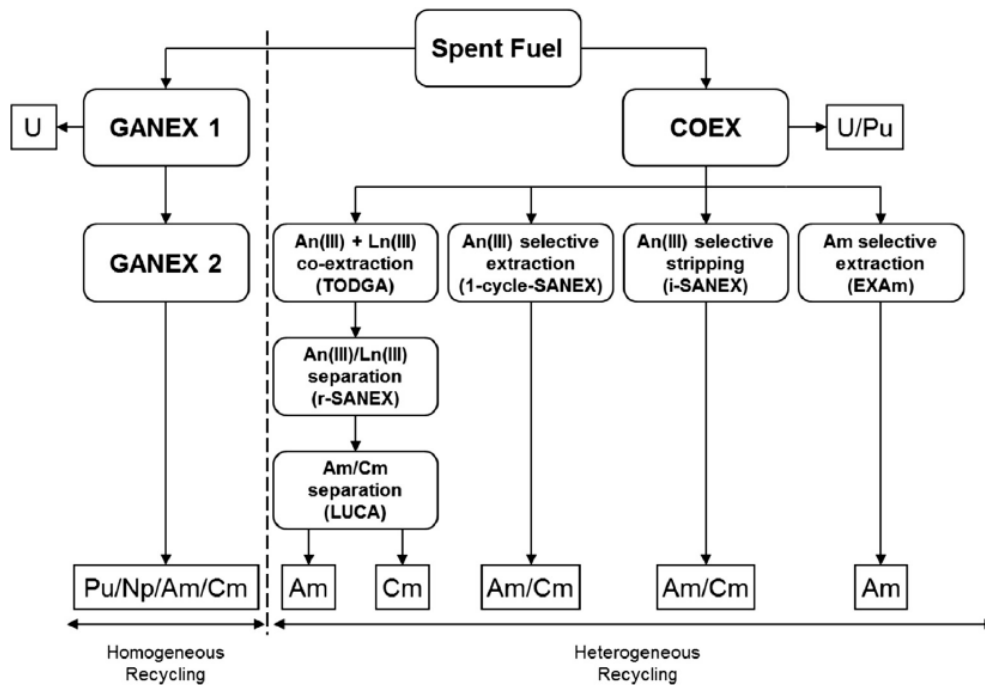


**Figure 1-1: Scheme of European hydrometallurgical partitioning processes.<sup>[19]</sup>**

Solvent extraction is the current technique for hydrometallurgical reprocessing methods of SNF. Two immiscible liquids (commonly one hydrophilic, one hydrophobic) are contacted. In the field of nuclear reprocessing, e.g., in the PUREX process, an aqueous nitric acid phase containing radionuclides of uranium, plutonium, minor actinides as well as fission products is contacted with an organic phase containing one or more extractants. During multistep countercurrent processes in pulsed columns or mixer-settler arrangements, the organic phase is contacted with the aqueous phase, allowing the extractant (ligand) to selectively extract the desired element(s) by the formation of chemical complexes. Following an equilibrium reaction (equation (1)), the nuclides of interest are distributed between the organic and aqueous phase, depending on the kinetics of the ‘forth’ and ‘back’ reaction. By selecting a suitable extracting agent, the equilibrium concentration of the desired nuclide(s) can be brought from the aqueous phase (before extraction) to the organic phase (after extraction).

In equation (2), the distribution ratio ( $D$ ) for a metal ion is shown for an extraction from the aqueous into an organic phase. The distribution ratio is defined as the quotient of the metal concentration in the organic phase divided by the metal concentration in the aqueous phase. The efficiency of a separation process is given by the separation factor ( $SF$ ), which is defined as the quotient of the distribution ratios of two metals (equation (3)). The separation of chemical elements is possible by solvent extraction, due to their different chemical properties. A separation of different isotopes of the same element (like it is done in enrichment plants) is not possible.



$$D_M = \frac{[M]_{\text{organic}}}{[M]_{\text{aqueous}}} \quad (2)$$

$$SF_{M_1, M_2} = \frac{D_{M_1}}{D_{M_2}} \quad (3)$$

The chemical characteristics of the lanthanide elements are quite similar to those of trivalent actinide elements. Therefore, an inter-actinide or inter-lanthanide separation requires tailor made ligand molecules as well as the combination of different process-steps or processes with differing ligand molecules. In the research and development for nuclear reprocessing, many processes were developed to separate uranium, plutonium and higher actinides like americium and curium from SNF. These actinide elements are either already used to produce fresh fuel for nowadays operating Gen II and Gen III fission reactors (MOX fuel (U, Pu)O<sub>2</sub>) or known to be suitable fissile material for advanced Gen IV reactor concepts (Am, Cm).

In a first process, uranium and plutonium are separated in the PUREX (Plutonium-Uranium Reduction Extraction) process.<sup>[20-21]</sup> The remaining high level liquid waste solution (HLLW) was for many years sent to vitrification for direct disposal. Within the development of closed, advanced fuel cycles (AFC), separation processes for the minor actinides (neptunium, americium, and curium) were developed. By separating the minor actinides as well as some long-lived fission products (mainly technetium and iodine), the long-term hazards of radioactive wastes can be reduced significantly by downsizing the radiotoxic and heat generating inventory of final geological disposal. Therefore, processes were developed to separate actinides and lanthanides together (An(III)/Ln(III)) from the remaining HLLW. The latter group-extraction (TODGA, Figure 1-1) requires additional separation processes, since the final goal is a selective actinide/americium and curium extraction.

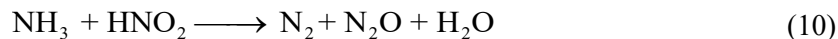
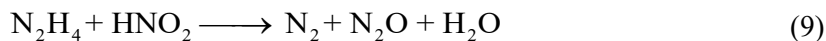
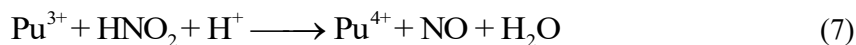
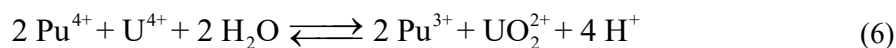
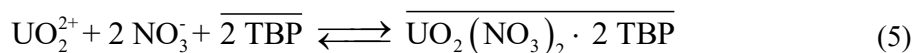
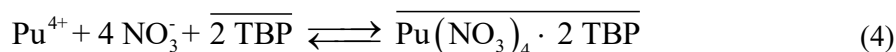
Due to the chemical similarities between trivalent actinides and lanthanides most processes being developed within the last decades contain a common An/Ln extraction-step from the PUREX HLLW leaving back fission products. This can be done by the DIAMEX (DIAMide Extraction) process.<sup>[22-23]</sup> Afterwards, a highly selective separation of the trivalent actinides is conducted. This is done by e.g. the r-SANEX (regular Selective Actinide Extraction) process.<sup>[24-26]</sup> Subsequent to the actinide separation, depending on the further utilization of the actinides, an Am/Cm separation is possible, e.g. by the LUCA process.<sup>[27]</sup>

#### (a) **PUREX-Process**

The process of Plutonium-Uranium Reduction Extraction (PUREX) is the worldwide most applied chemical technique for the reprocessing of SNF after their use in Light Water Reactors, developed in the United States in the 1940s.<sup>[20-21]</sup> In the PUREX process, SNF is dissolved in nitric acid before a solvent extraction process is applied, using tri-*n*-butyl phosphate (TBP) diluted in a paraffinic diluent (e.g. Exxsol D80, C11-C14 *n*-alkanes, *iso*-alkanes and cycloalkanes) as organic phase. Modern reprocessing facilities in

France, UK, Japan, and Russia all use versions of the PUREX process. Solvent extraction processes are conducted in pulsed columns, followed by purification steps.

In the first process step after dissolving SNF in nitric acid, uranium and plutonium are extracted in their tetravalent ( $\text{Pu}^{4+}$ ) or hexavalent ( $\text{UO}_2^{2+}$ ) form, as metal nitrates (equations (4) and (5))<sup>5</sup>. Subsequently, plutonium is reduced to its trivalent, inextractable form and stripped back to the aqueous phase using U(IV) as the reductant (equation (6)). Due to autocatalytic re-oxidation of Pu(III) by nitrous acid (equations (7) and (8)), a nitrous acid scavenger like hydrazine is added to the aqueous phase in the U/Pu separation step (equations (9) and (10)). Because of trace quantities of Pu(III) in the organic phase, a substantial excess of reductant is added to the organic phase to inhibit Pu(III) being re-oxidized to the tetravalent state.



In the last years, a growing international interest in partially closed (Plutonium recovery and use as MOX fuel) and fully closed (recovery of all minor actinides: Np, Pu, Am, Cm) nuclear fuel cycles occurred.<sup>[28]</sup> An alternative to the PUREX process is the more proliferation resistant COEX<sup>TM</sup> process (cf. Figure 1-1).<sup>[29]</sup> In this process, no plutonium separation is conducted. Parts of the separated uranium are guided back to the plutonium stream leading to a homogeneous (U,Pu)O<sub>2</sub> mixed oxide, which can be used to produce MOX fuel.

The separation of neptunium in addition to uranium and plutonium is possible within the PUREX process. However, for the recovery of americium and curium, advanced techniques and alternative separation methods are required. Additionally, for the further fission of TRU, advanced reactors are required like fast reactors (instead of the thermal neutron spectrum of LWRs) or accelerator driven systems (ADS).<sup>[30]</sup> Since the trivalent actinides are chemically very similar to trivalent lanthanides, new and highly selective partitioning processes have been developed. Additionally, new selective processes are under development

---

<sup>5</sup> Bars above the molecule symbols denote organic species.



for the even more complex separation of Am and Cm as well as for the heat generating fission products Cs and Sr.

In Figure 1-1, the COEX (CO-EXtraction) process is depicted, which is an adaption of the PUREX process. The main difference between PUREX and COEX is that in the latter one, plutonium is no longer purified alone but is always associated with uranium, providing an effective barrier against proliferation.<sup>[29]</sup>

**(b) Actinide/Lanthanide separation**

Subsequent to the uranium and plutonium separation, the separation of the minor actinides americium and curium is of interest within the P&T or P&C strategy, which can be done by the SANEX process. A recent version of the SANEX process uses 6,6'-bis(5,5,8,8-tetramethyl-5,6,7,8-tetrahydro-benzo[1,2,4]triazine-3-yl)-[2,2']-bipyridine (CyMe<sub>4</sub>BTBP, Figure 1-2) and *N,N,N',N'*-tetraoctyl diglycolamide (TODGA, Figure 1-2) in 1-octanol.<sup>[24]</sup>

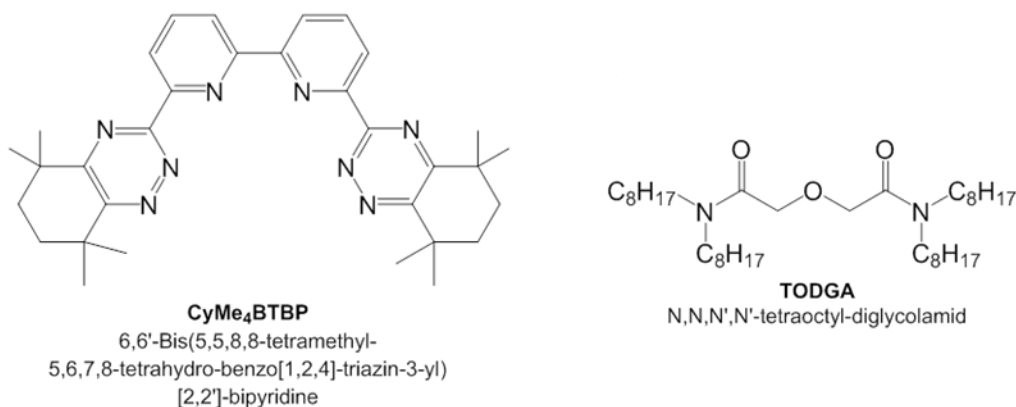


**Figure 1-2: Ligands CyMe<sub>4</sub>BTBP (left) and TODGA (right), used in the SANEX process.**

The flow sheet of the SANEX process is shown in Figure 1-3, as it was conducted at Forschungszentrum Jülich. The process consists of 20 stages, providing three main steps: extraction, scrubbing and stripping. In the first step, extraction, the ligand CyMe<sub>4</sub>BTBP extracts the trivalent actinides from the feed solution that enters the system at stage 12 of the counter-current process. However, TODGA acts as phase transfer agent. The scrubbing step is used for back-extraction of poorly co-extracted lanthanides to the feed solution, which leaves the system at stage 1 as Ln(III) raffinate. In stages 17 - 20, stripping of the An(III) is conducted, which means a back-extraction of the trivalent actinides to the aqueous phase forming the An(III) product.

In previous versions of this process, the DMDOHEMA ligand was used instead of TODGA as phase transfer agent.<sup>[25-26]</sup>

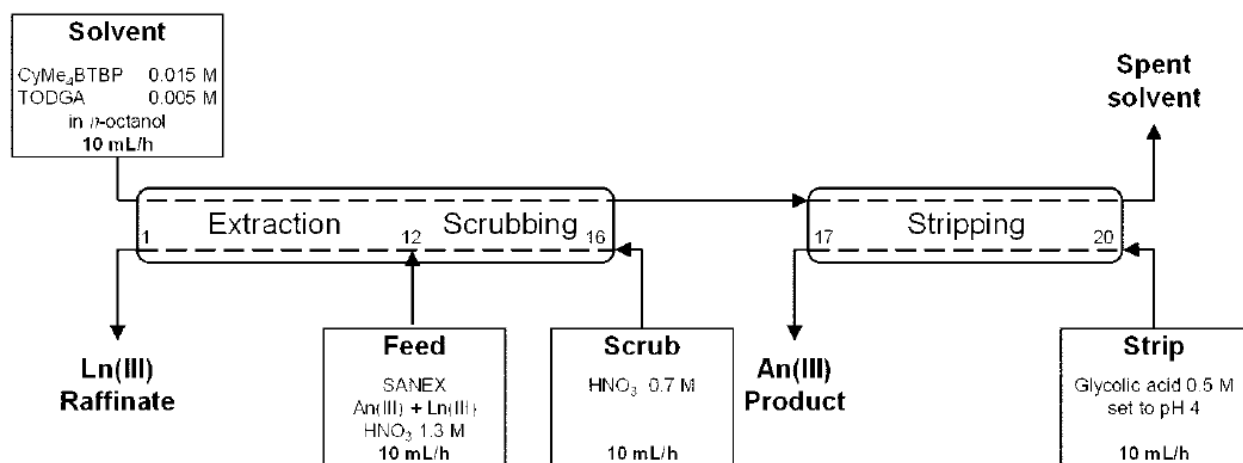


**Figure 1-3: Flow sheet of the SANEX process using CyMe<sub>4</sub>BTBP + TODGA as extractants.<sup>[24]</sup>**

Subsequent to this regular SANEX (r-SANEX) process, a process for the selective separation of Am(III) over Cm(III) was developed resulting in the LUCA (Lanthaniden Und Curium Americium Trennung, Lanthanide and Curium Americium Separation) process.<sup>[27]</sup> This process reaches an Am/Cm separation factor of 6-10, which was for many years the highest ever published  $SF_{Am/Cm}$ .<sup>[31]</sup>

A different approach aiming at the direct extraction of solely americium from the PUREX raffinate is the EXAm (EXtraction of Americium) process<sup>[32-33]</sup>, which is depicted in Figure 1-1. In this complex 6-step process, americium is extracted selectively from fission products, lanthanides as well as curium in 68 stages in total.

Further developments of the SANEX process, like the innovative-SANEX<sup>[34-37]</sup> and the one-cycle SANEX,<sup>[38-40]</sup> (cf. Figure 1-1) were conducted to directly extract the minor actinides Am and Cm from the PUREX raffinate avoiding the intermediate DIAMEX process. These SANEX processes were successfully demonstrated in miniature laboratory-scale centrifugal contractors at Forschungszentrum Jülich.<sup>[19]</sup>

A combination and further development of the above mentioned DIAMEX and SANEX processes is the so called GANEX (Group ActiNide EXtraction) process (cf. Figure 1-1). With the GANEX process, the group extraction of Np, Pu, Am and Cm is conducted in only one separation process.<sup>[9, 41-44]</sup>



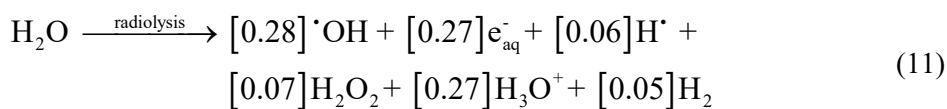
## 2. Radiolysis in nuclear reprocessing

As described above, solvent extraction processes are essential in hydrometallurgical nuclear reprocessing. Therefore, process conditions need to be predictable and well understood over the whole time of application. Since radionuclides of different decay types and –energies are present in different processes, the occurring effects of radioactive decay need to be understood. To describe the amount of energy deposited in matter, the linear energy transfer (LET) is defined as “the total energy lost per unit path” using the unit “eV nm<sup>-1</sup>”.[45] The LET is dependent on the nature of radiation ( $\alpha$ ,  $\beta$  or  $\gamma$  radiation of different energies) as well as on the matter being passed. A high LET means that energy is deposited in matter more quickly in higher amounts, while low LETs mean, charged particles or electrons can pass matter for longer distances, depositing lower amounts of energy per distance. Typically,  $\alpha$ -particles have high LETs causing high energy deposition in very limited path lengths. In contrast,  $\beta$ -particles (electrons) have low LETs which result in the deposition of smaller amounts of energy on longer, crooked paths (due to scattering).  $\gamma$ -rays, which are mainly photons, produce secondary electrons of small LETs.

For the successful design of processes and systems for nuclear reprocessing, hydrolytic and radiolytic degradation mechanisms need to be understood. Degradation of the solvent (ligand together with diluent) systems may lead to the production of interfering degradation products, decreases in ligand concentration and changes in solvent viscosity as well as in phase separation parameters.[46] All these effects can reduce metal extraction, separation factors and thus overall efficiency of the separation processes. Typical systems for An(III) separation are composed of an aqueous nitric acidic phase, which is contacted to an organic phase containing the ligand molecules only in millimolar concentrations. Due to this, radiolytic degradation occurs mostly in the nitric acidic as well as in the organic solvent phase. As a result, diluent molecules are ionized or excited producing highly reactive but short lived ionic and free-radical species. Subsequently, these species can undergo recombination reactions or reactions with ligand molecules. Therefore, ligand radiolysis is an indirect effect of diluent radiolysis. The variety of radiolytic degradation reactions was summarized in numerous publications.[46-55]

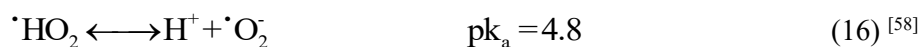
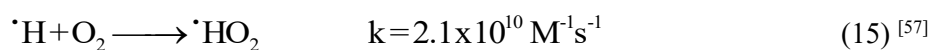
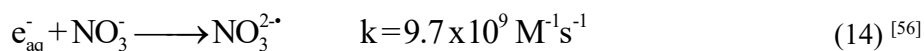
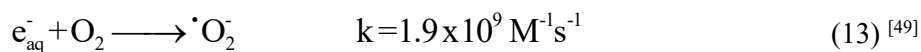
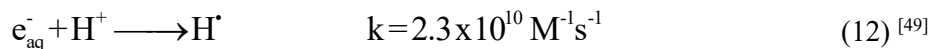
### 2.1. Radiolysis of the aqueous phase

In equation (11), water radiolysis by low LET particles is described with their corresponding yields (G values, given in  $\mu\text{mol J}^{-1}$ ).[49, 55]



The most reactive species from water radiolysis is the hydroxyl radical ( $\cdot\text{OH}$ ) besides hydrogen peroxide ( $\text{H}_2\text{O}_2$ ), the aqueous electron ( $e_{\text{aq}}^-$ ) and the hydrogen atom ( $\text{H}^\cdot$ ). In contrast, radiolysis by high LET particles like  $\text{He}^{2+}$  (e.g., from actinide decay) deposit their energy only in short ranges, leading mainly to direct recombination reactions due to the higher initial yields of radicals being built. As a result, finally, mainly molecular species ‘remain’.

Nitric acid is commonly used in numerous hydrometallurgical reprocessing techniques and processes (e.g. PUREX process). Therefore, the understanding of interactions with above mentioned reactive species is essential. Although oxidizing and reducing species are produced roughly equally, in aerated nitric acid, an oxidizing regime is predominant, since electrons and hydrogen atom radicals are scavenged as described in equations (12) to (16):

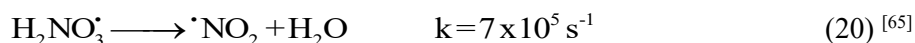
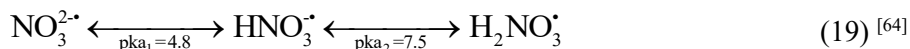


From equation (11), mainly hydrogen peroxide ( $H_2O_2$ ) as well as the highly reactive, oxidizing  $\cdot OH$  radical remain in solution. The latter one is able to undergo hydrogen abstraction reactions with organic ligand molecules, addition reactions to unsaturated hydrocarbons as well as electron transfer reactions to organic and aqueous solutes, as described by corresponding rate constants.<sup>[49, 59]</sup>

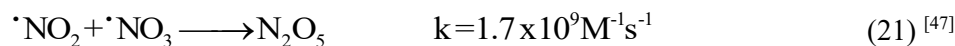
Additional to water radiolysis, direct as well as indirect radiolysis of nitric acid also generates reactive species. Nitric acid radiolysis was briefly reviewed by Katsumura.<sup>[60]</sup> The highly reactive  $\cdot NO_3$  radical is formed according to the following equations by direct radiolysis of the dissociated nitrate anion (equation (17)) as well as indirectly by the reaction of undissociated nitric acid with the hydroxyl radical (equation (18)).



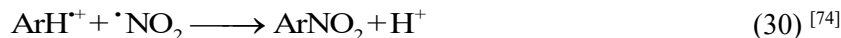
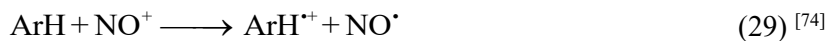
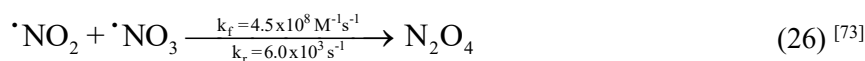
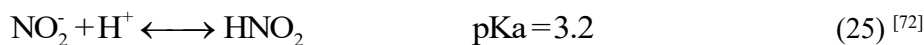
The resulting reactions of the produced  $\cdot NO_3$  radicals are comparable to those of  $\cdot OH$ , despite with lower reaction rates and decreased electrophilic character.<sup>[61-63]</sup> Besides the  $\cdot NO_3$  radical, the  $\cdot NO_2$  radical also occurs in acidic solutions being formed through the following equations from the product of equation (14) above:



Though the  $\cdot\text{NO}_2$  radical is less reactive, it was shown to be capable to add to unsaturated carbon bonds or producing nitrated derivatives of carbon-centered radicals.<sup>[66-68]</sup> Additionally, these nitrogen centered radicals can both react to  $\text{N}_2\text{O}_5$ , which decays to the powerful nitrating nitronium ion:

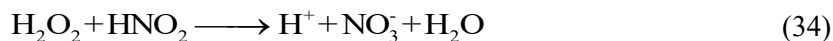


Another product of nitric acid radiolysis is  $\text{HNO}_2$ , nitrous acid, acting as catalyst for further nitration reactions. Its formations via direct and indirect radiolysis is shown in equations (23) to (27).<sup>6</sup> Starting from this, nitrosonium ions ( $\text{NO}^+$ ) are formed (equation (28)), which are finally able to perform nitration reactions on organic compounds like the aryl-moieties of the organic phase (thereafter “Ar”, Aryl) by electron transfer or addition, as shown in equations (29) to (30) and (31) to (33), respectively.



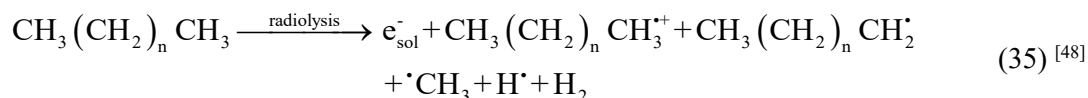
The maximum available yield of nitrous acid from radiolysis is limited by the radiolytically produced hydrogen peroxide as given in equation (34).<sup>[76-77]</sup>

<sup>6</sup> Radiolysis is not the only source of nitrous acid. Oxidation reactions of solution constituents can also be a source of  $\text{HNO}_2$ . However, radiolysis increases the yield of nitrous acid in the solution and thereby the yield of nitration reactions.

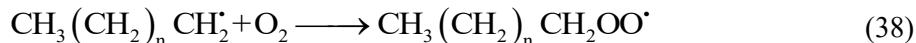
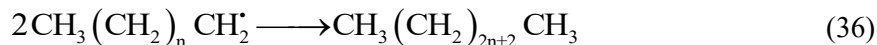


## 2.2. Radiolysis of the organic phase

In the organic phase of current processes for hydrometallurgical reprocessing normal and branched-chain alkanes and alcohols are widely used. The specific system of the work presented in this thesis uses 1-octanol as organic diluent for N-donor ligands and *n*-dodecane for DGA ligands. The radiolysis of alkanes is presented in equations (35) to (38).



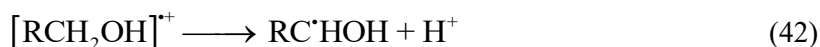
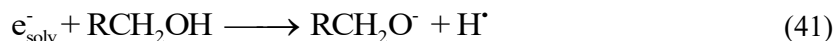
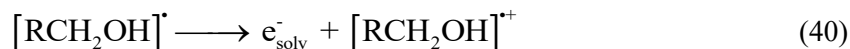
Yields of the different products are not given in the equation above, since they depend on the used alkane. In general, branched alkanes show higher yields in the range of 0.2-0.6  $\mu\text{molJ}^{-1}$  for  $\text{H}_2$  and about 0.005-0.1  $\mu\text{molJ}^{-1}$  of methane. For  $\text{C}_6$ - $\text{C}_{10}$  hydrocarbons, an  $\text{H}^*$  yield of 0.07  $\mu\text{molJ}^{-1}$  was reported,<sup>[78]</sup> which is in the range of water radiolysis (equation (11)). The carbon-centered radicals can further react by H-atom abstraction from the ligand molecules or other solvent molecules. Additionally, radical-radical addition reactions are possible, resulting in products of higher molecular weight (equation (36)). Another possibility is the disproportionation of two radical species (equation (37)) as well as the formation of peroxide species by oxygen addition (equation (38)).<sup>[79]</sup>



The unsaturated product of hydrocarbon radiolysis (equation (37)) is, like all unsaturated species, vulnerable to further radical addition reactions. In this specific system, the hydroxyl radical or the previously introduced N-centered radicals can perform radical addition reactions to this species. These species accumulate in solution and thereby change physical properties of the system leading to differences in e.g., viscosity, density, or process performance.

### 2.2.1. Radiolysis of alcohols

The radiolysis of alcohols that is given in equations (39) to (44) is briefly described in literature resulting in highly reactive  $\alpha$ -hydroxyalkyl radicals.<sup>[80-83]</sup>



For the N-donor ligand radiolysis presented in this work, 1-octanol was the organic diluent of choice. Decisive research on the  $^{60}\text{Co}$  gamma-radiolysis of 1-octanol, which was conducted by Yu *et al.*,<sup>[84]</sup> used UV-VIS, FT-IR, and GC techniques to examine occurring processes. The researchers found up to an absorbed dose of 100 kGy solely the absorption at 200 nm in UV-VIS spectrometry, which belongs to the  $\pi$ - $\sigma^*$  transition of the C-O bond. With increasing absorbed dose over 200, 300 and 600 to 900 kGy, two new absorption bands at 220 nm and 275 nm arose. These were dedicated to a  $\pi$ - $\pi^*$  and  $n$ - $\pi^*$  transition of a C=O bond, respectively. The occurrence of this C=O aldehyde bond, for the latter transition also revealed a fine structure that became more visible with increasing dose, showing higher yields of aldehyde with increasing dose. Additionally, the 200 nm bond gained an obvious redshift receiving doses > 300 kGy.

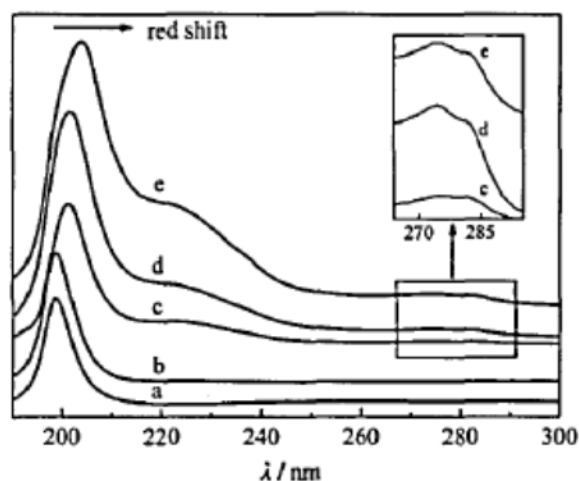
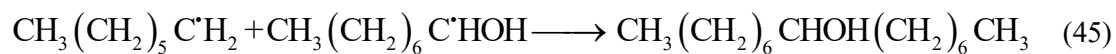


**Figure 2-1:** UV-VIS absorption spectra of 1-octanol in nitrogen, receiving doses of 0 (a), 100 (b), 200 (c), 300 (d), 600 (e) and 900 (f) kGy<sup>[84]</sup>



The formation of the aldehyde was proven by FT-IR measurements, where the formation of the aldehyde was found with an evolving absorption band after 100 kGy absorbed dose. With subsequent gas chromatographic examination (with a sample receiving 600 kGy), the formation of the main radiolysis product 1-octanal, the former found aldehyde, was further proven, while the additional radiolysis products *n*-heptane and 8-pentadecanol were found, as well.<sup>[84]</sup> The formation of the latter one proves, that besides the  $\alpha$ -C-H bond cleavage also C-C bond cleavage occurs forming free radicals of *n*-heptane, that react with free 1-octanol radicals forming the 8-pentadecanol product (equation (45)). This finding is of high relevance to this work, since we found these radiolysis products, *n*-heptane and 8-pentadecanol, in our samples, as well.



### 3. Ligands of interest for this work

Within the past years of European research on advanced processes for nuclear reprocessing, aiming at the partitioning of minor actinides from HLLW, the group of BT(B)P-type ligands was and is of high interest. Due to their fulfillment of the CHON principle,<sup>7,[85]</sup> as well as their ability to separate Am(III) and Cm(III) quantitatively from trivalent lanthanides, the 2,6-bistriazinylpyridines (BTPs) were early found to be promising for the use in highly selective separation processes.

### 3.1. Nitrogen donor ligands

In the presented work (Papers 1-5), investigations on the radiolytic processes and degradation of the ligands CyMe<sub>4</sub>BTBP and CyMe<sub>4</sub>BTPhen were made and published in several peer-reviewed journals.<sup>[86-90]</sup> The main findings and conclusions are summarized in chapter 5 of this thesis.

### 3.1.1. Development and evolution of N-donor ligands

The group of BT(B)P type nitrogen donor ligands, which is known to be highly selective to separate trivalent actinides (An(III)) over lanthanides (Ln(III)), has been further developed within the last decades.<sup>[54, 91]</sup> First reported by Case,<sup>[92]</sup> the group of 2,6-bis-triazinyl derivatives of pyridine, was further studied. Kolarik *et al.* suggested to use the group of 2,6-bis-(1,2,4-triazine-3-yl)pyridines (BTPs) for the selective Am(III) extraction from Eu(III), showing higher distribution ratios and separation factors than reported before for N-donor ligands.<sup>[93]</sup> In contrast to the earlier reported TPTZ (2,4,6-tri(2-pyridyl)-1,3,5-triazine) or BODO (2,6-bis-(benzoxazolyl)-4-dodecyloxy pyridine) ligands, the new tridentate soft nitrogen donor ligand does not longer need an additional lipophilic anion source (synergist, e.g.  $\alpha$ -bromocapric acid) to compensate the +3 charge of the An(III), since it is able to complex trivalent actinides using the nitrate ions out of nitric acid (as aqueous phase a PUREX raffinate solution is used).<sup>[91]</sup> Complexes being formed using BTP for Am(III) extraction are of the composition M:L<sub>3</sub>, namely Am(NO<sub>3</sub>)<sub>3</sub>(BTP)<sub>3</sub> and Am(NO<sub>3</sub>)<sub>3</sub>HNO<sub>3</sub>(BTP)<sub>3</sub>.<sup>[94-95]</sup> Due to the tridentate/terdentate coordination of BTP, the metal ions are coordinated by six triazine nitrogen atoms forming a distorted trigonal prismatic coordination sphere which is capped upon the rectangular faces with pyridine nitrogens.<sup>[96]</sup> The formed homoleptic complexes were found in the solid state as well as in solution.<sup>[94, 96-98]</sup> Actinide extraction was also implied to take place in the form of these homoleptic complexes.<sup>[99]</sup> Different alkyl substituents were introduced on the triazinyl rings to avoid solubility of the protonated molecules in the aqueous phase and therefore avoid extraction. Although pure triazine ligands appeared to be stable against radiolysis and hydrolysis, *n*Pr-BTP (2,6-bis(5,6-*n*-propyl-1,2,4-triazin-3-yl)pyridine) in octanol solutions in contact with nitric acid was found to be very sensitive against hydrolysis.<sup>[100]</sup> The  $\alpha$ -CH<sub>2</sub> position of the *n*-propyl side chains was identified to be the vulnerable position of the molecule and therefore, it was substituted by an isopropyl moiety which was found to be less susceptible against hydrolysis.<sup>[101]</sup>

On the other hand, even *i*Pr-BTP was not stable against radiolysis at all since the absorption of a  $\gamma$ -dose of 100 kGy led to a decrease in the  $D_{Am}$  and  $SF_{Am/Eu}$  of about 99 %. Mass spectrometric measures suggested

<sup>7</sup> The expression “CHON” describes a molecule, that only consists of the chemical elements carbon (C), hydrogen (H), oxygen (O) and nitrogen (N) and can therefore be easily combusted and released to the environment.

the addition of one or two diluent molecules to the ligand molecule forming addition products of *n*-octanol.<sup>[101]</sup> Even if there was no degradation mechanism identified, the not fully substituted  $\alpha$ -position of the propyl moiety was identified of being the most vulnerable part of the molecule. Therefore, a full substitution of the vulnerable  $\alpha$ -position was suggested. Since the synthesis of the fully substituted 2,6-bis-(5,6-di-*tert*-butyl-1,2,4-triazine-3-yl)pyridine was not successful, the class of annulated BTPs, the BATPs, was designed and tested.<sup>[98]</sup> As this simple BATPs also provided  $\alpha$ -CH<sub>2</sub> positions, the  $\alpha$ -benzylic positions were substituted with two methyl groups each resulting in the CyMe<sub>4</sub>BTP (2,6-bis(5,5,8,8-tetramethyl-5,6,7,8-tetrahydro-benzo[1,2,4]triazine-3-yl)pyridine) molecule.<sup>[98]</sup> Although this ligand reached a very high Am/Eu separation factor of >5000, radiolytic stability was unsatisfying after an absorbed dose of 100 kGy but at least improved in comparison to *i*Pr-BTP.<sup>[101]</sup> Additionally, CyMe<sub>4</sub>BTP required long times of contact to the aqueous phase to reach equilibrium, wherefore the malonamide DMDOHEMA (*N,N'*-dimethyl-*N,N'*-dioctyl-2-(2-hexoxyethyl)malonamide) was added to the system.<sup>[102]</sup>

Due to the high Am(III) distribution ratios, hindering the subsequent stripping steps, a second pyridine ring was added to the molecule leading to the 6,6'-bis(5,5,8,8-tetramethyl-5,6,7,8-tetrahydro-benzo[1,2,4]triazine-3-yl)[2,2']bipyridine (CyMe<sub>4</sub>BTBP, Figure 3-1a) ligand which shows very good extraction properties and hydrolytic stability. Therefore, it has been tested successfully for the use in continuous counter-current solvent extraction processes with genuine spent fuel (SANEX process, see section 1.2(b)) providing promising results.<sup>[25-26]</sup> In comparison to the CyMe<sub>4</sub>BTP ligand, radiolytic stability of CyMe<sub>4</sub>BTBP was found to be better, but still not satisfying, especially for higher doses. For both ligands, radiolytic stability, which is equal to final distribution ratios for americium, was favored using higher initial ligand concentrations.<sup>[101]</sup> Since qualitative as well as quantitative studies were not performed, it remained unclear whether the increased radiolytic stability stemmed from an inherently better stability of BABTPs or from their trivalent complex stoichiometry (M:L<sub>2</sub>) in contrast to BTPs and BATPs (M:L<sub>3</sub>). ESI-MS analyses of irradiated CyMe<sub>4</sub>BTBP in *n*-octanol did not reveal major heavier degradation compounds as they were found for *i*Pr-BTP.<sup>[101]</sup>

The inhibition of radiolytic degradation was studied by Nilsson *et al.*<sup>[80]</sup> In this study, the influence of *tert*-butyl-benzene and nitrobenzene (up to 10 vol%) on the radiolytic degradation of tE-BTP in 1-hexanol was examined. It was found that *tert*-butyl-benzene had no protective effect, since nitrobenzene preserved high D<sub>Am</sub> of tE-BTP with increasing concentration. Concluding, the influence of the aromatic  $\pi$ -system was negligible, while the NO<sub>2</sub>-moiety was found to be able to remove solvated electrons and  $\alpha$ -hydroxy alkyl radicals from diluent radiolysis.<sup>[80]</sup> The same observation was made for CyMe<sub>4</sub>BTBP in 1-octanol with 20 vol% nitrobenzene.<sup>[101]</sup>

Since the An(III) extraction rates of the CyMe<sub>4</sub>BTBP ligand are rather slow and the phase-transfer agent DMDOHEMA is needed to reach good extraction kinetics, further development was conducted. For metal complexation, the CyMe<sub>4</sub>BTBP ligand needs to change its thermodynamically preferred *trans*-conformation in solution to the *cis*-conformation, which is required for complexation.<sup>[103-104]</sup> The *cis*-locked 2,9-bis(1,2,4-triazine-3-yl)-1,10-phenanthroline (CyMe<sub>4</sub>BTPhen, Figure 3-1b) ligand already provides the required orientation of the nitrogen donor atoms, which accelerates complexation of An(III) and additionally leads to thermodynamically favored complexes compared to the CyMe<sub>4</sub>BTBP ligand.<sup>[105-106]</sup> Additionally, larger dipole moments of the CyMe<sub>4</sub>BTPhen ligand lead to an increased interaction of the molecule at the organic/aqueous interface leading to improved extraction kinetics.<sup>[107]</sup>

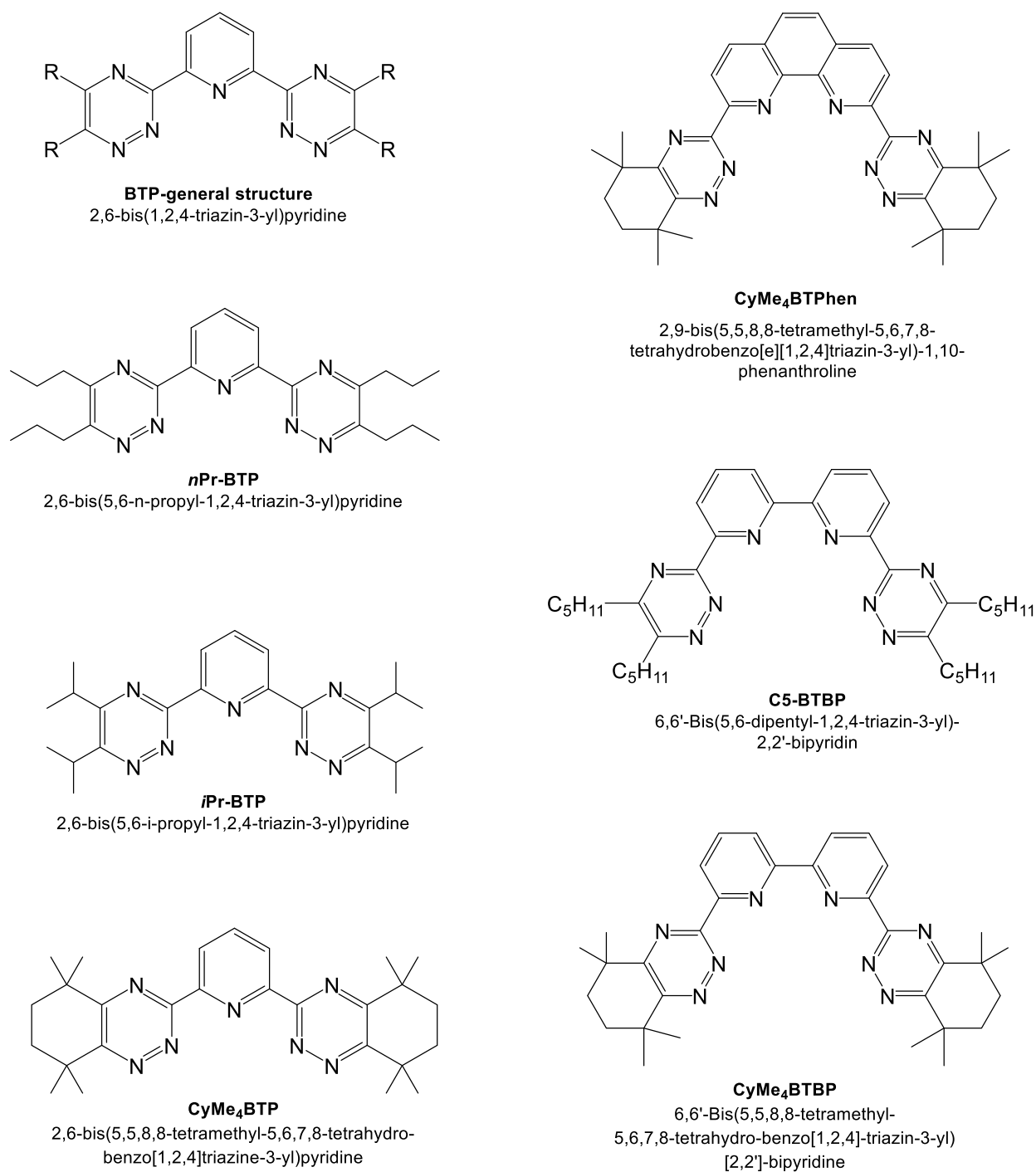
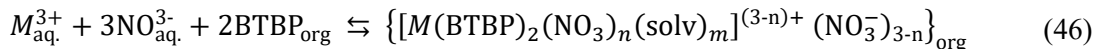


**Figure 3-1:** Selected molecules from the evolution of nitrogen-donor ligands.

For this work, out of the group of BTP-type ligands, CyMe<sub>4</sub>BTBP and CyMe<sub>4</sub>BTPhen were of interest. It is known from previous work<sup>[25, 108-110]</sup> that An(III) and Ln(III) extraction from nitric acid or nitrate solutions to the organic phase using CyMe<sub>4</sub>BTBP or C<sub>5</sub>-BTBP (*n*-pentane side chain) forms complexes of a 1:2 stoichiometry according to equation (46):



In solution, the 1:2 complexes were confirmed by ESI-MS, TRLFS and EXAFS techniques,<sup>[111-116]</sup> while in the solid state also 1:1 complexes were reported.<sup>[114-115, 117-119]</sup> The latter ones differ in the number of nitrate ions bound to the central metal ion, depending on the used preparation conditions. For the An(III)/Ln(III) separation, the chosen diluent showed great significance.<sup>[25, 120-121]</sup> The structures of Am(III) and Eu(III) complexes of the CyMe<sub>4</sub>BTBP ligand in different diluents (nitrobenzene, cyclohexanone, 1-hexanol, and 1-octanol) were resolved by Ekberg *et al.* using EXAFS (X-ray absorption fine structure) experiments.<sup>[122]</sup> Independent of the used diluent, [Am(CyMe<sub>4</sub>BTBP)<sub>2</sub>(NO<sub>3</sub>)<sub>2</sub>]<sup>2+</sup> and [Eu(CyMe<sub>4</sub>BTBP)<sub>2</sub>]<sup>3+</sup> were the predominant complexes found. The metal-nitrogen distance was about 0.1 Å shorter for the europium complex, which was explained by the slightly smaller ionic radius of europium(III) as well as different coordination numbers of eight and ten for Eu(III) and Am(III), respectively. The high charge density of the americium(III) complex is considerably compensated by the nitrate ion in the first coordination sphere, when only diluent shared or separated ion-pairs are formed.<sup>[122]</sup> Additionally, it was found that complex stability and solubility was increased with decreasing diluent permittivity (highest stability in 1-octanol, decreasing over 1-hexanol, cyclohexanone to nitrobenzene). In contrast, separation factors are decreasing in the same order, which means one has to find a balance between high separation factors (1-octanol) and high solubility (nitrobenzene).

### 3.1.2. Radiolytic degradation of BTBP-type ligands

The properties of C<sub>5</sub>-BTBP, a BTBP-type ligand containing four *n*-pentyl chains instead of the two tetramethylated cyclohexyl rings (in CyMe<sub>4</sub>BTBP), were extensively studied.<sup>[110, 123-128]</sup> With respect to radiolysis, it was found that while D<sub>Am</sub> decrease with increasing absorbed dose, D<sub>Eu</sub> remain as high as in fresh solution that not received irradiation.<sup>[124]</sup> Due to the linear alkyl substitutions, the C<sub>5</sub>-BTBP ligand was found to be vulnerable to radiolytic degradation, especially when aliphatic alcohols were used as diluent.<sup>[126]</sup> Most prominent radiolysis products were oxidized C<sub>5</sub>-BTBP compounds with partly degraded C<sub>5</sub> chains. Due to the high excess of diluent molecules compared to the ligand concentration, indirect ligand radiolysis as explained above (chapter 2.2) is most likely. This process of indirect radiolysis through an *in situ* formed radiolysis product of diluent radiolysis is referred to as sensitization effect and has already been observed for C<sub>5</sub>-BPP, a similar nitrogen donor ligand.<sup>[129]</sup> Experiments comparing the influence of the diluent with respect to similarity to the ligands side-group were conducted comparing C<sub>5</sub>-BTBP and CyMe<sub>4</sub>BTBP in 1-hexanol and cyclohexanone at low irradiation doses up to 27 kGy. It was found that the presence of a cyclic side-group, as in CyMe<sub>4</sub>BTBP, has an influence on increasing americium extraction, while europium extraction is not influenced by received dose.<sup>[125]</sup>

There has been work on product identification of bipyridine-type ligands before, like for the ligands C<sub>5</sub>-BTBP and C<sub>5</sub>-BPP.<sup>[126-130]</sup> For C<sub>5</sub>-BTBP, it was found that the dose rate of irradiation is of importance, since a lower dose rate and therefore a longer time needed to absorb the same amount of radiation leads to

higher yields in degradation products.<sup>[126]</sup> Additionally, the chosen diluent had an influence on ligand degradation. While the irradiated ligand in 1-hexanol yielded in high amounts of the degradation products, yields were much lower when cyclohexanone was used as diluent, despite same products occurred. This was explained by different ionizing potentials and the higher radiolytic stability (cyclic structure and stabilized radicals, unsaturated bond of the ketone group) of cyclohexanone. As radiolysis products, mainly oxidized side chains (=O and –OH) as well as lost side chains were found.<sup>[126]</sup>

Radiolysis experiments using the C<sub>5</sub>-BPP ligand in contrast showed a different behavior. Due to indirect radiolysis of the used diluent, 1-octanol, addition products of up to six 1-octanol radicals were found, while heavier reaction products were built in higher amounts with increasing dose.<sup>[129]</sup>

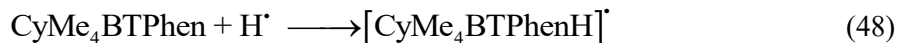
For CyMe<sub>4</sub>BTBP, a similar observation was made by Fermvik *et al.*<sup>[131]</sup> [“Paper VI” of her PhD thesis, probably not published]. Radiolysis experiments of CyMe<sub>4</sub>BTBP were conducted in cyclohexanone and 1-hexanol, respectively. Subsequently, Am distribution ratios were gained by solvent-extraction experiments. It is known that CyMe<sub>4</sub>BTBP builds complexes of a 1:2 stoichiometry according to equation (46), leading to distribution ratios proportional to the square of the ligand concentration. Assuming that distribution ratios would decrease with increasing absorbed dose due to radiolytic ligand degradation, a comparison of measured vs. calculated distribution ratios was made. It was shown, in contrast, that distribution ratios decreased but, for experiments using 1-hexanol as organic diluent, not to the expected extend. Therefore, the authors concluded that (some) radiolysis products are able to extract americium and europium as well. This observation was not made, when cyclohexanone was used as diluent. In the cited study, degradation product identification was conducted using mass spectrometry. Addition products of 1-hexanol as well as cyclohexanone to the ligand molecule were found up to four diluent molecules.

### 3.1.3. Pulse radiolysis of BT(B)Ps

For the understanding of the kinetics and mechanisms of radiolysis processes, the reactions of ligands with the reactive species are of high interest. The concentration of ligand molecules in solvent extraction processes is typically in the range of 10 to 20 mmol L<sup>-1</sup>, which is equal to an amount of ligand molecules in the solution of below 1 %. Therefore, like mentioned before, radiolysis of the diluent molecules or nitric acid are the predominant processes. The radiolysis of aliphatic alcohols was intensively studied and is well understood (chapter 2).<sup>[80-83, 132]</sup> As mentioned, the main products of alcohol radiolysis are the reducing solvated electrons (e<sup>-</sup><sub>solv</sub>), and hydroxyl radicals. By using steady state pulse radiolysis, we observed the lifetime of the solvated electron before it was absorbed by the ligand molecule (equation (47)). With increasing ligand concentration, we observed faster reaction rates resulting in shorter lifetimes of e<sup>-</sup><sub>solv</sub> (Schmidt *et al.*, Paper 5),<sup>[90]</sup> which is in good agreement with our previous work where it was shown, that the negative excess charge can be stabilized by the extended  $\pi$ -system of the ligand molecule (Szreder *et al.*, Paper 4).<sup>[133]</sup>



Additional experiments were conducted to clarify the role of nitric acid in the system. In contrast to experiments without acid in the system, no absorbance of solvated electrons was found when the organic solvent was pre-equilibrated with nitric acid. Instead, the solvated electrons were absorbed by protons (from dissociated acid) forming hydrogen atoms. As a result, fewer solvated electrons were available for ligand radiolysis. Instead, ligand radiolysis by the hydrogen atoms was observed (equation (48)):



Earlier, pulse radiolysis experiments of a number of BT(B)P ligands in 1-octanol were conducted by Sulich *et al.*<sup>[134]</sup>

The main findings and conclusions of our pulse radiolysis experiments were published in Schmidt *et al.*<sup>[90]</sup> (Paper 5, cf. chapter 10, List of Papers) and are summarized in chapter 6 of this thesis.

## 3.2. Diglycolamides (DGA)

### 3.2.1. Development and evolution of Diglycolamides

The group of diglycolamides (DGA, R=H: alkyl-3-oxapentane-1,5-diamide, Figure 3-2) has been investigated for their application in actinide solvent extraction for many years. Sasaki *et al.* investigated different DGAs varying the length and composition of the side chains ‘-R’.<sup>[135]</sup> He observed the derivatives with 4, 5 and 6 *N*-alkyl carbons (R= 4, 5, 6) being barely soluble in *n*-dodecane, while derivatives of 8 and 10 *N*-alkyl carbons (R= 8 and 10) were freely soluble in *n*-dodecane, a commonly used diluent for actinide solvent extraction. The latter derivatives complex and extract actinides and lanthanides with increasing distribution ratios as a function of the aqueous nitric acid concentration, following the order:  $\text{M}^{\text{III}}/\text{M}^{\text{IV}} > \text{M}^{\text{VI}} > \text{M}^{\text{V}}$ .

The octyl derivative, TODGA (R= C<sub>8</sub>H<sub>17</sub>, *N,N,N',N'*-tetraoctyldiglycolamide, Figure 3-2), was studied in detail on its applicability in nuclear reprocessing.<sup>[136-139]</sup> TODGA in combination with TBP (Tri-*n*-butylphosphate) in the industrial diluent TPH (hydrogenated tetra propylene, a mixture of linear and branched C12 alkanes) was found to selectively extract Eu(III), Am(III), Cm(III), Cf(III) and Th(IV) over a nitric acid range of 1-3 mol L<sup>-1</sup> from a simulated PUREX raffinate by Modolo *et al.*<sup>[140]</sup> Due to TODGAs strong complexation, holdback reagents were required to mitigate the co-extraction of Zr, Mo and Pd, the extraction of Sr was left as a problem.

As expressed above, TODGA can barely discriminate between An(III) and Ln(III) elements. In the collaborative European research project FP7 ACSEPT, methylated derivatives on the central carbon position (Me-TODGA, Me<sub>2</sub>-TODGA, Figure 3-2) were synthesized.<sup>[9, 141-142]</sup> With increasing methyl substitution, extraction efficiency decreased probably due to steric hindrance. Particularly for the GANEX process, Me-TODGA was found to be the most promising extractant. It was found that distribution ratios and loading capacity of the desired Ln(III) and An(III) elements remained acceptable, while the extraction efficiency of undesired fission products decreased.<sup>[142]</sup>

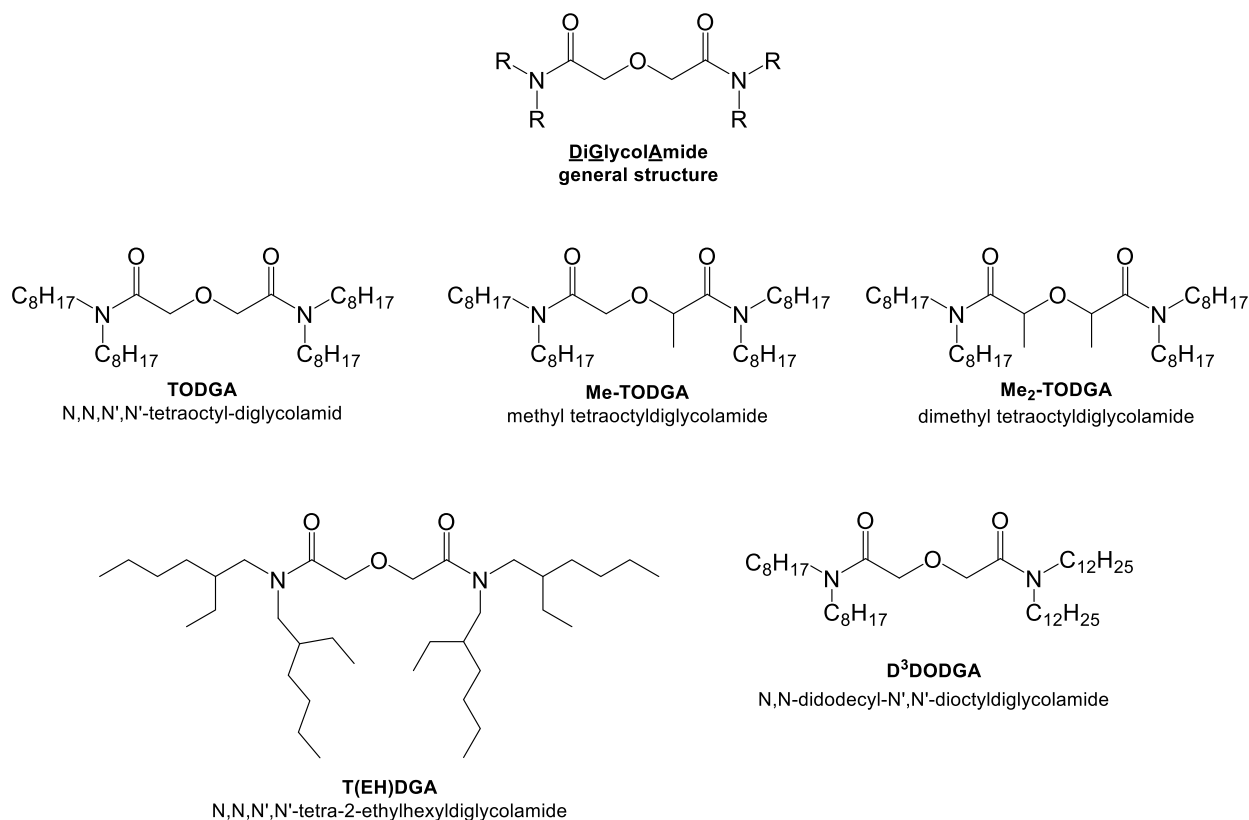


**Figure 3-2:** General structure of diglycolamide molecules (DGA) together with TODGA, its methylated forms Me-TODGA and Me<sub>2</sub>-TODGA, as well as T(EH)DGA and D<sup>3</sup>DODGA.

### 3.2.2. Radiolysis of Diglycolamides

Long-chained DGA molecules such as TODGA or T(EH)DGA were shown to be hydrolytically stable (Sugo *et al.*<sup>[143]</sup>, Modolo *et al.*<sup>[140]</sup>, Sharma *et al.*<sup>[144]</sup>) but are, depending on conditions, susceptible to radiolysis.<sup>[54, 140, 143, 145-152]</sup> TODGA itself was studied concerning its hydrolytic and radiolytic stability using different diluents. The molecule has an excellent solubility in saturated aliphatic hydrocarbons and extracts minor actinides like Am(III) and Cm(III) under high acidic conditions as well. Therefore, it was necessary to study the ligand's hydrolytic and radiolytic properties in order to apply TODGA in HLLW partitioning processes. Sugo *et al.* conducted a comparative study of TODGA and two more DGA ligands: *N,N'*-dioctyl-*N,N'*-dimethyl-2-(3'-oxapentadecyl)-propane-1,3-diamide (MA) and *N,N'*-dioctylhexamine (DOHA).<sup>[143]</sup> Additionally, product identification of radiolysis products was conducted. Hydrolysis experiments of 0.1 mol L<sup>-1</sup> in *n*-dodecane in contact with 3.0 mol L<sup>-1</sup> HNO<sub>3</sub> did not show any ligand degradation after stirring at room temperature for four weeks.<sup>[143]</sup>

Gamma-radiolysis experiments up to an absorbed dose of 500 kGy were conducted by Sugo *et al.*, using different TODGA concentrations from 0.01 to 1.57 mol L<sup>-1</sup> in *n*-dodecane, showing exponentially decreasing final ligand concentrations. The slope was depending on the initial TODGA concentration with the highest absolute slope using the smallest ligand concentration. It was therefore concluded, that the degradation of TODGA is enhanced in the presence of *n*-dodecane.<sup>[143]</sup> It was considered, that *n*-dodecane has a sensitization effect on all investigated amides. Therefore, radiolysis experiments were repeated us-



ing different solvent compositions of *n*-dodecane and benzene (100:0; 75:25; 50:50; 25:75; 0:100) showing decreasing radiolytic degradation with increasing share of benzene. This set of experiments proved the formerly considered sensitization effect.<sup>[143]</sup> Experiments on the effect of nitric acid (either without acid, pre-saturated as well as contacted during irradiation) did not show any protective effects.

Product identification of TODGA degradation products was conducted using FT-IR, NMR and GC/MS techniques. Four main radiolysis products were identified: dioctylamine (DOA), *N,N*-dioctylacetamide (DOAA), *N,N*-dioctylglycolamide (DOGA), and *N,N*-dioctylformamide (DOFA) (Figure 3-3). These compounds are results of bond cleavages of the N-C amide bond (a) (DOA), the C-O ether-bond (b) (DOAA, DOGA) as well as the C-C bond adjacent to the ether-bond (c) (DOFA). Bond cleavages (b) and (c) were considered as ‘typical’ reactions, while reaction (a) was found by GC to occur mainly in the presence of nitric acid. Reaction (b) occurred mainly in the absence of nitric acid, while reaction (c) was found to be the less reactive compared to the other two reactions.<sup>[143]</sup>

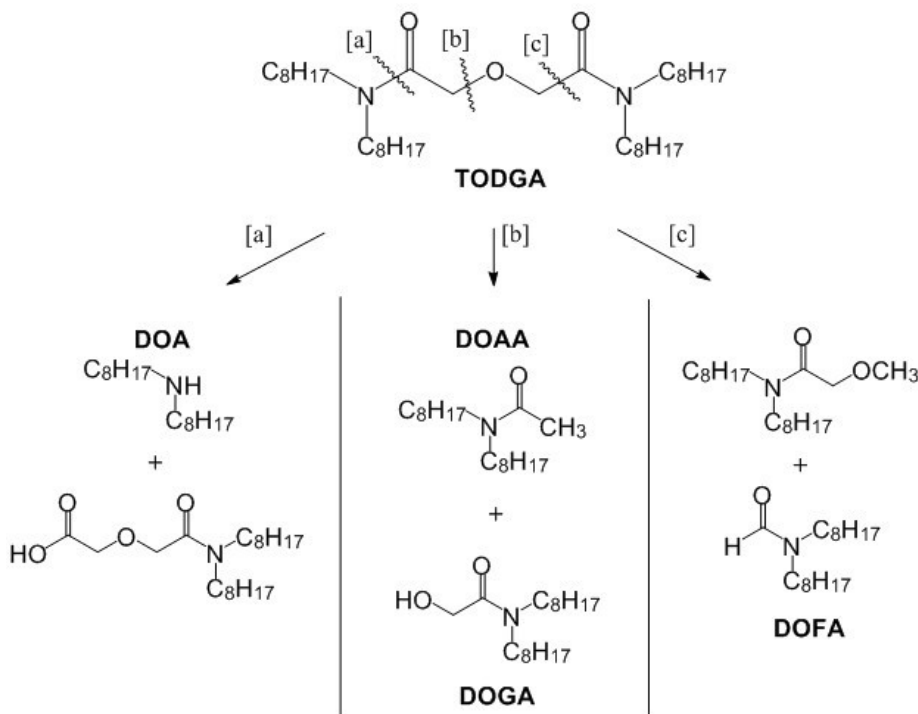


**Figure 3-3:** Schematic diagram of the radiolytic degradation of TODGA, based on Sugo *et al.*<sup>[143]</sup>

The radiolysis mechanism was found to be mainly resulting from electron-transfer reactions from diluent radical cations to the ligand molecules and Sugo *et al.*,<sup>[143]</sup> which was later proven in our work (Zarzana *et al.* (Paper 7)).<sup>[147]</sup> We found a protective effect of nitric acid depending on the used diluent. For TODGA in *n*-dodecane, for example, we observed only little effects on the dose constants for TODGA-degradation up to an absorbed dose of 400 kGy.<sup>[147]</sup> In contrast, irradiation experiments using TODGA in TPH being pre-contacted with nitric acid showed slightly protecting effects up to 1000 kGy absorbed dose, investigating the remaining TODGA concentration after irradiation. A clear protective effect was found using a diluent composed of a mixture of TPH and *n*-octanol.<sup>[146]</sup> The main sites for molecule degradation were found to be the functional diglycolamide group, specifically the C-O<sub>ether</sub> and N-C<sub>carbonyl</sub> bonds by Galán *et al.*<sup>[146]</sup> and later also in our work.<sup>[147]</sup>

Within the scope of this work, a study of gamma-radiolytic stability of the ligands Me-TODGA and Me<sub>2</sub>-TODGA (Paper 6)<sup>[153]</sup> as well as a comparison of gamma-radiolysis of TODGA and T(EH)DGA (Paper 7)<sup>[147]</sup> was conducted. Furthermore, the unsymmetrically substituted derivative *N,N*-didodecyl-*N',N'*-dioctyldiglycolamide (D<sup>3</sup>DODGA) was studied (Paper 8)<sup>[154]</sup>. A quantification of earlier identified radiolysis products of Me-TODGA was conducted as well (Paper 9).<sup>[155]</sup>

The main findings and conclusions of these works on diglycolamides are summarized in chapter 6.2 of this thesis.



## 4. Scope of the work and objectives

In this thesis, the radiolytic stability of two types of ligands is investigated, the 2,6-bis-triazinyl N-donor derivatives CyMe<sub>4</sub>BTBP (6,6'-bis(5,5,8,8-tetramethyl-5,6,7,8-tetrahydro-benzo[1,2,4]triazin-3-yl)[2,2']bipyridine) and CyMe<sub>4</sub>BTPhen (2,9-bis(1,2,4-triazin-3-yl)-1,10-phenantroline) (Figure 3-1), as well as the group of diglycolamides. For the group of DGAs (Figure 3-2), TODGA (*N,N,N',N'*-tetraoctyldiglycolamide) and its mono- and di-methylated derivatives (Me-TODGA and Me<sub>2</sub>-TODGA), the branched-chain TODGA derivative T(EH)DGA (*N,N,N',N'*-tetra-2-ethylhexyldiglycolamide) as well as the unsymmetrically substituted derivative *N,N*-didodecyl-*N',N'*-dioctyldiglycolamide (D<sup>3</sup>DODGA) are investigated.

### N-donor ligands

The focus of this work is a comparative study of the annulated N-donor ligands CyMe<sub>4</sub>BTBP and CyMe<sub>4</sub>BTPhen in 1-octanol solution in the light of possible future usage in minor actinide partitioning processes. The evolution of Am(III), Cm(III) and Eu(III) distribution ratios is observed as function of absorbed  $\gamma$ -dose. Molecular changes due to  $\gamma$ -radiolytic processes are analyzed by qualitative high resolution mass spectrometry. Additionally, quantitative measurements of the ligand molecules and semi-quantitative measurements of the formed radiolysis products are conducted. As final result, the degradation mechanisms of the systems are clarified.

### DGA-type ligands

The radiolytic stability and degradation mechanism of different TODGA derivatives, shown in Figure 3-2, are compared. For the investigation of effects of side chain modification, T(EH)DGA and D<sup>3</sup>DODGA are chosen. The derivatives Me-TODGA and Me<sub>2</sub>-TODGA are chosen, to investigate the effect of the methyl group(s) on their possible protective effect against radiolytic degradation.

Radiolytic degradation product identification is conducted, and a comparison to TODGA is made to analyze effects of side-chain and molecular backbone modification on radiolytic susceptibility of DGA-type compounds. In addition, the role of radiolytically formed diluent radical cations is elucidated with regard to the DGA degradation pathway. Besides the structural investigation and degradation product identification via mass spectrometric measures, the effect on actinide extraction (distribution ratios) is clarified.



## 5. Materials and Methods

### 5.1. Experiments using N-donor extractants

CyMe<sub>4</sub>BTBP and CyMe<sub>4</sub>BTPhen were purchased from Technocomm Ltd., Falkland, United Kingdom with a purity > 98 % and were used as received.

Solutions of 10 mmol L<sup>-1</sup> CyMe<sub>4</sub>BTBP or CyMe<sub>4</sub>BTPhen in 1-octanol (Merck, Darmstadt, Germany, analytical grade, > 99 %) were prepared and first irradiated under different conditions up to 413 kGy absorbed dose. In a later irradiation campaign, samples of CyMe<sub>4</sub>BTBP and CyMe<sub>4</sub>BTPhen in contact with 1 mol L<sup>-1</sup> nitric acid were irradiated to higher doses of 622 kGy. The <sup>60</sup>Co γ-source at Chalmers University, Gothenburg, Sweden was used (Gamma cell 220, Atomic Energy of Canada Ltd.). Due to the radioactive decay of <sup>60</sup>Co, the provided dose rate decreased from 9.8 to 8.7 kGy h<sup>-1</sup> during the experimental campaigns. The initial dose rate was determined using the ferrous-cupric dosimeter.<sup>[156]</sup> Samples of each ligand in 1-octanol solution were irradiated without, as well as in contact with nitric acidic solutions (Merck, Darmstadt, 65 %, analytical grade, diluted with demineralized water (18.2 MΩ cm)) of different concentrations (0.1, 1.0 and 4.0 mol L<sup>-1</sup> HNO<sub>3</sub>). Equal volumes (1 mL) of organic solvent and nitric acid were contacted during the irradiation experiments for which the samples were placed in the γ-source until the calculated dose was reached. To avoid pressurization during the irradiation experiment, the screw caps were not closed tightly. After removing the irradiated samples from the γ-source, phases were separated if necessary and the remaining organic phases were used for further analysis and solvent extraction experiments. In Figure 5-1, a set of samples is shown before (top) and after (bottom) irradiation.



**Figure 5-1:** Representative picture of a set of samples before (top) and after (bottom) irradiation.

In the solvent extraction experiments 500 μL of the irradiated organic phase were contacted with 500 μL fresh 1.0 mol L<sup>-1</sup> HNO<sub>3</sub> which was spiked with <sup>241</sup>Am (1.6 kBq), <sup>244</sup>Cm (1.6 kBq) and <sup>152</sup>Eu (2.8 kBq) tracer in 2 mL glass vials. Radioactive tracers were purchased from Isotopendienst M. Blasieg GmbH, Waldburg, Germany, Oak Ridge National Laboratory, Oak Ridge, USA, and Eckert and Ziegler Nuclitec GmbH, Braunschweig, Germany. The vials were shaken vigorously for 90 minutes in a shaking device (2,500 rpm) at 22°C to reach equilibrium. After centrifugation, the phases were separated, and aliquots of each phase were taken for analysis. Gamma spectroscopy was conducted using an HPGe (high-purity

germanium) detector system purchased from EG & G Ortec, Munich, Germany, and equipped with the GammaVision software. The  $\gamma$ -lines at 59.5 keV and 121.8 keV were analyzed for  $^{241}\text{Am}$  and  $^{152}\text{Eu}$ , respectively. Alpha measurements were carried out for  $^{241}\text{Am}$  (5486 keV) and  $^{244}\text{Cm}$  (5805 keV) using an Ortec Octète-pc eight chamber alpha measurement system equipped with PIPS detectors. Sample preparation for alpha measurement was done by homogenizing a 10  $\mu\text{L}$  alpha-spectroscopy sample in 100  $\mu\text{L}$  of a mixture of Zapon varnish and acetone (1:100 v/v). This mixture was distributed over a stainless-steel plate obtained from Berthold, Bad Wildbad, Germany. The sample was dried under a heating lamp and annealed into the stainless-steel plate by a gas-flame burner. The results are reported as distribution ratios  $D$ , as described in chapter 1.2. Given  $D$  values show an uncertainty of  $\pm 5\%$  within the range of  $0.01 < D < 100$ . Below and above these limits the uncertainties are lower than 20 % of the shown data. The minimum/maximum detectable distribution ratios were 0.002 and 500, respectively, due to the detection limits in either the organic or the aqueous phase.

Direct Infusion Mass Spectrometry measurements were performed using a Finnigan LCQ Fleet™ spherical Ion Trap LC/MSn instrument (Thermo Scientific) at the Institute of Inorganic Chemistry, Rež, Czech Republic. The specific experimental conditions can be found in Paper 5.<sup>[90]</sup>

Qualitative analyses for compound identification were performed using a hybrid linear ion trap FTICR (Fourier-Transform Ion Cyclotron Resonance) mass spectrometer LTQFT (Linear Tandem Quadrupole Fourier Transform) Ultra™ (Thermo Fisher Scientific, Bremen, Germany) coupled with an Agilent 1200 HPLC system (Agilent, Waldbronn, Germany). The specific experimental conditions can be found in Paper 5.<sup>[90]</sup> All shown spectra are formatted to be directly comparable to each other. Only peaks with a relative threshold of  $> 2\%$  were analyzed. All spectra were collected using data of the HPLC runs from 3 to 13 minutes for CyMe<sub>4</sub>BTBP and from 0 to 18 minutes for CyMe<sub>4</sub>BTPhen.

For quantitative mass spectrometric analyses, an HPLC-MS/MS method with APCI in positive ion mode as the ionization mode was developed and validated using a Triple Quadrupole Qtrap6500 instrument (ABSciex, Darmstadt, Germany) coupled with an Agilent 1260 HPLC system (Agilent, Waldbronn, Germany) to quantify the concentrations of CyMe<sub>4</sub>BTBP and CyMe<sub>4</sub>BTPhen after irradiation.

In all quantification experiments, data acquisition and processing were carried out using the software Analyst 1.6.1 (ABSciex, Darmstadt, Germany). For quantification the software Multiquant (ABSciex, Darmstadt, Germany) was used. The reproducibility for both ligands showed very good results with a variation coefficient  $\leq 6\%$ .

Pulse radiolysis experiments were conducted using the Laser-Electron Accelerator Facility (LEAF) at Brookhaven National Laboratory, which was described in detail by Wishart *et al.*<sup>[157]</sup> For irradiation experiments, 1-octanol solutions of CyMe<sub>4</sub>BTBP or CyMe<sub>4</sub>BTPhen were irradiated and lifetimes of the generated solvated electron ( $e^-_{\text{solv}}$ ) were observed in dependence of the ligand concentration, varying in the range from 2.5 to 10.0 mmol L<sup>-1</sup> CyMe<sub>4</sub>BTBP or CyMe<sub>4</sub>BTPhen, respectively. Additionally, the influence of nitric acid on  $e^-_{\text{solv}}$  absorbance by CyMe<sub>4</sub>BTPhen was tested in steady-state irradiation experiments using dried 1-octanol against 1-octanol contacted with 6.0 mol L<sup>-1</sup> HNO<sub>3</sub>. Samples were irradiated in 1.00 cm Suprasil semimicro cuvettes sealed with Teflon stoppers. The doses per pulse for these experiments were in the range 40–60 Gy. Time-resolved kinetics were obtained using an FND-100 silicon di-

ode detector and digitized using a LeCroy WaveRunner 640Zi oscilloscope (4 GHz, 8 bit). Interference filters (10 nm bandpass) were used for the wavelength selection of the analyzing light.<sup>[158]</sup>

## 5.2. Experiments using DGA extractants

The DGA molecules Me-TODGA and Me<sub>2</sub>-TODGA were synthesized according to the methodology described before<sup>[141]</sup> or purchased from Technocomm Ltd., Wellbrae, Scotland, which was also used as supplier for D<sup>3</sup>DODGA. TODGA and T(EH)DGA was supplied by Eichrome Industries, Darien, IL, US. All used chemicals were of analytical grade and were used without further purification.

For gamma irradiation experiments, two  $\gamma$ -sources were used. At CIEMAT (Spain), the Náyade facility, was used for experimental work resulting in Galán *et al.*<sup>[153]</sup> and Hubscher-Bruder *et al.*<sup>[155]</sup> (Papers 6 and 9, cf. chapter 10). For Galán *et al.*<sup>[153]</sup>, Zarzana *et al.*<sup>[147]</sup> and Roscioli-Johnson *et al.*<sup>[154]</sup> (Paper 6 to 8, cf. chapter 10), a Nordion Gamma Cell 220 <sup>60</sup>Co irradiator (Ottawa, Canada) at the Idaho National Lab (ID, US) was used. Details on the irradiation facilities can be taken from the corresponding publications.

### DAD/MS measurement procedure<sup>[153, 155]</sup>

The chemical composition of the irradiated TODGA, Me-TODGA and Me<sub>2</sub>-TODGA samples in Paper 6 was characterized by LC-DAD/MS or LC-HRMS. The HPLC-DAD measurements were performed by using a reverse phase C-18 column and CH<sub>3</sub>CN/H<sub>2</sub>O as the mobile phase at 205 nm.

HPLC-MS measurements in Papers 6 and 9 were performed using three different methods, which are described in detail in the corresponding publications.

### UHPLC-ESI-TOF-MS<sup>[147, 154]</sup>

For molecule-fragment identification, UHPLC-ESI-TOF-MS (ultra-high-performance liquid chromatograph coupled to an electrospray-ionization-quadrupole-time-of-flight mass spectrometer) experiments were conducted. Therefore, irradiated samples were diluted in HPLC-grade 2-propanol (Fisher Scientific, Pittsburg, PA, US) to receive concentrations in the low micromolar range. For experimental details, please see the corresponding publications.

### HPLC-APCI-FT-MS<sup>[154]</sup>

HPLC-APCI-FT-MS measurements were performed at Forschungszentrum Jülich using a hybrid linear ion trap FT-ICR mass spectrometer LTQFT Ultra™ (Thermo Fisher Scientific, Bremen, Germany) coupled with an Agilent 1200 system (Agilent, Waldbronn, Germany). Experimental details can be found in the corresponding publication. All data were processed using the Xcalibur software, version 2.0.

### Standard Preparation of TODGA and T(EH)DGA<sup>[147]</sup>

For the quantitative identification of DGA concentration after radiolysis, standards for TODGA and T(EH)DGA were prepared by serial dilution of unirradiated, non-acid contacted 0.05 mol L<sup>-1</sup> DGA solutions in dodecane with 2-propanol, to final concentrations ranging from 0.5  $\mu$ mol L<sup>-1</sup> to 5  $\mu$ mol L<sup>-1</sup>. These standards were used to construct a calibration curve using the integrated chromatographic peak areas for



the diglycolamides using the UHPLC-ESI-TOF-MS analytical method. Each sample result is the mean of 5 measurements and the error bars shown represent 99 % confidence intervals.

#### **Picosecond electron pulse radiolysis<sup>[147]</sup>**

Pulse radiolysis based transient absorption experiments were performed at the Brookhaven LEAF facility. Samples were irradiated in 1.00 cm Suprasil semimicro cuvettes sealed with Teflon stoppers. The doses per pulse for various experiments were in the range 20–40 Gy. Time-resolved kinetics were obtained using a Hamamatsu R1328-03 biplanar tube (rise time 60 ps) amplified using a B&H AC4020H20L1 amplifier (4 GHz), and digitized using LeCroy WaveRunner 640Zi oscilloscope (4 GHz). Interference filters were used for the wavelength selection of the analyzing light.

#### **Solvent extraction studies<sup>[155]</sup>**

The extraction experiments were performed according to the description above for N-donor-Ligand solvent extraction experiments (chapter 5.1).

#### **Microcalorimetric and van't Hoff studies<sup>[155]</sup>**

Microcalorimetric titrations were performed at  $25.00 \pm 0.05^\circ\text{C}$  using a 2277 thermal activity monitor microcalorimeter (TA instruments) according to the experimental details described in the corresponding publication.

## 6. Conclusions

The conclusion part of this thesis summarizes highlights of the attached Papers 1 to 10<sup>[86-88, 90, 133, 147, 153-155, 159]</sup> (cf. chapter 10, List of Papers).

### 6.1. Summary of the work on CyMe<sub>4</sub>BTBP and CyMe<sub>4</sub>BTPhen

The ligands CyMe<sub>4</sub>BTBP and CyMe<sub>4</sub>BTPhen were irradiated under different experimental conditions using a 0.01 mol L<sup>-1</sup> solution in 1-octanol. Neat organic solution was irradiated as well as organic solutions in contact to 0.1, 1.0 and 4.0 mol L<sup>-1</sup> nitric acid aqueous phases in glass vials using a <sup>60</sup>Co gamma source applying a dose rate of 9.8 to 8.7 kGy h<sup>-1</sup> to the samples. The irradiation experiments were stopped after receiving different absorbed doses up to 400 kGy. After these irradiation experiments, the organic phases were immediately separated from the aqueous phase in contact, if necessary, before solvent extraction as well as mass spectrometric experiments were conducted.

For Am(III), Cm(III) and Eu(III), we observed decreasing metal ion distribution ratios, as a function of absorbed dose for both ligands when irradiated without contact to an aqueous phase. For CyMe<sub>4</sub>BTBP, the *D* values decreased quickly, and the lower detection limit was reached within 200 kGy absorbed dose for An(III). CyMe<sub>4</sub>BTBP is a highly selective extractant for trivalent actinide ions<sup>[25]</sup> as indicated by the generally low *D* values measured for Eu(III) extraction. CyMe<sub>4</sub>BTPhen extracts trivalent metal ions with higher *D* values under the same conditions.<sup>[107]</sup> Therefore, all measured *D* values were found to be higher compared to CyMe<sub>4</sub>BTBP.

Furthermore, the decrease in *D* values did not proceed uniformly. We observed a ‘plateau’ for CyMe<sub>4</sub>BTPhen experiments in particular, which can be explained by formed radiolysis products, being able to extract trivalent metal ions themselves but also being prone to radiolytic degradation. The selectivity of the extractants in the solvent extraction experiments did not change much with increasing absorbed dose. Therefore, the radiolysis products also seem to be selective for trivalent actinide extraction.

Under most conditions of organic solvents being irradiated in contact with 0.1, 1, and 4 mol L<sup>-1</sup> HNO<sub>3</sub> solutions, the observed distribution ratios of both ligands were higher compared to the extraction series without contact to HNO<sub>3</sub> during irradiation. The selectivity of the extractants remained high as well.

The addition of nitric acid to the organic phase during irradiation led to a slower decrease in distribution ratios as function of absorbed dose, while 0.1 mol L<sup>-1</sup> HNO<sub>3</sub> had the slightest effect. For high nitric acid concentrations, An(III) distribution ratios for CyMe<sub>4</sub>BTPhen were even higher than before without nitric acid contact. This is partly due to a slight co-extraction of nitric acid in the irradiated solvent, causing slightly higher equilibrium nitric acid concentrations in the extraction experiments. We observed a comparable but less pronounced behavior for the Eu(III) *D* values, which cannot be explained by the co-extraction of nitric acid. Instead, this behavior is likely explained by the formation of radiolysis products which can extract trivalent metal ions themselves, as described above.

We cannot make a clear statement towards the comparison of the radiolytic stability for the two extractants based on the measured *D* values, as the initial *D* values already differ too much. Therefore, quantita-

tive information on the extractant concentration as a function of absorbed dose using mass spectrometric methods is discussed in Schmidt *et al.*<sup>[90]</sup> (Paper 5, cf. chapter 10).

Due to the high excess of diluent molecules over ligand molecules, indirect radiolysis of the ligand molecules is the dominantly occurring mechanism. These indirect radiolysis processes were described as sensitization effect for the radiolysis of amides in organic solutions by Sugo *et al.*<sup>[145]</sup> For TODGA and other amide ligands, we found mainly molecule destruction (chapter 6.2), whilst the aromatic systems of the N-donor ligands may stabilize the radical compound generated by the reaction of a solvated electron with the ligand molecule:



We conducted pulse radiolysis experiments with both ligands, to compare their behavior in terms of lifetime and subsequent reactions. Therefore, solvated electrons were generated in 1-octanol solution containing 2.5, 5.0, 7.5 and 10.0 mmol L<sup>-1</sup> CyMe<sub>4</sub>BTBP and CyMe<sub>4</sub>BTPPhen, respectively to react following equation (49).

Results are presented in Schmidt *et al.* (Paper 5)<sup>[90]</sup> depicting a faster reaction rate (faster decrease in absorbance) with increasing ligand concentration for both ligands. This is attributed to an increasing reaction rate of solvated electrons with the ligand molecules. Second-order rate constants (k) were calculated from the slopes and found to be  $(1.60 \pm 0.04) \times 10^9 \text{ L mol}^{-1} \text{ s}^{-1}$  for CyMe<sub>4</sub>BTBP and  $(1.05 \pm 0.03) \times 10^9 \text{ L mol}^{-1} \text{ s}^{-1}$  for CyMe<sub>4</sub>BTPPhen, which is in good agreement with Szreder *et al.* (Paper 4)<sup>[133]</sup> for CyMe<sub>4</sub>BTPPhen. These results imply that both ligands react rapidly with the solvated electron according to equation (49) and that CyMe<sub>4</sub>BTBP reacts faster than CyMe<sub>4</sub>BTPPhen. Additionally, we did not observe fragmentation of the molecule and we concluded, that the radical anion has a relatively long lifetime (stabilization according to paper 4) and is able to undergo further reactions.

To study the role of water and nitric acid during radiolysis, we conducted steady state pulse radiolysis experiments using solutions of 2.5 – 10.0 mmol L<sup>-1</sup> CyMe<sub>4</sub>BTPPhen in pure dried 1-octanol as well as in 1-octanol previously contacted with 6.0 mol L<sup>-1</sup> nitric acid. The absorbance of the solvated electrons was monitored as a function of time. For samples containing only the ligand molecule and 1-octanol, a clear absorbance of solvated electrons was found, whereas the acid contacted 1-octanol diluent did not show an absorbance of solvated electrons. In contrast to equation (49), where the solvated electrons were captured by ligand molecules forming ligand radical anions, the solvated electrons are captured by protons forming hydrogen atoms in the presence of dissociated nitric acid (equation (12), Paper 4). Due to this process, fewer solvated electrons are available to directly form ligand radical anions.

Analysis of the new absorbance kinetics under these contacted acidic 1-octanol conditions was also performed. We fitted the measured absorbance profiles to a standard pseudo-first-order growth and decay function, with the growth component value plotted against the ligand to obtain the second-order rate constants for hydrogen atom (H•) reaction



as  $k_6 = (3.18 \pm 0.08) \times 10^8 \text{ L mol}^{-1} \text{ s}^{-1}$  and  $(4.16 \pm 0.06) \times 10^8 \text{ L mol}^{-1} \text{ s}^{-1}$  for CyMe<sub>4</sub>BTBP and CyMe<sub>4</sub>BTPPhen, respectively.

### Mass spectrometry

Besides the above described, obvious effects of irradiation, which are reflected in the distribution ratios, the molecular changes due to radiolysis were of interest. Therefore, we conducted high resolution mass spectrometry (HRMS) measurements with prior high-performance liquid chromatography (HPLC).

Besides peaks of the protonated ligand species CyMe<sub>4</sub>BTBP and CyMe<sub>4</sub>BTPPhen species ( $M+H^+$ ), respectively, the most prominent radiolysis products were best described as addition products of the diluent 1-octanol. These addition products have been reported by Schmidt *et al.*<sup>[86-87, 90]</sup> (Papers 1, 2 and 5, cf. chapter 10). The results are in good agreement with literature, as was described in chapter 2.2 and equations (39) to (44).

The  $\alpha$ -hydroxyalkyl radicals (equation (39)) can react with the ligand molecules under formation of the observed addition products. The radiolysis products were identified as addition products with one or two of these  $\alpha$ -hydroxyoctyl radicals.

We could barely observe molecule fragments of  $m/z$  ratios lower than the parent molecule masses. The addition reaction of the  $\alpha$ -hydroxyoctyl radical seems to be more probable than ligand degradation, at least for the investigated dose range of up to 623 kGy absorbed dose. Interestingly, the identified addition-products were mainly found to be of two or sometimes four mass numbers higher, as explained in detail in Paper 5.<sup>[90]</sup> For these molecule species, reduced unsaturated bonds (addition of hydrogen radicals or molecules) of the aromatic system were found to be responsible, which can be explained by the relatively high yield of H<sub>2</sub> production by alcohol-radiolysis, compared to other diluents.<sup>[84, 160]</sup>

In agreement with Yu *et al.*,<sup>[84]</sup> we found addition products of the 1-octanol intermediate radiolysis products in the investigated system as well (Paper 5).<sup>[90]</sup> The corresponding addition products of the *n*-heptyl radical were found for CyMe<sub>4</sub>BTBP and CyMe<sub>4</sub>BTPPhen, respectively. We could observe the 8-hydroxypenta-decanyl radical addition products in their reduced form for CyMe<sub>4</sub>BTBP under both conditions. For CyMe<sub>4</sub>BTPPhen, the unreduced form was mainly observed under acidic conditions, while the reduced form was predominantly formed in neat organic solution. Additionally,  $m/z$  ratios of addition products with -16 mass units were found. We explained the difference of 16 mass units by the formal loss of one oxygen atom. Such a reaction could occur via the abstraction of one  $\cdot\text{OH}$ , followed by subsequent H $\cdot$  addition, albeit the reaction pathway can be more complex. The calculated  $m/z$  ratios for such reaction products are in very good agreement with measured  $m/z$  ratios and were also observed in the radiolysis of C5-BPP.<sup>[129]</sup>

In samples irradiated in contact to 1.0 mol/L<sup>-1</sup> nitric acid, we found the same peaks as for the samples irradiated without nitric acid contact, but with generally higher intensities of the parent molecule species. The addition products were similarly observed, but in contrast to the samples irradiated without acid contact, the M+1OctOH addition products were mainly present in the unreduced form. The reduced forms were only present in traces. Higher addition products with two  $\alpha$ -hydroxyoctyl radicals added were present in lower intensities, for CyMe<sub>4</sub>BTBP interestingly predominantly in the reduced form, while for CyMe<sub>4</sub>BTPPhen mainly in the unreduced form. We observed the *n*-heptyl and 8-hydroxypentadecanyl

radical addition products with only low intensities. 1-Octanol is known to extract considerable amounts of water and nitric acid when equilibrated with nitric acid solutions.<sup>[161-162]</sup> The considerably lower formation of radiolysis products is therefore attributed to the scavenging of reactive radicals in the organic phase by extracted water and nitric acid.<sup>[163]</sup> Therefore, contact with aqueous nitric acid solution during irradiation has a protective effect, especially on CyMe<sub>4</sub>BTBP, which confirms the observations from the solvent extraction experiments.

In Figure 6-1 and Figure 6-2, we show proposed reaction schemes for the radiolysis of CyMe<sub>4</sub>BTBP and CyMe<sub>4</sub>BTPhen, respectively, concluding the presented work on these two N-donor ligands. Additionally, we conducted quantification of the ligand molecules and semi-quantitative measurements of the above identified radiolysis products, which can be found in Schmidt *et al.*<sup>[90]</sup> (Paper 5).

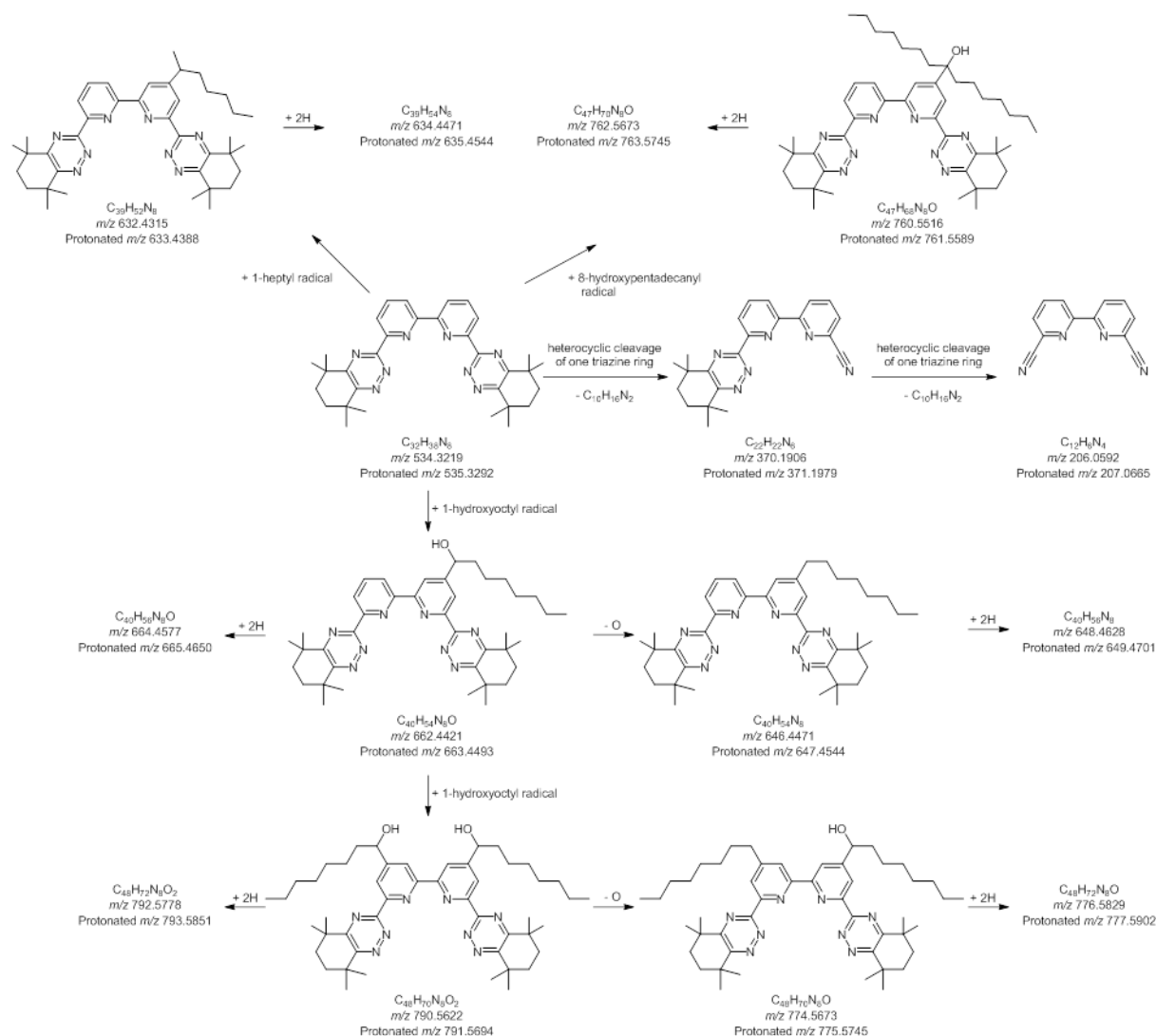


**Figure 6-1:** Suggested radiolysis reactions for CyMe<sub>4</sub>BTBP. Note that HRMS data does not give structural information and the shown structures (despite CyMe<sub>4</sub>BTBP) are only suggestions.

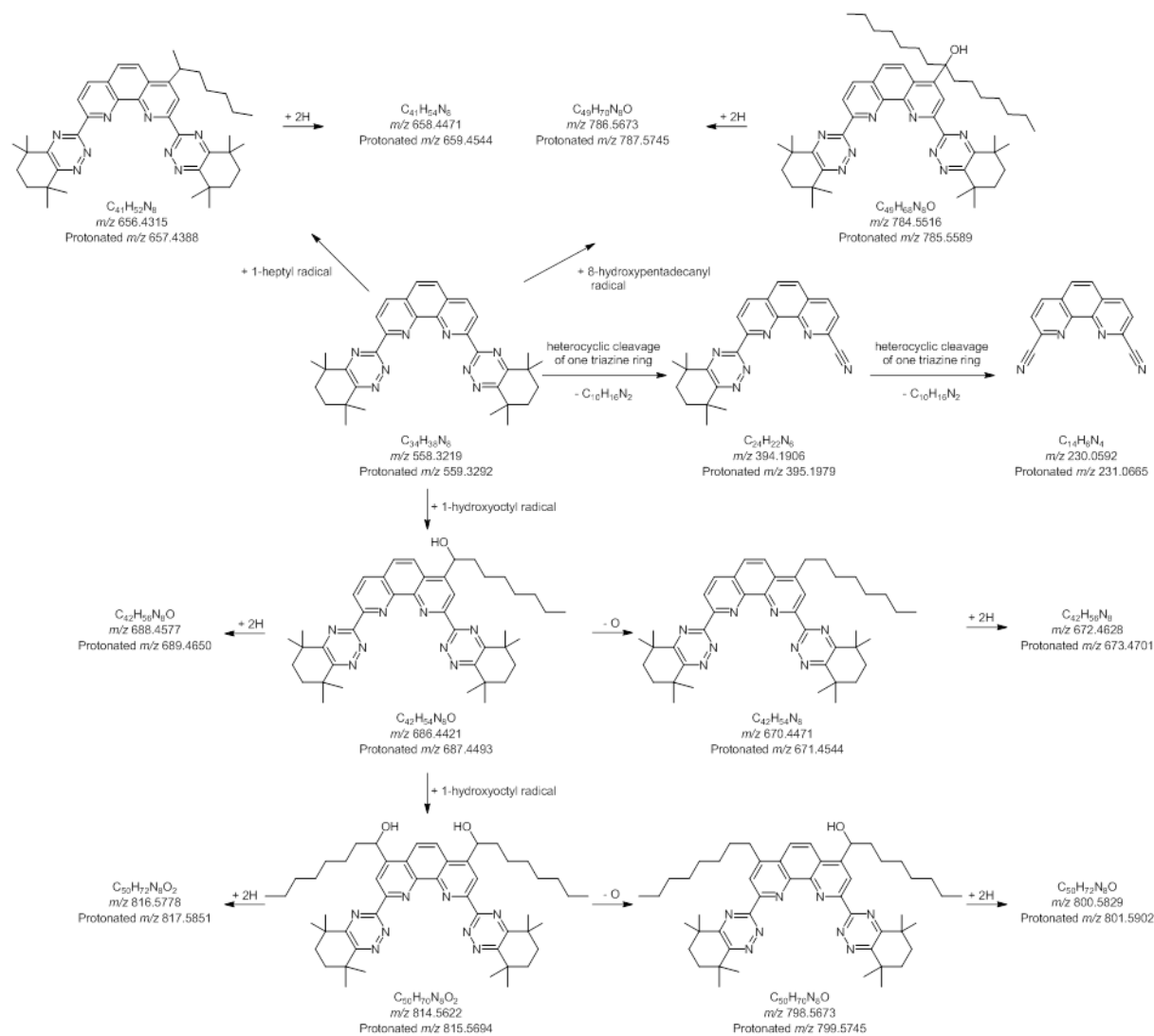


**Figure 6-2:** Suggested radiolysis reactions for CyMe<sub>4</sub>BTPPh. Note that HRMS data does not give structural information and the shown structures (despite CyMe<sub>4</sub>BTPPh) are only suggestions.

## 6.2. Summary of the work on DGA-type ligands

In this work, the influence of different substitutes to DGA molecules and their influence on radiolytic stability and actinide extraction was investigated. Therefore, on the one hand the substitution of the tetraoctyl side chains by symmetrically branched (T(EH)DGA) as well as asymmetrical (D<sup>3</sup>DODGA) side chains, and on the other hand the introduction of one or two methyl groups to the molecule backbone (Me-TODGA and Me<sub>2</sub>-TODGA) were investigated. For the substitution of the four symmetrical octyl moieties of the TODGA molecule, the branched ethylhexyl moieties were introduced resulting in T(EH)DGA (*N,N,N',N'*-tetra-2-ethylhexyldiglycolamide). This compound was successfully used by Lumetta *et al.* in the ALSEP (Actinide Lanthanide SEparation) process in combination with the soft donor ligand DTPA (diethylene-triamine pentaacetic acid) to gain a single extraction/strip cycle to separate actinides from lanthanides.<sup>[164-166]</sup>

Organic phases of TODGA and T(EH)DGA in *n*-dodecane were irradiated in the same concentration to compare radiolytic degradation in the presence and absence of aqueous nitric acid. Additionally, the kinetics of the *n*-dodecane radical cation with TODGA was measured. No differences in the  $\gamma$ -radiolysis of TODGA and T(EH)DGA in *n*-dodecane were found. Additionally, the influence of a contacted aqueous nitric acid phase during irradiation was negligible. Most vulnerable molecule bonds were found to be within the backbone of the molecule, not depending on the attached side chains (cf. Figure 6-3).<sup>[147]</sup> Especially the C-O<sub>ether</sub> (Compound III and IV), N-C<sub>carbonyl</sub> (Compound II) and the N-C<sub>side-chain</sub> (Compound I) bonds were found to be vulnerable. To a lesser extent, also the C-C<sub>carbonyl</sub> (Compound V and VI) was radiolytically attacked.

These results together with the measured very fast degradation pathway via *n*-dodecane radical cation charge transfer of  $k_2 = (9.7 \pm 1.1) \times 10^9 \text{ M}^{-1} \text{ s}^{-1}$  for TODGA indicating this to be the major degradation pathway, suggests the modification of the alkane side chains having no effect on the  $\gamma$ -radiolytic stability of TODGA derivatives.

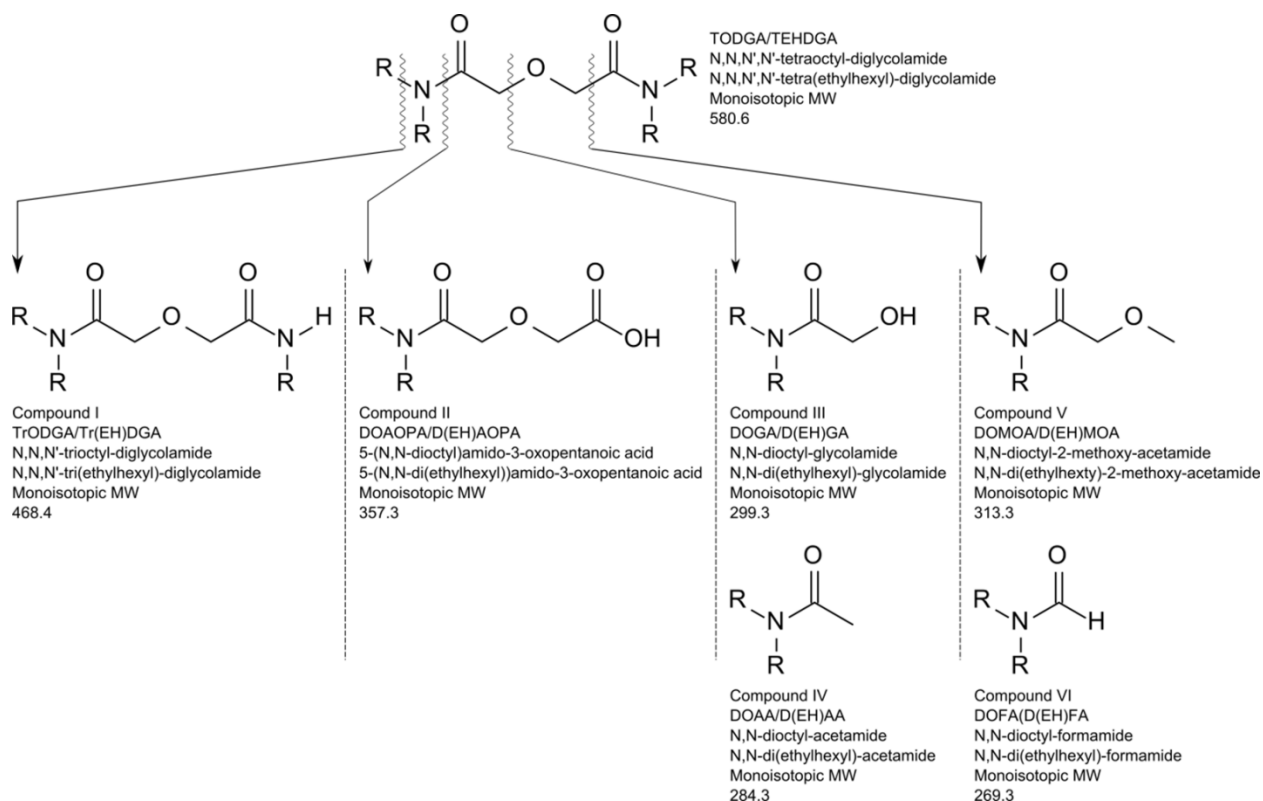


**Figure 6-3:** Proposed structures for radiolysis products observed for TODGA and T(EH)DGA with positive mode ESI-MS, where R is octyl for TODGA and ethylhexyl for T(EH)DGA.<sup>[147]</sup>

The studies on the slightly heavier D<sup>3</sup>DODGA molecule in comparison with TODGA and T(EH)DGA did not reveal differences in  $\gamma$ -radiolysis rates. Nevertheless, Wilden et al.<sup>[167]</sup> and Horne et al.<sup>[168]</sup> found a dependence between molecular weight and radiolysis rate for much lighter and heavier diglycolamides, later. In our experiments, the rate was not affected remarkably, neither by the presence of nitric acid nor by air sparging during radiolysis experiments. For the investigated DGA systems, the radical cation produced in the alkane diluent is the main reactive species for ligand radiolysis. The degradation chemistry, in contrast, was affected by nitric acid. In the presence of an aqueous nitric acidic phase during irradiation, major radiolytic degradation took place at the site of amide nitrogen atoms (cf. Figure 6-4)<sup>[154]</sup> resulting in higher fraction of degradation products from the rupture of N-C<sub>carbonyl</sub> (Compounds 2a, 2b, 3a, and 3b) and N-C<sub>alkyl</sub> (Compounds 1a and 1b,) bonds. In comparison with irradiation experiments without aqueous nitric acid contact, the C-O<sub>ether</sub> (Compounds 4a, 4b, 5a and 5b) and C-C<sub>carbonyl</sub> bonds (Compounds 6a and 6b) were broken rarely, resulting in a smaller fraction of all radiolysis products.



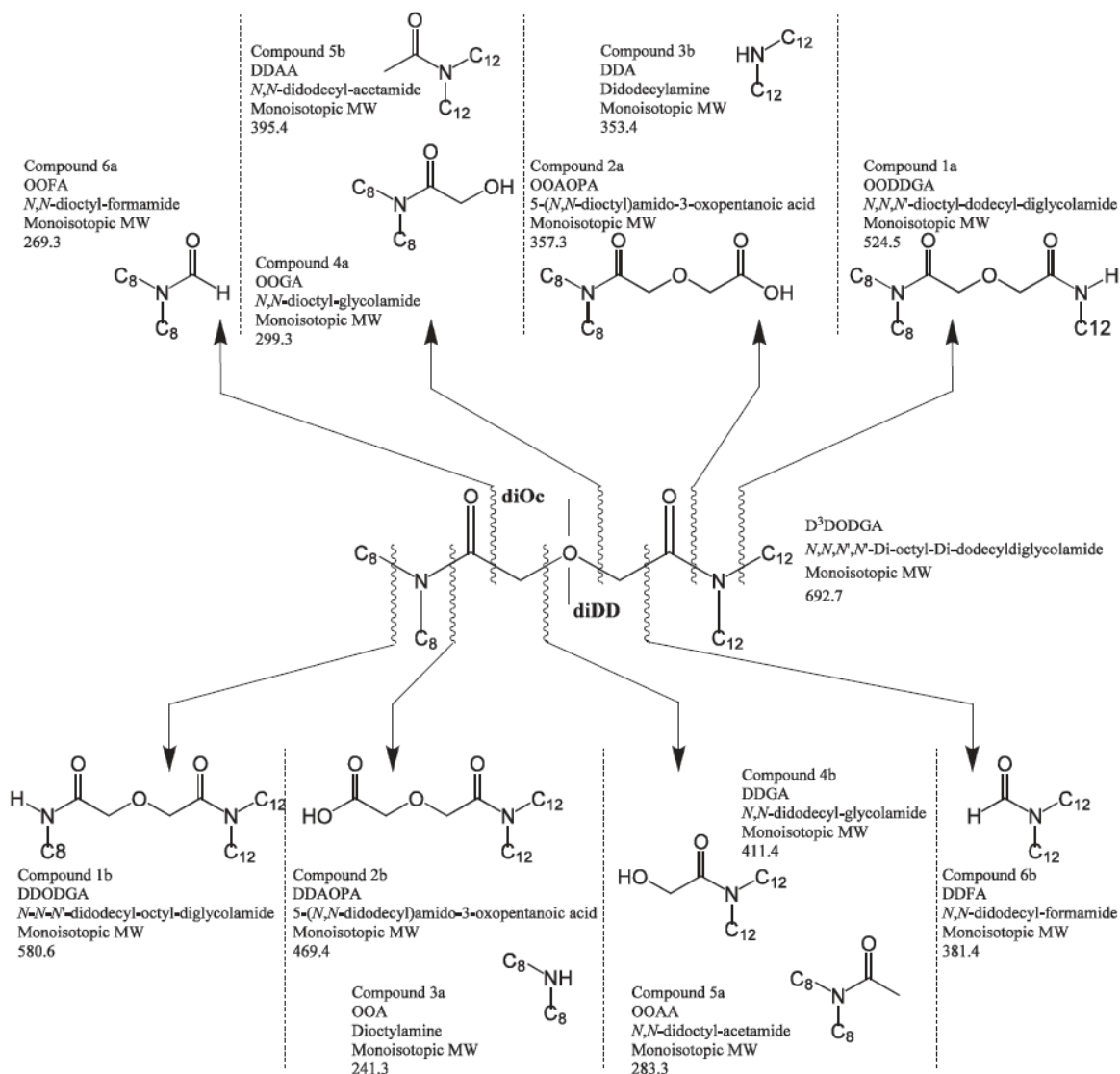


**Figure 6-4:** Proposed structures for radiolysis products observed for D<sup>3</sup>DODGA with positive-mode ESI-MS, where C<sub>8</sub> is C<sub>8</sub>H<sub>17</sub> and C<sub>12</sub> is C<sub>12</sub>H<sub>25</sub>.<sup>[154]</sup>

Since it was shown that substitutions of the four octyl chains of TODGA by different branched and straight chains did not affect radiolytic stability of DGA compounds, the backbone of the molecule was found to be the most vulnerable part of DGA molecules against radiolysis. Therefore, the methylated and di-methylated derivatives Me-TODGA and Me<sub>2</sub>-TODGA with the introduction of (a) methyl group(s) at the methylene carbon position(s) were synthesized during continued European research within the FP 7 ACSEPT project.<sup>[9, 141-142]</sup> It was found, that extraction efficiency decreased with increasing methyl substitution, due to steric hindrance. Nevertheless, Me-TODGA was found to be most promising, which its usage in the GANEX (Group ActiNide Extraction) process confirmed. It was proven, that the extraction of undesired fission products decreased, while distribution ratios and loading capacity of Ln(III) and An(III) remained acceptably high.<sup>[169]</sup>

Comparative studies of Me-TODGA and Me<sub>2</sub>-TODGA in TPH and *n*-dodecane indicated that the rupture of the O-C<sub>ether</sub> linkage was the main degradation taking place under  $\gamma$ -radiolysis. After introducing one methyl group to the TODGA molecule, the molecule was not protected against radiolysis at all. In contrast, Me-TODGA degraded faster compared to TODGA itself, possibly due to a weakening of the remaining unsubstituted C-O<sub>ether</sub> linkage resulting in the radiolysis products shown in Figure 6-5.

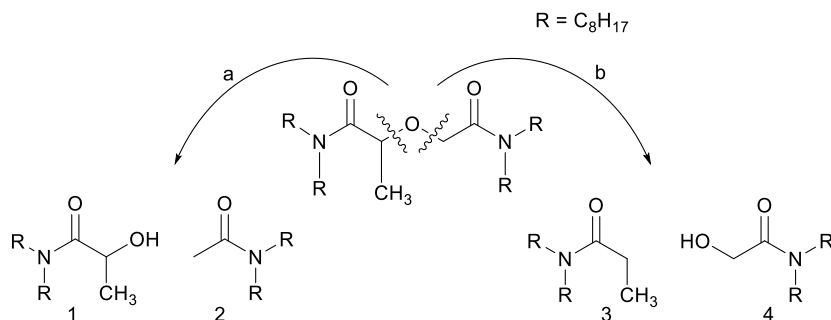


**Figure 6-5:** The four possible products of C-O<sub>ether</sub> linkage rupture for the unsymmetrical Me-TODGA.<sup>[153]</sup>

This was supported by the fact that radiolysis products from the rupture of the unsubstituted C-O<sub>ether</sub> linkage were most abundant. Substituting the diluent *n*-dodecane to TPH did not affect the results, indicating that besides the *n*-dodecane, also the radical cation is capable of electron transfer reactions with the DGAs. Nevertheless, for TPH lower dose constants were found, confirming the assumption that branched radical cations are expected to react slower due to their higher stability. Introducing a second methyl group at the unsubstituted C-O<sub>ether</sub> carbon atom further decreased the rate of radiolytic degradation. Besides this, the loss of one or, for Me<sub>2</sub>-TODGA, the loss of two octyl groups formed important degradation products besides the cleavage of the N-C<sub>carbonyl</sub> forming carboxylic acids. This effect was amplified in the presence of aqueous nitric acid during radiolysis. Figures of all identified degradation products can be found in Galán *et al.*<sup>[153]</sup> (Paper 6).

The influence of nitric acid was found to be much adverse than for other non-substituted DGAs, especially for Me<sub>2</sub>-TODGA. For all degradation products, higher yields were found in the presence of nitric acid. Therefore, methyl substitution seems to protect the hosting bond while activating other bonds within the molecule, especially towards reactions to reactive species coming from acid and water radiolysis. The most likely  $\cdot OH$  and  $\cdot NO_3$  radicals may react via  $\cdot H$  atom abstraction to the susceptible sites of Me-TODGA and Me<sub>2</sub>-TODGA. Nevertheless, the overall dose constants of these are comparable to those found for unsubstituted TODGA compounds.

In a following study, previously identified degradation products of Me-TODGA  $\gamma$ -radiolysis were investigated with respect to their ability to participate in actinide extraction. The presence of these degradation products can lead to undesired effects such as decrease in extraction efficiency and selectivity or deterioration of physical properties by third-phase formation. The examined degradation products are given in Figure 6-6.<sup>[155]</sup> Having the synthesized compounds as internal standard, HPLC-MS measurements of freshly irradiated 0.1 mol L<sup>-1</sup> Me-TODGA in TPH irradiated to 1000 kGy confirmed the previously thesis, that degradation path (a) from Figure 6-5 (bond cleavage at the unsubstituted side of the O<sub>ether</sub> atom) is

the preferred degradation path. Overall, it was proven that Me-TODGA is less resistant to radiolysis than TODGA itself.

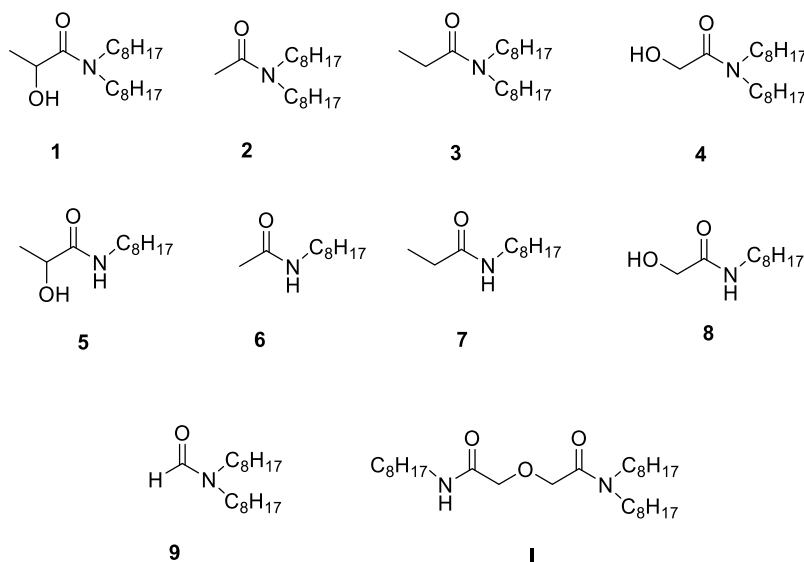


**Figure 6-6:** Structures of the degradation products of Me-TODGA (1-9) and TODGA (I).<sup>[155]</sup>

At high acidities, as they are found in numerous reprocessing processes, the 1- and 2-hydroxyamides are degradation products of main interest. Compounds 1 and 4 showed especially high affinity to Zr, Mo and Pd. A replacement of the hydroxy group in compound 1 by methoxy or acetoxy groups leads to decreasing Am(III) and Eu(III) extraction, underlining the importance of the hydroxy-group in metal extraction. A slope analysis of the main degradation compound (1) revealed an Am(III) and Eu(III) extraction via 1:4 complexes. In microcalorimetric studies, the compounds I, 1, 4 and 5 showed significant heat effects, related to strong interactions with the tested lanthanides La, Eu and Yb. The formation of 1:1 complexes, in contrast to 1:1, 1:2 and 1:3 complexes of TODGA and Me-TODGA with the lanthanides, is consistent with the formation of chelates.

Together with the results of T(EH)DGA and D<sup>3</sup>DODGA, the results of Me-TODGA and Me<sub>2</sub>-TODGA experiments show striking similarities in the degradation pathway. The degradation rates of the examined DGAs along with the identified degradation products strongly suggest the DGA molecule backbone being the most vulnerable part of the molecules. The side chains, independent if branched or not, are less relevant for the radiolytic stability.

## 7. List of Figures

Figure 1-1:	Scheme of European hydrometallurgical partitioning processes. <sup>[19]</sup> .....	5
Figure 1-2:	Ligands CyMe <sub>4</sub> BTBP (left) and TODGA (right), used in the SANEX process. ....	8
Figure 1-3:	Flow sheet of the SANEX process using CyMe <sub>4</sub> BTBP + TODGA as extractants. <sup>[24]</sup> .....	9
Figure 2-1:	UV-VIS absorption spectra of 1-octanol in nitrogen, receiving doses of 0 (a), 100 (b), 200 (c), 300 (d), 600 (e) and 900 (f) kGy <sup>[84]</sup> .....	15
Figure 3-1:	Selected molecules from the evolution of nitrogen-donor ligands.....	19
Figure 3-2:	General structure of diglycolamide molecules (DGA) together with TODGA, its methylated forms Me-TODGA and Me <sub>2</sub> -TODGA, as well as T(EH)DGA and D <sup>3</sup> DODGA. ....	23
Figure 3-3:	Schematic diagram of the radiolytic degradation of TODGA <sup>[143]</sup> .....	24
Figure 5-1:	Representative picture of a set of samples before (top) and after (bottom) irradiation. ....	29
Figure 6-1:	Suggested radiolysis reactions for CyMe <sub>4</sub> BTBP. Note that HRMS data does not give structural information and the shown structures (despite CyMe <sub>4</sub> BTBP) are only suggestions. ....	36
Figure 6-2:	Suggested radiolysis reactions for CyMe <sub>4</sub> BTPhen. Note that HRMS data does not give structural information and the shown structures (despite CyMe <sub>4</sub> BTPhen) are only suggestions. ....	37
Figure 6-3:	Proposed structures for radiolysis products observed for TODGA and T(EH)DGA with positive mode ESI-MS, where R is octyl for TODGA and ethylhexyl for T(EH)DGA. <sup>[147]</sup> .....	39
Figure 6-4:	Proposed structures for radiolysis products observed for D <sup>3</sup> DODGA with positive-mode ESI-MS, where C <sub>8</sub> is C <sub>8</sub> H <sub>17</sub> and C <sub>12</sub> is C <sub>12</sub> H <sub>25</sub> . <sup>[153]</sup> .....	40
Figure 6-5:	The four possible products of C-O <sub>ether</sub> linkage rupture for the unsymmetrical Me-TODGA. <sup>[152]</sup> .....	41
Figure 6-6:	Structures of the degradation products of Me-TODGA (1-9) and TODGA (I). <sup>[154]</sup> .....	42



## 8. References

1. <https://www.kernd.de/kernd-en/nuclear-power/npps-germany/>. (accessed 10.6.2021).
2. *Gesetz über die friedliche Nutzung der Kernenergie und zum Schutz gegen ihre Gefahren*; 1959.
3. *Gesetz zur geordneten Beendigung der Kernenergienutzung zur gewerblichen Erzeugung von Elektrizität*; 2002.
4. *Richtlinie 2011/70/EURATOM des Rates vom 19. Juli 2011 über einen Gemeinschaftsrahmen für die verantwortungsvolle und sichere Entsorgung abgebrannter Brennelemente und radioaktiver Abfälle*; 2011.
5. IAEA Joint Convention on the Safety of Spent Fuel Management and on the Safety of Radioactive Waste Management; INFCIRC/546; International Atomic Energy Agency; 24 December 1997; 1997.
6. Kommission Lagerung hoch radioaktiver Abfallstoffe Abschlussbericht der Kommission Lagerung hoch radioaktiver Abfallstoffe; 2016.
7. *Gesetz zur Suche und Auswahl eines Standortes für Wärme entwickelnde radioaktive Abfälle und zur Änderung anderer Gesetze (Standortauswahlgesetz, StandAG)*; 2013.
8. *Partitionierung und Transmutation nuklearer Abfälle, Chancen und Risiken in Forschung und Anwendung (acatech STUDIE)*. Herbert Utz Verlag: München, 2014.
9. Bourg, S.; Hill, C.; Caravaca, C.; Rhodes, C.; Ekberg, C.; Taylor, R.; Geist, A.; Modolo, G.; Cassayre, L.; Malmbeck, R.; Harrison, M.; de Angelis, G.; Espartero, A.; Bouvet, S.; Ouvrier, N. ACSEPT - Partitioning technologies and actinide science: Towards pilot facilities in Europe. Nucl. Eng. Des. **2011**, *241* (9), 3427-3435.
10. Bourg, S.; Geist, A.; Narbutt, J. SACSESS – the EURATOM FP7 project on actinide separation from spent nuclear fuels. Nukleonika **2015**, *60* (4 (Pt. II)), 809-814.
11. Geist, A.; Taylor, R.; Ekberg, C.; Guilbaud, P.; Modolo, G.; Bourg, S. The SACSESS Hydrometallurgy Domain — An Overview. Procedia Chem. **2016**, *21*, 218-222.
12. Bourg, S.; Adnet, J.; Geist, A.; Rhodes, C.; Hanson, B. GENIORS, a EU project on MOX fuel reprocessing in GEN IV systems, Proceedings of Management of Spent Fuel from Nuclear Power Reactors: Learning from the Past, Enabling the Future. Proceedings of an International Conference 2020.
13. Neumeier, S.; Deissmann, G.; Bosbach, D. Fachlicher Schlussbericht des BMBF Forschungsvorhabens "Verbundprojekt: Grundlegende Untersuchungen zur Immobilisierung Langlebiger Radionuklide mittels Einbau in Endlagerrelevante Keramiken (Conditioning)"; Forschungszentrum Jülich GmbH Institut für Energie- Und Klimaforschung - IEK-6: Nukleare Entsorgung Und Reaktorsicherheit; 2017.
14. Montel, J.-M. Minerals and design of new waste forms for conditioning nuclear waste. Comptes Rendus Geoscience **2011**, *343* (2), 230-236.

15. Bosbach, D.; Duro, L. Radiogeochemical aspects of nuclear waste disposal. Preface. *Journal of Contaminant Hydrology* **2008**, *102* (3-4), 173-173.
16. *BMWi, 7th Federal Energy Research Programme*; 2018.
17. Lyseid Authen, T.; Adnet, J.-M.; Bourg, S.; Carrott, M.; Ekberg, C.; Galán, H.; Geist, A.; Guilbaud, P.; Miguiditchian, M.; Modolo, G.; Rhodes, C.; Wilden, A.; Taylor, R. An overview of solvent extraction processes developed in Europe for advanced nuclear fuel recycling, Part 2 — homogeneous recycling. *Separation Science and Technology* **2022**, *57* (11), 1724-1744.
18. Geist, A.; Adnet, J.-M.; Bourg, S.; Ekberg, C.; Galán, H.; Guilbaud, P.; Miguiditchian, M.; Modolo, G.; Rhodes, C.; Taylor, R. An overview of solvent extraction processes developed in Europe for advanced nuclear fuel recycling, part 1 — heterogeneous recycling. *Separation Science and Technology* **2021**, *56* (11), 1866-1881.
19. Modolo, G.; Wilden, A.; Kaufholz, P.; Bosbach, D.; Geist, A. Development and demonstration of innovative partitioning processes (i-SANEX and 1-cycle SANEX) for actinide partitioning. *Progr. Nucl. Energ.* **2014**, *72*, 107-114.
20. McKibben, J.M. Chemistry of the PUREX process, Americal Chemical Society 135th National Meeting, Seattke, Washington, USA, 10 March 1983, 1983.
21. Birkett, J.E.; Carrott, M.J.; Fox, O.D.; Jones, C.J.; Maher, C.J.; Roube, C.V.; Taylor, R.J.; Woodhead, D.A. Recent Developments in the PUREX Process for Nuclear Fuel Reprocessing: Complexant Based Stripping for Uranium/Plutonium Separation. *Chimia* **2005**, *59* (12), 898-904.
22. Courson, O.; Lebrun, M.; Malmbeck, R.; Pagliosa, G.; Romer, K.; Satmark, B.; Glatz, J.P. Partitioning of minor actinides from HLLW using the DIAMEX process. Part 1 - Demonstration of extraction performances and hydraulic behaviour of the solvent in a continuous process. *Radiochim. Acta* **2000**, *88* (12), 857-863.
23. Malmbeck, R.; Courson, O.; Pagliosa, G.; Romer, K.; Satmark, B.; Glatz, J.P.; Baron, P. Partitioning of minor actinides from HLLW using the DIAMEX process. Part 2 - "Hot" continuous counter-current experiment. *Radiochim. Acta* **2000**, *88* (12), 865-871.
24. Modolo, G.; Wilden, A.; Daniels, H.; Geist, A.; Magnusson, D.; Malmbeck, R. Development and Demonstration of a new SANEX Partitioning Process for Selective Actinide(III)/Lanthanide(III) Separation using a mixture of CyMe<sub>4</sub>BTBP and TODGA. *Radiochim. Acta* **2013**, *101* (3), 155-162.
25. Geist, A.; Hill, C.; Modolo, G.; Foreman, M.R.S.J.; Weigl, M.; Gompfer, K.; Hudson, M.J.; Madic, C. 6,6'-Bis(5,5,8,8-tetramethyl-5,6,7,8-tetrahydro-benzo[1,2,4]triazin-3-yl)[2,2']bipyridine, an effective extracting agent for the separation of americium(III) and curium(III) from the lanthanides. *Solvent Extr. Ion Exch.* **2006**, *24* (4), 463-483.
26. Magnusson, D.; Christiansen, B.; Foreman, M.R.S.; Geist, A.; Glatz, J.P.; Malmbeck, R.; Modolo, G.; Serrano-Purroy, D.; Sorel, C. Demonstration of a SANEX Process in Centrifugal Contactors using the CyMe<sub>4</sub>-BTBP Molecule on a Genuine Fuel Solution. *Solvent Extr. Ion Exch.* **2009**, *27* (2), 97-106.

27. Modolo, G.; Kluxen, P.; Geist, A. Demonstration of the LUCA process for the separation of americium(III) from curium(III), californium(III), and lanthanides(III) in acidic solution using a synergistic mixture of bis(chlorophenyl)dithiophosphinic acid and tris(2-ethylhexyl)phosphate. *Radiochim. Acta* **2010**, 98 (4), 193-201.
28. OECD Trends towards Sustainability in the Nuclear Fuel Cycle - Executive Summary; OECD, Nuclear Energy Agency (NEA); 2011.
29. Senentz, G.; Drain, F.; Baganz, C. COEX Recycling Plant: A New Standard For An Integrated Plant, GLOBAL, Paris, 2009, p. 62-65.
30. H.Takano; T.Ikegami, *Activities on R&D of Partitioning and Transmutation in Japan*. OECD Nuclear Energy Agency: Issy-les-Moulineaux, France, 2003; Vol. NEA No. 4454, p 23.
31. Modolo, G.; Odoj, R. Method for separating trivalent americium from trivalent curium. European Patent EP1664359B1, 03.01.2007.
32. Rostaing, C.; Poinssot, C.; Warin, D.; Baron, P.; Lorrain, B. Development and Validation of the EXAm Separation Process for Single Am Recycling. *Procedia Chem.* **2012**, 7, 367-373.
33. Vanel, V.; Berthon, L.; Muller, J.; Miguiditchian, M.; Burdet, F. Modelling of americium stripping in EXAm process, ATALANTE2012, Montpellier, France, 02-07 September, 2012.
34. Wilden, A.; Modolo, G.; Sypula, M.; Geist, A.; Magnusson, D. The Recovery of An(III) in an innovative-SANEX process using a TODGA-based solvent and selective stripping with a hydrophilic BTP. *Proc. Chem.* **2012**, 7, 418-424.
35. Magnusson, D.; Geist, A.; Malmbeck, R.; Modolo, G.; Wilden, A. Flow-sheet design for an innovative SANEX process using TODGA and SO<sub>3</sub>-Ph-BTP. *Proc. Chem.* **2012**, 7, 245-250.
36. Sypula, M. Innovative SANEX process for trivalent actinides separation from PUREX raffinate. Dissertation, RWTH Aachen, 2013.
37. Wilden, A.; Modolo, G.; Kaufholz, P.; Sadowski, F.; Lange, S.; Sypula, M.; Magnusson, D.; Müllich, U.; Geist, A.; Bosbach, D. Laboratory-Scale Counter-Current Centrifugal Contactor Demonstration of an Innovative-SANEX Process Using a Water Soluble BTP. *Solvent Extr. Ion Exch.* **2015**, 33 (2), 91-108.
38. Wilden, A.; Schreinemachers, C.; Sypula, M.; Modolo, G. Direct Selective Extraction of Actinides (III) from PUREX Raffinate using a Mixture of CyMe<sub>4</sub>BTBP and TODGA as 1-cycle SANEX Solvent. *Solvent Extr. Ion Exch.* **2011**, 29 (2), 190-212.
39. Magnusson, D.; Geist, A.; Wilden, A.; Modolo, G. Direct Selective Extraction of Actinides (III) from PUREX Raffinate using a Mixture of CyMe<sub>4</sub>-BTBP and TODGA as 1-cycle SANEX Solvent Part II: Flow-sheet Design for a Counter-Current Centrifugal Contactor Demonstration Process. *Solvent Extr. Ion Exch.* **2013**, 31 (1), 1-11.
40. Wilden, A.; Modolo, G.; Schreinemachers, C.; Sadowski, F.; Lange, S.; Sypula, M.; Magnusson, D.; Geist, A.; Lewis, F.W.; Harwood, L.M.; Hudson, M.J. Direct Selective Extraction of Actinides (III) from PUREX Raffinate using a Mixture of CyMe<sub>4</sub>BTBP and TODGA as 1-cycle



SANEX Solvent Part III: Demonstration of a Laboratory-scale Counter-Current Centrifugal Contactor Process. *Solvent Extr. Ion Exch.* **2013**, *31* (5), 519-537.

41. Miguiditchian, M.; Chareyre, L.; Heres, X.; Hill, C.; Baron, P.; Masson, M. GANEX: Adaptation of the DIAMEX-SANEX process for the group actinide separation, Proceedings of Global 2007: Advanced Nuclear Fuel Cycles and Systems 2007, Boise, ID, United States, 9-13 September 2007, pp 550-552.
42. Adnet, J.-M.; Miguiditchian, M.; Hill, C.; Heres, X.; Lecomte, M.; Masson, M.; Brossard, P.; Baron, P. Development of New Hydrometallurgical Processes for Actinide Recovery: GANEX concept., Proceedings of GLOBAL 2005, Tsukuba, Japan, 9.-13.10.2005.
43. Miguiditchian, M.; Sorel, C.; Camès, B.; Bisel, I.; Baron, P.; Espinoux, D.; Calor, J.-N.; Viallesoubranne, C.; Lorrain, B.; Masson, M. HA demonstration in the Atalante facility of the GANEX 1<sup>st</sup> cycle for the selective extraction of Uranium from HLW, Proceedings of GLOBAL 2009, Paris, France, pp 1032-1035.
44. Miguiditchian, M.; Roussel, H.; Chareyre, L.; Baron, P.; Espinoux, D.; Calor, J.-N.; Viallesoubranne, C.; Lorrain, B.; Masson, M. HA demonstration in the Atalante facility of the GANEX 2<sup>nd</sup> cycle for the grouped TRU extraction, Proceedings of GLOBAL 2009, Paris, France, pp 1036-1040.
45. Vértes, A.; Nagy, S.; Klencsár, Z.; Lovas, R.G.; (Eds.), F.R. Handbook of Nuclear Chemistry. Chap. 23 Radiation Chemistry Springer Science+Business Media B.V. 2011: Dordrecht Heidelberg London New York, pp 1265-1332, **2011**.
46. Mincher, B.J. An overview of selected radiation chemical reactions affecting fuel cycle solvent extraction. *ACS Symp. Ser.* **2010**, *1046* (Nuclear Energy and the Environment), 181-192.
47. Katsumura, Y.; Jiang, P.Y.; Nagaishi, R.; Oishi, T.; Ishigure, K.; Yoshida, Y. Pulse radiolysis study of aqueous nitric acid solutions: formation mechanism, yield, and reactivity of NO<sub>3</sub> radical. *J. Phys. Chem.* **1991**, *95* (11), 4435-4439.
48. Spinks, J.W.T.; Woods, R.J., *An Introduction to radiation chemistry*. 3rd ed. ed.; Wiley: New York, 1990.
49. Buxton, G.V.; Greenstock, C.L.; Helman, W.P.; Ross, A.B. Critical Review of Rate Constants for Reactions of Hydrated Electrons, Hydrogen Atoms and Hydroxyl Radicals ( $\cdot\text{OH}/\text{O}\cdot$ ) in Aqueous Solution. *J. Phys. Chem. Ref. Data* **1988**, *17* (2), 513-886.
50. Jiang, P.Y.; Katsumura, Y.; Ishigure, K.; Yoshida, Y. Reduction Potential of the Nitrate Radical In Aqueous-Solution. *Inorg. Chem.* **1992**, *31* (24), 5135-5136.
51. Mincher, B.J.; Modolo, G.; Mezyk, S.P. Review Article: The Effects of Radiation Chemistry on Solvent Extraction: 1. Conditions in Acidic Solution and a Review of TBP Radiolysis. *Solvent Extr. Ion Exch.* **2009**, *27* (1), 1-25.
52. Mincher, B.J.; Modolo, G.; Mezyk, S.P. Review Article: The Effects of Radiation Chemistry on Solvent Extraction: 2. A Review of Fission-Product Extraction. *Solvent Extr. Ion Exch.* **2009**, *27* (3), 331-353.

53. Mincher, B.J.; Modolo, G.; Mezyk, S.P. Review Article: The Effects of Radiation Chemistry on Solvent Extraction 3: A Review of Actinide and Lanthanide Extraction. *Solvent Extr. Ion Exch.* **2009**, *27* (5&6), 579-606.
54. Mincher, B.J.; Modolo, G.; Mezyk, S.P. Review: The Effects of Radiation Chemistry on Solvent Extraction 4: Separation of the Trivalent Actinides and Considerations for Radiation-Resistant Solvent Systems. *Solvent Extr. Ion Exch.* **2010**, *28* (4), 415 - 436.
55. Mincher, B.J. 5.15 - Degradation Issues in Aqueous Reprocessing Systems. in *Comprehensive Nuclear Materials*, Konings, R.J.M., Elsevier: Oxford, pp 367-388, **2012**.
56. Elliot, A.J. A pulse radiolysis study of the temperature dependence of reactions involving H, OH and e-aq in aqueous solutions. *International Journal of Radiation Applications and Instrumentation. Part C. Radiation Physics and Chemistry* **1989**, *34* (5), 753-758.
57. Gordon, S.; Hart, E.J.; Thomas, J.K. The Ultraviolet Spectra of Transients Produced in the Radiolysis of Aqueous Solutions1. *The Journal of Physical Chemistry* **1964**, *68* (5), 1262-1264.
58. Bielski, B.H.J.; Cabelli, D.E.; Arudi, R.L.; Ross, A.B. Reactivity of HO<sub>2</sub>/O<sub>2</sub><sup>-</sup> Radicals in Aqueous Solution. *Journal of Physical and Chemical Reference Data* **1985**, *14* (4), 1041-1100.
59. *Reactivity of the Hydroxyl Radical in Aqueous Solutions*; Report of the United States National Bureau of Standards 46, National Bureau of Standards: Washington DC; 1973.
60. Katsumura, Y. NO<sub>2</sub> and NO<sub>3</sub> Radicals in the Radiolysis of Nitric Acid Solutions. Chap. 12 in *The Chemistry of Free Radicals: N-Centered Radicals*, Alfassi, Z.B., John Wiley & Sons: Chichester, pp 393-412, **1998**.
61. Neta, P.; Huie, R.E. Rate constants for reactions of nitrogen oxide (NO<sub>3</sub>) radicals in aqueous solutions. *The Journal of Physical Chemistry* **1986**, *90* (19), 4644-4648.
62. Shastri, L.; Huie, R.E. Rate constants for hydrogen abstraction reactions of NO<sub>3</sub> in aqueous solution. *International journal of chemical kinetics* **1990**, *22* (5), 505-512.
63. Neta, P.; Huie, R.E.; Ross, A.B. Rate Constants for Reactions of Inorganic Radicals in Aqueous Solution. *Journal of Physical and Chemical Reference Data* **1988**, *17* (3), 1027-1284.
64. Grätzel, M.; Henglein, A.; Taniguchi, S. Pulsradiolytische Beobachtungen über die Reduktion des NO<sub>3</sub><sup>-</sup>-Ions und über Bildung und Zerfall der persalpetrigen Säure in wäßriger Lösung. *Berichte der Bunsengesellschaft für physikalische Chemie* **1970**, *74* (3), 292-298.
65. Logager, T.; Sehested, K. Formation and Decay of Peroxynitrous Acid - A Pulse-Radiolysis Study. *J. Phys. Chem.* **1993**, *97* (25), 6664-6669.
66. Olah, G.A.; Lin, H.C.; Olah, J.A.; Narang, S.C. Electrophilic and free radical nitration of benzene and toluene with various nitrating agents. *Proceedings of the National Academy of Sciences* **1978**, *75* (3), 1045-1049.
67. Dzengel, J.; Theurich, J.; Bahnemann, D.W. Formation of nitroaromatic compounds in advanced oxidation processes: photolysis versus photocatalysis. *Environmental science & technology* **1999**, *33* (2), 294-300.

68. Ershov, B.G.; Gordeev, A.V.; Bykov, G.L.; Zubkov, A.A.; Kosareva, I.M. Synthesis of nitromethane from acetic acid by radiation-induced nitration in aqueous solution. *Mendeleev Communications* **2007**, *17* (5), 289-290.
69. Sworski, T.; Matthews, R.; Mahlman, H. Radiation chemistry of concentrated NaNO<sub>3</sub> solutions: Dependence of G (HNO<sub>2</sub>) on NaNO<sub>3</sub> concentration. *Adv. Chem. Ser.* **1968**, *82*, 164-181.
70. Nagaishi, R.; Jiang, P.-Y.; Katsumura, Y.; Ishigure, K. Primary yields of water radiolysis in concentrated nitric acid solutions. *Journal of the Chemical Society, Faraday Transactions* **1994**, *90* (4), 591-595.
71. Daniels, M. Radiolysis and photolysis of the aqueous nitrate system. *Adv. Chem. Ser.* **1968**, *82*, 153-163.
72. Lammel, G.; Perner, D.; Warneck, P. Decomposition of pernitric acid in aqueous solution. *Journal of Physical Chemistry* **1990**, *94* (15), 6141-6144.
73. Grätzel, M.; Henglein, A.; Lilie, J.; Beck, G. Pulsradiolytische untersuchung einiger elementarprozesse der oxydation und reduktion des nitritions. *Berichte der Bunsengesellschaft für physikalische Chemie* **1969**, *73* (7), 646-653.
74. Ridd, J.H. Some unconventional pathways in aromatic nitration. *Acta Chemica Scandinavica* **1998**, *52* (1), 11-22.
75. Turney, T.; Wright, G. Nitrous acid and nitrosation. *Chemical Reviews* **1959**, *59* (3), 497-513.
76. Vione, D.; Maurino, V.; Minero, C.; Borghesi, D.; Lucchiari, M.; Pelizzetti, E. New processes in the environmental chemistry of nitrite. 2. The role of hydrogen peroxide. *Environmental science & technology* **2003**, *37* (20), 4635-4641.
77. Bhattacharyya, P.K.; Veeraraghavan, R. Reaction between nitrous acid and hydrogen peroxide in perchloric acid medium. *International Journal of Chemical Kinetics* **1977**, *9* (4), 629-640.
78. Bishop, W.P.; Firestone, R.F. Radiolysis of liquid n-pentane. *The Journal of Physical Chemistry* **1970**, *74* (11), 2274-2284.
79. Alfassi, Z.B., *The Chemistry of Free Radicals: Peroxyl Radicals*. Wiley: New York, 1997.
80. Nilsson, M.; Andersson, S.; Ekberg, C.; Foreman, M.R.S.; Hudson, M.J.; Skarnemark, G. Inhibiting radiolysis of BTP molecules by addition of nitrobenzene. *Radiochim. Acta* **2006**, *94* (2), 103-106.
81. Mincher, B.J.; Arbon, R.E.; Knighton, W.B.; Meikrantz, D.H. Gamma-ray-induced degradation of PCBs in neutral isopropanol using spent reactor-fuel. *Appl. Radiat. Isot.* **1994**, *45* (8), 879-887.
82. Freeman, G.R. Radiolysis of Alcohols. *Actions Chim. Biol. Radiat.* **1970**, *14*, 73-134.
83. Symons, M.C.R.; Eastland, G.W. Radiation Mechanisms. Part 18. The Radiolysis of Alcohols: an Electron Spin Resonance Study. *J. Chem. Research (S)* **1977**, 254-255.
84. Yu, C.H.; Zhang, J.W.; Dai, J.; Peng, J.; Li, J.Q.; Zhai, M.L. Radiation Stability and Analysis of Radiolysis Product of 1-Octanol. *Acta Phys.-Chim. Sin.* **2010**, *26* (4), 988-992.

85. Madic, C.; Hudson, M.J. High-Level Liquid Waste Partitioning by Means of Completely Incinerable Extractants; EUR 18038 EN; European Commission; Luxembourg; 1998.
86. Schmidt, H.; Wilden, A.; Modolo, G.; Švehla, J.; Grüner, B.; Ekberg, C. Gamma radiolytic stability of CyMe<sub>4</sub>BTBP and effect of nitric acid. *Nukleonika* **2015**, *60* (4 (Pt. II)), 879-884.
87. Schmidt, H.; Wilden, A.; Modolo, G.; Bosbach, D.; Santiago-Schübel, B.; Hupert, M.; Švehla, J.; Grüner, B.; Ekberg, C. Gamma Radiolysis of the Highly Selective Ligands CyMe<sub>4</sub>BTBP and CyMe<sub>4</sub>BTPPhen: Qualitative and Quantitative Investigation of Radiolysis Products. *Procedia Chem.* **2016**, *21*, 32-37.
88. Koubský, T.; Schmidt, H.; Modolo, G.; Kalvoda, L. Simulation of UV/Vis Spectra of CyMe<sub>4</sub>BTBP and Some of its Degradation Products. *Procedia Chem.* **2016**, *21*, 509-516.
89. Szreder, T.; Kocia, R.; Schmidt, H.; Modolo, G. Selected Aspects of the SANEX System Radiation Chemistry, 13th DAE-BRNS Biennial Trombay Symposium on Radiation & Photochemistry (TSRP-2016) incorporating 6th Asia Pacific Symposium on Radiation Chemistry (APSRC-2016), TSRP - APSRC - 2016, Mumbai, India, 5 - 9 January, 2016.
90. Schmidt, H.; Wilden, A.; Modolo, G.; Bosbach, D.; Santiago-Schübel, B.; Hupert, M.; Mincher, B.J.; Mezyk, S.P.; Švehla, J.; Grüner, B. Gamma and pulsed electron radiolysis studies of CyMe<sub>4</sub>BTBP and CyMe<sub>4</sub>BTPPhen: Identification of radiolysis products and effects on the hydrometallurgical separation of trivalent actinides and lanthanides. *Radiation Physics and Chemistry* **2021**, *189*, 109696.
91. Ekberg, C.; Fermvik, A.; Retegan, T.; Skarnemark, G.; Foreman, M.R.S.; Hudson, M.J.; Englund, S.; Nilsson, M. An overview and historical look back at the solvent extraction using nitrogen donor ligands to extract and separate An(III) from Ln(III). *Radiochim. Acta* **2008**, *96* (4-5 EUROPART), 225-233.
92. Case, F.H. Preparation of 2,4-Bis-Triazinyl and 2,6-Bis-Triazinyl and Triazoliny Derivatives of Pyridine. *J. Heterocycl. Chem.* **1971**, *8* (6), 1043-1046.
93. Kolarik, Z.; Mullich, U.; Gassner, F. Selective extraction of Am(III) over Eu(III) by 2,6-ditriazolyl- and 2,6-ditriazinylpyridines. *Solvent Extr. Ion Exch.* **1999**, *17* (1), 23-32.
94. Denecke, M.A.; Rossberg, A.; Panak, P.J.; Weigl, M.; Schimmelpfennig, B.; Geist, A. Characterization and comparison of Cm(III) and Eu(III) complexed with 2,6-di(5,6-dipropyl-1,2,4-triazin-3-yl)pyridine using EXAFS, TRFLS, and quantum-chemical methods. *Inorg. Chem.* **2005**, *44* (23), 8418-8425.
95. Weigl, M.; Geist, A.; Müllich, U.; Gompfer, K. Kinetics of Americium(III) Extraction and Back Extraction with BTP. *Solvent Extraction and Ion Exchange* **2006**, *24* (6), 845-860.
96. Iveson, P.B.; Rivière, C.; Guillauneux, D.; Nierlich, M.; Thuéry, P.; Ephritikhine, M.; Madic, C. Selective complexation of uranium(III) over cerium(III) by 2,6-bis(5,6-dialkyl-1,2,4-triazin-3-yl)pyridines: 1H NMR and X-ray crystallography studies. *Chemical Communications* **2001**, (16), 1512-1513.
97. Berthet, J.-C.; Miquel, Y.; Iveson, P.B.; Nierlich, M.; Thuery, P.; Madic, C.; Ephritikhine, M. The affinity and selectivity of terdentate nitrogen ligands towards trivalent lanthanide and

- uranium ions viewed from the crystal structures of the 1 [ratio] 3 complexes. *J. Chem. Soc, Dalton Trans.* **2002**, (16), 3265-3272.
98. Hudson, M.J.; Boucher, C.E.; Braekers, D.; Desreux, J.F.; Drew, M.G.B.; Foreman, M.R.S.J.; Harwood, L.M.; Hill, C.; Madic, C.; Marken, F.; Youngs, T.G.A. New bis(triazinyl) pyridines for selective extraction of americium(III). *New J. Chem.* **2006**, *30* (8), 1171-1183.
  99. Madic, C.; Hudson, M.J.; Liljenzin, J.-O.; Glatz, J.-P.; Nannicini, R.; Facchini, A.; Kolarik, Z.; Odoj, R. Recent achievements in the development of partitioning processes of minor actinides from nuclear wastes obtained in the frame of the NEWPART European programme (1996-1999). *Prog. Nucl. Energy* **2002**, *40* (3-4), 523-526.
  100. Hill, C.; Guillaneux, D.; Berthon, L.; Madic, C. SANEX-BTP process development studies. *J. Nucl. Sci. Technol.* **2002**, (Suppl. 3), 309-312.
  101. Hill, C.; Berthon, L.; Madic, C. Study of the stability of BTP extractants under radiolysis, *Proceedings of GLOBAL 2005*, Tsukuba, Japan, 9-13 October, p 283.
  102. Spjuth, L. Solvent extraction studies with substituted malonamides and oligopyridines. Influence of structure and chemical properties on the extraction ability of trivalent actinides and lanthanides. Chalmers Univ. of Technology, Goeteborg (Sweden); Chalmers Univ. of Technology, Goeteborg (Sweden). Dept. of Nuclear Chemistry, 1999.
  103. Lewis, F.W.; Harwood, L.M.; Hudson, M.J.; Drew, M.G.B.; Wilden, A.; Sypula, M.; Modolo, G.; Vu, T.-H.; Simonin, J.-P.; Vidick, G.; Bouslimani, N.; Desreux, J.F. From BTBPs to BTPHens: The Effect of Ligand Pre-Organization on the Extraction Properties of Quadridentate Bis-Triazine Ligands. *Proc. Chem.* **2012**, *7*, 231-238.
  104. Lewis, F.W.; Harwood, L.M.; Hudson, M.J.; Drew, M.G.B.; Hubscher-Bruder, V.; Videva, V.; Arnaud-Neu, F.; Stamberg, K.; Vyas, S. BTBPs versus BTPHens: Some Reasons for Their Differences in Properties Concerning the Partitioning of Minor Actinides and the Advantages of BTPHens. *Inorg. Chem.* **2013**, *52* (9), 4993-5005.
  105. Sammes, P.G.; Yahioğlu, G. 1,10-Phenanthroline: a versatile ligand. *Chem. Soc. Rev.* **1994**, *23* (5), 327-334.
  106. Bencini, A.; Lippolis, V. 1,10-Phenanthroline: A versatile building block for the construction of ligands for various purposes. *Coord. Chem. Rev.* **2010**, *254* (17-18), 2096-2180.
  107. Lewis, F.W.; Harwood, L.M.; Hudson, M.J.; Drew, M.G.B.; Desreux, J.F.; Vidick, G.; Bouslimani, N.; Modolo, G.; Wilden, A.; Sypula, M.; Vu, T.-H.; Simonin, J.-P. Highly Efficient Separation of Actinides from Lanthanides by a Phenanthroline-Derived Bis-triazine Ligand. *J. Am. Chem. Soc.* **2011**, *133* (33), 13093-13102.
  108. Retegan, T.; Drew, M.; Ekberg, C.; Engdahl, E.L.; Hudson, M.J.; Fermvik, A.; Foreman, M.R.S.; Modolo, G.; Geist, A. Synthesis and Screening of t-Bu-CyMe<sub>4</sub>-BTBP, and Comparison with CyMe<sub>4</sub>-BTBP. *Solvent Extr. Ion Exch.* **2014**, DOI: 10.1080/07366299.07362014.07940767.
  109. Foreman, M.R.S.J.; Hudson, M.J.; Geist, A.; Madic, C.; Weigl, M. An investigation into the extraction of americium(III), lanthanides and D-block metals by 6,6'-bis-(5,6-dipentyl-1,2,4-triazin-3-yl)-2,2'-bipyridinyl (C-5-BTBP). *Solvent Extr. Ion Exch.* **2005**, *23* (5), 645-662.

110. Nilsson, M.; Ekberg, C.; Foreman, M.; Hudson, M.; Liljenzin, J.-O.; Modolo, G.; Skarnemark, G. Separation of actinides(III) from lanthanides(III) in simulated nuclear waste streams using 6,6'-bis-(5,6-dipentyl[1,2,4]triazin-3-yl)[2,2']bipyridinyl (C5-BTBP) in cyclohexanone. *Solvent Extr. Ion Exch.* **2006**, *24* (6), 823-843.
111. Retegan, T.; Berthon, L.; Ekberg, C.; Fermvik, A.; Skarnemark, G.; Zorz, N. Electrospray Ionization Mass Spectrometry Investigation of BTBP - Lanthanide(III) and Actinide(III) Complexes *Solvent Extr. Ion Exch.* **2009**, *27* (5&6), 663-682.
112. Vu, T.-H. Etude par spectrométrie de fluorescence de la solvation et de la complexation des ions Eu (III) et Cm (III) en milieu octanol et à l'interface avec l'eau. PhD thesis, Strasbourg 1, 2008.
113. Trumm, S.; Lieser, G.; Foreman, M.; Panak, P.J.; Geist, A.; Fanghanel, T. A TRLFS study on the complexation of Cm(III) and Eu(III) with 4-*t*-butyl-6,6'-bis-(5,6-diethyl-1,2,4-triazin-3-yl)-2,2'-bipyridine in a water/2-propanol mixture. *Dalton Trans.* **2010**, *39* (3), 923-929.
114. Steppert, M.; Cisarova, I.; Fanghanel, T.; Geist, A.; Lindqvist-Reis, P.; Panak, P.; Stepnicka, P.; Trumm, S.; Walther, C. Complexation of Europium(III) by Bis(dialkyltriazinyl)bipyridines in 1-Octanol. *Inorg. Chem.* **2012**, *51* (1), 591-600.
115. Whittaker, D.M.; Griffiths, T.L.; Helliwell, M.; Swinburne, A.N.; Natrajan, L.S.; Lewis, F.W.; Harwood, L.M.; Parry, S.A.; Sharrad, C.A. Lanthanide Speciation in Potential SANEX and GANEX Actinide/Lanthanide Separations Using Tetra-N-Donor Extractants. *Inorg. Chem.* **2013**, *52* (7), 3429-3444.
116. Bremer, A.; Whittaker, D.M.; Sharrad, C.A.; Geist, A.; Panak, P.J. Complexation of Cm(III) and Eu(III) with CyMe<sub>4</sub>-BTPhen and CyMe<sub>4</sub>-BTBP studied by time resolved laser fluorescence spectroscopy. *Dalton Trans.* **2014**, *43* (6), 2684-2694.
117. Foreman, M.R.S.; Hudson, M.J.; Drew, M.G.B.; Hill, C.; Madic, C. Complexes formed between the quadridentate, heterocyclic molecules 6,6'-bis-(5,6-dialkyl-1,2,4-triazin-3-yl)-2,2'-bipyridine (BTBP) and lanthanides(III): implications for the partitioning of actinides(III) and lanthanides(III). *Dalton Trans.* **2006**, (13), 1645-1653.
118. Drew, M.G.B.; Foreman, M.R.S.J.; Hill, C.; Hudson, M.J.; Madic, C. 6,6'-bis-(5,6-diethyl-[1,2,4]triazin-3-yl)-2,2'-bipyridyl the first example of a new class of quadridentate heterocyclic extraction reagents for the separation of americium(III) and europium(III). *Inorganic Chemistry Communications* **2005**, *8* (3), 239-241.
119. Lundberg, D.; Persson, I.; Ekberg, C. Crystal structure of [Eu (CyMe 4-BTBP) 2 κ 2 O, O'-(NO 3)](NO 3) 2 · n-C 8 H 17 OH and its structure in 1-octanol solution. *Dalton Transactions* **2013**, *42* (11), 3767-3770.
120. Löfström-Engdahl, E.; Aneheim, E.; Ekberg, C.; Foreman, M.; Hallerod, J.; Skarnemark, G. Extraction thermodynamics of Am(III) and Eu(III) using CyMe<sub>4</sub>-BTBP in various organic diluents. *J. Chem. Thermodyn.* **2014**, *76*, 64-69.
121. Andersson, S.; Ekberg, C.; Fermvik, A.; Liljenzin, J.; Magnusson, D.; Meridiano, Y.; Nilsson, M.; Retegan, T.; Skarnemark, G. Partitioning and Transmutation Annual Report; R-06-45, Swedish Nuclear Fuel and Waste Management Co., Stockholm; 2005.

122. Ekberg, C.; Löfstrom-Engdahl, E.; Aneheim, E.; Foreman, M.R.S.; Geist, A.; Lundberg, D.; Denecke, M.; Persson, I. The structures of CyMe<sub>4</sub>-BTBP complexes of americium(III) and europium(III) in solvents used in solvent extraction, explaining their separation properties. *Dalton Trans.* **2015**, DOI:10.1039/C5DT02859K.
123. Foreman, M.R.S.J.; Hudson, M.J.; Geist, A.; Madic, C.; Weigl, M. An Investigation into the Extraction of Americium(III), Lanthanides and D-Block Metals by 6,6'-Bis-(5,6-dipentyl-[1,2,4]triazin-3-yl)-[2,2']bipyridinyl (C5-BTBP). *Solvent Extr. Ion Exch.* **2005**, 23 (5), 645-662.
124. Nilsson, M.; Andersson, S.; Drouet, F.; Ekberg, C.; Foreman, M.; Hudson, M.; Liljenzin, J.-O.; Magnusson, D.; Skarnemark, G. Extraction Properties of 6,6'-Bis-(5,6-dipentyl-[1,2,4]triazin-3-yl)-[2,2']bipyridinyl (C5-BTBP). *Solvent Extr. Ion Exch.* **2006**, 24 (3), 299-318.
125. Retegan, T.; Ekberg, C.; Englund, S.; Fermvik, A.; Foreman, M.R.S.; Skarnemark, G. The behaviour of organic solvents containing C5-BTBP and CyMe<sub>4</sub>-BTBP at low irradiation doses. *Radiochim. Acta* **2007**, 95 (11), 637-642.
126. Fermvik, A.; Berthon, L.; Ekberg, C.; Englund, S.; Retegan, T.; Zorz, N. Radiolysis of solvents containing C5-BTBP: identification of degradation products and their dependence on absorbed dose and dose rate. *Dalton Trans.* **2009**, (32), 6421-6430.
127. Fermvik, A.; Grun, B.; Kvíčalová, M.; Ekberg, C. Semi-quantitative and quantitative studies on the gamma radiolysis of C5-BTBP. *Radiochim. Acta* **2011**, 99 (2), 113-119.
128. Fermvik, A.; Aneheim, E.; Gruner, B.; Hájková, Z.; Kvicalová, M.; Ekberg, C. Radiolysis of C5-BTBP in cyclohexanone irradiated in the absence and presence of an aqueous phase. *Radiochim. Acta* **2012**, 100 (4), 243-253.
129. Wilden, A.; Modolo, G.; Hupert, M.; Santiago-Schübel, B.; Löfström-Engdahl, E.; Halleröd, J.; Ekberg, C.; Mincher, B.J.; Mezyk, S.P. Gamma-radiolytic stability of solvents containing C5-BPP (2,6-Bis(5-(2,2-dimethylpropyl)-1H-pyrazol-3-yl)pyridine) for actinide(III)/lanthanide(III) separation. *Solvent Extr. Ion Exch.* **2016**, 34 (1), 1-12.
130. Fermvik, A.; Nilsson, M.; Ekberg, C. Radiolytic Degradation of Heterocyclic Nitrogen Containing Ligands from Low Dose-Rate Gamma Sources. in *Nuclear Energy and the Environment*, Vol. 1046, Wai, C.M.; Mincher, B.J., American Chemical Society: Washington, pp 215-229, **2010**.
131. Fermvik, A.; Aneheim, E.; Löfstrom-Engdahl, E.; Ekberg, C.; Gruner, B.; Hajkova, Z. Degradation of CyMe<sub>4</sub>-BTBP, an extractant developed for reprocessing, under high dose rate irradiations. unpublished **2011**.
132. Mincher, B.J.; Mezyk, S.P.; Elias, G.; Groenewold, G.S.; Riddle, C.L.; Olson, L.G. The Radiation Chemistry of CMPO: Part 1. Gamma Radiolysis. *Solvent Extr. Ion Exch.* **2013**, 31 (7), 715-730.
133. Szreder, T.; Schmidt, H.; Modolo, G. Fast radiation-induced reactions in organic phase of SANEX system containing CyMe<sub>4</sub>-BTPhen extracting agent. *Rad. Phys. Chem.* **2019**, 164, 108356.

134. Sulich, A.; Grodkowski, J.; Mirkowski, J.; Kocia, R. Reactions of ligands from BT(B)P family with solvated electrons and benzophenone ketyl radicals in 1-octanol solutions. Pulse radiolysis study. *J. Radioanal. Nucl. Chem.* **2014**, *300* (1), 415-421.
135. Sasaki, Y.; Sugo, Y.; Suzuki, S.; Tachimori, S. The Novel Extractants, Diglycolamides, for the Extraction of Lanthanides and Actinides in HNO<sub>3</sub>-*n*-dodecane System. *Solvent Extr. Ion Exch.* **2001**, *19* (1), 91-103.
136. Magnusson, D.; Christiansen, B.; Glatz, J.-P.; Malmbeck, R.; Modolo, G.; Serrano-Purroy, D.; Sorel, C. Demonstration of a TODGA based Extraction Process for the Partitioning of Minor Actinides from a PUREX Raffinate Part III: Centrifugal Contactor Run using Genuine Fuel Solution. *Solvent Extr. Ion Exch.* **2009**, *27* (1), 26-35.
137. Modolo, G.; Wilden, A.; Geist, A.; Magnusson, D.; Malmbeck, R. A review of the demonstration of innovative solvent extraction processes for the recovery of trivalent minor actinides from PUREX raffinate. *Radiochim. Acta* **2012**, *100* (8-9), 715-725.
138. Brown, J.; McLachlan, F.; Sarsfield, M.J.; Taylor, R.J.; Modolo, G.; Wilden, A. Plutonium loading of prospective grouped actinide extraction (GANEX) solvent systems based on diglycolamide extractants. *Solvent Extr. Ion Exch.* **2012**, *30* (2), 127-141.
139. Carrott, M.; Bell, K.; Brown, J.; Geist, A.; Gregson, C.; Hères, X.; Maher, C.; Malmbeck, R.; Mason, C.; Modolo, G.; Müllich, U.; Sarsfield, M.; Wilden, A.; Taylor, R. Development of a New Flowsheet for Co-Separating the Transuranic Actinides: The “EURO-GANEX” Process. *Solvent Extr. Ion Exch.* **2014**, *32* (5), 447-467.
140. Modolo, G.; Asp, H.; Schreinemachers, C.; Vijgen, H. Development of a TODGA based Process for Partitioning of Actinides from a PUREX Raffinate Part I: Batch Extraction Optimization Studies and Stability Tests. *Solvent Extr. Ion Exch.* **2007**, *25* (6), 703-721.
141. Iqbal, M.; Huskens, J.; Verboom, W.; Sypula, M.; Modolo, G. Synthesis and Am/Eu Extraction of Novel TODGA Derivatives. *Supramol. Chem.* **2010**, *22* (11), 827-837.
142. Wilden, A.; Modolo, G.; Lange, S.; Sadowski, F.; Beele, B.B.; Skerencak-Frech, A.; Panak, P.J.; Iqbal, M.; Verboom, W.; Geist, A.; Bosbach, D. Modified Diglycolamides for the An(III) + Ln(III) Co-separation: Evaluation by Solvent Extraction and Time-Resolved Laser Fluorescence Spectroscopy. *Solvent Extr. Ion Exch.* **2014**, *32* (2), 119-137.
143. Sugo, Y.; Sasaki, Y.; Tachimori, S. Studies on hydrolysis and radiolysis of N,N,N',N'-tetraoctyl-3-oxapentane-1,5-diamide. *Radiochim. Acta* **2002**, *90* (3), 161-165.
144. Sharma, J.N.; Ruhela, R.; Singh, K.K.; Kumar, M.; Janardhanan, C.; Achutan, P.V.; Manohar, S.; Wattal, P.K.; Suri, A.K. Studies on hydrolysis and radiolysis of tetra(2-ethylhexyl)diglycolamide (TEHDGA)/isodecyl alcohol/*n*-dodecane solvent system. *Radiochim. Acta* **2010**, *98* (8), 485-491.
145. Sugo, Y.; Izumi, Y.; Yoshida, Y.; Nishijima, S.; Sasaki, Y.; Kimura, T.; Sekine, T.; Kudo, H. Influence of diluent on radiolysis of amides in organic solution. *Radiat. Phys. Chem.* **2007**, *76* (5), 794-800.



146. Galan, H.; Nunez, A.; Espartero, A.G.; Sedano, R.; Durana, A.; de Mendoza, J. Radiolytic Stability of TODGA: Characterization of Degraded Samples under Different Experimental Conditions. *Proc. Chem.* **2012**, *7*, 195-201.
147. Zarzana, C.A.; Groenewold, G.S.; Mincher, B.J.; Mezyk, S.P.; Wilden, A.; Schmidt, H.; Modolo, G.; Wishart, J.F.; Cook, A.R. A Comparison of the  $\gamma$ -Radiolysis of TODGA and T(EH)DGA Using UHPLC-ESI-MS Analysis. *Solvent Extr. Ion Exch.* **2015**, *33* (5), 431-447.
148. Gujar, R.; Ansari, S.; Murali, M.; Mohapatra, P.; Manchanda, V. Comparative evaluation of tetra-2-ethylhexyl diglycolamide (T2EHDGA) for actinide partitioning. *J. Radioanal. Nucl. Chem* **2010**, *284*, 377-385.
149. Galán, H.; Murillo, M.T.; Sedano, R.; Núñez, A.; de Mendoza, J.; González-Espartero, A.; Prados, P. Hydrolysis and radiation stability of m-Xylylene Bis-diglycolamide: Synthesis and quantitative study of degradation products by HPLC–APCI+. *European Journal of Organic Chemistry* **2011**, *2011* (20), 3959.
150. Ruhela, R.; Sharma, J.N.; Tomar, B.S.; Singh, K.K.; Kumar, M.; Bajaj, P.N.; Hubli, R.C.; Suri, A.K. Studies on hydrolytic and radiolytic stability of N,N,N',N'-tetra-(2-ethylhexyl) thiodiglycolamide T(2EH)TDGA. *Radiochim. Acta* **2011**.
151. Gujar, R.B.; Ansari, S.A.; Bhattacharyya, A.; Kanekar, A.S.; Pathak, P.N.; Mohapatra, P.K.; Manchanda, V.K. Radiolytic Stability of N,N,N',N'-Tetraoctyl Diglycolamide (TODGA) in the Presence of Phase Modifiers Dissolved in n-Dodecane. *Solvent Extr. Ion Exch.* **2012**, *30* (3), 278-290.
152. Kalvoda, L.; Luštinec, J.; Koubský, T. Ab-initio Evaluation of Acid Influence on Chemical Stability of Hydrophilic Diglycolamides. *Frontiers in Molecular Biosciences*, 1317.
153. Galán, H.; Zarzana, C.A.; Wilden, A.; Núñez, A.; Schmidt, H.; Egberink, R.J.M.; Leoncini, A.; Cobos, J.; Verboom, W.; Modolo, G.; Groenewold, G.S.; Mincher, B.J. Gamma-Radiolytic Stability of New Methylated TODGA Derivatives for Minor Actinide Recycling. *Dalton Trans.* **2015**, *44* (41), 18049-18056.
154. Roscioli-Johnson, K.M.; Zarzana, C.A.; Groenewold, G.S.; Mincher, B.J.; Wilden, A.; Schmidt, H.; Modolo, G.; Santiago- , B. A Study of the  $\gamma$ -Radiolysis of N,N-Didodecyl-N',N'-Dioctyldiglycolamide Using UHPLC-ESI-MS Analysis. *Solvent Extr. Ion Exch.* **2016**, *34* (5), 439-453.
155. Hubscher-Bruder, V.; Mogilireddy, V.; Michel, S.; Leoncini, A.; Huskens, J.; Verboom, W.; Galan, H.; Núñez, A.; Cobos Sabate, J.; Modolo, G.; Wilden, A.; Schmidt, H.; Charbonnel, M.-C.; Guilbaud, P.; Boubals, N. Behaviour of the Extractant Me-TODGA Upon Gamma Irradiation: Quantification of the Degradation Compounds and Individual Influences on Complexation and Extraction. *New J. Chem.* **2017**, *41*, 13700-13711.
156. Bjergbakke, E. The Ferrous-Cupric Dosimeter. in *Manual on Radiation Dosimetry*, Holm, N.W.; Berry, R.J., Marcel Dekker Inc.: New York, pp 319-321, **1970**.
157. Wishart, J.F.; Cook, A.R.; Miller, J.R. The LEAF picosecond pulse radiolysis facility at Brookhaven National Laboratory. *Review of scientific instruments* **2004**, *75* (11), 4359-4366.

158. Mezyk, S.P.; Mincher, B.J.; Dhiman, S.B.; Layne, B.; Wishart, J.F. The role of organic solvent radical cations in separations ligand degradation. *J. Radioanal. Nucl. Chem.* **2016**, *307* (3), 2445-2449.
159. Wilden, A.; Lumetta, G.J.; Sadowski, F.; Schmidt, H.; Schneider, D.; Gerdes, M.; Law, J.D.; Geist, A.; Bosbach, D.; Modolo, G. An Advanced TALSPEAK Concept for Separating Minor Actinides. Part 2. Flowsheet Test with Actinide-Spiked Simulant. *Solvent Extr. Ion Exch.* **2017**, *35* (6), 396-407.
160. Swallow, A.J. Radiation Chemistry of the Liquid State: (2) Organic Liquids. Chap. 11 in *Radiation Chemistry - Principles and Applications*, Farhataziz; Rodgers, M.A.J., VCH Verlagsgesellschaft mbH: Weinheim, Germany, pp 351-375, **1987**.
161. Lang, B.E. Solubility of Water in Octan-1-ol from (275 to 369) K. *Journal of Chemical & Engineering Data* **2012**, *57* (8), 2221-2226.
162. Woodhead, D.; McLachlan, F.; Taylor, R.; Müllich, U.; Geist, A.; Wilden, A.; Modolo, G. Nitric Acid Extraction into a TODGA Solvent Modified with Octanol. *Solvent Extr. Ion Exch.* **2019**, *37* (2), 173-190.
163. Horne, G.P.; Zarzana, C.A.; Rae, C.; Cook, A.R.; Mezyk, S.P.; Zalupski, P.R.; Wilden, A.; Mincher, B.J. Does addition of 1-octanol as a phase modifier provide radical scavenging radioprotection for N, N, N', N'-tetraoctyldiglycolamide (TODGA)? *Physical Chemistry Chemical Physics* **2020**, *22* (43), 24978-24985.
164. Lumetta, G.J.; Gelis, A.V.; Carter, J.C.; Niver, C.M.; Smoot, M.R. The Actinide-Lanthanide Separation Concept. *Solvent Extr. Ion Exch.* **2014**, *32* (4), 333-347.
165. Gelis, A.V.; Lumetta, G.J. Actinide Lanthanide Separation Process-ALSEP. *Ind. Eng. Chem. Res.* **2014**, *53* (4), 1624-1631.
166. Wilden, A.; Kreft, F.; Schneider, D.; Paparigas, Z.; Modolo, G.; Lumetta, G.J.; Gelis, A.V.; Law, J.D.; Geist, A. Countercurrent Actinide Lanthanide Separation Process (ALSEP) Demonstration Test with a Simulated PUREX Raffinate in Centrifugal Contactors on the Laboratory Scale. *Applied Sciences* **2020**, *10* (20), 7217.
167. Wilden, A.; Mincher, B.J.; Mezyk, S.P.; Twight, L.; Rosciolo-Johnson, K.M.; Zarzana, C.A.; Case, M.E.; Hupert, M.; Stärk, A.; Modolo, G. Radiolytic and Hydrolytic Degradation of the Hydrophilic Diglycolamides. *Solvent Extr. Ion Exch.* **2018**, *36* (4), 347-359.
168. Horne, G.P.; Wilden, A.; Mezyk, S.P.; Twight, L.; Hupert, M.; Stärk, A.; Verboom, W.; Mincher, B.J.; Modolo, G. Gamma radiolysis of hydrophilic diglycolamide ligands in concentrated aqueous nitrate solution. *Dalton Trans.* **2019**, *48*, 17005–17013.
169. Wilden, A.; Modolo, G.; Lange, S.; Sadowski, F.; Kardhashi, D.; Li, Y.; Kowalski, P.; Beele, B.B.; Skerencak-Frech, A.; Panak, P.J.; Geist, A.; Rothe, J.; Dardenne, K.; Schäfer, S.; Wagner, A.T.; Roesky, P.W.; Verboom, W. Complex Structure of An and Ln Complexes with Modified Diglycolamides in Solution and Solid State using Different Speciation Techniques. Chap. 5.4 in *Institute of Energy and Climate Research IEK-6: Nuclear Waste Management Report 2013 / 2014 - Material Science for Nuclear Waste Management*, Vol. 327, Neumeier, S.; Klinkenberg, M.; Bosbach, D., Forschungszentrum Jülich GmbH: Zentralbibliothek, 52425 Jülich, pp 60-64, **2016**.



## 9. Acknowledgements

Mein besonderer Dank gilt Prof. Dr. Dirk Bosbach, welcher mir als mein Doktorvater die vorliegende Arbeit am Institut für Energie- und Klimaforschung, Abteilung Nukleare Entsorgung und Reaktorsicherheit (IEK-6) des Forschungszentrum Jülich GmbH ermöglicht hat. Vielen Dank für die Betreuung und Unterstützung in meiner Zeit am IEK-6 aber auch nach meinem Ausscheiden aus dem Institut.

Mein herzlicher Dank gilt Prof. Dr. Giuseppe Modolo und Dr. Andreas Wilden. Ich danke euch von Herzen für eure Betreuung und unermüdliche Geduld insbesondere in der Zeit nach meinem Ausscheiden aus dem IEK-6. Danke, dass ihr die Hoffnung in mich nicht aufgegeben habt und mich bis zum Ende der Promotion unterstützt und immer wieder ermutigt habt!

Financial support for this work was provided by the European Atomic Energy Community's 7<sup>th</sup> Framework Program project SACSESS – grant agreement No. FP7-Fission-2012-323-282. I would like to thank all members of the consortium for the fruitful discussions and for being such a good team.

Prof. Dr. Christian Ekberg at the CHALMERS university, Gothenburg, Sweden, to host me several times for irradiation experiments. Thanks also to Dr. Jenny Halleröd and Dr. Elin Löfström-Engdahl for the support (in the lab as well as in the free time) in CHALMERS as well as during several project meetings.

Dr. Thomasz Szreder for hosting me in Warsaw for common pulse radiolysis experiments.

Special thanks to my colleagues Dr. Bruce Mincher and Dr. Steve Mezyk for hosting me at Idaho National Lab and Brookhaven National Lab for common experiments, fruitful discussions, a common trip to the Yellowstone National Park, barbecues, and your support during the final preparation of this thesis.

Thanks to all my co-authors of the several papers we could publish together. We were such good teams, even across borders and continents.

Herzlichen Dank an meine Kolleginnen Dr. Beatrix Santiago-Schüble und Michelle Hupert für die unzähligen HPLC-HRMS Messungen und die zahlreichen Diskussionen zur Datenanalyse.

Ich bedanke mich bei allen meinen IEK-6 - Kollegen für das gute Miteinander und die gemeinsame Zeit. Mein besonderer Dank gilt Dr. Elena Mühr-Ebert, Dr. Simone Weigelt, Larissa Klaß, Jaqueline Holthausen, Dr. Peter Kaufholz, Dr. Steve Lange, Fabian Kreft und Dimitri Schneider für die fantastischen Zeiten in denen wir uns in verschiedenen Konstellationen ein Büro geteilt und die Pausen gemeinsam verbracht haben, sowie für eure Freundschaft.

Herzlichen Dank an meine Familie und Freunde. Ihr musstet eine Menge Geduld haben und oft konnte ich eure Fragen „Was macht die Doktorarbeit?“ leider nicht zufriedenstellend beantworten. Danke für eure Geduld, Unterstützung und Liebe. Mama und Papa, ich danke euch, dass ihr mir mein Studium und letztlich meinen Abschluss durch eure Unterstützung und Förderung ermöglicht habt.



## 10. List of Papers

### Paper 1<sup>[86]</sup>

Schmidt, H.; Wilden, A.; Modolo, G.; Švehla, J.; Gr<sup>ner</sup>, B.; Ekberg, C. Gamma radiolytic stability of CyMe<sub>4</sub>BTBP and effect of nitric acid. *Nukleonika* **2015**, *60* (4 (Pt. II)), 879-884.

DOI: 10.1515/nuka-2015-0156

#### Contribution:

In this work, I did gamma-radiolysis experiments, solvent extraction, HPLC-MS product identification as well as leading authorship.

### Paper 2<sup>[87]</sup>

Schmidt, H.; Wilden, A.; Modolo, G.; Bosbach, D.; Santiago-<sup>el</sup>, B.; Hupert, M.; Švehla, J.; Gr<sup>ner</sup>, B.; Ekberg, C. Gamma radiolysis of the highly selective ligands CyMe<sub>4</sub>BTBP and CyMe<sub>4</sub>BTPPhen: Qualitative and quantitative investigation of radiolysis products. *Procedia Chem.* **2016**, *21*, 32-37.

DOI: 10.1016/j.proche.2016.10.005

#### Contribution:

This work is a continuation of paper #1. I did gamma-radiolysis experiments, solvent extraction, HPLC-MS product identification as well as leading authorship.

### Paper 3<sup>[88]</sup>

Koubský, T.; Schmidt, H.; Modolo, G.; Kalvoda, L. Simulation of UV/VIS Spectra of CyMe<sub>4</sub>BTBP and some of its degradation products. *Procedia Chem.* **2016**, *21*, 509-516.

DOI: 10.1016/j.proche.2016.10.071

#### Contribution:

For this paper, I did all experimental work. The simulation work was mainly done by the leading author of this paper.

### Paper 4<sup>[133]</sup>

Szreder, T.; Schmidt, H.; Modolo, G. Fast radiation-induced reactions in organic phase of SANEX system containing CyMe<sub>4</sub>BTPPhen extracting agent. *Rad. Phys. Chem.* **2019**, *164*, 108356.

DOI: 10.1016/j.radphyschem.2019.108356

#### Contribution:

For this work, the leading author and I conducted pulse radiolysis experiments on 1-octanol as well as on the CyMe<sub>4</sub>BTPPhen system, and interpretation of the results together. Additionally, I participated in manuscript preparation.

### **Paper 5<sup>[90]</sup>**

Schmidt, H.; Wilden, A.; Modolo, G.; Bosbach, D.; Santiago-Schübel, B.; Hupert, M.; Mincher, B.J.; Mezyk, S.P.; Švehla, J.; Grüner, B. Gamma and pulsed electron radiolysis studies of CyMe<sub>4</sub>BTBP and CyMe<sub>4</sub>BTPhen: Identification of radiolysis products and effects on the hydrometallurgical separation of trivalent actinides and lanthanides. *Radiation Physics and Chemistry* **2021**, *189*, 109696.

DOI: 10.1016/j.radphyschem.2021.109696

#### **Contribution:**

This paper is a continuation of papers #1 and #2. I was leading author and conducted irradiation experiments, solvent extraction, and interpretation of the HPLC-MS results.

### **Paper 6<sup>[153]</sup>**

Galán, H., Zarzana, C.A., Wilden, A., Núñez, A., Schmidt, H., Egberink, R.J.M., Leoncini, A., Cobos, J., Verboom, W., Modolo, G., Groenewold, G.S., Mincher, B.J. Gamma-Radiolytic Stability of New Methylated TODGA Derivatives for Minor Actinide Recycling. *Dalton Trans.* **2015**, *44* (41), 18049-18056. DOI: 10.1039/c5dt02484f

#### **Contribution:**

For this work, solvent extraction experiments, analysis (gamma-spectrometry, results of ICP-MS), as well as product identification of mass spectrometric experiments were conducted mainly by A. Wilden and me. Additionally, I participated in paper preparation.

### **Paper 7<sup>[147]</sup>**

Zarzana, C.A.; Groenewold, G.S.; Mincher, B.J.; Mezyk, S.P.; Wilden, A.; Schmidt, H.; Modolo, G.; Wishart, J.F.; Cook, A.R. A Comparison of the  $\gamma$ -Radiolysis of TODGA and T(EH)DGA Using UHPLC-ESI-MS Analysis. *Solvent Extr. Ion Exch.* **2015**, *33* (5), 431-447. DOI: 10.1080/07366299.2015.1012885

#### **Contribution:**

For this work, solvent extraction experiments analysis (gamma-spectrometry, results of ICP-MS), as well as product identification of mass spectrometric experiments were conducted mainly by A. Wilden and me. Additionally, I participated in paper preparation.

### **Paper 8<sup>[154]</sup>**

Roscioli-Johnson, K.M.; Zarzana, C.A.; Groenewold, G.S.; Mincher, B.J.; Wilden, A.; Schmidt, H.; Modolo, G.; Santiago-Schübel, B. A Study of the  $\gamma$ -Radiolysis of N,N-Didodecyl-N',N'-Dioctyldiglycolamide Using UHPLC-ESI-MS Analysis. *Solvent Extr. Ion Exch.* **2016**, *34* (5), 439-453.

DOI: 10.1080/07366299.2016.1212540

#### **Contribution:**

For this work, solvent extraction experiments, analysis (gamma-spectrometry, results of ICP-MS) as well as product identification of mass spectrometric experiments were conducted mainly by A. Wilden and me. Additionally, I participated in paper preparation.

**Paper 9<sup>[155]</sup>**

Hubscher-Bruder, V.; Mogilireddy, V.; Michel, S.; Leoncini, A.; Huskens, J.; Verboom, W.; Galan, H.; Núñez, A.; Cobos Sabate, J.; Modolo, G.; Wilden, A.; Schmidt, H.; Charbonnel, M.-C.; Guilbaud, P.; Boubals, N. Behaviour of the Extractant Me-TODGA Upon Gamma Irradiation: Quantification of the Degradation Compounds and Individual Influences on Complexation and Extraction. *New J. Chem.* **2017**, *41*, 13700-13711.

DOI: 10.1039/C7NJ02136D

**Contribution:**

For this work, solvent extraction experiments as well as their analysis (gamma-spectrometry, results of ICP-MS) using the synthesized degradation products of TODGA and Me-TODGA were conducted mainly by A. Wilden and me. Additionally, I participated in paper preparation.

**Paper 10<sup>[159]</sup>**

Wilden, A.; Lumetta, G.J.; Sadowski, F.; Schmidt, H.; Schneider, D.; Gerdes, M.; Law, J.D.; Geist, A.; Bosbach, D.; Modolo, G. An Advanced TALSPEAK Concept for Separating Minor Actinides. Part 2. Flowsheet Test with Actinide-Spiked Simulant. *Solvent Extr. Ion Exch.* **2017**, *35* (6), 396-407.

DOI: 10.1080/07366299.2017.1368901

**Contribution:**

For this work, solvent extraction experiments as well as their analysis (gamma-spectrometry, results of ICP-MS) were conducted in the IEK-6, Forschungszentrum Jülich, in which I was involved.





## Paper 1<sup>[86]</sup>

Schmidt, H.; Wilden, A.; Modolo, G.; Švehla, J.; Grüner, B.; Ekberg, C. Gamma radiolytic stability of CyMe<sub>4</sub>BTBP and effect of nitric acid. *Nukleonika* **2015**, *60* (4 (Pt. II)), 879-884.

DOI: 10.1515/nuka-2015-0156

### Contribution:

In this work, I did gamma-radiolysis experiments, solvent extraction, HPLC-MS product identification as well as leading authorship.





# Gamma radiolytic stability of CyMe<sub>4</sub>BTBP and the effect of nitric acid

Holger Schmidt,  
Andreas Wilden,  
Giuseppe Modolo,  
Jaroslav Švehla,  
Bohumir Grüner,  
Christian Ekberg

**Abstract.** The highly selective nitrogen donor ligand CyMe<sub>4</sub>BTBP for An(III) separation by solvent extraction was irradiated in a <sup>60</sup>Co γ-source under varying conditions. Organic solutions of 10 mmol/L ligand in 1-octanol were contacted with different concentrations of nitric acid to observe the influence of an aqueous phase during irradiation. In subsequent liquid-liquid extraction experiments, distribution ratios of <sup>241</sup>Am and <sup>152</sup>Eu were determined. Distribution ratios decreased with increasing absorbed dose when irradiation was performed in the absence of nitric acid. With addition of nitric acid, initial distribution ratios remained constant over the whole examined dose range up to 300 kGy. For qualitative determination of radiolysis products, HPLC-MS measurements were performed. The protective effect of nitric acid was confirmed, since in samples irradiated with acid contact, no degradation products were observed, but only addition products of the 1-octanol molecule to the CyMe<sub>4</sub>BTBP molecule.

**Key words:** CyMe<sub>4</sub>BTBP • gamma radiolysis • liquid-liquid extraction • nitric acid • partitioning • protective effect

H. Schmidt, A. Wilden, G. Modolo<sup>✉</sup>  
Institut für Energie- und Klimaforschung, Nukleare  
Entsorgung und Reaktorsicherheit (IEK-6),  
Forschungszentrum Jülich GmbH (FZJ),  
52425 Jülich, Germany,  
Tel.: +49 2461 61 4896, Fax: +49 2461 61 2450,  
E-mail: g.modolo@fz-juelich.de

J. Švehla, B. Grüner  
Institute of Inorganic Chemistry, Academy of Sciences  
of the Czech Republic,  
Hlavni 1001, 25068 Husinec-Rež, Czech Republic

C. Ekberg  
Nuclear Chemistry & Industrial Materials Recycling,  
Department of Chemical and Biochemical Engineering,  
Chalmers University of Technology,  
Kemigården 4, 41296 Gothenburg, Sweden

Received: 23 June 2015

Accepted: 15 September 2015

## Introduction

Within international research in partitioning and transmutation (P&T), the separation of trivalent actinides (An(III)) from the chemical similar trivalent lanthanides (Ln(III)) is a main task that was comprehensively studied within the last two decades [1–3].

The investigated solvent extraction processes often follow the plutonium uranium reduction extraction (PUREX) process, in which uranium and plutonium are recycled from dissolved spent nuclear fuel solutions. For An(III) separation, a two-cycle concept, the so-called DIAMEX-SANEX concept, was developed [4]. In the first cycle the trivalent actinides were co-separated together with the lanthanides in the diamide extraction (DIAMEX) process [5, 6]. In the subsequent selective actinide extraction (SANEX) process, An(III) were selectively partitioned using the highly selective nitrogen donor ligand CyMe<sub>4</sub>BTBP (6,6'-bis(5,5,8,8-tetramethyl-5,6,7,8-tetrahydro-benzo[1,2,4]-triazin-3-yl)-[2,2']-bipyridine) (Fig. 1) [7, 8]. A hot SANEX process demonstration was conducted using a genuine feed solution containing Ln(III) as well as Am(III) and Cm(III). Those An(III) were selectively extracted, whereas the lanthanides were routed to the raffinate stream [9]. In further work this SANEX process was modified to be able to extract the actinides directly from PUREX raffinate [10–12].

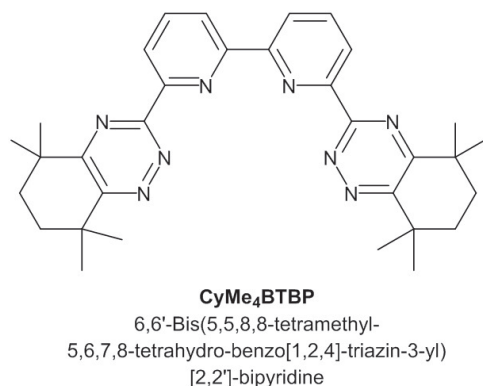


**Fig. 1.** Chemical structure of the CyMe<sub>4</sub>BTBP ligand.

For the development of processes on an industrial scale, one main issue to consider is the detailed knowledge of radiolytic stability of the chemicals used since a solvent would be in contact for longer times with highly radioactive process streams. Degradation of the solvent may lead to the production of interfering degradation products, decreases in ligand concentration and changes in solvent viscosity as well as phase separation parameters [13]. This degradation may result in losses in selectivity and affinity for target metal extraction.

Radiolytic degradation of the BTBP ligand family was investigated previously [14–16]. A variety of different BTBP molecules was developed, such as C5-BTBP (6,6'-bis(5,6-dipentyl-[1,2,4]triazin-3-yl)-[2,2']bipyridine) or the annulated MF2-BTBP (4-tert-butyl-6,6'-bis-(5,5,8,8-tetramethyl-5,6,7,8-tetrahydro-benzo[1,2,4]triazin-3-yl)[2,2']-bipyridine) and tested for their process performance [17]. Since it was proven that annulated BTBPs are much more stable towards radiolytic degradation than the tetra alkyl substituted BTBPs, those annulated systems were further investigated. Finally, the CyMe<sub>4</sub>BTBP system was chosen as reference system in European research, resulting in the above mentioned SANEX process. Radiolytic stability of the SANEX solvent (CyMe<sub>4</sub>BTBP + DMDOHEMA (*N,N'*-dimethyl-*N,N'*-dioctylhexylethoxymalonamide) in octanol) was studied by Magnusson *et al.* [18]. They investigated the radiolytic degradation for alpha as well as gamma radiation depending on the absorbed dose. The degradation of the extractant was found to be more severe for gamma radiolysis, as the reduction of distribution ratios was 40% higher compared to alpha radiolysis. This was explained by the higher LET of alpha radiation yielding in denser radiation tracks, allowing much faster recombination of radicals formed than in the case of gamma radiation [18].

The presence of an aqueous phase during irradiation of C5-BTBP in cyclohexanone was studied by Fermvik *et al.* [19]. It was found that in the presence of an aqueous phase the degradation of the extractant increased. A general review of the radiation chemistry of selective ligands for trivalent actinide recovery was published by Mincher *et al.* [20]. Su-

lich *et al.* examined the radiolysis of CyMe<sub>4</sub>BTBP in 1-octanol pre-equilibrated with nitric acid using electron pulse radiolysis [21]. They added benzophenone and observed a protective effect on the ligand which was attributed to the addition of the aromatic ketone in higher concentration than the ligand, preferentially reacting with solvated electrons.

In this work, the radiolytic degradation of CyMe<sub>4</sub>BTBP in 1-octanol and the influence of an aqueous phase in contact during irradiation were investigated. Experiments were conducted without an aqueous phase as well as in contact to different diluted nitric acid solutions.

## Experimental part

CyMe<sub>4</sub>BTBP was purchased from Technocomm Ltd., Falkland, United Kingdom with a purity >98%. 1-Octanol (analytical grade, >99%) and concentrated nitric acid (65%, analytical grade) were purchased from Merck, Darmstadt, Germany.

## Radiolysis experiments

Solutions of CyMe<sub>4</sub>BTBP in 1-octanol (10 mmol/L) were irradiated either without contact to an aqueous phase or in contact to different diluted nitric acid solutions (0.1, 1.0 and 4.0 mol/L HNO<sub>3</sub>). The irradiation was performed at the Department of Chemical and Biochemical Engineering at the Chalmers University of Technology in Gothenburg, Sweden. A <sup>60</sup>Co γ-source (Gammacell 220, Atomic Energy of Canada Ltd.) with a dose rate of ~9.5 kGy/h was used and samples were irradiated up to absorbed doses of 300 kGy. With increasing absorbed dose, the color of the former light yellow organic phase turned into a more reddish/orange color, which could indicate degradation of the pyridine moieties.

## Liquid-liquid extraction

After removing the irradiated samples from the Gammacell, phases were separated (if necessary) and batch shaking experiments were performed. In each experiment 500 μL of the irradiated organic phase were contacted with 500 μL fresh 1.0 mol/L HNO<sub>3</sub> which was spiked with an <sup>241</sup>Am (1.6 kBq) and a <sup>152</sup>Eu (2.8 kBq) tracer. The samples were vigorously mixed for 90 min in a shaking device (2500 rpm) at 22°C and after centrifugation the phases were separated and aliquots of each phase were taken for analysis. Gamma spectroscopy was performed with a high-purity germanium detector obtained from EG&G Ortec, Munich, Germany and equipped with the Gamma Vision software. The gamma lines at 59.5 keV and 121.8 keV were analyzed for <sup>241</sup>Am and <sup>152</sup>Eu, respectively. The results are reported as distribution ratios *D* ( $D = [M_{org}]/[M_{aq}]$ ), which have an uncertainty of ±5%, and where detection limits are  $500 > D > 0.002$ .

## HPLC-MS experiments

MS measurements were performed using a Finnigan LCQ Fleet<sup>TM</sup> spherical Ion Trap LC/MS<sub>n</sub> instrument (Thermo Scientific). All mass spectra were measured with APCI interface. 25  $\mu$ L of the samples of initial concentration of the ligand were diluted to a volume of 1.0 mL with acetonitrile (for LC-MS, Aldrich, gradient grade). Mass spectra from direct infusion by a syringe were measured with APCI in positive mode. Conditions used for APCI interface: flow rate from a syringe infusion pump: 10  $\mu$ L/min; sheath gas flow 15 L/min; auxiliary gas flow at 7 L/min, source voltage: 3.75 kV, vaporizer temperature 400°C; capillary temperature 250°C; capillary voltage 48 V, tube lens voltage 100 V and mass range from 50 to 2000.

## Results and discussion

The radiolytic stability of CyMe<sub>4</sub>BTBP was first studied in the liquid-liquid extraction experiments using solvents irradiated to different doses up to 300 kGy. The irradiated samples were then analyzed by high-pressure liquid chromatography mass spectrometry (HPLC-MS) to determine the radiolysis products.

### Liquid-liquid extraction experiments

Figure 2 shows the distribution ratios of <sup>241</sup>Am and <sup>152</sup>Eu as a function of absorbed dose for initially 10 mmol/L CyMe<sub>4</sub>BTBP in 1-octanol, when the organic phase was irradiated without contact to an aqueous phase. Both, the americium and europium distribution ratios decreased with increasing absorbed dose, in line with observations from Magnusson *et al.* [18] who used a mixture of CyMe<sub>4</sub>BTBP + DMDOHMA in octanol. Decreasing distribution ratios were observed up to an absorbed dose of

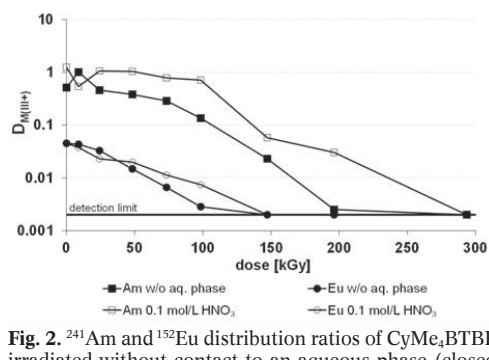


**Fig. 2.** <sup>241</sup>Am and <sup>152</sup>Eu distribution ratios of CyMe<sub>4</sub>BTBP irradiated without contact to an aqueous phase (closed symbols) and in contact with 0.1 mol/L nitric acid (open symbols) as a function of the absorbed dose. Organic phase: initially 0.01 mol/L ligand in 1-octanol, irradiated by <sup>60</sup>Co  $\gamma$  radiation, dose rate  $\sim$ 9.5 kGy/h. Aqueous phase: fresh 1 mol/L HNO<sub>3</sub>, spiked with <sup>241</sup>Am and <sup>152</sup>Eu tracer; 90 min shaking time, 22°C.

200 kGy (europium: 100 kGy), where the detection limit was reached. A linear decrease in distribution ratios was observed for europium (circles). For americium (squares), a delayed decrease in distribution ratios was found. After 75 kGy absorbed dose the slope of decreasing distribution ratios became steeper.

This could be explained by the formation of an intermediate species (see HPLC-MS section) that is also able to extract Am(III) to a certain amount, but is prone to radiolytic degradation with increasing dose itself. This behavior suggests there is no direct and exclusive degradation of the ligand by direct gamma irradiation alone but predominantly through indirect radiolysis [22–24]. It is well known, that during irradiation reactive radicals are formed mainly by radiolysis of the diluent, which can react with the extractant molecules (see discussion HPLC-MS, Eqs. (1)–(4)). Diluent molecules are present in much higher concentration than extractant molecules and are therefore more available for direct radiolysis.

The effect of nitric acid during irradiation was studied. Therefore, the organic solvent was irradiated in contact with different nitric acid concentrations from 0.1 to 4.0 mol/L HNO<sub>3</sub>. For diluted 0.1 mol/L nitric acid, we could observe just slightly increased distribution ratios (Fig. 2). Irradiation experiments performed in contact with 1.0 mol/L nitric acid resulted in much higher distribution ratios. The observed distribution ratios did not decrease with increasing dose and the Am(III)/Eu(III) separation factor ( $SF_{M1/M2} = D_{M1}/D_{M2}$ ) remained at the initial level with no observable changes (Fig. 3).

Obviously, the extracting system was protected by nitric acid against gamma radiation. The protection mechanism still needs to be resolved and in future experiments the individual influences of nitrate, acidity and water content will be studied. However, the added nitric acid seems to scavenge radicals built during radiolysis of the diluent. With increasing concentration of nitric acid from 0.1 mol/L to 1.0 mol/L, this scavenging became more effective until no reduction of distribution ratios was observed even at the highest doses studied here (300 kGy). Increase of the nitric acid concentration to 4.0 mol/L during irradiation

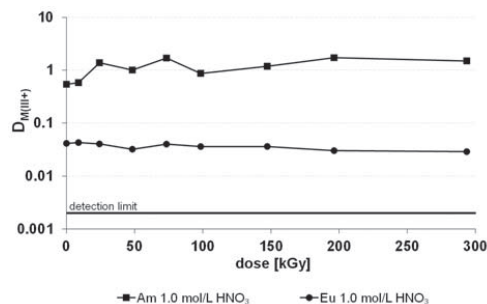


**Fig. 3.** <sup>241</sup>Am and <sup>152</sup>Eu distribution ratios of CyMe<sub>4</sub>BTBP irradiated in contact with 1.0 mol/L nitric acid as a function of the absorbed dose. Organic phase: initially 0.01 mol/L ligand in 1-octanol, irradiated by <sup>60</sup>Co  $\gamma$  radiation, dose rate  $\sim$ 9.5 kGy/h. Aqueous phase: fresh 1 mol/L HNO<sub>3</sub>, spiked with <sup>241</sup>Am and <sup>152</sup>Eu tracer; 90 min shaking time, 22°C.

showed no further improvement. For clarification of the radiolysis mechanism HPLC-MS measurements were conducted to identify the radiolysis products and to investigate the influence of nitric acid addition on the radiolysis mechanism.

### HPLC-MS analysis

Qualitative HPLC-MS analysis was performed to identify the radiolysis products of the gamma irradiated ligand solutions. Results of the liquid-liquid extraction studies suggest that there is at least one new species formed during irradiation in contact with nitric acid that is also able to extract the actinides. In neat samples (no irradiation, no contact to nitric acid, but prepared at the same time as the samples for irradiation) only the molecule peak was found  $m/z = (M + H^+) = 535.4$  u. When irradiating the organic samples without contact to an aqueous phase, several different fragments were built with increasing yield towards increasing dose (Fig. 4). Products with heavier and lighter masses were detected suggesting also the degradation of extractant molecules.

In samples irradiated in contact with nitric acid, mainly one product was found with  $m/z = 663.4$  u, which may be an addition product of one 1-octanol molecule to the CyMe<sub>4</sub>BTBP molecule. However, the HPLC-MS method does not give structural information. Lighter masses than the  $M + H^+$  peak were only observed in negligible abundances.

The radiolysis of alcohols, such as isopropanol or hexanol, mainly results in the highly reactive  $\alpha$ -hydroxy radicals as described in the literature by Eqs. (1)–(4) [25–29]. The reaction of diluent radicals with extractant molecules was reported as sensitization effect [30, 31].

- (1)  $RCH_2OH + \rightarrow [RCH_2OH]^{\bullet}$
- (2)  $[RCH_2OH]^{\bullet} \rightarrow e^- + [RCH_2OH]^{\bullet+}$
- (3)  $e^- \rightarrow e^-_{\text{solv}}$
- (4)  $[RCH_2OH]^{\bullet+} + RCH_2OH \rightarrow RC^{\bullet}HOH + RCH_2OH_2^+$

According to this mechanism, it is very likely that during irradiation experiments,  $\alpha$ -hydroxyoctyl

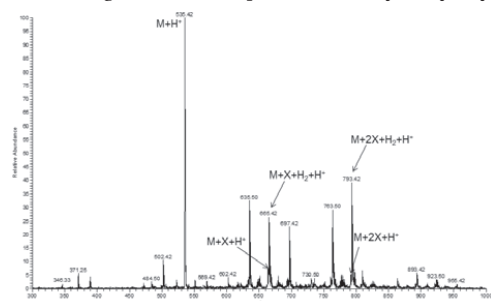


**Fig. 4.** CyMe<sub>4</sub>BTBP irradiated without contact to an aqueous phase to an absorbed dose of 100 kGy.

**Table 1.** Calculated mass to charge ratios for CyMe<sub>4</sub>BTBP and  $\alpha$ -hydroxyoctyl adducts. ( $M = \text{CyMe}_4\text{BTBP}$ ;  $X = \alpha$ -hydroxyoctyl ( $\text{CH}_3(\text{CH}_2)_6\text{C}^{\bullet}\text{HOH}$ ))

	Calculated $m/z$ ratio	Molecular formula
$M + H^+$	535.33 u	$\text{C}_{32}\text{H}_{59}\text{N}_8^+$
$M + X + H^+$	663.45 u	$\text{C}_{40}\text{H}_{55}\text{N}_8\text{O}^+$
$M + 2X + H^+$	791.57 u	$\text{C}_{48}\text{H}_{71}\text{N}_8\text{O}_2^+$

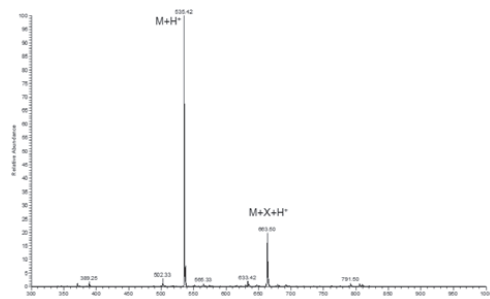


**Fig. 5.** CyMe<sub>4</sub>BTBP irradiated in contact to 1 mol/L  $\text{HNO}_3$  to an absorbed dose of 100 kGy.

radicals were formed and reacted with the ligand molecule. This is in good agreement with the observed  $m/z$  ratios, especially in samples irradiated in contact with nitric acid, where exclusively  $M + X + H^+$  ( $X = \alpha$ -hydroxyoctyl ( $\text{CH}_3(\text{CH}_2)_6\text{C}^{\bullet}\text{HOH}$ )) was found (Table 1, Fig. 5). Based on the results from the liquid-liquid extraction, we assume that the reaction of the  $\alpha$ -hydroxyoctyl is taking place on the 'periphery' of the ligand molecule. The tetradentate binding pocket made up by the nitrogen donor groups of CyMe<sub>4</sub>BTBP, should not be occupied [32]. In the literature, radiolysis of nitric acid is well described and especially radical scavenging by  $\text{HNO}_3$ ,  $\text{NO}_2$  or  $\text{H}^+$  seems to be likely [33–40]. The individual influences of  $\text{HNO}_3$ ,  $\text{NO}_2$  or  $\text{H}^+$  will therefore be investigated and further detailed investigations of the radiolysis mechanism are planned (e.g. using pulse radiolysis). In samples irradiated without contact with an aqueous phase, also the higher addition product containing two  $\alpha$ -hydroxyoctyl groups ( $M + 2X + H^+$ ) was found (Fig. 4). The  $m/z$  ratio of this species is 791.75 which is present in the sample at a relatively low abundance. The dominating species is found to be  $M + 2X + \text{H}_2 + H^+$  ( $m/z = 793.59$ ). This observation is also true for the  $M + X$  product. This seems to be the product of the reduction of one of the double-bonds in the molecule.

### Conclusions and outlook

The gamma radiolysis of the highly selective nitrogen donor ligand CyMe<sub>4</sub>BTBP was investigated in solution and the influence of nitric acid contact during irradiation was tested. A protection of CyMe<sub>4</sub>BTBP against radiolytic degradation was found for solutions irradiated in contact with nitric acid. In contrast to irradiation experiments without contact to nitric acid solutions, no decrease in  $^{241}\text{Am}$  and  $^{152}\text{Eu}$  distribu-



tion ratios was observed. As nitric acid is commonly used in partitioning processes for trivalent actinide separation, this protective effect plays a crucial role for the long-term performance of the used solvents.

A large number of radiolysis products was found in qualitative HPLC-MS measurements of samples irradiated without contact to an aqueous phase. In contrast, only the formation of 1-octanol adducts to the extractant was observed in samples irradiated in contact with nitric acid. The protective effect of nitric acid reduced the formation of other degradation products and the adducts are believed to potentially be able to extract trivalent actinides, as distribution ratios remained constant.

As the next step, it is planned to perform high resolution mass spectroscopy to further identify the radiolysis products and to synthesize 1-octanol adducts to CyMe<sub>4</sub>BTBP. These synthesized molecules will then also be tested for their extraction abilities within the current European SACSESS project. Additionally, the CyMe<sub>4</sub>BTBP molecule, which is the current reference molecule in European research, will be compared to the very promising molecule CyMe<sub>4</sub>BTPPhen, where the bipyridine moiety is replaced by a phenanthroline functionality to fix the molecule in the *cis*-conformation resulting in a thermodynamically more favored metal-ligand complexation.

**Acknowledgments.** Financial support for this research is provided by the European Atomic Energy Community's 7th Framework Programme project SACSESS – grant agreement no. FP7-Fission-2012-323-282.

## References

- OECD-NEA. (2011). *Potential benefits and impacts of advanced nuclear fuel cycles with actinide partitioning and transmutation*. Issy-les-Moulineaux, France: O. Publishing OECD-NEA. (NEA no. 6894).
- González-Romero, E. M. (2011). Impact of partitioning and transmutation on the high level waste management. *Nucl. Eng. Des.*, 241, 3436–3444. DOI: 10.1016/j.nucengdes.2011.03.030.
- Modolo, G., Geist, A., & Miguiditchian, M. (2015). Minor actinide separations in the reprocessing of spent nuclear fuels: recent advances in Europe. In R. Taylor (Ed.), *Reprocessing and recycling of spent nuclear fuel* (pp. 245–287). Oxford: Woodhead Publishing.
- Baron, P., Hérès, X., Lecomte, M., & Masson, M. (2001). Separation of the minor actinides: the DIAMEX-SANEX concept. In Proceedings of the International Conference on Future Nuclear Systems, GLOBAL'01, 9–13 September 2001. Paris, France.
- Courson, O., Lebrun, M., Malmbeck, R., Pagliosa, G., Romer, K., Satmark, B., & Glatz, J. P. (2000). Partitioning of minor actinides from HLLW using the DIAMEX process. Part 1 – Demonstration of extraction performances and hydraulic behaviour of the solvent in a continuous process. *Radiochim. Acta*, 88, 857–863. DOI: 10.1524/ract.2000.88.12.857.
- Malmbeck, R., Courson, O., Pagliosa, G., Romer, K., Satmark, B., Glatz, J. P., & Baron, P. (2000). Partitioning of minor actinides from HLLW using the DIAMEX process. Part 2 – “Hot” continuous counter-current experiment. *Radiochim. Acta*, 88, 865–871. DOI: 10.1524/ract.2000.88.12.865.
- Geist, A., Hill, C., Modolo, G., Foreman, M. R. S. J., Weigl, M., Gompper, K., Hudson, M. J., & Madic, C. (2006). 6,6'-Bis(5,5,8,8-tetramethyl-5,6,7,8-tetrahydro-benzo[1,2,4]triazin-3-yl)[2,2']bipyridine, an effective extracting agent for the separation of americium(III) and curium(III) from the lanthanides. *Solvent Extr. Ion Exch.*, 24, 463–483. DOI: 10.1080/07366290600761936.
- Foreman, M. R. S., Hudson, M. J., Drew, M. G. B., Hill, C., & Madic, C. (2006). Complexes formed between the quadridentate, heterocyclic molecules 6,6'-bis-(5,6-dialkyl-1,2,4-triazin-3-yl)-2,2'-bipyridine (BTBP) and lanthanides(III): implications for the partitioning of actinides(III) and lanthanides(III). *Dalton Trans.*, 13, 1645–1653. DOI: 10.1039/B511321k.
- Magnusson, D., Christiansen, B., Foreman, M. R. S., Geist, A., Glatz, J. P., Malmbeck, R., Modolo, G., Serrano-Purroy, D., & Sorel, C. (2009). Demonstration of a SANEX process in centrifugal contactors using the CyMe<sub>4</sub>-BTBP molecule on a genuine fuel solution. *Solvent Extr. Ion Exch.*, 27, 97–106. DOI: 10.1080/07366290802672204.
- Wilden, A., Schreinemachers, C., Sypula, M., & Modolo, G. (2011). Direct selective extraction of actinides (III) from PUREX raffinate using a mixture of CyMe<sub>4</sub>BTBP and TODGA as 1-cycle SANEX solvent. *Solvent Extr. Ion Exch.*, 29, 190–212. DOI: 10.1080/07366299.2011.539122.
- Magnusson, D., Geist, A., Wilden, A., & Modolo, G. (2013). Direct selective extraction of actinides (III) from PUREX raffinate using a mixture of CyMe<sub>4</sub>-BTBP and TODGA as 1-cycle SANEX solvent. Part II: Flow-sheet design for a counter-current centrifugal contactor demonstration process. *Solvent Extr. Ion Exch.*, 31, 1–11. DOI: 10.1080/07366299.2012.700596.
- Wilden, A., Modolo, G., Schreinemachers, C., Sadowski, F., Lange, S., Sypula, M., Magnusson, D., Geist, A., Lewis, F. W., Harwood, L. M., & Hudson, M. J. (2013). Direct selective extraction of actinides (III) from PUREX raffinate using a mixture of CyMe<sub>4</sub>BTBP and TODGA as 1-cycle SANEX solvent. Part III: Demonstration of a laboratory-scale counter-current centrifugal contactor process. *Solvent Extr. Ion Exch.*, 31, 519–537. DOI: 10.1080/07366299.2013.775890.
- Mincher, B. J. (2010). An overview of selected radiation chemical reactions affecting fuel cycle solvent extraction. *ACS Symp. Ser.*, 1046, 181–192. DOI: 10.1021/bk-2010-1046.ch015.
- Hill, C., Berthon, L., & Madic, C. (2005). Study of the stability of BTP extractants under radiolysis. In Proceedings of the GLOBAL 2005, 9–13 October (p. 283). Tsukuba, Japan.
- Retegan, T., Ekberg, C., Englund, S., Fermvik, A., Foreman, M. R. S., & Skarnemark, G. (2007). The behaviour of organic solvents containing C5-BTBP and CyMe<sub>4</sub>-BTBP at low irradiation doses. *Radiochim. Acta*, 95, 637–642. DOI: 10.1524/ract.2007.95.11.637.
- Fermvik, A., Berthon, L., Ekberg, C., Englund, S., Retegan, T., & Zorz, N. (2009). Radiolysis of solvents containing C5-BTBP: identification of degradation products and their dependence on absorbed dose and dose rate. *Dalton Trans.*, 32, 6421–6430. DOI: 10.1039/b907084b.
- Fermvik, A., Ekberg, C., Englund, S., Foreman, M. R. S. J., Modolo, G., Retegan, T., & Skarnemark, G. (2009). Influence of dose rate on the radiolytic stability of a BTBP solvent for actinide(III)/lanthanide(III)



- separation. *Radiochim. Acta*, 97, 319–324. DOI: 10.1524/ract.2009.1615.
18. Magnusson, D., Christiansen, B., Malmbeck, R., & Glatz, J. P. (2009). Investigation of the radiolytic stability of a CyMe<sub>4</sub>-BTBP based SANEX solvent. *Radiochim. Acta*, 97, 497–502. DOI: 10.1524/ract.2009.1647.
  19. Fermvik, A., Aneheim, E., Grüner, B., Hájková, Z., Kvalicová, M., & Ekberg, C. (2012). Radiolysis of C5-BTBP in cyclohexanone irradiated in the absence and presence of an aqueous phase. *Radiochim. Acta*, 100, 273–282. DOI: 10.1524/ract.2012.1908.
  20. Mincher, B. J., Modolo, G., & Mezyk, S. P. (2010). Review: The effects of radiation chemistry on solvent extraction 4: Separation of the trivalent actinides and considerations for radiation-resistant solvent systems. *Solvent Extr. Ion Exch.*, 28, 415–436. DOI: 10.1080/07366299.2010.485548.
  21. Sulich, A., Grodkowski, J., Mirkowski, J., & Kocia, R. (2014). Reactions of ligands from BT(B)P family with solvated electrons and benzophenone ketyl radicals in 1-octanol solutions. Pulse radiolysis study. *J. Radioanal. Nucl. Chem.*, 300, 415–421. DOI: 10.1007/s10967-014-3021-5.
  22. Mincher, B. J., & Mezyk, S. P. (2009). Radiation chemical effects on radiochemistry: A review of examples important to nuclear power. *Radiochim. Acta*, 97, 519–534. DOI: 10.1524/ract.2009.1646.
  23. Mincher, B. J., Modolo, G., & Mezyk, S. P. (2009). The effects of radiation chemistry on solvent extraction: 1. Conditions in acidic solution and a review of TBP radiolysis. *Solvent Extr. Ion Exch.*, 27, 1–25. DOI: 10.1080/07366290802544767.
  24. Mincher, B. J. (2015). Radiation chemistry in the reprocessing and recycling of spent nuclear fuels. In R. Taylor (Ed.), *Reprocessing and recycling of spent nuclear fuel* (pp. 191–211). Oxford: Woodhead Publishing.
  25. Nilsson, M., Andersson, S., Ekberg, C., Foreman, M. R. S., Hudson, M. J., & Skarnemark, G. (2006). Inhibiting radiolysis of BTP molecules by addition of nitrobenzene. *Radiochim. Acta*, 94, 103–106. DOI: 10.1524/ract.2006.94.2.103.
  26. Mincher, B. J., Arbon, R. E., Knighton, W. B., & Meikrantz, D. H. (1994). Gamma-ray-induced degradation of PCBs in neutral isopropanol using spent reactor-fuel. *Appl. Radiat. Isot.*, 45, 879–887. DOI: 10.1016/0969-8043(94)90219-4.
  27. Freeman, G. R. (1970). Radiolysis of alcohols. *Actions Chim. Biol. Radiat.*, 14, 73–134.
  28. Mincher, B. J., Mezyk, S. P., Elias, G., Groenewold, G. S., Riddle, C. L., & Olson, L. G. (2013). The radiation chemistry of CMPO: Part 1. Gamma radiolysis. *Solvent Extr. Ion Exch.*, 31, 715–730. DOI: 10.1080/07366299.2013.815491.
  29. Symons, M. C. R., & Eastland, G. W. (1977). Radiation mechanisms. Part 18. The radiolysis of alcohols: an electron spin resonance study. *J. Chem. Res., Suppl.*, 254–255.
  30. Sugo, Y., Sasaki, Y., & Tachimori, S. (2002). Studies on hydrolysis and radiolysis of N,N,N',N'-tetraoctyl-3-oxapentane-1,5-diamide. *Radiochim. Acta*, 90, 161–165. DOI: 10.1524/ract.2002.90.3.2002.161.
  31. Sugo, Y., Izumi, Y., Yoshida, Y., Nishijima, S., Sasaki, Y., Kimura, T., Sekine, T., & Kudo, H. (2007). Influence of diluent on radiolysis of amides in organic solution. *Radiat. Phys. Chem.*, 76, 794–800. DOI: 10.1016/j.radphyschem.2006.05.008.
  32. Steppert, M., Cisarova, I., Fanghanel, T., Geist, A., Lindqvist-Reis, P., Panak, P., Stepnicka, P., Trumm, S., & Walther, C. (2012). Complexation of europium(III) by bis(dialkyltriazinyl)bipyridines in 1-octanol. *Inorg. Chem.*, 51, 591–600. DOI: 10.1021/ic202119x.
  33. Mezyk, S. P., Cullen, T. D., Elias, G., & Mincher, B. J. (2010). Aqueous nitric acid radiation effects on solvent extraction process chemistry. *ACS Symp. Ser.*, 1046, 193–203. DOI: 10.1021/bk-2010-1046.ch016.
  34. Mincher, B. J. (2012). Degradation issues in aqueous reprocessing systems. *Compr. Nucl. Mater.*, 5, 367–388. DOI: 10.1016/b978-0-08-056033-5.00104-x.
  35. Mincher, B. J., Mezyk, S. P., & Martin, L. R. (2008). A pulse radiolysis investigation of the reactions of tributyl phosphate with the radical products of aqueous nitric acid irradiation. *J. Phys. Chem. A*, 112, 6275–6280. DOI: 10.1021/jp802169v.
  36. Harwood, L. M., Lewis, F. W., Hudson, M. J., John, J., & Distler, P. (2011). The separation of americium(III) from europium(III) by two new 6,6'-bistriazinyl-2,2'-bipyridines in different diluents. *Solvent Extr. Ion Exch.*, 29, 551–576. DOI: 10.1080/10496475.2011.556989.
  37. Joshi, R., Pathak, P. N., Manchanda, V. K., Sarkar, S. K., & Mukherjee, T. (2010). Reactions of N,N-dihexyloctanamide with nitrate and dodecane radicals: a pulse radiolysis study. *Res. Chem. Intermed.*, 36, 503–510. DOI: 10.1007/s11164-010-0161-2.
  38. Neta, P., & Huie, R. E. (1986). Rate constants for reactions of nitrogen oxide (NO<sub>2</sub>) radicals in aqueous solutions. *J. Phys. Chem.*, 90, 4644–4648. DOI: 10.1021/j100410a055.
  39. Katsumura, Y. (1998). NO<sub>2</sub> and NO<sub>3</sub> radicals in radiolysis of nitric acid solutions. In Z. B. Alfassi (Ed.), *The chemistry of free radicals: N-centered radicals* (pp. 393–412). Weinheim: Wiley.
  40. Katsumura, Y., Jiang, P. Y., Nagaishi, R., Oishi, T., Ishigure, K., & Yoshida, Y. (1991). Pulse radiolysis study of aqueous nitric acid solutions: formation mechanism, yield, and reactivity of NO<sub>3</sub> radical. *J. Phys. Chem.*, 95, 4435–4439. DOI: 10.1021/j100164a050.

## Paper 2<sup>[87]</sup>

Schmidt, H.; Wilden, A.; Modolo, G.; Bosbach, D.; Santiago-Schübel, B.; Hupert, M.; Švehla, J.; Grüner, B.; Ekberg, C. Gamma radiolysis of the highly selective ligands CyMe4BTBP and CyMe4BTPhen: Qualitative and quantitative investigation of radiolysis products. *Procedia Chem.* 2016, 21, 32-37.

DOI: 10.1016/j.proche.2016.10.005

Contribution:

This work is a continuation of paper #1. I did gamma-radiolysis experiments, solvent extraction, HPLC-MS product identification as well as leading authorship.



5<sup>th</sup> International ATALANTE Conference on Nuclear Chemistry for Sustainable Fuel Cycles

## Gamma radiolysis of the highly selective ligands CyMe<sub>4</sub>BTBP and CyMe<sub>4</sub>BTPPhen: Qualitative and quantitative investigation of radiolysis products

Holger Schmidt<sup>a</sup>, Andreas Wilden<sup>a</sup>, Giuseppe Modolo<sup>a\*</sup>, Dirk Bosbach<sup>a</sup>, Beatrix Santiago-Schübel<sup>b</sup>, Michelle Hupert<sup>b</sup>, Jaroslav Švehla<sup>c</sup>,  
Bohumir Grüner<sup>c</sup>, Christian Ekberg<sup>d</sup>

<sup>a</sup>Forschungszentrum Jülich GmbH, Institute of Energy and Climate Research IEK-6: Nuclear Waste Management, 52425 Jülich, D

<sup>b</sup>Forschungszentrum Jülich GmbH, Central Institute for Engineering, Analytics (ZEA-3), 52425 Jülich, D

<sup>c</sup>Institute of Inorganic Chemistry, Academy of Sciences, Hlavni 1001, 25068 Husinec-Rež, CZ

<sup>d</sup>Department of Chemical and Biochemical Engineering, Chalmers University of Technology, 41296 Gothenburg, SE

---

### Abstract

The highly selective nitrogen donor ligands CyMe<sub>4</sub>BTBP and CyMe<sub>4</sub>BTPPhen were  $\gamma$ -irradiated under identical experimental conditions in 1-octanol with and without contact to nitric acid solution. Subsequently, solvent extraction experiments were carried out to evaluate the stability of the extractants against  $\gamma$ -radiation monitoring Am(III) and Eu(III) distribution ratios. Generally, decreasing distribution ratios with increasing absorbed dose were detected for both molecules. Furthermore, qualitative mass spectrometric analyses were performed and ligand concentrations were determined by HPLC-DAD after irradiation to investigate the radiolysis mechanism. An exponential decrease with increasing absorbed dose was observed for both ligands with a faster rate for CyMe<sub>4</sub>BTPPhen. Main radiolysis products indicated the addition of one or more diluent molecules (1-octanol) to the ligand via prior production of  $\alpha$ -hydroxyoctyl radicals from diluent radiolysis. The addition of nitric acid during the irradiation lead to a remarkable stabilization of the system, as the extraction of Am(III) and Eu(III) did not change significantly over the whole examined dose range. Quantification of the remaining ligand concentration on the other hand showed decreasing concentrations with increasing absorbed dose. The stabilization of D values is therefore explained by the formation of 1-octanol addition products which are also able to extract the studied metal ions.

© 2016 The Authors. Published by Elsevier B.V. This is an open access article under the CC BY-NC-ND license

(<http://creativecommons.org/licenses/by-nc-nd/4.0/>).

Peer-review under responsibility of the organizing committee of ATALANTE 2016

\* Corresponding author. Tel.: +49 2461 61-4896; fax: +49 2461 61-2450.

E-mail address: [g.modolo@fz-juelich.de](mailto:g.modolo@fz-juelich.de)

**Keywords:** N-donor ligands; gamma radiolysis; solvent extraction; mass spectrometry, CyMe<sub>4</sub>BTBP, CyMe<sub>4</sub>BTPhen

## 1. Introduction

Within the past and current European research on the development of new separation processes for the partitioning of minor actinides (MA: Np, Am and Cm) from highly active nuclear waste solutions, the group of BTBPs was developed and found to be very efficient. Especially the separation of the trivalent actinides Am(III) and Cm(III) from trivalent lanthanides (Ln(III)) is crucial. Therefore, the group of soft nitrogen donor ligands such as BTBPs is very promising, since it also fulfills the CHON principle.<sup>[1]</sup> Radiolytic as well as chemical stability are important aspects for a potential ligand application in industrial partitioning processes. The annulated 6,6'-bis(1,2,4-triazin-3-yl)-2,2'-bipyridine ligands appeared to be more stable against radiolytic degradation than the tetra-*n*-alkyl substituted derivatives such as C5-BTBP.<sup>[2-4]</sup> The CyMe<sub>4</sub>BTBP (6,6'-bis(5,5,8,8-tetramethyl-5,6,7,8-tetrahydro-benzo[1,2,4]-triazin-3-yl)-[2,2']-bipyridine) ligand (Fig. 1a) was successfully studied and finally chosen as European reference molecule for MA partitioning.<sup>[3, 5-8]</sup> Due to rather slow extraction rates of CyMe<sub>4</sub>BTBP, a derivative, CyMe<sub>4</sub>BTPhen (2,9-bis(5,5,8,8-tetramethyl-5,6,7,8-tetrahydro-benzo[1,2,4]-triazin-3-yl)-1,10-phenanthroline) (Fig. 1b), was invented. This new ligand showed faster extraction kinetics, which is caused by its rigidity and the juxtaposition of the N-donor atoms in *cis* conformation that leads to a faster as well as thermodynamically favored complex formation.<sup>[9-11]</sup>

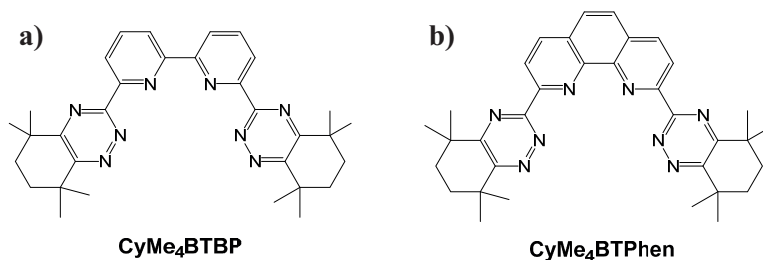


Fig. 1: Investigated ligand molecules CyMe<sub>4</sub>BTBP (a) and CyMe<sub>4</sub>BTPhen (b), which were irradiated as 10 mmol/L solutions in 1-octanol.

In this paper, we will study and compare the radiolytic stability of the before mentioned ligands CyMe<sub>4</sub>BTBP and CyMe<sub>4</sub>BTPhen and its influence on the actinide/lanthanide extraction. Therefore, radiolysis experiments were conducted at the Department of Chemical and Biochemical Engineering at the Chalmers University of Technology in Gothenburg, Sweden. A description of the gamma radiolysis experiments as well as liquid-liquid extraction can be found in our previous work.<sup>[12]</sup> Furthermore, quantitative and qualitative analyses were performed and the influence of nitric acid contact during irradiation was investigated. These measurements were done at the Institute of Inorganic Chemistry, Academy of Sciences, Husinec-Rež, Czech Republic.<sup>[12-13]</sup>

## 2. Results and Discussion

CyMe<sub>4</sub>BTBP and CyMe<sub>4</sub>BTPhen were irradiated in parallel (<sup>60</sup>Co, dose rate ~9.5 kGy/h) in 1-octanol solution (10 mmol/L) with and without contact to 1.0 mol/L nitric acid. Liquid-liquid extraction studies were performed and distribution ratios of <sup>241</sup>Am and <sup>152</sup>Eu were measured. For both ligands, decreasing Am(III)/Eu(III) D-values were observed with increasing absorbed dose, while CyMe<sub>4</sub>BTPhen started at higher initial distribution ratios (Fig. 2, filled symbols). This effect did not occur when the organic phase was irradiated in contact with a 1.0 mol/L nitric acid solution (Fig. 2, open symbols). Under these conditions, distribution ratios for both nuclides remained high. For CyMe<sub>4</sub>BTPhen in contact with nitric acid, an increasing/ decreasing behavior in the low-dose area for D<sub>Am</sub> was observed. This phenomenon could be attributed to a radiolytic buildup of extracting species (increasing D-values), which are prone to radiolysis themselves with increasing absorbed dose (decreasing D-values).

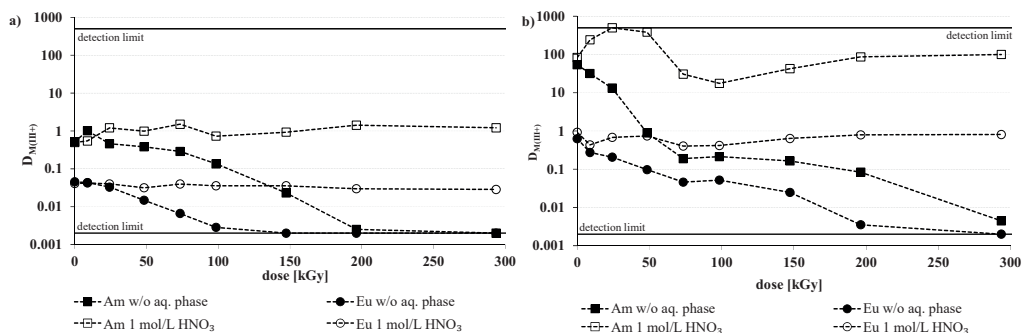


Fig. 2: Distribution ratios of  $^{241}\text{Am}$  and  $^{152}\text{Eu}$  as function of absorbed dose. Extraction experiment after  $\gamma$ -radiolysis of 10 mmol/L CyMe<sub>4</sub>BTBP (a, left) and CyMe<sub>4</sub>BTPhen (b, right) in 1-octanol. Irradiation was conducted as pure organic solution (filled symbols) and as organic solution in contact to 1.0 mol/L HNO<sub>3</sub> (open symbols).

Additional to solvent extraction studies, we conducted mass spectrometric measurements of the irradiated samples. Results for the CyMe<sub>4</sub>BTBP ligand can be found in Fig. 3 and data for the CyMe<sub>4</sub>BTPhen ligand are presented in Fig. 4 (with M = CyMe<sub>4</sub>BTBP/ CyMe<sub>4</sub>BTPhen and X =  $\alpha$ -hydroxyoctyl moiety, RC•HOH). Irradiation experiments of both ligands in contact with 1.0 mol/L nitric acid led to less different radiolysis products (Fig. 3b, Fig. 4b). Detected m/z ratios correspond mainly to addition products of the organic diluent, 1-octanol on the ligand molecules (X). These species (M+X, M+2X, M+3X) were also present in organic samples irradiated without nitric acid contact, but especially the M+X species could only be found in lower intensities.

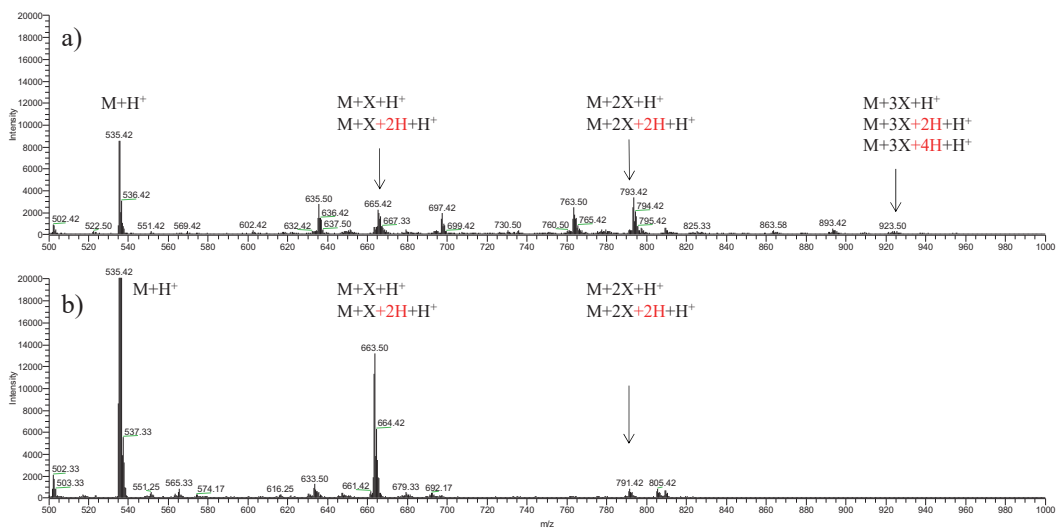


Fig. 3: Mass spectra of 10 mmol/L CyMe<sub>4</sub>BTBP in 1-octanol irradiated as organic solution without a) and with b) contact to 1.0 mol/L HNO<sub>3</sub>. Absorbed dose: 100 kGy. (Data were presented before)<sup>[12]</sup>

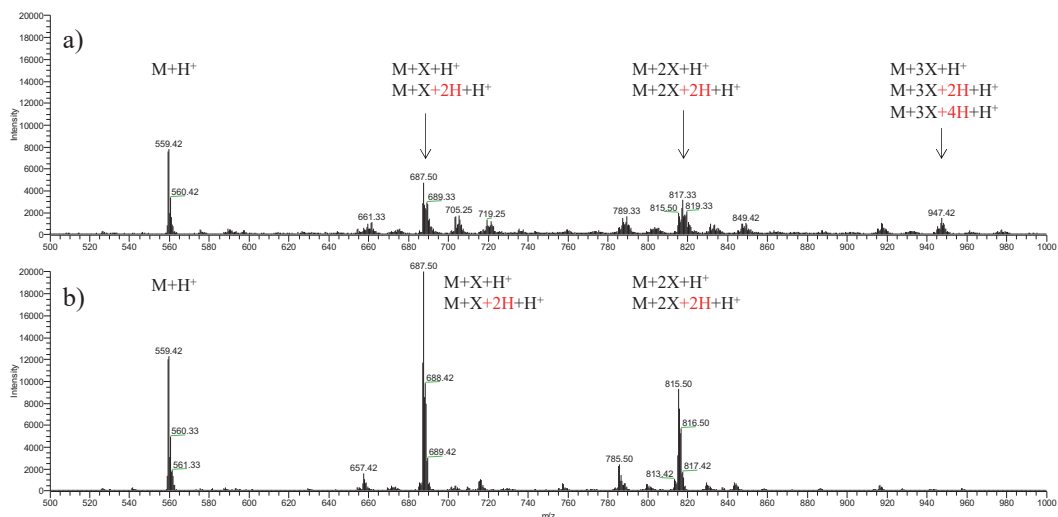
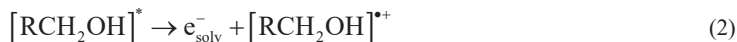


Fig. 4: Mass spectra of 10 mmol/L CyMe<sub>4</sub>BTPhen in 1-octanol irradiated as organic solution without a) and with b) contact to 1.0 mol/L HNO<sub>3</sub>. Absorbed dose: 100 kGy.

Furthermore, in irradiated solvents without nitric acid contact (Fig. 3b, Fig. 4b), the 1-octanol addition products were mainly formed with +2 and +4 higher mass units than the predicted molar masses ( $m/z$  ratio,  $z=1$ ) of 1-octanol addition products. These products could also be found in irradiated organic solutions in contact with nitric acid, but in contrast, the “pure”  $M+X$ ,  $M+2X$  and  $M+3X$  species were the dominant products here. The mechanism of alcohol radiolysis was described before:<sup>[14-17]</sup>



Following equations (1) and (2), a solvated electron and the octanol radical cation are formed during alcohol radiolysis. The solvated electron is able to react with new alcohol molecules resulting in hydrogen radicals (3) that are able to attack unsaturated bonds of the ligand molecules. This saturation leads to products with two mass units higher molar weight per saturated bond. When organic phases were irradiated in contact with nitric acid, hydrogen radicals and other reactive species were probably scavenged by  $NO_2^\bullet$  and  $NO_3^\bullet$  radicals that were formed during nitric acid radiolysis.<sup>[18]</sup> This scavenging reactions prevent double bonds from being saturated, in contrast to organic solutions irradiated without contact to nitric acid.

Equations (4) and (5) illustrate the formation of  $\alpha$ -hydroxyoctyl radicals, which can further react with the extractants to form 1-octanol addition products observed in the MS spectra (Fig. 3 and Fig. 4). This observation of 1-octanol molecule addition to N-donor ligands was made before by Wilden *et al.*<sup>[17]</sup> For both ligands, not only addition products of one 1-octanol molecule were found, but also two- and three-fold addition products were detected ( $M+X$ ,  $M+2X$  and  $M+3X$ ), while the  $M+3X$  addition product was only found in irradiated samples of pure organic phase without contact to a nitric acid phase. The formation of those addition products has no adverse effect

on extraction, since distribution ratios remained constantly high. Therefore, we predict the addition of 1-octanol radicals (X) takes place somewhere in the outer periphery of the molecules, as the nitrogen donor site binds to the metal ions. For sterical reasons, the pyridine moieties and the additional bond between those two in the CyMe<sub>4</sub>BTPhen molecule should be the preferred addition positions. New simulation results from Koubský *et al.* indicate the meta position of the pyridine moiety as the most probable position in the CyMe<sub>4</sub>BTBP molecule.<sup>[19]</sup>

Quantitative analyses were carried out to confirm this observation. Results can be found in Fig. 5, which shows decreasing concentrations for both ligands with increasing absorbed dose. After 196 kGy absorbed dose, nearly no ligand is left in both cases (CyMe<sub>4</sub>BTBP: 1%, CyMe<sub>4</sub>BTPhen: 0.5%). Irradiated samples in contact with nitric acid showed also decreasing ligand concentrations for both ligands, although the degradation was less severe. Especially CyMe<sub>4</sub>BTBP was protected even at higher doses. After 293 kGy absorbed dose, 53% of the initial concentration were left, whereas only 7% CyMe<sub>4</sub>BTPhen were remaining. This is in clear contrast to the results from solvent extraction (Fig. 2), which lets us conclude, that at least one of the new formed species is also able to extract Am(III) and Eu(III) to the organic phase.

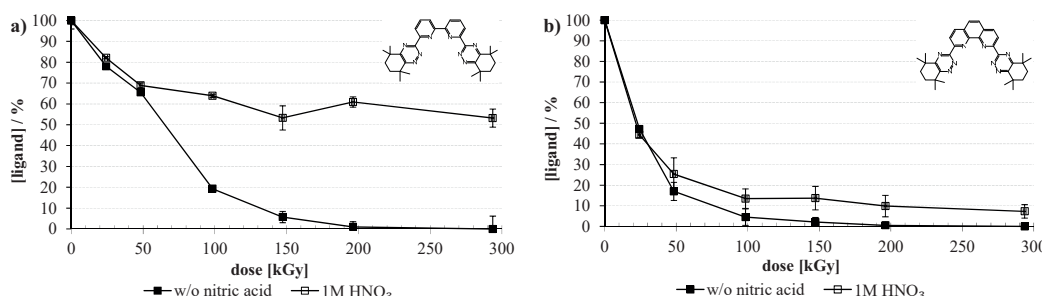


Fig. 5: Quantitative analysis of a) CyMe<sub>4</sub>BTBP and b) CyMe<sub>4</sub>BTPhen. Shown are irradiation experiments of neat organic solution (10 mmol/L ligand in 1-octanol) as filled symbols and organic solution in contact with 1.0 mol/L nitric acid as open symbols.

## Conclusion

The highly selective soft N-donor ligands CyMe<sub>4</sub>BTBP and CyMe<sub>4</sub>BTPhen were compared and studied under identical conditions for their radiolytic stability. A significant protective effect when irradiated in contact with nitric acid was found for both ligand molecules, especially with regard to distribution ratios, which remained nearly constant. Mass spectrometric analyses showed mainly the formation of 1-octanol addition products. A partial hydrogenation of those addition products was observed, which is attributed to the formation of hydrogen, hydrogen atoms and other reducing species through diluent radiolysis. Quantification of the ligand species itself showed a higher stability of the CyMe<sub>4</sub>BTBP ligand when irradiated in contact with acid in comparison to CyMe<sub>4</sub>BTPhen, for which the protective effect was much smaller. This acid protecting effect could also be seen in mass spectrometric measurements in which much higher intensities of the addition products in comparison to pure ligand molecules were detected.

## Acknowledgements

Financial support for this research is provided by the European Atomic Energy Community's 7<sup>th</sup> Framework program project SACSESS – grant agreement No. FP7-Fission-2012-323-282.



## References

1. Panak, P.J.; Geist, A. Complexation and Extraction of Trivalent Actinides and Lanthanides by Triazinylpyridine N-Donor Ligands. *Chem. Rev.* 2013, 113 (2), 1199-1236.
2. Hill, C.; Berthon, L.; Madic, C. Study of the stability of BTP extractants under radiolysis, Proceedings of GLOBAL 2005 2005, Tsukuba, Japan, 9-13 October, p 283.
3. Retegan, T.; Ekberg, C.; Englund, S.; Fermvik, A.; Foreman, M.R.S.; Skarnemark, G. The behaviour of organic solvents containing C5-BTBP and CyMe4-BTBP at low irradiation doses. *Radiochim. Acta* 2007, 95 (11), 637-642.
4. Fermvik, A.; Berthon, L.; Ekberg, C.; Englund, S.; Retegan, T.; Zorz, N. Radiolysis of solvents containing C5-BTBP: identification of degradation products and their dependence on absorbed dose and dose rate. *Dalton Trans.* 2009,(32), 6421-6430.
5. Geist, A.; Hill, C.; Modolo, G.; Foreman, M.R.S.J.; Weigl, M.; Gompper, K.; Hudson, M.J.; Madic, C. 6,6'-Bis(5,5,8,8-tetramethyl-5,6,7,8-tetrahydro-benzo[1,2,4]triazin-3-yl)[2,2']bipyridine, an effective extracting agent for the separation of americium(III) and curium(III) from the lanthanides. *Solvent Extr. Ion Exch.* 2006, 24 (4), 463-483.
6. Magnusson, D.; Christiansen, B.; Foreman, M.R.S.; Geist, A.; Glatz, J.P.; Malmbeck, R.; Modolo, G.; Serrano-Purroy, D.; Sorel, C. Demonstration of a SANEX Process in Centrifugal Contactors using the CyMe4-BTBP Molecule on a Genuine Fuel Solution. *Solvent Extr. Ion Exch.* 2009, 27 (2), 97-106.
7. Foreman, M.R.S.; Hudson, M.J.; Drew, M.G.B.; Hill, C.; Madic, C. Complexes formed between the quadridentate, heterocyclic molecules 6,6'-bis-(5,6-dialkyl-1,2,4-triazin-3-yl)-2,2'-bipyridine (BTBP) and lanthanides(III): implications for the partitioning of actinides(III) and lanthanides(III). *Dalton Trans.* 2006,(13), 1645-1653.
8. Retegan, T.; Ekberg, C.; Dubois, I.; Fermvik, A.; Skarnemark, G.; Wass, T.J. Extraction of Actinides with Different 6,6'-Bis(5,6-Dialkyl-[1,2,4]-Triazin-3-yl)-[2,2']-Bipyridines (BTBPs). *Solvent Extr. Ion Exch.* 2007, 25 (4), 417-431.
9. Lewis, F.W.; Harwood, L.M.; Hudson, M.J.; Drew, M.G.B.; Wilden, A.; Sypula, M.; Modolo, G.; Vu, T.-H.; Simonin, J.-P.; Vidick, G.; Bouslimani, N.; Desreux, J.F. From BTBPs to BTPPhs: The Effect of Ligand Pre-Organization on the Extraction Properties of Quadridentate Bis-Triazine Ligands. *Proc. Chem.* 2012, 7, 231-238.
10. Lewis, F.W.; Harwood, L.M.; Hudson, M.J.; Drew, M.G.B.; Hubscher-Bruder, V.; Videva, V.; Arnaud-Neu, F.; Stamberg, K.; Vyas, S. BTBPs versus BTPPhs: some reasons for their differences in properties concerning the partitioning of minor actinides and the advantages of BTPPhs. *Inorg. Chem.* 2013, 52 (9), 4993-5005.
11. Lewis, F.W.; Harwood, L.M.; Hudson, M.J.; Drew, M.G.B.; Desreux, J.F.; Vidick, G.; Bouslimani, N.; Modolo, G.; Wilden, A.; Sypula, M.; Vu, T.-H.; Simonin, J.-P. Highly Efficient Separation of Actinides from Lanthanides by a Phenanthroline-Derived Bis-triazine Ligand. *J. Am. Chem. Soc.* 2011, 133 (33), 13093-13102.
12. Schmidt, H.; Wilden, A.; Modolo, G.; Svehla, J.; Grüner, B.; Ekberg, C. Gamma radiolytic stability of CyMe4BTBP and effect of nitric acid. *Nukleonika* 2015, 60 (4), 879-884.
13. Fermvik, A.; Grüner, B.; Kvičalová, M.; Ekberg, C. Semi-quantitative and quantitative studies on the gamma radiolysis of C5-BTBP. *Radiochim. Acta* 2011, 99 (2), 113-119.
14. Mincher, B.J.; Arbon, R.E.; Knighton, W.B.; Meikrantz, D.H. Gamma-ray-induced degradation of PCBs in neutral isopropanol using spent reactor-fuel. *Appl. Radiat. Isot.* 1994, 45 (8), 879-887.
15. Freeman, G.R. Radiolysis of alcohols. *Actions Chim. Biol. Radiat.* 1970, 14, 73-134.
16. Swallow, A.J. Radiation Chemistry of the Liquid State: (2) Organic Liquids. Chap. 11 in *Radiation Chemistry - Principles and Applications*, Farhat Aziz; Rodgers, M.A.J., VCH Verlagsgesellschaft mbH: Weinheim, Germany, pp 351-375, 1987.
17. Wilden, A.; Modolo, G.; Hupert, M.; Santiago-Schübel, B.; Löfström-Engdahl, E.; Halleröd, J.; Ekberg, C.; Mincher, B.J.; Mezyk, S.P. Gamma-radiolytic stability of solvents containing C5-BPP (2,6-Bis(5-(2,2-dimethylpropyl)-1H-pyrazol-3-yl)pyridine) for actinide(III)/lanthanide(III) separation. *Solvent Extr. Ion Exch.* 2016, 34 (1), 1-12.
18. Katsumura, Y. NO<sub>2</sub>• and NO<sub>3</sub>• Radicals in Radiolysis of Nitric Acid Solutions. Chap. 12 in *The Chemistry of Free Radicals: N-Centered Radicals*, Alfassi, Z.B., Wiley: Weinheim, pp 393-412, 1998.
19. Koubsky, T.; Schmidt, H.; Modolo, G.; Kalvoda, L. Simulation of UV/vis spectra of CyMe4-BTBP and some of its degradation products. *Proc. Chem.* 2016, same issue.

## Paper 3<sup>[88]</sup>

Koubský, T.; Schmidt, H.; Modolo, G.; Kalvoda, L. Simulation of UV/VIS Spectra of CyMe<sub>4</sub>BTBP and some of its degradation products. *Procedia Chem.* **2016**, *21*, 509-516.

DOI: 10.1016/j.proche.2016.10.071

Contribution:

For this paper, I did all experimental work. The simulation work was mainly done by the leading author of this paper.



5<sup>th</sup> International ATALANTE Conference on Nuclear Chemistry for Sustainable Fuel Cycles

## Simulation of UV/vis spectra of CyMe<sub>4</sub>BTBP and some of its degradation products

Tomáš Koubský<sup>a\*</sup>, Holger Schmidt<sup>b</sup>, Giuseppe Modolo<sup>b</sup>, Ladislav Kalvoda<sup>a</sup>

<sup>a</sup>Czech Technical University in Prague, Department of Solid State Engineering, Trojanova 13, Prague 12000, Czech Republic

<sup>b</sup>Forschungszentrum Jülich GmbH, Institut für Energie- und Klimaforschung - Nukleare Entsorgung und Reaktorsicherheit - (IEK 6), Jülich, Germany.

---

### Abstract

Wet extraction and selective separation methods of actinide elements from highly active spent nuclear fuel constitutes a key step in the current waste reprocessing technologies. The quadridentate 6,6'-bis(1,2,4-triazin-3-yl)-2,2'-bipyridine ligands (BTBPs) form a very promising group of extraction agents investigated at recent. Radiation decay process of one of the BTBPs representatives, CyMe<sub>4</sub>BTBP, is indirectly analyzed by simulating the UV-Visible absorption spectra of the original compound and one proposed possible CyMe<sub>4</sub>BTBP and 1-octanol adduct and comparing the obtained courses with experimentally observed data. Ab-initio TDDFT approach using 6-31++G(d,p) basis set and wB97X, CAM-B3LYP, LC-wPBE functionals is applied. Partial agreement of the simulated and experimental data is found and discussed.

© 2016 The Authors. Published by Elsevier B.V. This is an open access article under the CC BY-NC-ND license (<http://creativecommons.org/licenses/by-nc-nd/4.0/>).

Peer-review under responsibility of the organizing committee of ATALANTE 2016

**Keywords:** CyMe<sub>4</sub>-BTBP; ab-initio DFT; TDDFT; UV-Vis spectra; gamma irradiation

---

### 1. Introduction

During several past decades, much effort has been spent on development of wet extraction and selective separation methods of actinide elements from highly active spent nuclear fuel. The latter constitute a key step in the current waste reprocessing technologies.<sup>1</sup>

---

\* Corresponding author. Tel.: +420-22435-8638 ; fax: +420-22435-8601.

E-mail address: [tomas.koubsky@tfjfi.cvut.cz](mailto:tomas.koubsky@tfjfi.cvut.cz)

One strategy for reducing the radiotoxicity of the remaining waste involves partitioning and transmutation of the long-lived minor actinides into shorter-lived or stable elements by neutron fission. However, it is, at first, necessary to separate the actinides from the lanthanides and other fission products due to the high cross sections of lanthanides for neutron capture. Therefore, separation of the radioactive minor actinides from the lanthanides itself represents one of the main challenges of today's nuclear waste reprocessing.<sup>2</sup>

It has been shown that ligands with soft N-donor atoms can distinguish between the actinides and lanthanides. Among others, the N-heterocyclic ligand class have emerged as a particularly promising one: the quadridentate 6,6'-bis(1,2,4-triazin-3-yl)-2,2'-bipyridine ligands (BTBPs) with its representative CyMe<sub>4</sub>BTBP (Figure 1). In general, the BTBP ligands can be considered as currently the most suitable ligands for the herein mentioned separation tasks.<sup>3,4</sup>

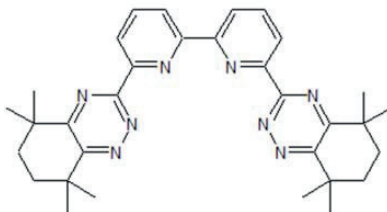


Figure 1: Chemical formula of CyMe<sub>4</sub>BTBP

To evaluate the applicability of extractants for process development, it is necessary to demonstrate not only their good extraction and selective properties, but also their resistance against degradation caused by contact of the extracting phase with highly radioactive solutions and highly concentrated nitric acid. Detailed investigation of the degradation mechanisms of CyMe<sub>4</sub>BTBP and identification of its degradation products is thus very desirable in relation to the further extraction process development.

In this paper, we present results of quantum mechanical simulations of one type of the expected major degradation products. The structure guess was made according to measured mass spectra of CyMe<sub>4</sub>BTBP 1-octanol solution before and after irradiation. Together with that, we present evolution of UV-Visible absorption spectra measured on the same experimental system and compare them with the simulated spectra calculated both for the pure CyMe<sub>4</sub>BTBP and the selected degradation product by several quantum mechanical simulation methods.

## 2. Computational / experimental details

For the geometrical optimizations, the Density Functional Theory (DFT) method was used as implemented in the Gaussian 09 code, with the hybrid exchange-correlation functional B3LYP<sup>5,6,7,8</sup> and the 6-31G(d,p) basis set. The PCM cavity approximation of solvent is used with 1-octanol.<sup>9</sup> For the simulation of UV-Visible absorption spectra, the time-dependent DFT (TDDFT) method was used together with the 6-31++G(d,p) basis and three different long range corrected exchange and correlation functionals: wB97X<sup>10</sup>, CAM-B3LYP<sup>11</sup>, and LC-wPBE<sup>12,13,14</sup>. These three different methods were used in order to evaluate the level of the possible dependence of the calculated electronic excitations on the applied ab-initio theory level. Comparison of the results obtained by the three selected widely used methods provides an estimate of such dependence. The relaxation level of transition state was confirmed by subsequent vibrational analysis.

## 3. Results and discussion

### 3.1. CyMe<sub>4</sub>BTBP molecular structure

As already shown, the free BTBP-type ligands are expected to adopt the 'trans' conformation (the molecule is close to C<sub>2h</sub> symmetry; trans-CyMe<sub>4</sub>BTBP in Figure 2), where the central bond between two pyridine rings comprises the center of symmetry; the 'cis' conformation (C<sub>2v</sub> point group) is less energetically favored.<sup>4,15</sup> The

results calculated for CyMe<sub>4</sub>BTBP confirmed such expectation: the ‘cis’ conformation is 5.7 kcal/mol higher in energy than the ‘trans’ conformation possessing the activation energy 8.1 kcal/mol. Accordingly, we further assume that majority of CyMe<sub>4</sub>BTBP molecules in the solution adopt the ‘trans’ conformation. The further investigation shows that also the torsion angle of the triazine-pyridine bonds plays a role in the total energy of the molecule. Turning of such bond by 180 degrees with respect to the complexing conformation (bond L; trans-CyMe<sub>4</sub>BTBP-L in Figure 2) causes the drop in energy of about 0.3 kcal/mol. Changing the torsion angle of the second triazine-pyridine bond has the same effect (see Table 1)

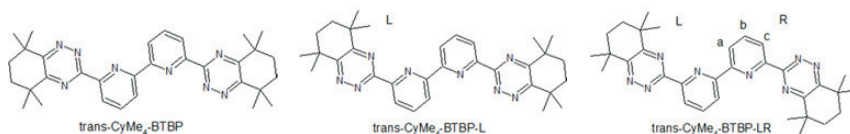


Fig. 2. Chemical conformations of CyMe<sub>4</sub>-BTBP. In the trans-CyMe<sub>4</sub>BTBP-LR structure, the probable position of the C8H17O group are marked (a, b, and c).

Table 1. Energy of different CyMe<sub>4</sub>BTBP conformations.

Molecular system	potential energy (kcal/mol)
trans-CyMe <sub>4</sub> BTBP-LR	0.00
trans-CyMe <sub>4</sub> BTBP-L	0.27
trans-CyMe <sub>4</sub> BTBP	0.63
cis-CyMe <sub>4</sub> BTBP	6.30

### 3.2. Prevailing reaction products

The HPLC-MS analysis of irradiated CyMe<sub>4</sub>BTBP solutions in 1-octanol showed that in such case no degradation of the distribution ratios occurs and the resulting solution contains, in addition to the original CyMe<sub>4</sub>BTBP molecules, some adduct of 1-octanol to CyMe<sub>4</sub>BTBP.<sup>16</sup> It is thus plausible to expect that the core structure of the adducts - involving the vicinity of the complexing nitrogen atoms - remains the same as in CyMe<sub>4</sub>BTBP. Based on this assumption, we have selected three positions where the octanol can be attached to the CyMe<sub>4</sub>BTBP molecule (see trans-CyMe<sub>4</sub>BTBP-LR in Figure 2) and optimized the structures (marked A, B, C in figure 3).

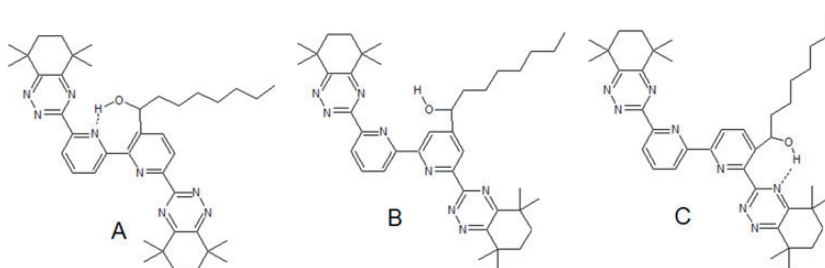


Fig. 3. Chemical structures of the investigated adducts of CyMe<sub>4</sub>BTBP and 1-octanol.

In this case, the role of torsion of the triazine-pyridine bond is further complicated by the interaction of the alpha-hydroxyoctyl function group with the remaining structure. Therefore, the core conformation is not identical in this case with the above described trans-CyMe<sub>4</sub>BTBP-LR conformation, most favorable in case of the original CyMe<sub>4</sub>BTBP molecule. After the geometrical optimization, the energy of formation was calculated and compared

for all three structures. The obtained energetic difference between the structures A, B, C is small, presumably comparable to the energy of thermal vibrations.

Assuming that the attachment of the alpha-hydroxyoctyl group runs through the nucleophilic substitution, the most susceptible position of the reaction should be position 'b' thanks to the inductive effect. Surprisingly, the structure B is not the one showing the lowest energy. On the other hand, in structures A and C, the possibility of an H-bond creation between the alpha-hydroxyoctyl group and the neighboring triazine or pyridine group arises equalizing likely the preference of the 'b' position and causing that the structures A and C can successfully compete with the structure B. The conformations of A, B, and C with the lowest energy are depicted in Figure 3 and their energy is presented in Table 2. Since the energy differences of the structures A, B, and C are small and significantly sensitive to small possible conformation changes, all three structures should be incorporated in further investigations.

Table 2. Energy of formation calculated for the optimized molecular structures.

Molecular system	potential energy (kcal/mol)
product A	0.00
product B	0.64
product C	4.00

### 3.3. UV-Visible absorption spectra

The experimental UV-Visible absorption spectra recorded before and after several different doses of gamma irradiation are presented in figure 4. With the absorbed dose increasing up to 200 kGy, the broad absorption bands between 220 - 300 nm decrease in intensity. Further irradiation results in a slight reversal of the intensity decay in the range of longer wavelengths (~ 240 - 320 nm). The short wavelengths absorption is steadily growing with the absorbed dose. Within a close vicinity of the wavelength point located at ca. 215 nm, the observed spectral courses corresponding to the different irradiation doses are intersecting, suggesting thus the possibility that the observed spectral changes can be interpreted by a chemical transition of the initial CyMe<sub>4</sub>BTBP molecules into a mixture of products characterized (in average) by a stronger extinction in the region at the "left" and a weaker extinction at the "right" from the intersection region. Remarkably, the spectrum measured after irradiation with 300 kGy dose digresses from the previous monotonic spectral evolution both in sense of the red shift of the intersection point and the reversal of the extinction decay in the region of wavelengths longer than 240 nm. Such behavior can suggest that the original CyMe<sub>4</sub>BTBP molecules are already depleted and some next step of the radiation decay starts to proceed.

In order to confirm selection of the representative products A, B, and C, the UV-Visible absorption spectra were simulated for both CyMe<sub>4</sub>BTBP and the chosen degradation products and the results compared with the experimental data. The spectra obtained for original CyMe<sub>4</sub>BTBP molecule are presented in figure 5. The result obtained with the wB97XD functional can be perhaps preferred because of a closer similarity of the calculated spectral course with the experimental one as well as due to the fact that the CAM-B3LYP functional has provided very similar results and supported the reliability of them.

The calculated envelope curves are featuring four absorption maxima within the studied region for LC-wPBE; the short-wavelength maximum predicted by xB97XD (~ 198 nm) is very weak and coincides with the shoulder of the stronger band localized at ca ~ 220 nm in case of the CAM-B3LYP. The spectra obtained with wB97XD and CAM-B3LYP are close to each other in the region of longer wavelengths but differ in the oscillator strength and position of the high energy band. Much weaker absorption of the latter is predicted by CAM-B3LYP. The spectral course calculated using LC-wPBE is comparable in shape to the ones obtained with wB97XD and CAM-B3LYP, but the positions of maxima show all a 15-20 nm blue shift. With exception of the results obtained with CAM-B3LYP functional, the simulated spectra contain the same number of absorption maxima as the experimental courses; however, the calculated band positions show all a significant blue shift (~ -30 nm for the spectra calculated with wB97XD and CAM-B3LYP) compared with the experimental ones. Energetic shift of such extent (0.3-0.4 eV) and direction have been already reported in connection with TDDFT simulations of electronic excitations in small organic molecules.<sup>17</sup>

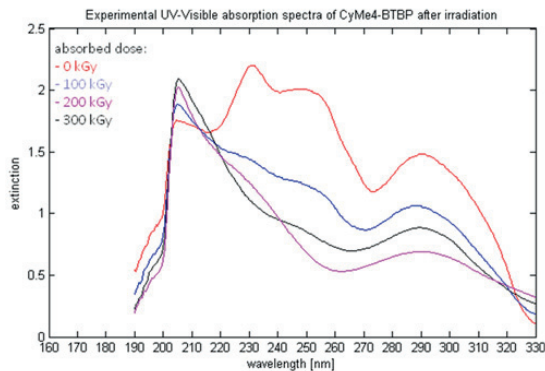


Fig. 4. Experimental absorption spectra of CyMe<sub>4</sub>BTBP in 1-octanol after various absorbed doses with absorption maxima at 205.0 nm, 231.5 nm, and 290.5 nm.

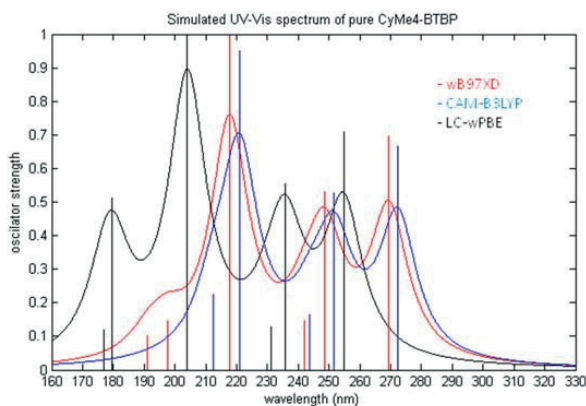


Fig. 5. Simulated absorption spectra of CyMe<sub>4</sub>BTBP by TDDFT / wB97XD, CAM-B3LYP, LC-wPBE.

Spectral positions of electronic transitions calculated for the molecular fragments A, B, and C (figure 6) are similar to those obtained for CyMe<sub>4</sub>BTBP but the computed oscillator strength of the most intense absorption band at ~ 220 nm is remarkably reduced. Again, the spectrum calculated with LC-wPBE is blue-shifted in respect to the two other spectra. The very weak maximum at the blue-side shoulder of the 220 nm band is missing in case of the C-structure and wB97XD and CAM-B3LYP functionals; however, the maximum is preserved in the LC-wPBE spectra. The apparent differences in the intensity and position of the two maxima at ~ 250 nm and ~ 270 nm between A, B, and C are probably linked to the different torsion angles of the triazine-pyridine bonds. The effect appears in the results obtained with all three applied theoretical methods. Taking in account the already mentioned systematic shift in energy between the calculated and experimental spectra, and the fact that the real experimental absorption spectrum is composed from contributions of all thermodynamically feasible molecular structures existing in the solution under test, the simulated spectra qualitatively agree with the observed evolution of the experimental spectra in the spectral region ~ 215-320 nm. On the other hand, the observed increase of extinction in the region of short wavelengths is not copied by the simulated spectra of the compounds A, B, and C. In this regard, the closest match provides the LC-wPBE functional.



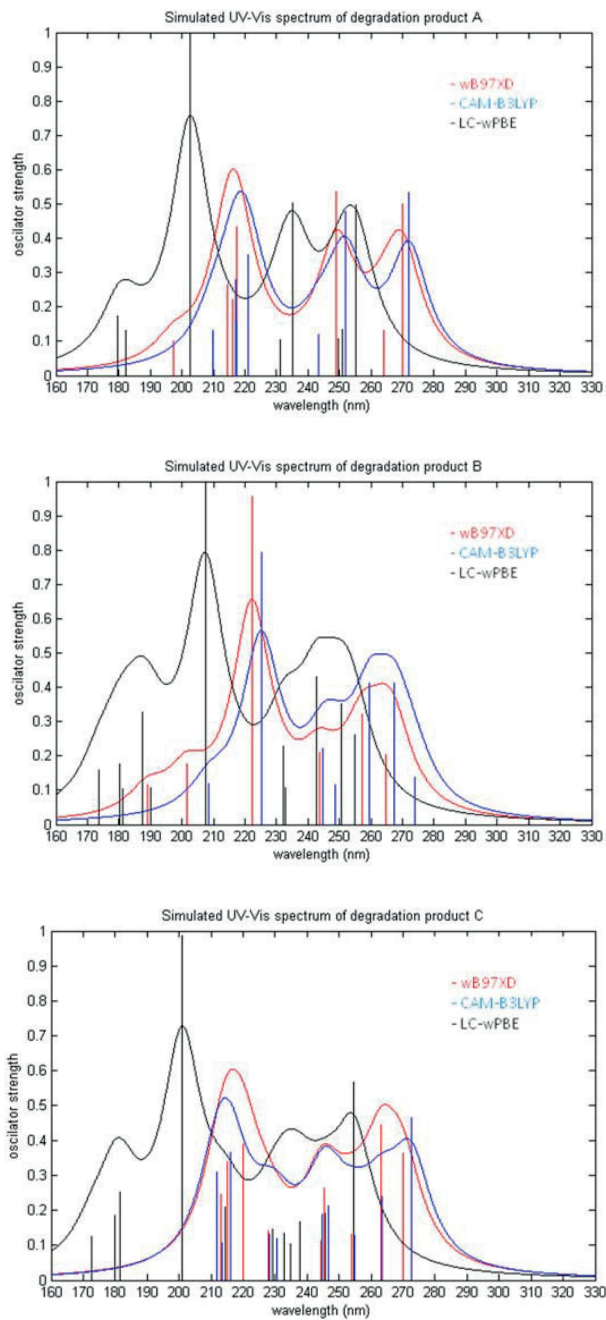


Fig. 6. Simulated absorption spectra of the structures A, B, and C by TDDFT / wB97XD, CAM-B3LYP, LC-wPBE.

Evaluation of the electronic transitions obtained with the wB97XD functional shows that the main excitations occur predominantly between the  $\pi$  orbitals energetically close to the HOMO and the  $\pi^*$  orbitals close to the LUMO (the details are not presented due to the restricted article extend). We furthermore note that because the dominant orbitals involved in the electronic transitions are only weakly affected by the presence of the 1-octanol chain, no substantial change of the UV-Vis. spectra can be expected due to the changing the binding positions 'a', 'b', and 'c'.

#### 4. Conclusions

The molecular structure of CyMe<sub>4</sub>BTBP and three possible degradation products were optimized by the quantum mechanical simulation methods and its molecular structure features were investigated. For the original structure and three probable degradation products selected on the basis of the HPLC-MS analysis, UV-Visible spectra were simulated and compared with the experimental results. The different simulation methods were found to be qualitatively in agreement. The changes in simulated spectra between the original ligand and the products with one 1-octanol group attached correlate at least qualitatively with the observed evolution of the experimental spectra at the longer measured wavelengths. However, the extinction enhancement with the absorbed dose that is observed at the high energy end of the experimental spectra has no adequate counterpart in the simulated results. Thus, a larger group of the possible products of the CyMe<sub>4</sub>BTBP radiation induced transformation must be considered and tested.

The real experimental spectra are measured at thermodynamic conditions allowing for existence of thermally excited molecular conformations contributed thus to the resulting spectral course. Fitting of the experimental spectrum by a simulated course constructed as a weighted average of the selected, most thermodynamically feasible molecular/conformation constituents could provide us with an improved level of the agreement between the experimental and the simulated results. Results obtained with the use of such procedure will be presented in the forthcoming article.

#### Acknowledgements

This work has been carried out under the European SACSESS Project (FP7-Fission-2012-323-282). Methodical support is acknowledged of the Student Grant System of the Czech Technical University in Prague (Grant No. SGS13/219/OHK4/3T/14) and the Czech Science Foundation (grant No. 14-36566G). Access to computing and storage facilities owned by parties and projects contributing to the National Grid Infrastructure MetaCentrum, provided under the programme 'Projects of Large Infrastructure for Research, Development, and Innovations' (LM2010005) is greatly appreciated. The authors would like to thank prof. Jaroslav Burda for invaluable discussions.

#### References

1. Madić C. Overview of the Hydrometallurgical and Pyrometallurgical Processes Studied Worldwide for the Partitioning of High Active Nuclear Wastes. Proc. of OCDE-NEA 6th Information Exchange Meeting on P&T: Madrid; 2000, p. 53-6.
2. Mathur JN, Murali MS, Nash KL. Actinide partitioning - A review. *Solvent Extraction and Ion Exchange*. 2001; **19**: 357-390.
3. Geist A, Hill C, Modolo G, Foreman M, Weigl M, Gompfer K, Hudson MJ. 6,6'-Bis(5,5,8,8-tetramethyl-5,6,7,8-tetrahydrobenzo[1,2,4]triazin-3-yl) [2,2'] bipyridine, an Effective Extracting Agent for the Separation of Americium(III) and Curium(III) from the Lanthanides. *Solvent Extraction and Ion Exchange*. 2006; **24**: 463-483.
4. Foreman M, Hudson MJ, Drew MGB, Hill C, Madić C. Complexes formed between the quadridentate, heterocyclic molecules 6,6'-bis-(5,6-dialkyl-1,2,4-triazin-3-yl)-2,2'-bipyridine (BTBP) and lanthanides(III): implications for the partitioning of actinides(III) and lanthanides(III). *Dalton Transactions*. 2006; **13**: 1645-1653.
5. Becke AD. Density - functional thermochemistry. III. The role of exact exchange. *J. Chem. Phys.* 1993; **98**: 5648-5652.
6. Lee C, Yang W, Parr RG. Development of the Colle-Salvetti correlation-energy formula into a functional of the electron density. *Phys. Rev. B*. 1988; **37**: 785-789.
7. Vosko SH, Wilk L, Nusair M. Accurate spin-dependent electron liquid correlation energies for local spin density calculations: A critical analysis. *Can. J. Phys.* 1980; **58**: 1200-1211.
8. Stephens PJ, Devlin FJ, Chabalowski CF, Frisch MJ. Ab Initio Calculation of Vibrational Absorption and Circular Dichroism Spectra Using Density Functional Force Fields. *J. Phys. Chem.* 1994; **98**: 11623-11627.
9. Tomasi J, Mennucci B, Cammi R. 2005. Quantum mechanical continuum solvation models. *Chemical Review*. 2005; **105**: 2999-3093.
10. Chai JD, Head-Gordon M. Systematic optimization of long-range corrected hybrid density functionals. *J. Chem. Phys.* 2008; **128**: 084106.

11. Yanai T, Tew D, Handy N. A new hybrid exchange-correlation functional using the Coulomb-attenuating method (CAM-B3LYP). *Chem. Phys. Lett.* 2004; **393**: 51-57.
12. Vydrov OA, Scuseria GE. Assessment of a long range corrected hybrid functional. *J. Chem. Phys.* 2006; **125**: 234109.
13. Vydrov OA, Heyd J, Krukau A, Scuseria GE. Importance of short-range versus long-range Hartree-Fock exchange for the performance of hybrid density functionals. *J. Chem. Phys.* 2006; **125**: 074106.
14. Vydrov OA, Scuseria GE, Perdew JP. Tests of functionals for systems with fractional electron number. *J. Chem. Phys.* 2007; **126**: 154109.
15. Lewis FW, Harwood LM, Hudson MJ, Drew MGB, Hubscher-Bruder V, Videva V, Arnaud-Neu F, Stamberg K, Vyas S. BTBPs versus BTPPhens: Some Reasons for Their Differences in Properties Concerning the Partitioning of Minor Actinides and the Advantages of BTPPhens. *Inorganic Chemistry*. 2013; **52**: 4993-5005.
16. Schmidt H, Wilden A, Modolo G, Švehla J, Grüner B, Ekberg C. Gamma radiolytic stability of CyMe<sub>4</sub>BTBP and the effect of nitric acid. *NUKLEONIKA* 2015; **60**: 879-884.
17. Furche F, Rappoport D. Density functional methods for excited states: equilibrium structure and electronic spectra. *Theoretical and Computational Chemistry*. 2005; **16**: 93-128.

## Paper 4<sup>[133]</sup>

Szreder, T.; Schmidt, H.; Modolo, G. Fast radiation-induced reactions in organic phase of SANEX system containing CyMe<sub>4</sub>BTPhen extracting agent. *Rad. Phys. Chem.* **2019**, *164*, 108356.

DOI: 10.1016/j.radphyschem.2019.108356

### Contribution:

For this work, the leading author and I conducted pulse radiolysis experiments on 1-octanol as well as on the CyMe<sub>4</sub>BTPhen system, and interpretation of the results together. Additionally, I participated in manuscript preparation.





# Fast radiation-induced reactions in organic phase of SANEX system containing CyMe<sub>4</sub>-BTPPh extracting agent

T. Szreder<sup>a,\*</sup>, H. Schmidt<sup>b</sup>, G. Modolo<sup>b</sup>

<sup>a</sup> Institute of Nuclear Chemistry and Technology, Dorodna 16, 03-195, Warsaw, Poland

<sup>b</sup> Forschungszentrum Jülich GmbH, Nukleare Entsorgung und Reaktorsicherheit (IEK-6) Leo-Brandt-Straße, 52428, Jülich, Germany

## ARTICLE INFO

### Keywords:

Radiation chemistry  
Pulse radiolysis  
SANEX  
Minor actinide extraction  
1-Octanol  
CyMe<sub>4</sub>-BTPPh  
Spent nuclear fuel reprocessing  
Nuclear science

## ABSTRACT

The mechanism of radiation-induced fast reactions occurring in the early stages in the 1-octanol system containing 2,9-Bis-(5,5,8,8-tetramethyl-5,6,7,8-tetrahydro-benzo (Herbst et al., 2011; Nash et al., 2015; Bourg et al., 2015)triazin-3-yl)- (Herbst et al., 2011; Panak and Geist, 2013)phenanthroline (CyMe<sub>4</sub>-BTPPh) extracting agent were studied. This is a simplified model of the r-SANEX organic phase for the selective actinide(III)/lanthanide (III) separation. Effects of various scavengers as well as water content were under consideration. Radiation chemical yield of  $e_s^-$  ( $G(e_s^-)$ ) and their molar absorption coefficient ( $\epsilon(e_s^-)$ ) in 1-octanol were found to be 130(10) nmol J<sup>-1</sup> and 18500(700) M<sup>-1</sup> cm<sup>-1</sup>, respectively. Rate constants of  $e_s^-$  reactions with H<sup>+</sup>, O<sub>2</sub>, CyMe<sub>4</sub>-BTPPh and its protonated form were found to be 1.5(3) × 10<sup>9</sup>, 1.0(1) × 10<sup>10</sup>, 1.85(9) × 10<sup>9</sup>, 1.9(6) × 10<sup>9</sup> M<sup>-1</sup> s<sup>-1</sup>, respectively. The C<sub>37</sub> value for scavenging of dry electrons ( $e_{dry}^-$ ) by CyMe<sub>4</sub>-BTPPh was equal to 30.4(8) mM. Rate constants of H<sup>+</sup> reactions with CyMe<sub>4</sub>-BTPPh and its protonated form were found to be < 7.2 × 10<sup>9</sup> and 4.3(9) × 10<sup>9</sup> M<sup>-1</sup> s<sup>-1</sup>, respectively. A relatively good extraction performance of the system studied under exposition to high radiation doses was explained on the basis of hydroxyoctyl substitution in a phenanthroline aromatic ring.

## 1. Introduction

Separation of plutonium and uranium from the spent nuclear fuel in various versions of the Plutonium and Uranium Recovery by Extraction (PUREX) process has been used by the industry in several countries for many years (Herbst et al., 2011; Nash et al., 2015). Such approach significantly saves energy resources and reduces potential radiotoxicity hazard of wastes from approximately 250 000 to 10 000 years. Further reduction of radiotoxicity and heat loading, and hence the footprint of a geological disposal facility can be achieved by minor actinide (MA) transmutation followed by their separation from PUREX raffinate (Poinssot et al., 2015; Bourg et al., 2015; Modolo et al., 2015). Multi-step concepts, e.g. the diamide extraction (DIAMEX) followed by regular selective actinide extraction (r-SANEX), processes, have been developed to separate the MA. Alternatively single cycle processes were proposed, such as the 1-cycle SANEX, innovative SANEX, and EXAM processes (Modolo et al., 2015; Wilden et al., 2011, 2015).

Bis(triazinyl)pyridines (BTPs) ligands were proposed for the selective separation of trivalent actinides from lanthanides (r-SANEX). Development of that type of ligands was the first attempt of intentional structural modifications to adopt molecules for the nuclear fuel cycle

(Hudson et al., 2013; Bobrowski et al., 2016). The first generation of BTPs (e.g. 2,6-bis(5,6-dialkyl-1,2,4-triazin-3-yl)pyridine) (Fig. 1) was vulnerable both to oxidative and radiolytic degradation (Panak and Geist, 2013). Since degradation was proposed to be initiated by H-atom abstraction from the benzylic position of the alkyl substituents on the triazine, efforts were made to replace them by the groups less susceptible to hydrogen abstraction. Especially, the substituents without H atoms at the vulnerable positions were tested. A compromise between stability, extractant solubility and extraction capabilities of the newly designed molecules was found for cyclohexyl moieties substituted with methyl groups in the benzylic positions (CyMe<sub>4</sub>, Fig. 1) (Panak and Geist, 2013). Furthermore, in order to eliminate problems with stripping-back ligated metal ions, the improved structure based on a bipyridine skeleton was designed leading to 6,6'-bis(5,5,8,8-tetramethyl-5,6,7,8-tetrahydro-benzo-1,2,4-triazin-3-yl)-2,2'-bipyridine (CyMe<sub>4</sub>-BTBP, Fig. 1) (Hudson et al., 2013). The CyMe<sub>4</sub>-BTBP ligand is currently considered as an European standard for development of selective actinide separation (Panak and Geist, 2013). In addition, it was shown that extraction kinetics of CyMe<sub>4</sub>-BTBP can be improved by intramolecular pre-organization of the molecule in which the 2,2'-bipyridine moiety was replaced by a 1, 10-phenanthroline leading

\* Corresponding author.

E-mail address: [t.szreder@ichtj.waw.pl](mailto:t.szreder@ichtj.waw.pl) (T. Szreder).

<https://doi.org/10.1016/j.radphyschem.2019.108356>

Received 28 December 2018; Received in revised form 31 May 2019; Accepted 6 June 2019

Available online 07 June 2019

0969-806X/© 2019 Elsevier Ltd. All rights reserved.

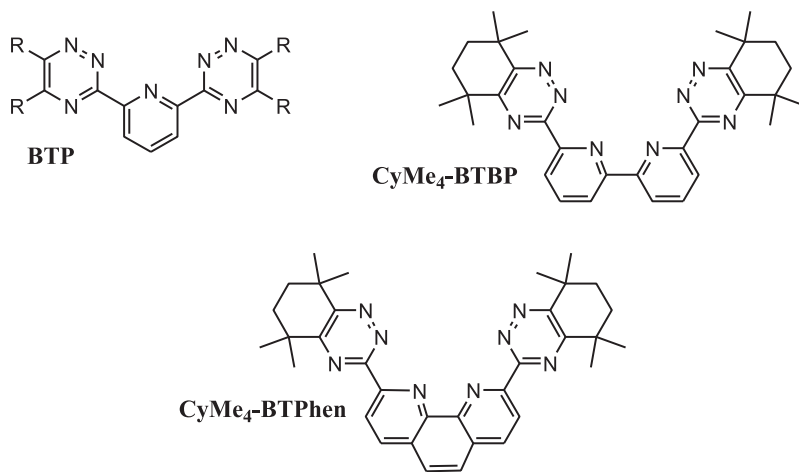


Fig. 1. Structures of BTP, CyMe<sub>4</sub>-BTBP and CyMe<sub>4</sub>-BTPhen ligands.

ultimately to 2,9-Bis-(5,5,8,8-tetramethyl-5,6,7,8-tetrahydro-benzo (Herbst et al., 2011; Nash et al., 2015; Bourg et al., 2015)triazin-3-yl)-(Herbst et al., 2011; Panak and Geist, 2013)phenanthroline (CyMe<sub>4</sub>-BTPhen, Fig. 1).

Typically, concentrations of these ligands in extraction system do not exceed 10 mM. This is mostly due to their limited solubility in organic diluents (e.g. the solubility of CyMe<sub>4</sub>-BTBP in 1-octanol-based diluents is in the range of 10–20 mM (Panak and Geist, 2013)). At these concentrations a direct interaction of ionizing radiation with the ligands is very unlikely. Thus, the observed deterioration in the extraction performance in irradiated systems is mainly due to secondary reactions of radicals, radical-ions and permanent products (generated from the diluents) with the ligands. Several diluents were proposed for r-SANEX system. Various cyclohexanone derivatives, phenyl trifluoromethyl sulfone, neat 1-octanol, and 1-octanol in mixture with hydrocarbons (kerosene, up to 30%) were used (Panak and Geist, 2013; Hallerod et al., 2015; Anaheim et al., 2012). The latter system is the most promising (Panak and Geist, 2013). In our studies, we focused on 1-octanol as a simplified model of the r-SANEX diluent. Knowledge of the mechanism of radiation induced reactions in the CyMe<sub>4</sub>-BTPhen/1-octanol system occurring in the early stages was the main aim of the studies. Effects of typical scavengers as well as water content in the system was also under consideration.

## 2. Materials and methods

2,9-Bis-(5,5,8,8-tetramethyl-5,6,7,8-tetrahydro-benzo (Herbst et al., 2011; Nash et al., 2015; Bourg et al., 2015)triazin-3-yl)-(Herbst et al., 2011; Panak and Geist, 2013)phenanthroline (CyMe<sub>4</sub>-BTPhen, Fig. 1.) was obtained from Technocomm LTD (UK) with a purity of 99 % and used as received. All other chemicals were purchased from Sigma-Aldrich with the highest available purity. Water purified in the Direct Q3UV (Merck Millipore) system was used in all experiments.

Pulse radiolysis experiments with fast optical absorption detection were carried out at the Institute of Nuclear Chemistry and Technology in Warsaw, Poland. The pulse radiolysis set-up is based on the LAE-10 linear electron accelerator delivering 10 ns pulses with an electron energy of about 10 MeV. The 150 W xenon arc lamp E7536 (Hamamatsu Photonics K.K) was used as a monitoring light source. The respective wavelengths were selected either by a MSH 301 (Lot Oriol Gruppe) monochromator with resolution 2.4 nm or by bandpass filters (Standa Ltd) with FWHM about 40 nm above 750 nm. The intensity of

the analyzing light was measured by means of PMT R955 (Hamamatsu) below 750 nm, and by Si amplified diode PDA10A (Thorlabs) up to 1150 nm. A signal from the detector was digitized using a WaveSurfer 104MXs-B (1 GHz, 10 GS/s, LeCroy) oscilloscope and then send to PC for further processing. In order to avoid photodecomposition and/or photobleaching effects in the samples, the UV or VIS cut-off filters were used. However, no evidence of such effects was found within the time domains monitored. If necessary, a water filter was used to eliminate near IR wavelengths. All experiments were performed in a standard quartz cell with an optical pathlength of 1 cm and at 22 °C.

The total dose per pulse was determined before each series of experiments by a thiocyanate dosimeter (an N<sub>2</sub>O-saturated aqueous solution containing 10 mM KSCN) using  $G \times \epsilon = 5.048 \times 10^{-3} \text{ mol J}^{-1} \text{ M}^{-1} \text{ cm}^{-1}$  (Buxton and Stuart, 1995; Schuler et al., 1980) for the (SCN)<sub>2</sub><sup>-</sup> radical anion at 472 nm. Doses absorbed in 1-octanol systems were corrected for the electron density by a factor of 0.848.

The content of water was determined before pulse irradiation by the Karl-Fischer coulometric titration method (C20 Coulometric KF Titrator, Mettler Toledo). We make an effort to limit water contents in our samples up to 3 % by weight even though solubility of water in 1-octanol ranges between 4.7 and 5.05 % (Szreder and Kocia, 2015; Backlund et al., 1984). This is because higher concentrations cause occasionally phase separation during a storage or even during experiments.

For pulse radiolysis all samples were prepared by dissolution of known quantity of solute in exact volume of 1-octanol. Concentration of solute were low enough to prevent precipitation or phase separation.

Quantum calculations were performed using a Gaussian 09 software and visualized by evaluation version of Chemcraft 1.8 on a PC class computer.

## 3. Results

### 3.1. Initial stages of 1-octanol radiolysis

A time evolution of transient absorption spectra recorded after the electron pulse in 1-octanol is shown in Fig. 2. The spectra obtained at the short time domain (up to 4 us) are dominated by a broad absorption band in the UV-VIS range (with  $\lambda_{\text{max}} \approx 670 \text{ nm}$ ) with a tail in the near IR. This absorption band was unequivocally assigned to the solvated electrons (e<sub>s</sub>) based on the literature data (Sulich et al., 2014; Hentz and Kenney-Wallace, 1972, 1974).

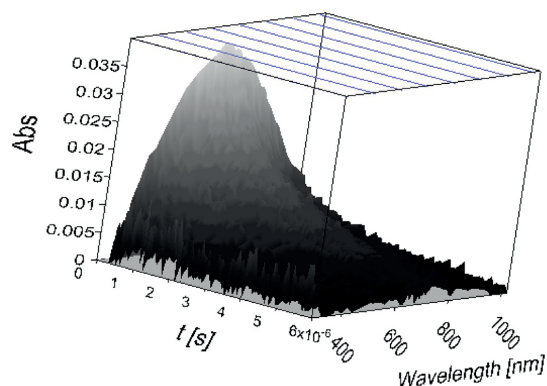


Fig. 2. Time evolution of transient absorption spectra recorded in neat 1-octanol purged with Ar, 21 Gy, water content  $\sim 0.06$  % by weight.

An initial radiation chemical yield of  $e_s^-$  ( $G(e_s^-)$ ) was calculated based on experiments involving pyrene (Pyr). A second-order rate constant for the reaction of Pyr with  $e_s^-$  (eq. (1)) in 1-octanol was measured in this work and found to be  $1.8(1) \times 10^9 \text{ M}^{-1} \text{ s}^{-1}$ . In the short time scale (up to 150 ns) and high concentration of Pyr (above 5 mM) this reaction can be considered quantitative. At this condition the rate of decay of the  $e_s^-$  absorption at 670 nm ( $\text{Abs}(e_s^-, 670 \text{ nm})$ ) corresponds nearly to the formation rate of the well-known Pyr radical anion ( $\text{Pyr}^{\cdot-}$ ) absorption at 495 nm (Okada et al., 1982) ( $\text{Abs}(\text{Pyr}^{\cdot-}, 495 \text{ nm})$ ) as it is shown in Fig. 3a. Small discrepancy is due to contribution of  $e_s^-$  absorption at 495 nm.



The plot of a linear correlation between  $\text{Abs}(e_s^-, 670 \text{ nm})$  and  $\text{Abs}(\text{Pyr}^{\cdot-}, 495 \text{ nm})$  corrected by subtraction of overlapped  $e_s^-$  absorption at 495 nm ( $\text{Abs}(495 \text{ nm})$ ) is shown in Fig. 3b. The relation between the slope of this plot and molar absorption coefficient of  $e_s^-$  ( $\epsilon(e_s^-, 670 \text{ nm})$ ) in 1-octanol is given by eq. (2).

$$\text{slope} = -\epsilon(e_s^-, 670 \text{ nm}) / \epsilon(\text{Pyr}^{\cdot-}, 495 \text{ nm}) + \text{const.} \quad (2)$$

Resulting  $\epsilon(e_s^-, 670 \text{ nm})$  value equal to  $18500 (700) \text{ M}^{-1} \text{ cm}^{-1}$  was obtained as an average of data collected from experiments with various concentration of Pyr (up to 27 mM). The molar absorption coefficient of  $\text{Pyr}^{\cdot-}$  ( $\epsilon(\text{Pyr}^{\cdot-}, 495 \text{ nm})$ )  $4.92 \times 10^4 \text{ M}^{-1} \text{ cm}^{-1}$  used for these calculations was taken from literature (Hentz and Kenney-Wallace, 1974). The value of  $\epsilon(e_s^-, 670 \text{ nm})$  obtained in this work is in good agreement with the previously reported  $\epsilon(e_s^-, 670 \text{ nm})$  in 1-octanol ranging from  $15000$  to  $20000 \text{ M}^{-1} \text{ cm}^{-1}$  (Hall and Kenney-Wallace, 1978; Jay-Gerin and Ferradini, 1994). Eventually, it leads to  $G(e_s^-)$  value equal to  $130(10) \text{ nmol J}^{-1}$  which is higher than the reported range of  $70$ – $100 \text{ nmol J}^{-1}$  (Sulich et al., 2014; Jay-Gerin and Ferradini, 1994; Hentz and Kenney-Wallace, 1974). Partially it is due to the fact that previous results do not take into account differences in electron density between 1-octanol and water based dosimeters.

It is worthy to note that an organic phase of the extraction system contains a considerable amount of water due to contact with an aqueous phase. The solubility limit of water in 1-octanol ranges between  $4.7$  and  $5.05$  % by weight (Szreder and Kocia, 2015; Backlund et al., 1984). It corresponds to concentration, molar and electron fraction ranges:  $2.16$ – $2.32 \text{ mol dm}^{-3}$ ,  $0.263$ – $0.278$  and  $0.0460$ – $0.0494$ , respectively. A bathochromic shift of the absorption maximum of the  $e_s^-$  band from  $670 \text{ nm}$  to  $700 \text{ nm}$  which is accompanied by an increasing absorption of about  $10$  % was observed in 1-octanol containing  $2.9$  % of water (see Fig. 4). This is not surprising since  $\lambda_{\text{max}}$  and the corresponding molar absorption coefficient of  $e_s^-$  in water are  $715 \text{ nm}$  and

$19700 \text{ M}^{-1} \text{ cm}^{-1}$ , respectively (Torche and Marignier, 2016). Similar effects were reported previously in alcohol/water systems (Arai and Sauer, 1966; Leu et al., 1983). In general,  $e_s^-$  in binary mixtures reveals only one absorption band. The location of the maximum of this absorption band is usually between the maxima of absorption bands of  $e_s^-$  observed in neat components. However, shift and intensity of the maximum as well as width at half height of the band are not linearly correlated with the molar composition of mixtures. This is due to favourable and specific solvation interaction of one solvent. Moreover, in some water/alcohol binary systems  $G(e_s^-)$  was higher than those observed in both neat solvents (Leu et al., 1983). The experimental error of our method does not allow us to separate the fraction of absorption corresponding to increase of  $G(e_s^-)$  and/or  $\epsilon(e_s^-)$  values.

It is well known from previous studies, that electron deficiency species (often called holes) generated upon ionization of 1-octanol undergo a fast ion-molecule reaction with an intact alcohol molecule (eq. (3)). This reaction leads mostly to C-centered radicals but not exclusively limited to  $\alpha$ -hydroxyalkyl radicals (Bobrowski et al., 2016). These radicals show moderate reducing properties.



Contribution of  $\cdot\text{OH}$  generated as a consequence of direct ionization of water in 1-octanol on ligand degradation seems to be negligible. This is due to the relatively low electron fraction of water in 1-octanol  $0.046$ – $0.0494$  at solubility limit as well as fast reaction of  $\cdot\text{OH}$  with 1-octanol. Rate constant of this reaction in aqueous solution was found to be  $5.2 \times 10^9 \text{ dm}^3 \text{ mol}^{-1} \text{ s}^{-1}$  (Scholes and Willson, 1967).

### 3.2. Reaction of CyMe<sub>4</sub>-BTPPh with electrons

A faster decay of the transient absorbance at  $670 \text{ nm}$  (assigned to  $e_s^-$  in 1-octanol), in respect to a neat solvent, was observed in the presence of CyMe<sub>4</sub>-BTPPh. This is due to the reaction of  $e_s^-$  with ligand (eq. (4)).



The dependence of pseudo-first order decay rate constant on the ligand concentration is shown in Fig. 5a. The resulting second order rate constant (calculated from the slope in Fig. 5a) was found to be  $1.85(9) \times 10^9 \text{ M}^{-1} \text{ s}^{-1}$  ( $k_4$ ). This value is very similar to those previously found for CyMe<sub>4</sub>-BTP and CyMe<sub>4</sub>-BTBP equal to  $2.4(2) \times 10^9 \text{ M}^{-1} \text{ s}^{-1}$  and  $1.7(3) \times 10^9 \text{ M}^{-1} \text{ s}^{-1}$ , respectively (Sulich et al., 2014). A value of almost an order of magnitude higher ( $1.5$ – $1.8) \times 10^{10} \text{ M}^{-1} \text{ s}^{-1}$  was previously found for the reaction of  $e_s^-$  with the model compound – 1, 10-phenanthroline in aqueous solution (Teplý et al., 1980).

Interestingly, a decreasing of initial absorbance of  $e_s^-$  with increasing ligand concentration was observed (see Fig. 5b). This might suggest that the CyMe<sub>4</sub>-BTPPh ligand also reacts with dry electrons ( $e_{\text{dry}}^-$ ). Typically, scavenging of  $e_{\text{dry}}^-$  is described by the  $C_{37}$  parameter. This parameter corresponds to a concentration of scavenger capable to decrease initial  $G(e_s^-)$  by factor of  $36.7\%$  ( $e^-$ ) and can be calculated according to the formula  $\varphi(c) = \varphi_0 \exp(-c/C_{37})$ , where  $\varphi$  is in any quantity proportional to  $G(e_s^-)$  and  $\varphi_0$  is a corresponding value not affected by scavenger (for a neat solvent). The  $C_{37}$  value for the system studied was found to be  $30.4(8) \text{ mM}$  showing moderate scavenging capabilities.

Similar experiments were performed for 1-octanol containing  $2.9$  % of water. In principle, results are the same within an experimental error. The respective rate constant and  $C_{37}$  obtained in that system were  $1.7(1) \times 10^9 \text{ M}^{-1} \text{ s}^{-1}$  and  $31.1(4) \text{ mM}$ , respectively.

It is reasonable to assume that the reactions of ligand with both  $e_{\text{dry}}^-$  and  $e_s^-$  lead to a radical anion of CyMe<sub>4</sub>-BTPPh (CyMe<sub>4</sub>-BTPPh $^{\cdot-}$ ). Structure of CyMe<sub>4</sub>-BTPPh $^{\cdot-}$  was examined based on the HF 6-311G(d,p) and B3LYP 6-311++(d,p) level of theory. Calculations



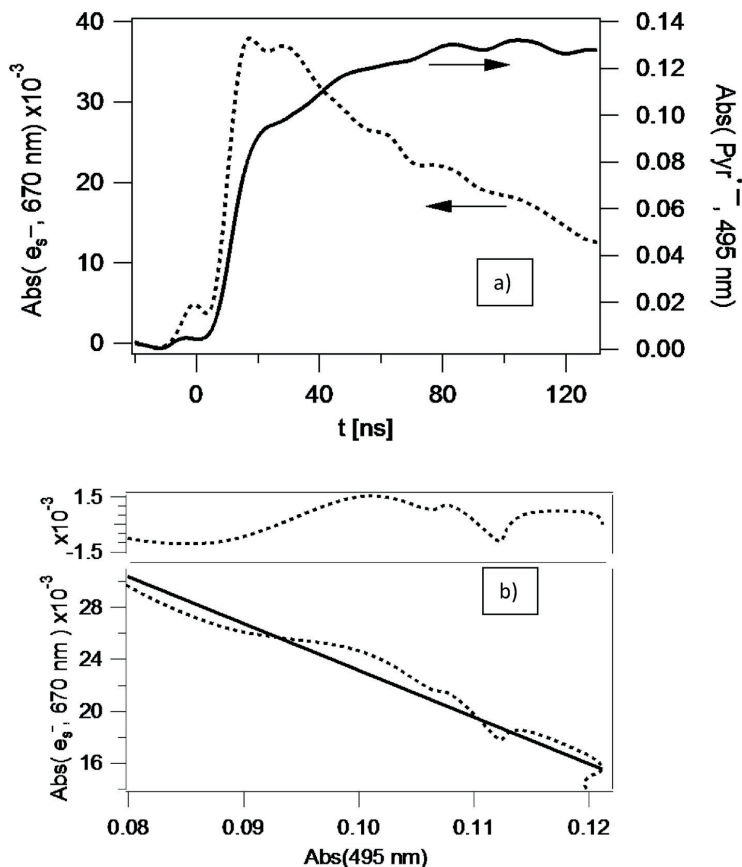


Fig. 3. a) Transient absorption profiles recorded at 670 nm (e<sub>s</sub><sup>-</sup>, dotted line) and 495 nm (Pyr<sup>-</sup>, straight line) for the Pyr (5.31 mM)/1-octanol system after 10 ns electron pulse irradiation (Ar saturated, 19 Gy, water contents 0.06 % by weight). b) Plot of the correlation between e<sub>s</sub><sup>-</sup> absorption at 670 nm (Abs(e<sub>s</sub><sup>-</sup>, 670 nm)) and Pyr<sup>-</sup> absorption at 495 nm corrected by subtraction of overlapped e<sub>s</sub><sup>-</sup> absorption at 495 nm (Abs(495 nm)) (dotted line) with linear fitting (straight line, slope = -0.361(4)) and residual analysis in the top.

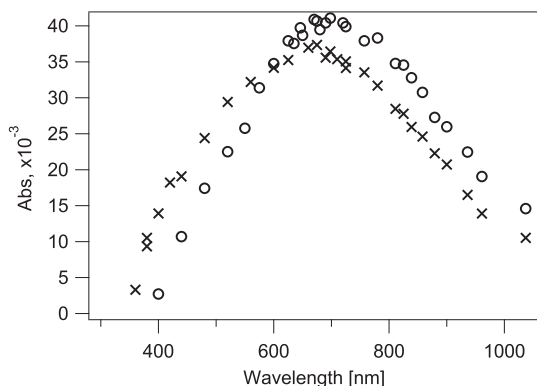


Fig. 4. Transient absorption spectra of pulse irradiated, Ar saturated 1-octanol containing 0.06 (x) and 2.9 % (o) of water (by weight), recorded 50 ns after electron pulse (20 Gy).

show an extended delocalization of an excess electron on aromatic fragments of ligand molecule (see Fig. 6) with a highest electron density on triazine moieties. This effect contributes to stabilization of the system. In addition, no molecule fragmentation was observed. Thus, it is likely that the life-time of these species is relatively long so they may undergo further reactions with other transients (e.g. reproducing ligand).

It is worthy to mention, that the absorption spectrum of CyMe<sub>4</sub>-BTPhen<sup>-</sup> was not observed, even for a solution containing relatively high concentration of a ligand ~11 mM and irradiated with a dose as high as 23 Gy per pulse. This is quite surprising, since experimental data for a model molecule – 1, 10-phenanthroline (Shida, 1988) as well as theoretical calculations for the radical anion of the ligand (CyMe<sub>4</sub>-BTPhen<sup>-</sup>) revealed distinct absorption bands located in the VIS region. The most plausible explanation is a low molar absorption coefficient of the studied species.

### 3.3. Nitric acid effects

Extraction of minor actinides takes place from an aqueous phase acidified by nitric acid (HNO<sub>3</sub>). In principle, the concentration of HNO<sub>3</sub> in aqueous phase is around 1 M (Panak and Geist, 2013), which

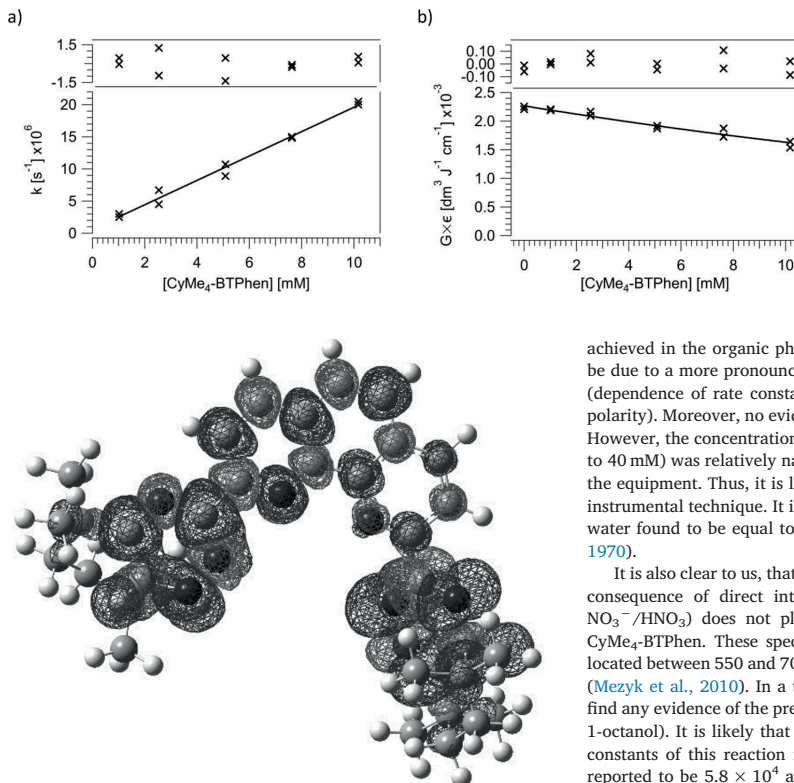


Fig. 6. Spin density of an excess electron on CyMe<sub>4</sub>-BTPhen, calculated by the B3LYP 6-311++(d,p) method.

corresponds to 90 mM HNO<sub>3</sub> present in the organic 1-octanol phase being in contact (Geist, 2010). Molar and electron fractions of HNO<sub>3</sub> in 90 mM 1-octanol solution are equal to 0.014 and 0.0061, respectively. The presence of HNO<sub>3</sub> in 1-octanol may affect radiation chemistry of the system due to an effective e<sub>s</sub><sup>-</sup> scavenging by both protons (H<sup>+</sup>) and nitrate anions (NO<sub>3</sub><sup>-</sup>) and also by protonation of the ligand.

The reaction of e<sub>s</sub><sup>-</sup> with H<sup>+</sup> (eq. (5)) was studied in a perchloric acid (HClO<sub>4</sub>)/1-octanol solution. It is well known the ClO<sub>4</sub><sup>-</sup> anion does not react neither with e<sub>dir</sub><sup>-</sup> nor e<sub>s</sub><sup>-</sup>.



The second-order rate constant of reaction 5 was measured in this work and was found to be  $1.5(3) \times 10^9 \text{ M}^{-1} \text{ s}^{-1}$  ( $k_5$ ) based on a pseudo-first order rate constant of e<sub>s</sub><sup>-</sup> decay dependence on the HClO<sub>4</sub> concentration. It is likely, that this reaction is reversible as it was observed in aqueous systems (Bobrowski et al., 2016; Garrett et al., 2005). However, it must be strongly shifted towards the product. In the range of HClO<sub>4</sub> concentration investigated (up to 40 mM) no evidence for H<sup>+</sup> reaction with e<sub>dir</sub><sup>-</sup> was found. This is in agreement with the C<sub>37</sub> value reported in water which is as high as 10 M (Gauduel, 1995). Neither rate constant of reaction 5 nor reactivity towards e<sub>dir</sub><sup>-</sup> in 1-octanol was affected by water contents up to 2.9 % by weight.

Within an experimental error no difference in e<sub>s</sub><sup>-</sup> decay kinetics was found when HClO<sub>4</sub> was replaced by HNO<sub>3</sub>. This is surprising, since the reported reaction of NO<sub>3</sub><sup>-</sup> with e<sub>s</sub><sup>-</sup> in aqueous systems is relatively fast with a rate constant equal to  $9.7 \times 10^9 \text{ M}^{-1} \text{ s}^{-1}$  (Buxton et al., 1988). It seems that this reaction is irrelevant or full dissociation of HNO<sub>3</sub> is not

Fig. 5. a) The dependence of pseudo-first order rate constant of e<sub>s</sub><sup>-</sup> decay (measured at 670 nm) on CyMe<sub>4</sub>-BTPhen concentration, b)  $G \times \epsilon$  values calculated based on an initial absorbance at 670 nm as a function of CyMe<sub>4</sub>-BTPhen concentration (20 Gy, water content 0.10 % by weight, Ar saturated solution). Straight lines represent fitting to experimental data, residue analysis is shown on the top of plots.

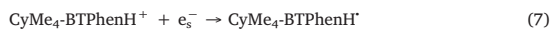
achieved in the organic phase studied. Partially, this observation may be due to a more pronounced ion – ion interaction in non-polar media (dependence of rate constants of reacting charged species on solvent polarity). Moreover, no evidence of NO<sub>3</sub><sup>-</sup> reaction with e<sub>dir</sub><sup>-</sup> was found. However, the concentration range of HNO<sub>3</sub> used in our experiment (up to 40 mM) was relatively narrow due to limitation of time resolution of the equipment. Thus, it is likely that C<sub>37</sub> value was out of limits of our instrumental technique. It is supported by a relatively high C<sub>37</sub> value in water found to be equal to 0.55 M (Lam and Hunt, 1975; Wolff et al., 1970).

It is also clear to us, that a low concentration of NO<sub>3</sub><sup>-</sup> (generated as a consequence of direct interaction of the ionization radiation with NO<sub>3</sub><sup>-</sup>/HNO<sub>3</sub>) does not play any significant role in degradation of CyMe<sub>4</sub>-BTPhen. These species are characterized by absorption bands located between 550 and 700 nm as it was observed in aqueous solution (Mezyk et al., 2010). In a time domain of our observation we did not find any evidence of the presence of them (even for 200 mM of HNO<sub>3</sub> in 1-octanol). It is likely that NO<sub>3</sub><sup>-</sup> reacts with 1-octanol molecules. Rate constants of this reaction in aqueous and acetonitrile solutions were reported to be  $5.8 \times 10^4$  and  $8.4 \times 10^4 \text{ M}^{-1} \text{ s}^{-1}$ , respectively (Mezyk et al., 2010).

The first protonation of CyMe<sub>4</sub>-BTPhen takes place at the phenantroline ring, which is described by eq. (6) with pK<sub>a</sub> = 3.1(1) (Lewis et al., 2011).

$$K_a = \frac{([CyMe_4 - BTPhen]_0 - [CyMe_4 - BTPhenH^+])([H^+]_0 - [CyMe_4 - BTPhenH^+])}{[CyMe_4 - BTPhenH^+]} \quad (6)$$

Subsequent pK<sub>a</sub> values are rather low and equal to 0.3(1), 0.2(1) and 0.03(3) for second, third and fourth protonation, respectively. In the organic phase with an HNO<sub>3</sub> concentration of 90 mM, about 95 % of CyMe<sub>4</sub>-BTPhen molecules are protonated (CyMe<sub>4</sub>-BTPhenH<sup>+</sup>). Taking into account the limitation of time resolution of our pulse radiolysis setup, we investigated reaction of e<sub>s</sub><sup>-</sup> with CyMe<sub>4</sub>-BTPhenH<sup>+</sup> (eq. (7)) in 1-octanol containing [H<sup>+</sup>]<sub>0</sub> = 5.8 mM and [CyMe<sub>4</sub>-BTPhen]<sub>0</sub> in the range of 0–5.7 mM.



At these conditions an equilibrated concentration [CyMe<sub>4</sub>BTPhenH<sup>+</sup>] can be calculated by solution of the quadratic eq. (8) derived from eq. (6).

$$[CyMe_4BTPhenH^+]^2 - ([CyMe_4BTPhen]_0 + [H^+]_0 + K_a) [CyMe_4BTPhenH^+] + [CyMe_4BTPhen]_0 [H^+]_0 = 0 \quad (8)$$

The observed rate constant ( $k_{obs}$ ) of absorbance decay at 670 nm (corresponding to the decay of e<sub>s</sub><sup>-</sup>) for this system is given by formula (eq. (9)), where  $k(H^+) = 1.5 \times 10^9 \text{ M}^{-1}$ ,  $k(CyMe_4-BTPhen) = 1.85 \times 10^9 \text{ M}^{-1}$  and  $k(CyMe_4-BTPhenH^+)$  are the rate constants of e<sub>s</sub><sup>-</sup> reactions with H<sup>+</sup>, CyMe<sub>4</sub>-BTPhen and CyMe<sub>4</sub>-BTPhenH<sup>+</sup>, respectively.

$$k_{obs} = k(H^+) [H^+] + k(CyMe_4-BTPhen) [CyMe_4-BTPhen] + k(CyMe_4-$$

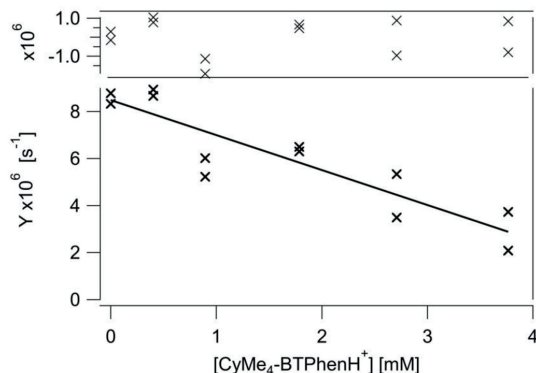


Fig. 7. Graphical representation of equation (9) for 1-octanol system containing  $[H^+]_0 = 5.8 \text{ mM}$  and  $[CyMe_4-BTPhen]_0$  in the range of 0–5.7 mM with a linear fitting (intersection =  $8.5(5) \times 10^6 \text{ s}^{-1}$ , slope =  $-1.4(2) \times 10^9 \text{ M}^{-1} \text{ s}^{-1}$ ) and residual analysis at the top (20 Gy, water contents 0.46 % by weight).

$$BTPhenH^+ [CyMe_4-BTPhenH^+] \quad (9)$$

Equation (9) can be transformed to a linear form – eq. (10), and plotted as it is shown in Fig. 7.

$$Y = \text{slope} \times [CyMe_4-BTPhenH^+] + k(H^+) [H^+]_0 \quad (10)$$

where:  $Y = k_{obs} - k(CyMe_4-BTPhen) [CyMe_4-BTPhen]_0$

$$\text{slope} = k(CyMe_4-BTPhenH^+) - k(CyMe_4-BTPhen) - k(H^+)$$

Based on a slope of the fitting line in Fig. 7, the obtained value of  $k(CyMe_4-BTPhenH^+)$  is equal to  $1.9(6) \times 10^9 \text{ M}^{-1} \text{ s}^{-1}$  ( $k_7$ ). The rate constant obtained is the same (within an experimental error) as the rate constant for the respective reaction of non-protonated ligand confirming a diffusion-controlled or closed to a diffusion-controlled reaction mechanism. It is worthy to note that relatively high level of uncertainty is due to a narrow concentration range of  $CyMe_4-BTPhen$  used in our experiments.

It is also possible that  $CyMe_4-BTPhen$  and its protonated form can be reduced by hydroxyoctyl radicals (species generated from 1-octanol holes in reaction 3). The reaction of hydroxyalkyl radicals with 1, 10-phenanthroline and its protonated form in aqueous solution was observed before (Mulazzani et al., 1979; Teplý et al., 1980) but it was significantly slower than reduction by  $e_s^-$ . It was not possible to study this reaction in our system due to the lack of product absorption in the available spectral range.

### 3.4. Oxygen reaction with solvated electrons

The ability of molecular oxygen ( $O_2$ ) to react with  $e_s^-$  according to (eq. (11)) is well known. The second-order rate constant of this reaction in 1-octanol was calculated by measuring the pseudo-first order rate constants of  $e_s^-$  decay as function of  $O_2$  in the solvent purged by various  $O_2/Ar$  mixture composition. The  $O_2$  concentrations in 1-octanol were calculated by using Henry Fugacity equal to 91.42 MPa (Bo et al., 1993). The rate constant ( $k_{r1}$ ) obtained  $1.0(1) \times 10^{10} \text{ M}^{-1} \text{ s}^{-1}$  is independent of water concentration up to 2.9 %. As it was expected, this value is lower than those observed in methanol and ethanol ( $1.9 \times 10^{10}$  to  $2.1 \times 10^{10} \text{ M}^{-1} \text{ s}^{-1}$  and  $1.9 \times 10^{10}$  to  $2.0 \times 10^{10} \text{ M}^{-1} \text{ s}^{-1}$ ), respectively. This fact can be rationalized by a higher viscosity of 1-octanol in comparison to methanol and ethanol.



It is also worthy to note that radiation resistance studies of extraction systems were generally performed in sealed vessels with limiting diffusion of  $O_2$  into organic phase. In addition, the applied irradiation doses are as high as 1 MGy. Since  $O_2$  plays a significant role in scavenging both  $e_s^-$  and  $H^\cdot$  as well as it has the ability to regenerate phenanthroline substrate upon the irradiation (Mulazzani et al., 1979) it is important to take into account its depletion in irradiated systems.

### 3.5. Reaction with $H^\cdot$

The spectrum of an  $H^\cdot$  adduct to model compound – 1, 10-phenanthroline was observed in aqueous solution (Mulazzani et al., 1979). However, we did not record any absorption which can be assigned to corresponding  $H^\cdot$  adduct to  $CyMe_4-BTPhen$ . Therefore, it is likely that these species are characterized either by low molar absorption coefficient or alternatively they are formed on triazine moieties with no bands in the region studied.

Since Pyr is capable to scavenge  $H^\cdot$  forming the adduct  $PyrH^\cdot$  with characteristic band peaking at 400–405 nm (Zhang and Thomas, 1994), we used this feature to study kinetics of  $H^\cdot$  addition to  $CyMe_4-BTPhen$  by a competition. Our observations do not lead to an exact value but clearly show that this reaction is at least 10-fold slower than the reaction leading to  $PyrH^\cdot$  formation. The kinetics of  $PyrH^\cdot$  formation was not measured in 1-octanol, however, the rate constant of this reaction was found to be  $7.2 \times 10^9 \text{ M}^{-1} \text{ s}^{-1}$  in methanol (Zhang and Thomas, 1994).

The transient absorption spectrum recorded in acidified (80 mM of  $H^+$ ) 1-octanol solution of  $CyMe_4-BTPhen$  is shown in Fig. 8. At these experimental conditions, the ligand exists mostly in a protonated form and  $e_s^-$  is converted by forming an additional amount of  $H^\cdot$  (reaction 5).

Two absorption bands can be distinguished in the spectrum recorded 800 ns after the pulse: the first one with  $\lambda_{max} \approx 630 \text{ nm}$  and the second one with  $\lambda_{max} \approx 450 \text{ nm}$  or below. By comparison with a pulse-irradiated, acidified solution of 1, 10-phenanthroline this spectrum can be assigned to the  $H^\cdot$  adduct to a protonated form of the ligand –  $CyMe_4-BTPhenH_2^{+}$ . The adduct of  $H^\cdot$  to protonated 1, 10-phenanthroline is characterized by a similar absorption bands peaking at  $\lambda = 430$  and  $660 \text{ nm}$  (Teplý et al., 1980). The rate constant of  $CyMe_4-BTPhenH_2^{+}$  formation (eq. (12)) was measured in this work and was found to be  $4.3(9) \times 10^6 \text{ M}^{-1} \text{ s}^{-1}$  ( $k_{12}$ ) based on a dependence of a pseudo-first order rate constant signal growing at 450 nm on a concentration of  $CyMe_4-BTPhenH^+$ . For a protonated form of 1,10-phenanthroline in aqueous solution the rate constant of this reaction was almost one order

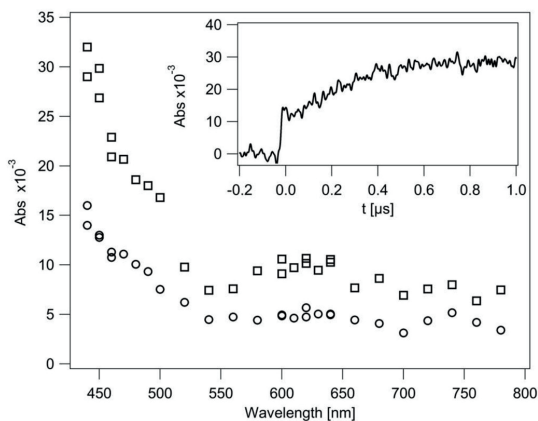


Fig. 8. Transient absorption spectra recorded in irradiated, Ar saturated, 1-octanol with 80 mM HCl and 8.5 mM  $CyMe_4-BTPhen$  50 ns (○) and 800 ns (□) after the electron pulse, insert shows time profile recorded at 450 nm (19 Gy, water contents 0.46 % by weight).

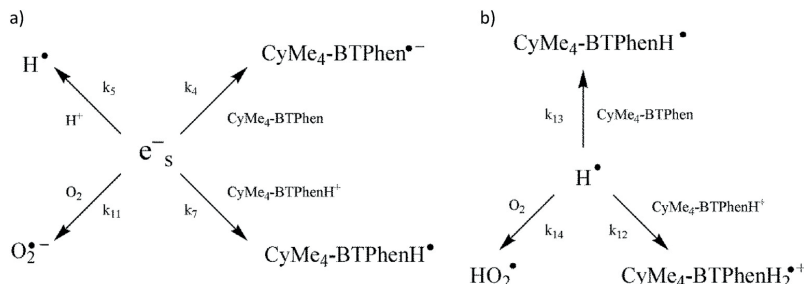


Fig. 9. The reaction scheme involving a)  $e_s^-$  and b)  $H^\bullet$  in 1-octanol based r-SANEX extraction system containing CyMe<sub>4</sub>-BTPhen ligand.

Table 1

Rate constant of fast reactions taking place in r-SANEX system based on 1-octanol diluent with CyMe<sub>4</sub>-BTPhen ligand.

rate constant	value [ $M^{-1} s^{-1}$ ]
$k_4$	$1.85(9) \times 10^9$
$k_5$	$1.5(3) \times 10^9$
$k_7$	$1.9(6) \times 10^9$
$k_{11}$	$1.0(1) \times 10^{10}$
$k_{12}$	$4.3(9) \times 10^8$
$k_{13}$	$< 7.2 \times 10^8$

of the magnitude higher and equal to  $3.3 \times 10^9 M^{-1} s^{-1}$  (Teply et al., 1980).



Mass spectra of permanent products for irradiated 1-octanol solutions of CyMe<sub>4</sub>-BTPhen (Schmidt et al., 2016) and aqueous solution of 1, 10-phenanthroline containing alcohols (Teply et al., 1980) show hydroxyalkyl adducts as a main, final product regardless presence or absence of acid. However, it is clear that significant alteration of ligand radiation chemistry occurs in the presence of  $H^+$  as it is shown by actinide/lanthanide performance extraction upon irradiation (Schmidt et al., 2016). It is possible that a hydroxyalkyl substitution in phenanthroline moiety dominates in an acidified solution. Positions 2 and 4 in phenanthroline are vulnerable for this kind of reaction (Teply et al., 1980). However, in the case of CyMe<sub>4</sub>-BTPhen triazine substituent is in position 2. Therefore, the radiolysis product does not affect the binding centre of the ligand and no deterioration of extraction efficiency is observed up to 300 kGy dose even though only traces of initial quantity of CyMe<sub>4</sub>-BTPhen can be detected in extraction system exposed to 100 kGy (Schmidt et al., 2016). On the other hand, in the absence of acid substitution of triazine ring leads to damaging of binding centre. It is likely that in both cases reaction with  $H^\bullet$  initiate this transformation.

#### 4. Conclusions

Solvated electrons ( $e_s^-$ ) and hydrogen atoms ( $H^\bullet$ ) are the two most reactive species generated during 1-octanol (diluent of r-SANEX extraction system) irradiation. Radiation chemical yield of  $e_s^-$  ( $G(e_s^-)$ ) and its molar absorption coefficient ( $\epsilon(e_s^-)$ ) in 1-octanol were found to be 130(10) mmol  $J^{-1}$  and 18500(700)  $M^{-1} cm^{-1}$ , respectively. Both species undergo fast reactions with the ligand CyMe<sub>4</sub>-BTPhen and other scavengers present in the extraction system according to the scheme shown in Fig. 9. All rate constants describing investigated reactions and findings in this work were collected together in Table 1 for readability improvement.

Moreover, the CyMe<sub>4</sub>-BTPhen ligand is capable to scavenge dry electrons with  $C_{37}$  equal to 30.4(8) mM.

#### Acknowledgments

The authors wish to thank prof. K. Bobrowski for helping in paper preparation and fruitful discussions.

Investigations were partially supported by the Euratom-Fission Collaborative Project SACSESS, FP7-Fission-2012-323282, co-financed by the Grant No. 2924/7. PR-EURATOM/2013/2 donated by the Ministry of Science and Higher Education (Poland) (TS).

#### References

- Aneheim, E., Bauhn, L., Ekberg, C., Foreman, M., Löfström-Engdahl, E., 2012. Extraction experiments after radiolysis of a proposed GANEX solvent-effect of time. *Procedia Chem.* 7, 123–129. <https://doi.org/10.1016/j.proche.2012.10.022>.
- Arai, S., Sauer, M.C., 1966. Absorption spectra of solvated electron in polar liquids - dependence on temperature and composition of mixtures. *J. Chem. Phys.* 44 (6), 2297–2305. <https://doi.org/10.1063/1.1727037>.
- Backlund, S., Hoiland, H., Vikholm, I., 1984. Water-alcohol interactions in the 2-phase system water-alcohol-alkane. *J. Solut. Chem.* 13 (10), 749–755. <https://doi.org/10.1007/BF00649012>.
- Bo, S.Q., Battino, R., Wilhelm, E., 1993. Solubility of gases in liquids. 19. Solubility of He, Ne, Ar, Kr, Xe, N<sub>2</sub>, O<sub>2</sub>, CH<sub>4</sub>, CF<sub>4</sub>, and SF<sub>6</sub> in normal 1-alkanols n-C<sub>4</sub>H<sub>9</sub>O<sub>1</sub>OH (1 less-than-or-equal-to 1 less-than-or-equal-to 11) at 298.15 K. *J. Chem. Eng. Data* 38 (4), 611–616. <https://doi.org/10.1021/Jc00012a035>.
- Bobrowski, K., Skotnicki, K., Szreder, T., 2016. Application of radiation chemistry to some selected technological issues related to the development of nuclear energy. *Top. Curr. Chem.* 374 (5), 147–194. <https://doi.org/10.1007/s41061-016-0058-7>.
- Bourg, S., Geist, A., Narbut, J., 2015. SACSESS - the EURATOM FP7 project on actinide separation from spent nuclear fuels. *Nukleonika* 60, 809–814. <https://doi.org/10.1515/nuka-2015-0152>.
- Buxton, G.V., Stuart, C.R., 1995. Reevaluation of the thiocyanate dosimeter for pulse-radiolysis. *J. Chem. Soc., Faraday Trans.* 91 (2), 279–281. <https://doi.org/10.1039/Ft9959100279>.
- Buxton, G.V., Greenstock, C.L., Helman, W.P., Ross, A.B., 1988. Critical-review of rate constants for reactions of hydrated electrons, hydrogen-atoms and hydroxyl radicals ( $\cdot OH/\cdot O^-$ ) in aqueous solution. *J. Phys. Chem. Ref. Data* 17 (2), 513–886.
- Garrett, B.C., Dixon, D.A., Camaioni, D.M., Chipman, D.M., Johnson, M.A., Jonah, C.D., Kimmel, G.A., Miller, J.H., Rescigno, T.N., Rossky, P.J., Xantheas, S.S., Colson, S.D., Laufer, A.H., Ray, D., Barbara, P.F., Bartels, D.M., Becker, K.H., Bowen Jr., K.H., Bradforth, S.E., Carmichael, I., Coe, J.V., Corrales, L.R., Cowin, J.P., Dupuis, M., Eisenthal, K.B., Franz, J.A., Gutowski, M.S., Jordan, K.D., Kay, B.D., Laverne, J.A., Lymar, S.V., Madey, T.E., McCurdy, C.W., Meisel, D., Mukamel, S., Nilsson, A.R., Orlando, T.M., Petrik, N.G., Pimblott, S.M., Rustad, J.R., Schenter, G.K., Singer, S.J., Tokmakoff, A., Wang, L.S., Wettig, C., Zwier, T.S., 2005. Role of water in electron-initiated processes and radical chemistry: issues and scientific advances. *Chem. Rev.* 105 (1), 355–390. <https://doi.org/10.1021/cr030453x>.
- Gauduel, Y., 1995. Femtosecond optical spectroscopy in liquids: applications to the study of reaction dynamics. *J. Mol. Liq.* 63 (1), 1–54. [https://doi.org/10.1016/0167-7322\(94\)00782-R](https://doi.org/10.1016/0167-7322(94)00782-R).
- Geist, A., 2010. Extraction of nitric acid into alcohol: kerosene mixtures. *Solvent Extr. Ion Exch.* 28 (5), 596–607. <https://doi.org/10.1080/07366299.2010.499286>.
- Hall, G.E., Kenney-Wallace, G.A., 1978. Nanosecond laser measurements of optical-absorption coefficients of electrons in polar fluids. *Chem. Phys.* 32 (2), 313–322. [https://doi.org/10.1016/0301-0104\(78\)87063-3](https://doi.org/10.1016/0301-0104(78)87063-3).
- Hallerod, J., Ekberg, C., Foreman, M., Engdahl, E.L., Aneheim, E., 2015. Stability of phenyl trifluoromethyl sulfone as diluent in a grouped actinide extraction process. *J. Radioanal. Nucl. Chem.* 304 (1), 287–291. <https://doi.org/10.1007/s10967-014-3657-1>.
- Hentz, R.R., Kenney-Wallace, G., 1972. Optical-absorption of solvated electrons in alcohols and their mixtures with alkanes. *J. Phys. Chem.* 76 (20), 2931–2933. <https://doi.org/10.1021/J100646a028>.
- Hentz, R.R., Kenney-Wallace, G.A., 1974. The influence of molecular-structure on optical-

- absorption spectra of solvated electrons in alcohols. *J. Phys. Chem.* 78 (5), 514–519. <https://doi.org/10.1021/J100598a011>.
- Herbst, R.S., Baron, P., Nilsson, M., 2011. Standard and advanced separation: PUREX processes for nuclear fuel reprocessing. In: Nash, K.L., Lumetta, G.J. (Eds.), *Advanced Separation Techniques for Nuclear Fuel Reprocessing and Radioactive Waste Treatment*. Woodhead Publishing, pp. 141–175.
- Hudson, M.J., Lewis, F.W., Harwood, L.M., 2013. The circuitous journey from malonamides to BTPhens: ligands for separating actinides from lanthanides. In: In: Michael, H. (Ed.), *Strategies and Tactics in Organic Synthesis*, vol. 9. Academic Press, pp. 177–202.
- Jay-Gerin, J.P., Ferradini, C., 1994. Compilation of some physicochemical properties of solvated electrons in polar liquids. *Journal de chimie physique* 91 (2), 173–187. <https://doi.org/10.1051/jcp/1994910173>.
- Lam, K.Y., Hunt, J.W., 1975. Picosecond pulse-radiolysis .6. Fast electron reactions in concentrated solutions of scavengers in water and alcohols. *Int. J. Radiat. Phys. Chem.* 7 (2–3), 317–338. [https://doi.org/10.1016/0020-7055\(75\)90072-8](https://doi.org/10.1016/0020-7055(75)90072-8).
- Leu, A.D., Jha, K.N., Freeman, G.R., 1983. Solvent structure effects on electron thermalization ranges in water alcohol mixed-solvents - preferred eamax values for E-S in alcohols. *Can. J. Chem.* 61 (6), 1115–1119. <https://doi.org/10.1139/V83-199>.
- Lewis, F.W., Harwood, L.M., Hudson, M.J., Drew, M.G., Desreux, J.F., Vidick, G., Bouslimani, N., Modolo, G., Wilden, A., Sypula, M., Vu, T.H., Simonin, J.P., 2011. Highly efficient separation of actinides from lanthanides by a phenanthroline-derived bis-triazine ligand. *J. Am. Chem. Soc.* 133 (33), 13093–13102. <https://doi.org/10.1021/ja203378m>.
- Mezyk, S.P., Cullen, T.D., Elias, G., Mincher, B.J., 2010. Aqueous nitric acid radiation effects on solvent extraction process chemistry. In: *Nuclear Energy and the Environment*, vol. 1046. American Chemical Society, pp. 193–203 ACS Symposium Series, vol. 1046.
- Modolo, G., Geist, A., Miguirditchian, M., 2015. Minor actinide separations in the reprocessing of spent nuclear fuels: recent advances in Europe. In: Taylor, R. (Ed.), *Reprocessing and Recycling of Spent Nuclear Fuel*. Woodhead Publishing, Oxford, pp. 245–287.
- Mulazzani, Q.G., Emmi, S., Fuochi, P.G., Venturi, M., Hoffman, M.Z., Simic, M.G., 1979. One-electron reduction of aromatic nitrogen-heterocycles in aqueous-solution - 2,2'-bipyridine and 1,10-phenanthroline. *J. Phys. Chem.* 83 (12), 1582–1590. <https://doi.org/10.1021/J100475a006>.
- Nash, K.L., Nilsson, M., 2015. Introduction to the reprocessing and recycling of spent nuclear fuels. In: Taylor, R. (Ed.), *Reprocessing and Recycling of Spent Nuclear Fuel*. Woodhead Publishing, Oxford, pp. 3–25.
- Okada, T., Karaki, I., Mataga, N., 1982. Picosecond laser photolysis studies of hydrogen-atom transfer-reaction via heteroexcimer state in pyrene primary and pyrene secondary aromatic amine systems - role of hydrogen-bonding interaction between amino group of donor and pi-electrons of acceptor in the heteroexcimer. *J. Am. Chem. Soc.* 104 (25), 7191–7195. <https://doi.org/10.1021/ja00389a049>.
- Panak, P.J., Geist, A., 2013. Complexation and extraction of trivalent actinides and lanthanides by triazinylpyridine N-donor ligands. *Chem. Rev.* 113 (2), 1199–1236. <https://doi.org/10.1021/cr3003399>.
- Poinssot, C., Boullis, B., Bourg, S., 2015. Role of recycling in advanced nuclear fuel cycles. In: Taylor, R. (Ed.), *Reprocessing and Recycling of Spent Nuclear Fuel*. Woodhead Publishing, Oxford, pp. 27–48.
- Schmidt, H., Wilden, A., Modolo, G., Bosbach, D., Santiago-Schübel, B., Hupert, M., Švehla, J., Grüner, B., Ekberg, C., 2016. Gamma radiolysis of the highly selective ligands CyMe4BTBP and CyMe4BTPhen: qualitative and quantitative investigation of radiolysis products. *Procedia Chem.* 21, 32–37. <https://doi.org/10.1016/j.proche.2016.10.005>.
- Scholes, G., Willson, R.L., 1967. Gamma-radiolysis of aqueous thymine solutions - determination of relative reaction rates of OH radicals. *Trans. Faraday Soc.* 63 (540P), 2983–8. <https://doi.org/10.1039/Tf9676302983>.
- Schuler, R.H., Patterson, L.K., Janata, E., 1980. Yield for the scavenging of OH radicals in the radiolysis of N<sub>2</sub>O-saturated aqueous-solutions. *J. Phys. Chem.* 84 (16), 2088–2089. <https://doi.org/10.1021/J100453a020>.
- Shida, T., 1988. *Electronic Absorption Spectra of Radical Ions*. Elsevier, Amsterdam, Oxford, New York, Tokyo.
- Sulich, A., Grodkowski, J., Mirkowski, J., Kocia, R., 2014. Reactions of ligands from BT(B) P family with solvated electrons and benzophenone ketyl radicals in 1-octanol solutions. Pulse radiolysis study. *J. Radioanal. Nucl. Chem.* 300 (1), 415–421. <https://doi.org/10.1007/s10967-014-3021-5>.
- Szreder, T., Kocia, R., 2015. Electron beam irradiation of r-SANEX and i-SANEX solvent extraction systems: analysis of gaseous products. *Nukleonika* 60, 899–905. <https://doi.org/10.1515/nuka-2015-0157>.
- Teplý, J., Janovský, I., Mehnert, R., Brede, O., 1980. Pulse radiolytic study of unstable intermediates in the radiolysis of aqueous solutions of 1,10-phenanthroline. *Radiat. Phys. Chem.* 15 (2), 169–175. [https://doi.org/10.1016/0146-5724\(80\)90128-4](https://doi.org/10.1016/0146-5724(80)90128-4).
- Torche, F., Marignier, J.L., 2016. Direct evaluation of the molar absorption coefficient of hydrated electron by the isosbestic point method. *J. Phys. Chem. B* 120 (29), 7201–7206. <https://doi.org/10.1021/acs.jpcc.6b04796>.
- Wilden, A., Schreinemachers, C., Sypula, M., Modolo, G., 2011. Direct selective extraction of actinides (III) from PUREX raffinate using a mixture of CyMe<sub>4</sub>BTBP and TODGA as 1-cycle SANEX solvent. *Solvent Extr. Ion Exch.* 29 (2), 190–212. <https://doi.org/10.1080/07366299.2011.539122>.
- Wilden, A., Modolo, G., Kaufholz, P., Sadowski, F., Lange, S., Sypula, M., Magnusson, D., Müllich, U., Geist, A., Bosbach, D., 2015. Laboratory-scale counter-current centrifugal contactor demonstration of an innovative-SANEX process using a water soluble BTP. *Solvent Extr. Ion Exch.* 33 (2), 91–108. <https://doi.org/10.1080/07366299.2014.952532>.
- Wolff, R.K., Bronskil, M.J., Hunt, J.W., 1970. Picosecond pulse radiolysis studies .2. Reactions of electrons with concentrated scavengers. *J. Chem. Phys.* 53 (11), 4211–4215. <https://doi.org/10.1063/1.1673923>.
- Zhang, G.H., Thomas, J.K., 1994. Pyrene radical formation in pulse-radiolysis of liquid methanol. *J. Phys. Chem.* 98 (45), 11714–11718. <https://doi.org/10.1021/J100096a014>.

## Paper 5<sup>[90]</sup>

Schmidt, H.; Wilden, A.; Modolo, G.; Bosbach, D.; Santiago-Schübel, B.; Hupert, M.; Mincher, B.J.; Mezyk, S.P.; Švehla, J.; Grüner, B. Gamma and pulsed electron radiolysis studies of CyMe<sub>4</sub>BTBP and CyMe<sub>4</sub>BTPhen: Identification of radiolysis products and effects on the hydrometallurgical separation of trivalent actinides and lanthanides. *Radiation Physics and Chemistry* **2021**, *189*, 109696.

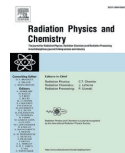
DOI: 10.1016/j.radphyschem.2021.109696

### Contribution:

This paper is a continuation of papers #1 and #2. I was leading author and conducted irradiation experiments, solvent extraction and interpretation of the HPLC-MS results.







# Gamma and pulsed electron radiolysis studies of CyMe<sub>4</sub>BTBP and CyMe<sub>4</sub>BTPhen: Identification of radiolysis products and effects on the hydrometallurgical separation of trivalent actinides and lanthanides

Holger Schmidt<sup>a</sup>, Andreas Wilden<sup>a,\*</sup>, Giuseppe Modolo<sup>a</sup>, Dirk Bosbach<sup>a</sup>,  
Beatrix Santiago-Schübel<sup>b</sup>, Michelle Hupert<sup>b</sup>, Bruce J. Mincher<sup>c</sup>, Stephen P. Mezyk<sup>d</sup>,  
Jaroslav Švehla<sup>e</sup>, Bohumir Grüner<sup>e</sup>, Christian Ekberg<sup>f</sup>

<sup>a</sup> Forschungszentrum Jülich GmbH, Institut für Energie- und Klimaforschung - Nukleare Entsorgung und Reaktorsicherheit (IEK-6), 52428, Jülich, Germany

<sup>b</sup> Forschungszentrum Jülich GmbH, Zentralinstitut für Engineering, Elektronik und Analytik (ZEA-3), 52428, Jülich, Germany

<sup>c</sup> Idaho National Laboratory, Idaho Falls, ID, 83415, USA

<sup>d</sup> California State University at Long Beach, Department of Chemistry and Biochemistry, Long Beach, CA, 90840, USA

<sup>e</sup> Institute of Inorganic Chemistry, Czech Academy of Sciences, Hlavní 1001, 25068, Rež, Czech Republic

<sup>f</sup> Chalmers University of Technology, Nuclear Chemistry, Department of Chemical and Biochemical Engineering, 41296, Gothenburg, Sweden

## ARTICLE INFO

### Keywords:

Nuclear waste treatment  
Used nuclear fuel  
Radiolysis  
Solvent extraction  
N-Donor extractants

## ABSTRACT

The radiolytic stability of the highly selective ligands CyMe<sub>4</sub>BTBP and CyMe<sub>4</sub>BTPhen against ionizing gamma radiation was studied in 1-octanol solution. CyMe<sub>4</sub>BTBP and CyMe<sub>4</sub>BTPhen are important extractants for a potential treatment of used nuclear fuel. They were studied under identical experimental conditions to directly compare the effects of gamma and pulsed electron radiolysis on the ligands and systematically study the influence of structural changes in the ligand backbone. Distribution ratios of Am<sup>3+</sup>, Cm<sup>3+</sup> and Eu<sup>3+</sup>, the residual concentration of CyMe<sub>4</sub>BTBP and CyMe<sub>4</sub>BTPhen in solution, and the formation of radiolysis products were studied as a function of absorbed gamma dose and presence of an acidic aqueous phase during irradiation. Quantitative and semi-quantitative analyses were used to elucidate the radiolysis mechanism for both ligands. Addition products of alpha-hydroxyoctyl radicals formed through radiolysis of the 1-octanol diluent to the ligand molecules were identified as the predominant radiolysis products. These addition products also extract trivalent metal ions, as distribution ratios remained high although the parent molecule concentrations decreased. Therefore, the utilization time of a solvent using these extractants under the harsh conditions of used nuclear fuel treatment could be considerably longer than expected. Understanding the radiolysis mechanism is crucial for designing more radiation resistant extractants.

## 1. Introduction

The hydrometallurgical treatment of used nuclear fuel is currently under investigation by several countries and international collaborative projects, as it may offer benefits in terms of resource savings and improved final disposal, and contribute to the sustainability of the nuclear fuel cycle and public acceptance (OECD-NEA, 2011; Veliscek-Carolan, 2016; Poinssot et al., 2016; Serp et al., 2017; Geist et al., 2020; Seidl et al., 2021). Detailed knowledge of the radiolytic degradation of organic ligands used in advanced processes for the hydrometallurgical treatment of used nuclear fuel is crucial for the design of these processes

and their safe operation (Mincher and Mezyk, 2009; Mincher et al., 2009). As different organics are used in the processes (diluent, extractants, complexants, buffers, etc.), different degradation mechanisms, radiolytic vulnerabilities, sensitive functional groups and effects of additives need to be considered and understood. With this knowledge, modifications of the molecular structures can help protect these organic species against radiolytic degradation. Consequences of radiolytic ligand degradation are molecular alterations which may lead to changes in solvent properties (e.g. density, viscosity), separation effectiveness (affinity and selectivity), or formation of precipitates (Mincher et al., 2010a).

\* Corresponding author.

E-mail address: [a.wilden@fz-juelich.de](mailto:a.wilden@fz-juelich.de) (A. Wilden).

<https://doi.org/10.1016/j.radphyschem.2021.109696>

Received 30 April 2021; Received in revised form 22 June 2021; Accepted 30 June 2021

Available online 10 July 2021

0969-806X/© 2021 The Authors. Published by Elsevier Ltd. This is an open access article under the CC BY license (<http://creativecommons.org/licenses/by/4.0/>).



The group of BT(B)P-type nitrogen donor ligands is known to be highly selective for trivalent actinides (An(III)) over lanthanides (Ln(III)), and different members of this class of ligands have been used in different separation processes over the last decades (Veliscek-Carolan, 2016; Geist et al., 2020; Ekberg et al., 2008; Magnusson et al., 2009a; Panak and Geist, 2013; Wilden et al., 2013; Modolo et al., 2015; Geist and Panak, 2021). Kolarik et al. first suggested the use of 2,6-bis-(1,2,4-triazine-3-yl)pyridines (BTP-type ligands) for selective Am(III) extraction (Kolarik et al., 1999). After identifying the  $\alpha$ -CH<sub>2</sub> position in the alkyl side-chain of the tested ligands to be the most vulnerable position, different branched and annulated modifications were synthesized and tested (Hill et al., 2002, 2005). CyMe<sub>4</sub>BTP (2,6-bis(5,5,8,8-tetra-methyl-5,6,7,8-tetrahydro-benzo[1,2,4]triazine-3-yl)pyridine) was found to have beneficial extraction properties with acceptable radiolytic stability (Hudson et al., 2006). However, due to the high An(III) distribution ratios, effective back-extraction of An(III) was problematic. Therefore, a second pyridine ring was added to the molecule backbone yielding 6,6'-bis(5,5,8,8-tetramethyl-5,6,7,8-tetrahydro-benzo[1,2,4]triazine-3-yl)[2,2']bipyridine (CyMe<sub>4</sub>BTBP, Fig. 1), which showed very good extraction properties and stability (Geist et al., 2006). Therefore, the ligand was used in several European process demonstrations for the selective separation of An(III), like the r-SANEX (Modolo et al., 2013, 2014), 1-cycle-SANEX (Wilden et al., 2011, 2013; Modolo et al., 2014; Magnusson et al., 2013) and the CHALMEX processes (Aneheim et al., 2010, 2011, 2012a, 2013; Halleröd et al., 2015; Authen et al., 2021). The r-SANEX process has also been tested successfully on genuine spent fuel on the laboratory scale (Magnusson et al., 2009a). Similar to the BTP ligands, it was found that the radiolysis of BTBP ligands is induced in  $\alpha$ -CH<sub>2</sub> positions of the side-chain, e.g. for the C5-BTBP ligand (Fermvik et al., 2009, 2010, 2011, 2012; Mincher et al., 2010b). Due to the linear alkyl substitutions, the C5-BTBP ligand was found to be very susceptible to radiolytic degradation, especially when aliphatic alcohols were used as diluent (Fermvik et al., 2009). Aliphatic alcohols are often used as diluents to increase the concentration of ligands that are only sparingly soluble in alkane diluents, or as phase modifiers to suppress third phase formation (Berthon et al., 2021; Geist and Modolo, 2009). The major radiolysis products were found to be  $\alpha$ -oxidized C5-BTBP compounds with partially degraded C<sub>5</sub> chains. Due to the high excess of diluent molecules compared to extractant molecules, indirect radiolysis via a reaction with highly reactive species formed *in situ* by diluent radiolysis is most likely. This effect is referred to as sensitization effect (Sugo et al., 2002, 2007). The hydrolytic (Nicolas et al., 2011) and radiolytic stability of CyMe<sub>4</sub>BTBP was further studied in different chemical conditions (e.g. in different diluents) and for different irradiation conditions (i.e. alpha- and gamma irradiation, as well as electron- and ion-beam) and CyMe<sub>4</sub>BTBP was found to be sufficiently stable for its application in the hydrometallurgical treatment of used nuclear fuel (Halleröd et al., 2015; Retegan et al., 2007; Magnusson et al., 2009b; Aneheim et al., 2012b; Sulich et al., 2014).

Since An(III) extraction rates with the CyMe<sub>4</sub>BTBP ligand in 1-octanol are rather low and a phase-transfer agent (like DMDOHEMA (Geist et al., 2006) or TODGA (Modolo et al., 2008)) is needed to reach good extraction kinetics, further development was conducted. For metal complexation, the CyMe<sub>4</sub>BTBP ligand needs to rearrange from the thermodynamically preferred *trans*-conformation to the *cis*-conformation (Lewis et al., 2011, 2012, 2013). The *cis*-locked 2,9-bis(1,2,

4-triazin-3-yl)-1,10-phenantroline (CyMe<sub>4</sub>BTPhen, Fig. 1) ligand provides the required *cis*-conformation in a pre-organized molecular structure. Due to its preorganization, the complex formation is thermodynamically favored compared to CyMe<sub>4</sub>BTBP and the complexation is accelerated (Lewis et al., 2011).

The  $\gamma$ -radiolysis of CyMe<sub>4</sub>BTPhen has been investigated to a much lesser extent compared to CyMe<sub>4</sub>BTBP (Zhou et al., 2014; Distler et al., 2015; Kondé et al., 2016; Szreder et al., 2019; Zsabka et al., 2020). Distler and Kondé et al. investigated the radiolytic stability of CyMe<sub>4</sub>BTBP and CyMe<sub>4</sub>BTPhen in phenyl trifluoromethyl sulfone (FS-13) and CyMe<sub>4</sub>BTPhen in cyclohexanone diluents. They concluded that the stability of the extractant is higher in FS-13 compared to cyclohexanone-type diluents and that addition products of diluent radicals to the parent molecules are formed (Distler et al., 2015; Kondé et al., 2016). Zsabka et al. studied the radiolysis of CyMe<sub>4</sub>BTPhen in the ionic liquid tri-*n*-octylmethylammonium nitrate (Zsabka et al., 2020). Both groups observed increasing metal ion distribution ratios as a function of absorbed dose, assuming the formation of radiolysis products that are able to extract metal ions similar to the ligand itself.

In this study, we present comparative  $\gamma$ -radiolysis studies of the highly selective nitrogen donor ligands CyMe<sub>4</sub>BTBP and CyMe<sub>4</sub>BTPhen with respect to the extraction of Am(III), Cm(III), and Eu(III) with irradiated solvents as well as qualitative and (semi-)quantitative analyses of the solutions. The major radiolysis products are identified and (semi-)quantified as a function of absorbed dose, and the influence of the presence of nitric acid during irradiation is studied. This paper describes the results of collaborative work within the European projects SACSESS and GENIORS and collaborative work with US-DOE laboratories and should be understood as continuation of our previous work, where we investigated the effect of  $\gamma$ -radiolysis on the An(III)/Ln(III) separation via solvent extraction using CyMe<sub>4</sub>BTBP and CyMe<sub>4</sub>BTPhen in comparison (Schmidt et al., 2015, 2016).

## 2. Materials and methods

**CAUTION:** ionizing radiation and handling of radioactive material is hazardous. Refer to local safety precautions, legislation, and associated regulations. CyMe<sub>4</sub>BTBP and CyMe<sub>4</sub>BTPhen were purchased from Technocomm Ltd. (Wellbrae, Falkland, Scotland) and were used as received. Solutions of 10 mmol L<sup>-1</sup> CyMe<sub>4</sub>BTBP or CyMe<sub>4</sub>BTPhen in 1-octanol (Merck, Darmstadt, Germany, analytical grade, >99%) were prepared and first irradiated under different conditions up to 413 kGy absorbed dose. In a later irradiation campaign, samples of CyMe<sub>4</sub>BTBP and CyMe<sub>4</sub>BTPhen in contact with 1 mol L<sup>-1</sup> nitric acid were irradiated to higher doses of 622 kGy. The <sup>60</sup>Co  $\gamma$ -source at Chalmers University, Gothenburg, Sweden was used (Gamma cell 220, Atomic Energy of Canada Ltd.). Due to the radioactive decay of <sup>60</sup>Co, the provided dose rate decreased from 9.8 to 8.7 kGy h<sup>-1</sup> during the experimental campaigns. Doses are reported relative to the initial dose rate determined using the ferric-cupric dosimeter without electron density corrections (Bjergbakke et al., 1970). The ferric-cupric dosimeter is used as standard technique at Chalmers, also taking into account the high dose-rate of the <sup>60</sup>Co  $\gamma$ -source. Samples of each ligand in 1-octanol solution were irradiated without, as well as in contact with nitric acid solutions (Merck, Darmstadt, 65%, analytical grade, diluted with demineralized water (18.2 M $\Omega$  cm)) of different concentrations (0.1, 1.0 and 4.0 mol L<sup>-1</sup> HNO<sub>3</sub>). Organic phases were used without prior pre-equilibration. Equal volumes (1 mL) organic solvent and nitric acid were contacted during the irradiation experiments for which the samples were placed in the  $\gamma$ -source, until the calculated dose was reached. To avoid pressurization during the irradiation experiment, the screw caps were not closed tightly. Nevertheless, the samples are considered deaerated due to positive pressure generated by radiolysis. Small amounts of oxygen that may diffuse into the samples are continuously consumed by radiolysis. After removing the irradiated samples from the  $\gamma$ -source, phases were separated if necessary and the remaining organic phases were used for

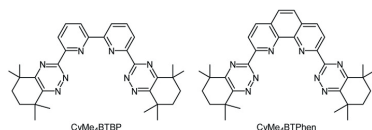


Fig. 1. Extractants investigated in this study: CyMe<sub>4</sub>BTBP (left) and CyMe<sub>4</sub>BTPhen (right).

further analysis and solvent extraction experiments.

In the solvent extraction experiments 500  $\mu\text{L}$  of the irradiated organic phase were contacted with 500  $\mu\text{L}$  fresh  $1.0 \text{ mol L}^{-1} \text{ HNO}_3$  which was spiked with  $^{241}\text{Am}$  (1.6 kBq),  $^{244}\text{Cm}$  (1.6 kBq) and  $^{152}\text{Eu}$  (2.8 kBq) tracer in 2 mL glass vials. The organic phases irradiated without contact to an aqueous phase or in contact with 0.1 and  $4.0 \text{ mol L}^{-1} \text{ HNO}_3$  were also directly contacted with  $1.0 \text{ mol L}^{-1} \text{ HNO}_3$  to avoid washing out degradation compounds. Radioactive tracers were purchased from Isotopendienst M. Blaseg GmbH, Waldburg, Germany, Oak Ridge National Laboratory, Oak Ridge, USA, and Eckert and Ziegler Nuclitec GmbH, Braunschweig, Germany. The vials were shaken vigorously for 90 min in a shaking device (2,500 rpm) at  $22^\circ\text{C}$  to reach equilibrium. After centrifugation, the phases were separated, and aliquots of each phase were taken for analysis. Gamma spectroscopy was conducted using an HPGe (high-purity germanium) detector system purchased from EG & G Ortec, Munich, Germany, and equipped with the GammaVision software. The  $\gamma$ -lines at 59.5 keV and 121.8 keV were analyzed for  $^{241}\text{Am}$  and  $^{152}\text{Eu}$ , respectively. Alpha measurements were carried out for  $^{241}\text{Am}$  (5486 keV) and  $^{244}\text{Cm}$  (5805 keV) using an Ortec Octète-pc eight chamber alpha measurement system equipped with PIPS detectors. Sample preparation for alpha measurement was done by homogenizing a  $10 \mu\text{L}$  alpha-spectroscopy sample in  $100 \mu\text{L}$  of a mixture of Zapon varnish and acetone (1:100 v/v). This mixture was distributed over a stainless-steel plate obtained from Berthold, Bad Wildbad, Germany. The sample was dried under a heating lamp and annealed into the stainless-steel plate by a gas-flame burner. The results are reported as distribution ratios  $D$ , which were calculated by dividing the measured metal activity of the organic phase by the metal activity of the aqueous phase ( $D = [\text{M}^{3+}_{\text{org}}]/[\text{M}^{3+}_{\text{aq}}]$ ). Given  $D$  values show an uncertainty of  $\pm 5\%$  within the range of  $0.01 < D < 100$ . The minimum/maximum detectable distribution ratios were 0.002 and 500, respectively, due to the detection limits in either the organic or the aqueous phase.

Direct Infusion Mass Spectrometry measurements were performed using a Finnigan LCQ Fleet<sup>TM</sup> spherical Ion Trap LC/MS<sub>n</sub> instrument (Thermo Scientific) at the Institute of Inorganic Chemistry, ReZ, Czech Republic. All mass spectra were measured with APCI interface.  $25 \mu\text{L}$  of the samples of initial concentration of the ligand were diluted to a volume of  $1.0 \text{ mL}$  with acetonitrile (for LC-MS, Aldrich, Gradient Grade). Mass Spectra from direct infusion by a syringe were measured with APCI in positive mode. Conditions used for APCI interface: Flow rate from a syringe infusion pump  $10 \mu\text{L min}^{-1}$ ; Sheath gas flow  $15 \text{ L min}^{-1}$ ; Auxiliary gas flow  $7 \text{ L min}^{-1}$ ; Source Voltage  $3.75 \text{ kV}$ ; Vaporizer Temperature  $400^\circ\text{C}$ ; Capillary Temperature  $250^\circ\text{C}$ ; Capillary Voltage  $48 \text{ V}$ ; Tube Lens Voltage  $100 \text{ V}$  and mass range from 50 to 2000.

Qualitative analyses for compound identification were performed using a hybrid linear ion trap FTICR (Fourier-Transform Ion Cyclotron Resonance) mass spectrometer LTQFT (Linear Tandem Quadrupole Fourier Transform) Ultra<sup>TM</sup> (Thermo Fisher Scientific, Bremen, Germany) coupled with an Agilent 1200 HPLC system (Agilent, Waldbronn, Germany). The mass spectrometer was first tuned and calibrated in the positive mode following the standard optimization procedure for all voltages and settings: Source Type: APCI; Source Voltage  $6.00 \text{ kV}$ ; Capillary Voltage  $34.00 \text{ V}$ ; Tube Lens Voltage  $80.00 \text{ V}$ ; Capillary Temperature  $275.00^\circ\text{C}$ ; APCI Vaporizer Temperature  $400.00^\circ\text{C}$ ; Sheath Gas Flow  $50.00 \text{ a.u.}$ ; Aux Gas Flow  $5.00 \text{ a.u.}$  Mass spectra were recorded in full scan from 100 to  $1000 \text{ Da}$  with a resolution of 100,000 at  $m/z$  400. For the detection of radiolysis products, first a separation was carried out on the reversed phase column Zorbax Eclipse Plus C18 from Agilent ( $3.8 \mu\text{m}$  particles  $100 \times 4.6 \text{ mm}$ ) in a gradient run with solvent A (water with  $0.1\%$  formic acid) and solvent B (acetonitrile with  $0.1\%$  formic acid) as shown in Table 1. All data were processed using the XCalibur software version 2.0. For better visibility, peaks with an intensity  $>100,000$  counts (which only occurred for the ligand molecules themselves) were cut off in all shown spectra to increase visibility of peaks with lower intensity (radiolysis products). All shown spectra are formatted to be directly comparable to each other. Only peaks with a

**Table 1**

Gradient used in the LC separation.

Time	Solvent A	Solvent B
0–2 min	40%	60%
2–10 min	Decrease to 2%	Increase to 98%
10–25 min	2%	98%
25–31 min	40%	60%

relative threshold of  $>2\%$  were analyzed. All spectra were collected using data of the HPLC runs from 3 to 13 min for CyMe<sub>4</sub>BTBP and from 0 to 18 min for CyMe<sub>4</sub>BTPhen.

For quantitative mass spectrometric analyses, an HPLC-MS/MS method with APCI in positive ion mode was developed and validated using a Triple Quadrupole Qtrap6500 instrument (ABSciex, Darmstadt, Germany) coupled with an Agilent 1260 HPLC system (Agilent, Waldbronn, Germany) to quantify the concentrations of CyMe<sub>4</sub>BTBP and CyMe<sub>4</sub>BTPhen after irradiation. For CyMe<sub>4</sub>BTBP, a Phenyl-X phase column from Thermo Scientific was used ( $2.6 \mu\text{m}$  particles,  $100 \times 4.6 \text{ mm}$ ) at  $40^\circ\text{C}$  in an isocratic run with  $95\%$  methanol and  $5\%$   $5 \text{ mmol L}^{-1}$  ammonium-acetate buffer at pH 6.5. Optimum separation performance for CyMe<sub>4</sub>BTBP was observed using a flow rate of  $700 \mu\text{L min}^{-1}$  over 15 min. The reversed phase column Nucleodur C18 Gravity SB phase from Macherey-Nagel ( $3 \mu\text{m}$  particles,  $150 \times 4.6 \text{ mm}$ ) with an isocratic run ( $98\%$  methanol and  $2\%$  water +  $0.1\%$  formic acid) at  $40^\circ\text{C}$ , over 15 min, with a flow rate of  $600 \mu\text{L min}^{-1}$  and an injection volume of  $10 \mu\text{L}$  showed the best separation performance for CyMe<sub>4</sub>BTPhen.

For the detection, the Multiple Reaction Monitoring (MRM) method was used with optimized method parameters for both ligands (Table 2). Mass spectrometer settings were: Curtain Gas 30 units; Gas 1 60 units; Gas 2 60 units; Temperature  $350^\circ\text{C}$ ; Needle Current (NC)  $3 \mu\text{A}$ ; Enhanced Potential  $10 \text{ V}$ . In all quantification experiments, data acquisition and processing were carried out using the software Analyst 1.6.1 (ABSciex, Darmstadt, Germany). For quantification the software Multiquant (ABSciex, Darmstadt, Germany) was used. The reproducibility for both ligands showed very good results with a variation coefficient  $\leq 6\%$ .

Pulse radiolysis experiments were conducted using the Laser-Electron Accelerator Facility (LEAF) at Brookhaven National Laboratory (NY, USA), which was described in detail by Wishart et al. (2004). For irradiation experiments, 1-octanol solutions of CyMe<sub>4</sub>BTBP or CyMe<sub>4</sub>BTPhen were irradiated and lifetimes of the generated solvated electron ( $e^-_{\text{solv}}$ ) was observed in dependence of the ligand concentration, varying in the range from  $2.5$  to  $10.0 \text{ mmol L}^{-1}$  CyMe<sub>4</sub>BTBP or CyMe<sub>4</sub>BTPhen, respectively. Additionally, the influence of nitric acid on  $e^-_{\text{solv}}$  absorbance by CyMe<sub>4</sub>BTPhen was tested in steady-state irradiation experiments using dried 1-octanol against 1-octanol contacted with  $6.0 \text{ mol L}^{-1} \text{ HNO}_3$ , which yields an approximate organic  $\text{HNO}_3$  concentration of  $1.5 \text{ mol L}^{-1} \text{ HNO}_{3,\text{org}}$  (Geist, 2010). Samples were irradiated in  $1.00 \text{ cm}$  Suprasil semimicro cuvettes sealed with Teflon stoppers. The doses per pulse for these experiments were in the range  $40\text{--}60 \text{ Gy}$ . Time-resolved kinetics were obtained using an FND-100 silicon diode detector and digitized using a LeCroy WaveRunner 640Zi oscilloscope

**Table 2**

Optimized reaction parameters for the ligand fragmentation.

Ligand	Fragment	Collision Energy	Cell Exit Potential	Declustering Potential
CyMe <sub>4</sub> BTBP	$m/z$ 535.1 to $m/z$ 505.3	69 V	10 V	241 V
CyMe <sub>4</sub> BTBP	$m/z$ 535.1 to $m/z$ 371.2	69 V	10 V	241 V
CyMe <sub>4</sub> BTPhen	$m/z$ 559.1 to $m/z$ 529.3	67 V	6 V	200 V
CyMe <sub>4</sub> BTPhen	$m/z$ 559.1 to $m/z$ 395.2	67 V	24 V	200 V

(4 GHz, 8 bit). Interference filters (10 nm bandpass) were used for the wavelength selection of the analyzing light (Mezyk et al., 2016).

### 3. Results and discussion

The radiolytic stability of the highly selective ligands CyMe<sub>4</sub>BTBP and CyMe<sub>4</sub>BTPhen was studied in parallel to compare the effects of radiolysis. 10 mmol L<sup>-1</sup> solutions in 1-octanol were irradiated without contact to an aqueous phase, as well as in contact with 0.1, 1.0 and 4.0 mol L<sup>-1</sup> HNO<sub>3</sub>. After irradiation, phases were separated when needed and the irradiated solvent phases were further studied. <sup>241</sup>Am, <sup>244</sup>Cm and <sup>152</sup>Eu distribution ratios were determined in extraction experiments using fresh 1.0 mol L<sup>-1</sup> HNO<sub>3</sub>. Europium was used as a representative for trivalent lanthanides. Mass spectrometric analyses of the irradiated solvent phases were performed to identify the radiolysis products of the ligand molecules and to (semi-) quantify the remaining extractant and radiolysis product concentrations to investigate the radiolysis mechanism of both ligands. The radiolysis mechanism was further studied using pulsed electron radiolysis.

#### 3.1. Solvent extraction

Fig. 2 shows the Am<sup>3+</sup> and Eu<sup>3+</sup> distribution ratios for CyMe<sub>4</sub>BTBP and CyMe<sub>4</sub>BTPhen as a function of absorbed dose. Curium was found to behave like americium under all tested conditions, with just slightly lower *D* values. Corresponding Cm data is shown in the Supplementary Information (Fig. S1). We found decreasing metal ion distribution ratios for both ligands as a function of absorbed dose when irradiated without contact to an aqueous phase. For CyMe<sub>4</sub>BTBP the *D* values decreased

quickly and the lower detection limit of the *D* values was reached within 200 kGy absorbed dose for <sup>241</sup>Am<sup>3+</sup>. CyMe<sub>4</sub>BTBP is a highly selective extractant for trivalent actinide ions (Geist et al., 2006), as indicated by the generally low *D* values measured for Eu<sup>3+</sup> extraction. Therefore, the lower detection limit of the <sup>152</sup>Eu<sup>3+</sup> *D* values was reached much earlier, within 100–150 kGy absorbed dose. CyMe<sub>4</sub>BTPhen extracts trivalent metal ions with higher *D* values under the same conditions (Lewis et al., 2011). Therefore, all measured *D* values were generally higher compared to CyMe<sub>4</sub>BTBP. Furthermore, the decrease in *D* values did not proceed uniformly. Instead, up to ca. 75 kGy absorbed dose, *D* values decreased quickly, while a much slower decrease was observed between 75 and 300 kGy. This behavior cannot be explained by a decrease in extractant concentration due to radiolysis alone. As we show below, some of the formed radiolysis products seem to be able to extract trivalent metal ions themselves. The stepwise reduction in *D* values for CyMe<sub>4</sub>BTPhen could therefore be due to the build-up of a radiolysis product which also extracts trivalent metal ions, which is then prone to radiolytic degradation itself. The selectivity of the extractants in the solvent extraction experiments did not change much with increasing absorbed dose. Therefore, the radiolysis products also seem to be selective for trivalent actinide extraction.

During process operation, the organic solvent will be irradiated in contact with nitric acid solutions. Therefore, we tested the extraction of trivalent metal ions for solvents irradiated in contact with 0.1, 1, and 4 mol L<sup>-1</sup> HNO<sub>3</sub> solutions. After irradiation, the phases were separated, and the irradiated organic phases were contacted with fresh 1 mol L<sup>-1</sup> HNO<sub>3</sub> containing trace metal ions. These results are also shown in Fig. 2. Under most conditions, the observed distribution ratios were higher compared to the extraction series without addition of HNO<sub>3</sub> during

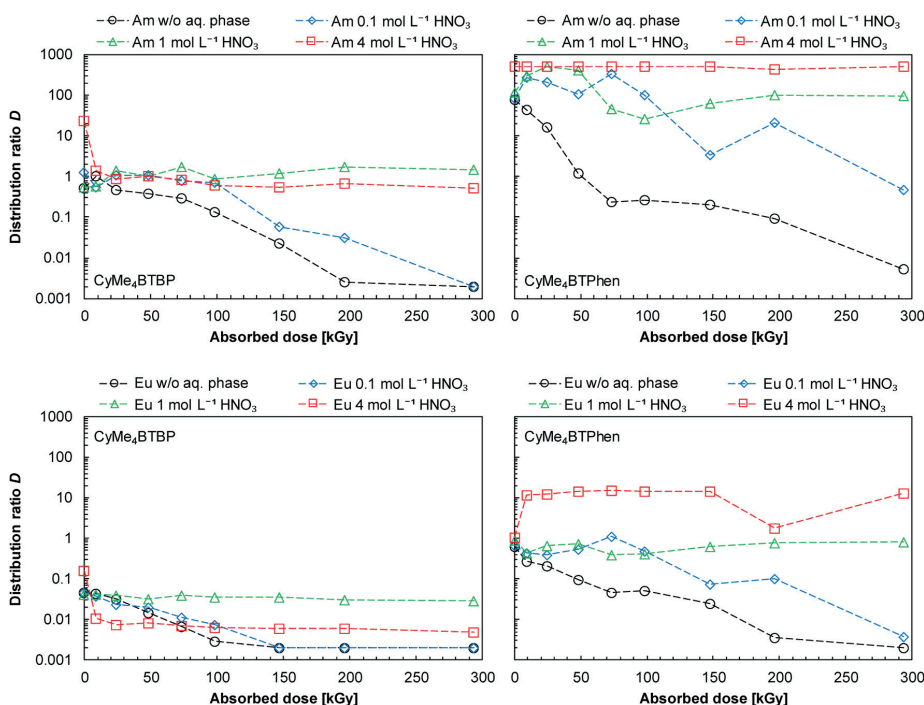


Fig. 2. Am<sup>3+</sup> (top) and Eu<sup>3+</sup> (bottom) distribution ratios as a function of absorbed dose for CyMe<sub>4</sub>BTBP (left) and CyMe<sub>4</sub>BTPhen (right). Extraction experiments after  $\gamma$ -irradiation of solutions of 10 mmol L<sup>-1</sup> ligand in 1-octanol without and with contact to 0.1, 1.0 and 4.0 mol L<sup>-1</sup> HNO<sub>3</sub>. The solvent extraction experiments were conducted using the irradiated solvent phase and fresh 1.0 mol L<sup>-1</sup> HNO<sub>3</sub> spiked with <sup>241</sup>Am, <sup>244</sup>Cm, and <sup>152</sup>Eu tracer. Given *D* values show an uncertainty of  $\pm 5\%$  within the range of  $0.01 < D < 100$ .

irradiation, and the selectivity of the extractants remained high. The estimated annual dose to a solvent in used nuclear fuel treatment differs in the range 250 kGy to 125 MGy, depending on fuel type and burn-up (Fermvik et al., 2010; Magnusson et al., 2009b; Logunov et al., 2006). The results show that both ligands can be used in a continuous separation process for many extraction cycles, as the ligands will likely be used in contact with higher nitric acid concentrations during the extraction steps (where fission products with high gamma dose rate are present). The addition of 0.1 mol L<sup>-1</sup> HNO<sub>3</sub> during irradiation caused a slower decrease of *D* values as a function of absorbed dose. For CyMe<sub>4</sub>BTBP the lower detection limit of the *D* values was reached after 300 kGy absorbed dose for <sup>241</sup>Am<sup>3+</sup>. For 1 and 4 mol L<sup>-1</sup> HNO<sub>3</sub> the CyMe<sub>4</sub>BTBP *D* values remained relatively constant up to 300 kGy. Interestingly, the contact with 1 and 4 mol L<sup>-1</sup> HNO<sub>3</sub> during irradiation caused increased *D* values for CyMe<sub>4</sub>BTPhen. This is partly due to a slight co-extraction of nitric acid in the irradiated solvent, causing slightly higher equilibrium nitric acid concentrations in the extraction experiments. In the series irradiated in contact with 4 mol L<sup>-1</sup> HNO<sub>3</sub>, the Am<sup>3+</sup> *D* values were very high over the whole range of absorbed doses studied. The Eu<sup>3+</sup> *D* values increased at 10 kGy absorbed dose and remained almost constant for higher absorbed doses. The Am<sup>3+</sup> *D* values of the series irradiated in contact with 1 mol L<sup>-1</sup> HNO<sub>3</sub> first shows an increase of *D* values up to ca. 50 kGy, then a slight decrease between 50 and 100 kGy, and another increase up to 300 kGy. A comparable, but less pronounced behavior, was also observed for the Eu<sup>3+</sup> *D* values. Such a behavior cannot be explained by the co-extraction of nitric acid. Instead, this behavior is likely explained by the formation of radiolysis products which can extract trivalent metal ions themselves, as described above. Similar behavior was observed for CyMe<sub>4</sub>BTPhen in FS-13 (Kondé et al., 2016), as well as CyMe<sub>4</sub>BTPhen in the ionic liquid tri-*n*-octylmethylammonium nitrate (Zsabka et al., 2020). A lower decrease in *D* values for solvents irradiated in contact with HNO<sub>3</sub> solutions was also observed for C5-BPP (2,6-bis(5-(2,2-dimethylpropyl)-1H-pyrazol-3-yl)pyridine, another highly selective N-Donor extractant) in a mixture of kerosene, 1-octanol and 2-bromohexanoic acid (Wilden et al., 2016). A clear statement towards the comparison of the radiolytic stability for the two extractants cannot be made based on the measured *D* values, as the initial *D* values already differ too much. Therefore, quantitative information on the extractant concentration as a function of absorbed dose using mass spectrometric methods is discussed below.

### 3.2. Identification of radiolysis products

Following the results of solvent extraction experiments, additional irradiation experiments were conducted to study the irradiated solvents using mass spectrometric techniques. Based on the extraction results, we decided to perform these experiments with solvents irradiated without contact to an aqueous phase and in contact with 1.0 mol L<sup>-1</sup> nitric acid only. These two experimental conditions showed the most interesting results in the solvent extraction experiments, clearly indicating that changes in the CyMe<sub>4</sub>BTBP and CyMe<sub>4</sub>BTPhen molecular structures took place. The aim of the mass spectrometric measurements was to measure the extractant concentration in the irradiated solvents, as well as to identify and if possible, to semi-quantify the radiolysis products. Quantitative analyses were only possible for the parent CyMe<sub>4</sub>BTBP and CyMe<sub>4</sub>BTPhen molecules. For the radiolysis products no calibration standards were available and thus, a quantification was not possible. Instead, the measured intensities in the HPLC-MS spectra are discussed (semi-quantification). For the identification of radiolysis products, we used high resolution mass spectrometry (HR-MS) measurements with prior high-performance liquid chromatography (HPLC). Samples irradiated in contact with 1.0 mol L<sup>-1</sup> nitric acid to moderate absorbed doses of ca. 100 kGy were most suitable for radiolysis product identification, as they included the parent molecules as well as the radiolysis products in enough quantities. Fig. 3 shows exemplary mass spectra of CyMe<sub>4</sub>BTBP and CyMe<sub>4</sub>BTPhen solutions irradiated to 132 kGy absorbed dose without contact to an aqueous phase. The mass spectra from all irradiated samples of both extractants irradiated without (10–413 kGy) or with (10–623 kGy) nitric acid contact are shown in the Supplementary Information (Figs. S2–S5). Nitric acid contacted samples were irradiated to higher doses, as the solvent extraction experiments suggested a protective effect and thus higher absorbed doses were necessary to result in notable degradation.

The peaks found at *m/z* 535.3291 and 559.3290 were assigned to the protonated CyMe<sub>4</sub>BTBP and CyMe<sub>4</sub>BTPhen species (M+H<sup>+</sup>), respectively. The measured *m/z* ratios were in very good agreement with *m/z* ratios calculated from the proposed molecular formulae, as shown in Table 3 and Table 4. Sodiated species were detected at *m/z* 557.3113 and 581.3109 (M+Na<sup>+</sup>), as sodium is widespread in glassware, solvents, and the mass spectrometer ion sources. The CyMe<sub>4</sub>BTPhen + Na<sup>+</sup> species is better visible compared to the CyMe<sub>4</sub>BTBP + Na<sup>+</sup> species, which

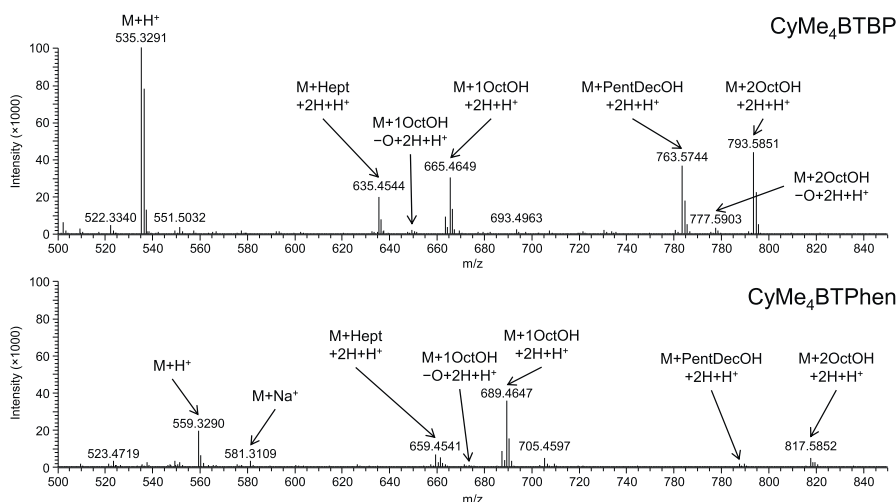


Fig. 3. Mass spectra of 10 mmol L<sup>-1</sup> CyMe<sub>4</sub>BTBP (top) and CyMe<sub>4</sub>BTPhen (bottom) in 1-octanol irradiated to 132 kGy absorbed dose without contact to nitric acid. M = CyMe<sub>4</sub>BTBP or CyMe<sub>4</sub>BTPhen, OctOH =  $\alpha$ -hydroxyoctyl, PentDecOH = 8-hydroxypentadecanyl, Hept = heptyl.



**Table 3**

Overview of the identified species in irradiated CyMe<sub>4</sub>BTBP samples. *m/z* ratios were calculated using the given molecular formulae and compared to the measured *m/z* ratios.

M = CyMe<sub>4</sub>BTBP, OctOH =  $\alpha$ -hydroxyoctyl, PentDecOH = 8-hydroxypentadecanyl, Hept = heptyl.

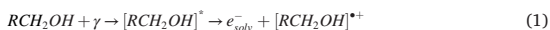
CyMe <sub>4</sub> BTBP species	Measured <i>m/z</i> ratio	Calculated <i>m/z</i> ratio	Molecular formula
Dicarbonitrile	207.0665	207.0665	C <sub>12</sub> H <sub>7</sub> N <sub>4</sub> <sup>+</sup>
Carbonitrile	371.1979	371.1979	C <sub>22</sub> H <sub>23</sub> N <sub>4</sub> <sup>+</sup>
M + H <sup>+</sup>	535.3291	535.3292	C <sub>32</sub> H <sub>39</sub> N <sub>4</sub> <sup>+</sup>
M + Na <sup>+</sup>	557.3113	557.3112	C <sub>32</sub> H <sub>38</sub> N <sub>4</sub> Na <sup>+</sup>
M + Hept + H <sup>+</sup>	633.4387	633.4388	C <sub>39</sub> H <sub>53</sub> N <sub>4</sub> <sup>+</sup>
M + Hept + 2H + H <sup>+</sup>	635.4544	635.4544	C <sub>39</sub> H <sub>55</sub> N <sub>4</sub> <sup>+</sup>
M + 1OctOH – O + 2H + H <sup>+</sup>	649.4700	649.4701	C <sub>40</sub> H <sub>57</sub> N <sub>4</sub> <sup>+</sup>
M + 1OctOH + H <sup>+</sup>	663.4490	663.4493	C <sub>40</sub> H <sub>55</sub> N <sub>4</sub> O <sup>+</sup>
M + 1OctOH + 2H + H <sup>+</sup>	665.4649	665.4650	C <sub>40</sub> H <sub>57</sub> N <sub>4</sub> O <sup>+</sup>
M + PentDecOH + H <sup>+</sup>	761.5770	761.5589	C <sub>47</sub> H <sub>69</sub> N <sub>4</sub> O <sup>+</sup>
M + PentDecOH + 2H + H <sup>+</sup>	763.5744	763.5745	C <sub>47</sub> H <sub>71</sub> N <sub>4</sub> O <sup>+</sup>
M + 2OctOH – O + 2H + H <sup>+</sup>	777.5903	777.5902	C <sub>48</sub> H <sub>73</sub> N <sub>4</sub> O <sup>+</sup>
M + 2OctOH + H <sup>+</sup>	791.5695	791.5694	C <sub>48</sub> H <sub>71</sub> N <sub>4</sub> O <sub>2</sub> <sup>+</sup>
M + 2OctOH + 2H + H <sup>+</sup>	793.5851	793.5851	C <sub>48</sub> H <sub>73</sub> N <sub>4</sub> O <sub>2</sub> <sup>+</sup>

**Table 4**

Overview of the identified species in irradiated CyMe<sub>4</sub>BTPhen samples. *m/z* ratios were calculated using the given molecular formulae and compared to the measured *m/z* ratios. M = CyMe<sub>4</sub>BTPhen, OctOH =  $\alpha$ -hydroxyoctyl, PentDecOH = 8-hydroxypentadecanyl, Hept = heptyl.

CyMe <sub>4</sub> BTPhen species	Measured <i>m/z</i> ratio	Calculated <i>m/z</i> ratio	Molecular formula
Dicarbonitrile	231.0665	231.0665	C <sub>14</sub> H <sub>7</sub> N <sub>4</sub> <sup>+</sup>
Carbonitrile	395.1978	395.1979	C <sub>24</sub> H <sub>23</sub> N <sub>4</sub> <sup>+</sup>
M + H <sup>+</sup>	559.3290	559.3292	C <sub>34</sub> H <sub>39</sub> N <sub>4</sub> <sup>+</sup>
M + Na <sup>+</sup>	581.3109	581.3112	C <sub>34</sub> H <sub>38</sub> N <sub>4</sub> Na <sup>+</sup>
M + Hept + H <sup>+</sup>	657.4385	657.4388	C <sub>41</sub> H <sub>53</sub> N <sub>4</sub> <sup>+</sup>
M + Hept + 2H + H <sup>+</sup>	659.4541	659.4544	C <sub>41</sub> H <sub>55</sub> N <sub>4</sub> <sup>+</sup>
M + 1OctOH – O + 2H + H <sup>+</sup>	673.4698	673.4701	C <sub>42</sub> H <sub>57</sub> N <sub>4</sub> <sup>+</sup>
M + 1OctOH + H <sup>+</sup>	687.4491	687.4493	C <sub>42</sub> H <sub>55</sub> N <sub>4</sub> O <sup>+</sup>
M + 1OctOH + 2H + H <sup>+</sup>	689.4647	689.4650	C <sub>42</sub> H <sub>57</sub> N <sub>4</sub> O <sup>+</sup>
M + PentDecOH + H <sup>+</sup>	785.5587	785.5589	C <sub>49</sub> H <sub>69</sub> N <sub>4</sub> O <sup>+</sup>
M + PentDecOH + 2H + H <sup>+</sup>	787.5745	787.5745	C <sub>49</sub> H <sub>71</sub> N <sub>4</sub> O <sup>+</sup>
M + 2OctOH – O + 2H + H <sup>+</sup>	801.5907	801.5902	C <sub>50</sub> H <sub>73</sub> N <sub>4</sub> O <sup>+</sup>
M + 2OctOH + H <sup>+</sup>	815.5696	815.5694	C <sub>50</sub> H <sub>71</sub> N <sub>4</sub> O <sub>2</sub> <sup>+</sup>
M + 2OctOH + 2H + H <sup>+</sup>	817.5852	817.5851	C <sub>50</sub> H <sub>73</sub> N <sub>4</sub> O <sub>2</sub> <sup>+</sup>
M + 2OctOH + 4H + H <sup>+</sup>	819.6016	819.6008	C <sub>50</sub> H <sub>75</sub> N <sub>4</sub> O <sub>2</sub> <sup>+</sup>

occurs in smaller intensity below the label threshold limit in Fig. 3 (but still well measured). The most prominent radiolysis products found in the measured mass spectra were best described as addition products of the diluent 1-octanol. Longer chained alcohols are known to yield  $\alpha$ -hydroxyalkyl radicals and other radiolysis products under irradiation (Mincher et al., 1994, 2010b; Freeman, 1970; Symons and Eastland, 1977; Swallow, 1987; Nilsson et al., 2006). The most important radiolysis reactions for longer chained alcohols are summarized in equations (1)–(4):



The initial products formed during alcohol radiolysis are solvated electrons ( $e_{solv}^-$ ) and the corresponding alcohol radical cations ( $[RCH_2OH]^+$ ), Equation (1). The radical cations decompose to form  $\alpha$ -hydroxyalkyl radicals (2). The solvated electron can react with protons to yield the hydrogen radical  $H^*$  (3) (Buxton et al., 1988). Hydrogen radicals commonly react with diluent molecules via hydrogen atom abstraction also resulting in the formation of carbon-centered  $\alpha$ -hydroxyalkyl radicals (4). The  $\alpha$ -hydroxyalkyl radicals can react with the ligand molecules with the formation of the observed addition products. The radiolysis products were identified as addition product with one or two of these  $\alpha$ -hydroxyoctyl radicals (OctOH). The *m/z* ratios of the M+3OctOH+H<sup>+</sup> products were only found with very low intensities in a few samples. Interestingly, lower *m/z* ratios than the parent molecule masses were barely observed. The addition reaction with the  $\alpha$ -hydroxyoctyl radical seems to be more probable than ligand degradation, at least for the investigated dose range of up to 623 kGy absorbed dose. This is partly explained by the relatively low concentration (0.01 mol L<sup>-1</sup>) of CyMe<sub>4</sub>BTBP or CyMe<sub>4</sub>BTPhen compared to the diluent 1-octanol (ca. 6.4 mol L<sup>-1</sup>, equals ca. 640 times higher concentration). Therefore, the radiolysis of diluent molecules is expected to be the preferred interaction of the incoming gamma rays producing the highly reactive diluent radicals. These diluent radicals then react with the ligand molecules, which is frequently referred to as indirect radiolysis (Mincher et al., 2010a). The reactivity of such diluent radicals depends on the nature of the diluent and was referred to as the sensitization effect (Sugo et al., 2002, 2007). Intensities of the different 1-octanol addition products decreased with the number of additions (see Fig. 3). The reaction of extractant molecules with diluent radicals was described previously by Fermvik et al. for the radiolysis of CyMe<sub>4</sub>BTBP in cyclohexanone and 1-hexanol (Fermvik, 2011), and by Wilden et al. for the radiolysis of C5-BPP (Wilden et al., 2016), a related nitrogen donor ligand. Zsabka et al. recently observed addition reactions of the cations of an ionic liquid to the CyMe<sub>4</sub>BTPhen ligand, as well (Zsabka et al., 2020).

We assume that the  $\alpha$ -hydroxyoctyl radical addition reaction takes place via H<sup>\*</sup> atom abstraction from the parent molecules. This should yield addition products with *m/z* ratios of 663.4493 and 687.4493 in the protonated forms for the M+1OctOH addition products of CyMe<sub>4</sub>BTBP and CyMe<sub>4</sub>BTPhen, respectively. However, both *m/z* ratios were only found at trace levels. Instead, *m/z* ratios with two and in some cases four mass units higher compared to the expected species were found predominantly. This could be explained by the additional reduction of one or two unsaturated bonds in the ligand molecules. This reduction is likely caused by reactions with reducing species (e.g. hydrogen radicals (H<sup>\*</sup>) or H<sub>2</sub>), formed by diluent radiolysis (cf. equations (3) and (4)) (Mincher and Mezyk, 2009). The yield of H<sub>2</sub> production by radiolysis is relatively high in alcohols, compared to other diluents (Swallow, 1987; Yu et al., 2010). The reduction of one C=C bond in the M+1OctOH molecule results in calculated *m/z* ratios of 665.4650 and 689.4650 (protonated form) for CyMe<sub>4</sub>BTBP and CyMe<sub>4</sub>BTPhen, respectively (*m/z* ratios 665.4649 and 689.4647 in Fig. 3 labelled M+1OctOH+2H + H<sup>+</sup>). Similar reduction products were observed for the addition of two  $\alpha$ -hydroxyoctyl radicals and other addition products for both ligands. Fig. 3 shows that these reduced species were found predominantly.

Another possible route for the formation of addition products would be the initial reaction of an extractant with a solvated electron to form the extractant radical anion. This route was proposed by Szreder et al. (2019), showing that in addition to equation (3), the extended  $\pi$ -system of the ligand molecules should also be able to incorporate and stabilize the solvated electron (cf. equation (5)).



Yu et al. further reported the formation of *n*-heptane and pentadecan-8-ol (via addition of heptyl with  $\alpha$ -hydroxyoctyl radicals) among others in <sup>60</sup>Co irradiated 1-octanol solution of up to 600 kGy

absorbed dose (Yu et al., 2010). These products are also likely produced by radical reactions with the intermediate formation of the *n*-heptyl and 8-hydroxypentadecanyl radicals. We observed the corresponding addition products of the *n*-heptyl radical with  $m/z$  633.4387 and 657.4385 of the protonated species for CyMe<sub>4</sub>BTBP and CyMe<sub>4</sub>BTPhen, respectively (Tables 3 and 4). Again, the reduced forms ( $m/z$  635.4544 and 659.4541) were predominantly found. The 8-hydroxypentadecanyl radical addition products were found in their reduced form at  $m/z$  763.5744 for CyMe<sub>4</sub>BTBP under both conditions. For CyMe<sub>4</sub>BTPhen, the unreduced form ( $m/z$  785.5587) was mainly observed under acidic conditions, while the reduced form ( $m/z$  787.5745) was predominantly formed in neat organic solution. Additionally,  $m/z$  ratios of addition products with  $-16$  mass units ( $M+1\text{OctOH}-16$ ,  $M+2\text{OctOH}-16$ ) were found. The difference of 16 mass units could be explained by the formal loss of one oxygen atom. Such a reaction could occur via the abstraction of one OH $\cdot$ , followed by subsequent H $\cdot$  addition, albeit the reaction pathway can be more complex. The calculated  $m/z$  ratios for such reaction products are in very good agreement with measured  $m/z$  ratios and was also observed in the radiolysis of C5-BPP (Wilden et al., 2016). The mass spectra shown in Fig. 3 showed the most abundant radiolysis products in the range of  $m/z$  500–1000 for better visibility. The only identified CyMe<sub>4</sub>BTBP radiolysis products with lower  $m/z$  ratios as the parent molecule were found to be 6'-(5,5,8,8-tetramethyl-5,6,7,8-tetrahydrobenzo[e][1,2,4]-triazin-3-yl)-[2,2'-bipyridine]-6-carbonitrile and [2,2'-bipyridine]-6,6'-dicarbonitrile ("Carbonitrile" and "Dicarbonitrile" in Table 3, see also Fig. S6). The carbonitrile has been observed before by Fermvik et al. for the radiolysis of CyMe<sub>4</sub>BTBP in cyclohexanone and 1-hexanol (Fermvik, 2011), and Nicolas et al. for the hydrolysis of CyMe<sub>4</sub>BTBP (Nicolas et al., 2011). The dicarbonitrile was found only in extremely small amounts. Comparable compounds were found for the radiolysis of CyMe<sub>4</sub>BTPhen in very small amounts as well (Table 4, see also Fig. S7). All identified molecules and ligand fragments are summarized in Tables 3 and 4 for CyMe<sub>4</sub>BTBP and CyMe<sub>4</sub>BTPhen, respectively.

Figs. S8 and S9 show proposed reaction schemes for the radiolysis of CyMe<sub>4</sub>BTBP and CyMe<sub>4</sub>BTPhen, respectively, summarizing the different reactions described in this paper. We were not able yet to determine the molecular structures of the addition products. Irradiation experiments using ligand solutions in deuterated 1-octanol and subsequent  $^1\text{H}$  and  $^{13}\text{C}$ -NMR analyses were not successful. Afsar et al. synthesized chloro-

and bromo-CyMe<sub>4</sub>BTBP with the addition of the halides in 4-position of the pyridine ring, which were able to extract trivalent metal ions (Afsar et al., 2016). Therefore, we chose to show the radical addition products substituted at this position in Figs. S8 and S9, although the exact structure is unknown. The substitution in 4-position of the pyridine ring would also explain the preservation of the extraction properties as discussed above.

Fig. 4 shows exemplary mass spectra of CyMe<sub>4</sub>BTBP and CyMe<sub>4</sub>BTPhen solutions irradiated to 132 kGy in contact with 1.0 mol L<sup>-1</sup> nitric acid (all mass spectra are shown in Figure S2 to Figs. S2–S5). In principle, the same peaks were found as for the samples irradiated without nitric acid contact (Fig. 3), but with generally higher intensities of the parent molecule species ( $M+H^+$ ). The addition products were similarly observed, but in contrast to the samples irradiated without acid contact, the  $M+1\text{OctOH}$  addition products were mainly found in the unreduced form. The reduced forms ( $+2\text{H}$ ) were only found in traces. Higher addition products with two  $\alpha$ -hydroxyoctyl radicals added ( $M+2\text{OctOH}$ ) were present in lower intensities, for CyMe<sub>4</sub>BTBP interestingly predominantly in the reduced form, while for CyMe<sub>4</sub>BTPhen mainly in the unreduced form. The *n*-heptyl and 8-hydroxypentadecanyl radical addition products were found with low intensities. 1-Octanol is known to extract considerable amounts of water and nitric acid when equilibrated with nitric acid solutions (Lang, 2012; Woodhead et al., 2019). The considerably lower formation of radiolysis products is therefore attributed to the scavenging of reactive radicals in the organic phase by extracted water and nitric acid (Horne et al., 2020). Therefore, contact with aqueous nitric acid solution during irradiation has a protective effect, especially on CyMe<sub>4</sub>BTBP. This confirms the observations from the solvent extraction experiments and will be described more quantitatively in the following discussion.

### 3.3. (Semi-) quantification of radiolysis products

Quantitative analyses of irradiated samples were carried out to measure the decrease in ligand concentration as a function of absorbed dose. Freshly prepared solutions of 10 mmol L<sup>-1</sup> CyMe<sub>4</sub>BTBP or CyMe<sub>4</sub>BTPhen in 1-octanol were used for calibration and as references. Fig. 5 shows the measured ligand concentrations in organic solutions irradiated without and with contact to 0.1 and 1.0 mol L<sup>-1</sup> nitric acid as a function of the absorbed dose from HPLC-MS. The data shows some

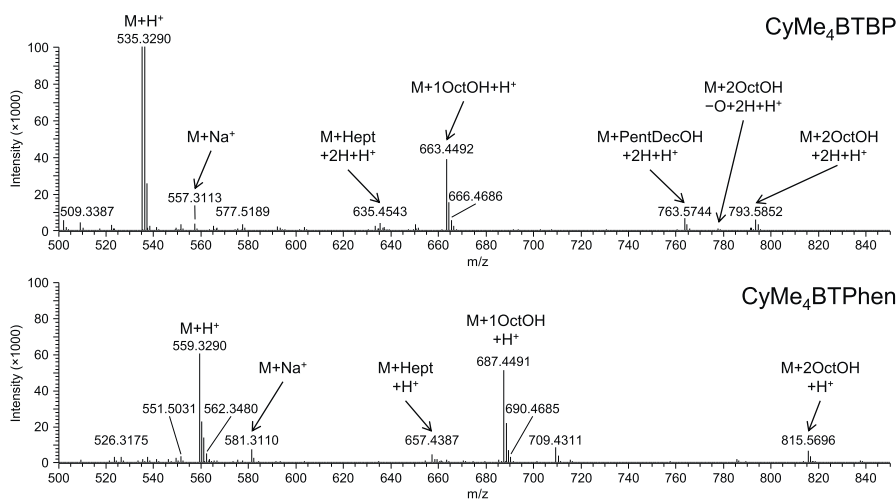


Fig. 4. Mass spectra of 10 mmol L<sup>-1</sup> CyMe<sub>4</sub>BTBP (top) and CyMe<sub>4</sub>BTPhen (bottom) in 1-octanol irradiated to 132 kGy absorbed dose in contact with 1.0 mol L<sup>-1</sup> nitric acid. M = CyMe<sub>4</sub>BTBP or CyMe<sub>4</sub>BTPhen, OctOH =  $\alpha$ -hydroxyoctyl, PentDecOH = 8-hydroxypentadecanyl, Hept = heptyl.

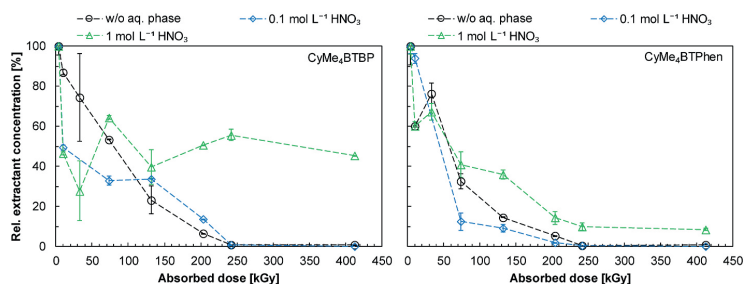


Fig. 5. Decrease of the CyMe<sub>4</sub>BTBP (left) and CyMe<sub>4</sub>BTPPh (right) concentration as a function of the absorbed dose. Data is normalized to the measured concentration in the unirradiated sample. 10 mmol L<sup>-1</sup> solutions of CyMe<sub>4</sub>BTBP and CyMe<sub>4</sub>BTPPh in 1-octanol were irradiated without and with contact to 0.1 and 1.0 mol L<sup>-1</sup> HNO<sub>3</sub> and analyzed by HPLC HR-MS.

scattering but generally compares well with additional data obtained from direct infusion mass spectrometry (not shown) (Schmidt et al., 2016). For solutions irradiated without contact to nitric acid a steep decrease in the remaining ligand concentration was observed. This is in good agreement with results from solvent extraction, assuming the observed decreasing distribution ratios resulting from the decreasing concentration of the ligand molecules (Fig. 2). The ligand degradation without acid contact occurred within the same dose range for both ligands. After 250 kGy absorbed dose, the remaining CyMe<sub>4</sub>BTBP and CyMe<sub>4</sub>BTPPh concentrations were below the detection limit. For the organic solutions irradiated in contact with 0.1 mol L<sup>-1</sup> HNO<sub>3</sub>, no protective effect was found. In contrast, degradation of both ligands seemed

to be even higher under these conditions. This is contradictory to the solvent extraction results, where higher distribution ratios were observed when the solvents were irradiated in contact with 0.1 mol L<sup>-1</sup> HNO<sub>3</sub>. For irradiation of the organic phases in contact with 1.0 mol L<sup>-1</sup> nitric acid, higher final ligand concentrations were found up to 413 kGy absorbed dose. For CyMe<sub>4</sub>BTBP, the final concentration was nearly 45%, while in the case of CyMe<sub>4</sub>BTPPh roughly 10% of the initial ligand concentration remained. In comparison with results from solvent extraction, the low ligand concentration of CyMe<sub>4</sub>BTPPh was surprising, since high americium distribution ratios were found for both ligands after radiolysis (Fig. 2).

As the parent molecule concentrations decreased with increasing

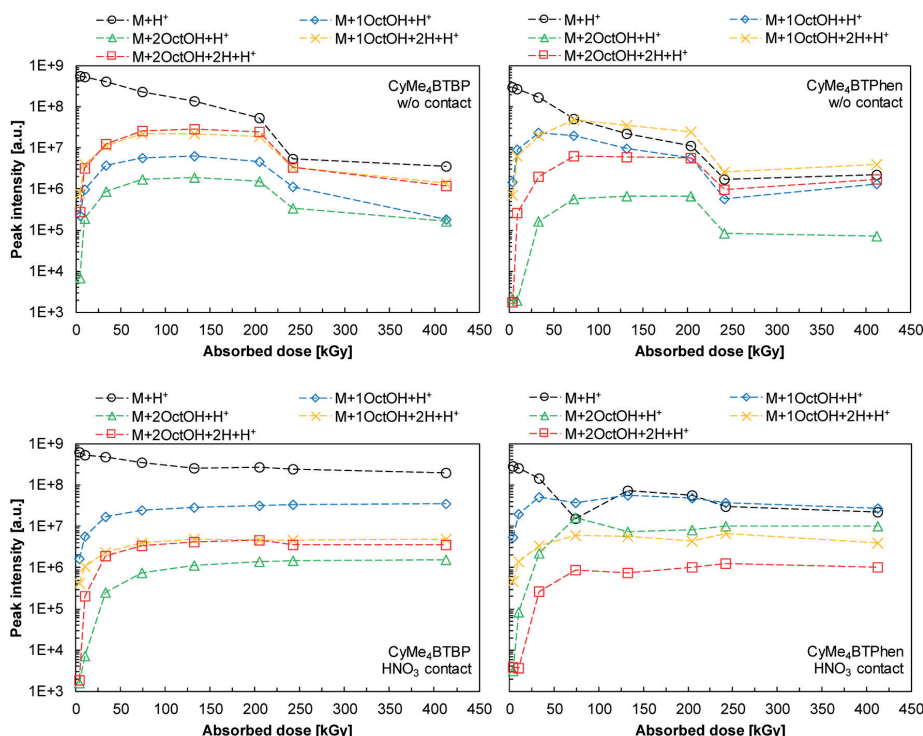


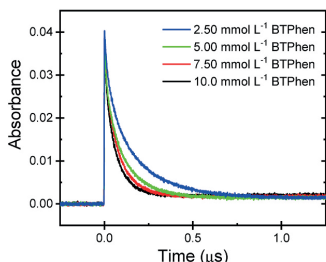
Fig. 6. Peak intensities of the parent molecules and the radiolysis products as a function of the absorbed dose for CyMe<sub>4</sub>BTBP (left) and CyMe<sub>4</sub>BTPPh (right), irradiated without contact to an aqueous phase (top) or in contact with 1.0 mol L<sup>-1</sup> HNO<sub>3</sub> (bottom). Measured *m/z* ratios of the fragments are given in Tables 3 and 4.

absorbed dose, but  $\text{An}^{3+}$  extraction was nearly not influenced, our previous assumption that at least one of the observed radiolytic addition products is also capable of extracting  $\text{An}^{3+}$  is confirmed. Similar observations were made by Fermvik (2011). The ligand concentration after radiolysis and calculated theoretical americium distribution ratios were determined and compared with measured  $D$  values. The values for cyclohexanone were in good agreement, but for 1-hexanol higher distribution ratios were observed than calculated based on the remaining ligand concentration. In subsequent mass spectrometric measurements, addition products of up to three solvent molecules to  $\text{CyMe}_4\text{BTBP}$  were found, comparable with our findings.

The quantification of radiolysis products in irradiated samples was not possible directly, as analytical standards were not available. Instead, the measured intensities of the mass spectrometric runs were interpreted. Fig. 6 shows the results of these semi-quantitative measurements of the ligand molecules and the addition products of one and two  $\alpha$ -hydroxyoctyl radicals ( $\text{M}+1\text{OctOH}$  and  $\text{M}+2\text{OctOH}$ ) as a function of the absorbed dose for  $\text{CyMe}_4\text{BTBP}$  and  $\text{CyMe}_4\text{BTPhen}$  solutions irradiated without contact to an aqueous phase or in contact with  $1.0 \text{ mol L}^{-1}$   $\text{HNO}_3$ . The quantitative measurements and semi quantification results using HR-MS intensities were in good agreement for the parent molecules (the  $\text{M}+\text{H}^+$   $m/z$  intensities). Without contact to an aqueous phase (Fig. 6, top) a quick decrease in the parent molecule peak intensities over several orders of magnitude was observed, comparable to the quantitative measurements shown in Fig. 5. The radiolysis products' intensities increase to a maximum at ca. 200 kGy after which their intensities decrease with higher doses. In contrast, radiolytic degradation of  $\text{CyMe}_4\text{BTBP}$  and  $\text{CyMe}_4\text{BTPhen}$ , as well as degradation of the radiolysis products themselves is reduced significantly by  $1.0 \text{ mol L}^{-1}$  nitric acid contact during irradiation (Fig. 6, bottom). After a slight initial degradation of the ligand molecules and buildup of the addition products, the intensities of the ligand molecules as well as the  $\text{M}+1\text{OctOH}$  and  $\text{M}+2\text{OctOH}$  addition products remain relatively constant up to 400 kGy. The semi-quantification data again suggests a higher stability of  $\text{CyMe}_4\text{BTBP}$  compared to  $\text{CyMe}_4\text{BTPhen}$  under these conditions, as  $\text{CyMe}_4\text{BTPhen}$  peak intensities further decrease with increasing dose.

### 3.4. Steady state pulse radiolysis

Solvated electrons were generated in 1-octanol solution containing 2.5, 5.0, 7.5 and  $10.0 \text{ mmol L}^{-1}$   $\text{CyMe}_4\text{BTBP}$  and  $\text{CyMe}_4\text{BTPhen}$ , respectively, and their lifetime and subsequent reaction with the ligand molecules following equation (5) was recorded. The results in Fig. 7 show that for both ligands, a faster reaction rate (faster decrease in absorbance) was detected with increasing ligand concentration. This is attributed to an increasing reaction rate of solvated electrons with the ligand molecules. Second-order rate constants ( $k$ ) were calculated from the slopes in Fig. 7 and found to be  $(1.60 \pm 0.04) \times 10^9 \text{ L mol}^{-1} \text{ s}^{-1}$  for  $\text{CyMe}_4\text{BTBP}$  and  $(1.05 \pm 0.03) \times 10^9 \text{ L mol}^{-1} \text{ s}^{-1}$  for  $\text{CyMe}_4\text{BTPhen}$ .



These results imply that both ligands react rapidly with the solvated electron according to equation (5) and that  $\text{CyMe}_4\text{BTBP}$  reacts faster than  $\text{CyMe}_4\text{BTPhen}$ . Molecular orbital calculations by Szreder et al. showed that the excess electron is delocalized within the structure of the  $\text{CyMe}_4\text{BTPhen}$  radical anion with the highest electron density on the triazinyl moieties, which contribute in stabilizing the system (Szreder et al., 2019). Additionally, no fragmentation of the molecule was observed and it was concluded that the radical anion has a relatively long life-time and is able to undergo further reactions. Szreder et al. measured a rate constant of  $(1.85 \pm 0.09) \times 10^9 \text{ L mol}^{-1} \text{ s}^{-1}$  for the reaction of  $\text{CyMe}_4\text{BTPhen}$  with the solvated electron in 1-octanol, which is in good agreement with our results (Szreder et al., 2019). Further steady-state irradiation experiments under oxidizing and reducing conditions are planned in the future to clarify the role of solvated electrons in molecule degradation. To study the role of water and nitric acid during radiolysis, steady state pulse radiolysis experiments were conducted using solutions of  $2.5\text{--}10.0 \text{ mmol L}^{-1}$   $\text{CyMe}_4\text{BTPhen}$  in pure dried 1-octanol as well as in 1-octanol previously contacted with  $6.0 \text{ mol L}^{-1}$  nitric acid. The absorbance of the solvated electrons was monitored as a function of time (Fig. 8). For samples containing only the ligand molecule and 1-octanol, a clear absorbance of solvated electrons was found, whereas the acid contacted 1-octanol solvent did not show an absorbance of solvated electrons. In contrast to equation (5), where the solvated electrons were captured by ligand molecules forming ligand radical anions, in the presence of dissociated nitric acid the solvated electrons are captured by protons or nitrate anions to form hydrogen atoms (equation (3)) and other transient species. Due to this process, fewer solvated electrons are available to directly form ligand radical anions.

Analysis of the new absorbance kinetics under these contacted acidic octanol conditions was also performed, as shown in Fig. 8. The measured absorbance profiles were fitted to a standard pseudo-first-order growth and decay function, with the growth component value plotted against the ligand concentration (Fig. 8, Bottom Left and Bottom Right) to obtain the second-order rate constants for hydrogen atom ( $\text{H}^\bullet$ ) reaction



as  $k_6 = (3.18 \pm 0.08) \times 10^8 \text{ L mol}^{-1} \text{ s}^{-1}$  and  $(4.16 \pm 0.06) \times 10^8 \text{ L mol}^{-1} \text{ s}^{-1}$  for  $\text{CyMe}_4\text{BTBP}$  and  $\text{CyMe}_4\text{BTPhen}$ , respectively.

### 4. Conclusions

The gamma radiolysis of  $\text{CyMe}_4\text{BTBP}$  and  $\text{CyMe}_4\text{BTPhen}$  in 1-octanol solution with and without contact with nitric acid was studied comparatively to examine the influence of structural changes in the ligand backbone on the radiolytic stability. Solvent extraction experiments showed that irradiation of the pure solvent lead to a rapid decrease in distribution ratios of the tested trivalent actinide and lanthanide ions ( $\text{Am}^{3+}$ ,  $\text{Cm}^{3+}$ ,  $\text{Eu}^{3+}$ ) for both ligands, and an almost

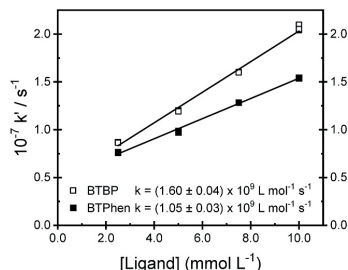
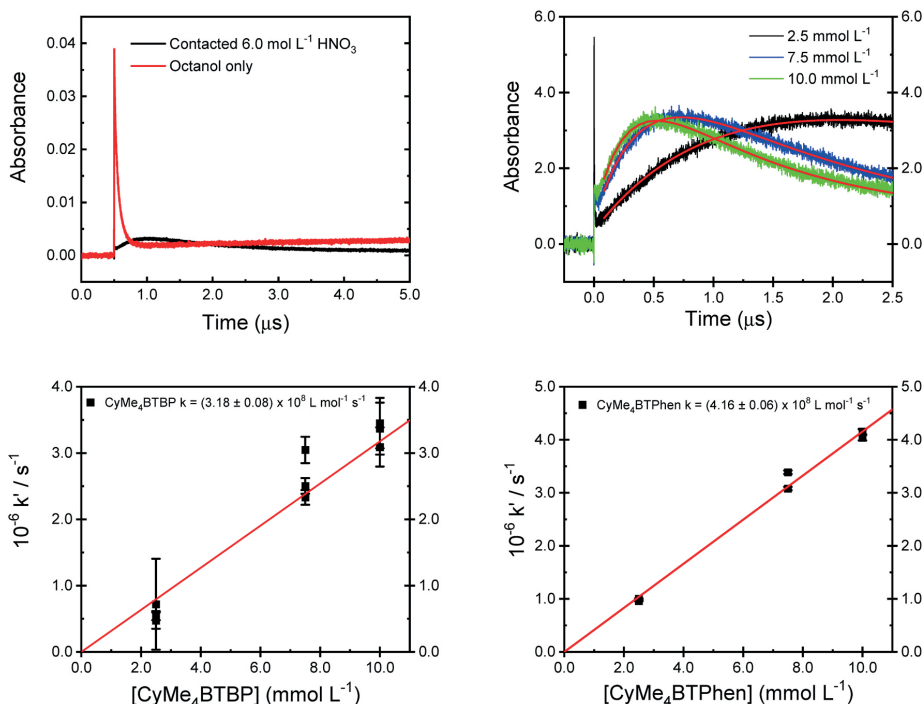


Fig. 7. Left: Decay kinetics of the solvated electron in 1-octanol at 640 nm for different concentrations of  $\text{CyMe}_4\text{BTPhen}$ . Right: Calculated second-order rate constants for solvated electron reaction with  $\text{CyMe}_4\text{BTBP}$  and  $\text{CyMe}_4\text{BTPhen}$  as obtained from fitting pseudo-first-order kinetics to the observed decay data for the different ligand concentrations in 1-octanol (cf. equation (5)).





**Fig. 8.** **Top Left:** Absorbance decays of the solvated electron in the presence of 10.0 mmol L<sup>-1</sup> CyMe<sub>4</sub>BTBP in pure 1-octanol (red) and 1-octanol contacted with 6.0 mol L<sup>-1</sup> HNO<sub>3</sub> (black). **Top Right:** CyMe<sub>4</sub>BTPhen concentration dependence of the new growth following solvated electron decay observed at 640 nm. Solid red lines are calculated fits using a pseudo-first-order growth and decay kinetic model. **Bottom Left:** Second-order rate constant determination for H<sup>•</sup> atom reaction with CyMe<sub>4</sub>BTBP in 1-octanol, with calculated rate constant of  $k = (3.18 \pm 0.08) \times 10^9 \text{ L mol}^{-1} \text{ s}^{-1}$ . **Bottom Right:** Second-order rate constant determination for H<sup>•</sup> atom reaction with CyMe<sub>4</sub>BTPhen in 1-octanol, with calculated rate constant of  $k = (4.16 \pm 0.06) \times 10^8 \text{ L mol}^{-1} \text{ s}^{-1}$ . (For interpretation of the references to colour in this figure legend, the reader is referred to the Web version of this article.)

complete loss of extraction at 200–300 kGy absorbed dose. Irradiation of the solvents in contact with nitric acid solution showed a stabilization (CyMe<sub>4</sub>BTBP), or even an increase (CyMe<sub>4</sub>BTPhen) of the metal ion distribution ratios and preservation of the high selectivity of the extractants. This is attributed to the formation of radiolysis products that are good An<sup>3+</sup> extractants with high selectivity themselves. Radiolysis products were identified by high-resolution mass spectrometric analyses. Comparable radiolysis products were found for both ligands, mainly formed through addition of diluent radicals formed by prior reaction of diluent molecules with the incident gamma radiation, following an indirect radiolysis mechanism. Although no direct information on the location of the addition site of the  $\alpha$ -hydroxyoctyl and other radicals to the ligand molecule is available from the mass spectrometric measurements, the retention of good extraction properties of solvents irradiated in contact with nitric acid implies a substitution in the outer region of the ligand backbones, *i.e.* outside the binding cleft which accommodates the target metal ion. Quantification of the remaining ligand concentrations in irradiated solvents and semi quantification of radiolysis products further fortified that assumption. The quantification showed that the CyMe<sub>4</sub>BTBP concentrations after receiving a certain dose were higher than the CyMe<sub>4</sub>BTPhen concentrations, and hence CyMe<sub>4</sub>BTBP can be considered more stable against radiolysis. However, from an applications point of view, a solvent extraction process might be operated longer with CyMe<sub>4</sub>BTPhen, as metal ion distribution ratios are higher after the same dose than for CyMe<sub>4</sub>BTBP. Further irradiation experiments employing loop radiolysis tests in a continuous operation mode will be necessary to finally decide

which ligand could be better used in the hydrometallurgical treatment of used nuclear fuel. Steady state pulse radiolysis experiments showed that the solvated electron presumably is the main reactive species in the radiolysis of CyMe<sub>4</sub>BTBP and CyMe<sub>4</sub>BTPhen in 1-octanol. When solvents were irradiated in contact with nitric acid, solvated electrons were preferentially captured by nitric acid instead of reacting with the ligands or the 1-octanol diluent, resulting in a partial protection of the ligand molecules. Our future research aims at better understanding the observed protective effect of nitric acid. Additionally, the molecular structures of the formed addition products must be clarified. This will also enable the development of improved extractants with enhanced radiation stability and better extraction properties.

#### CRediT authorship contribution statement

**Holger Schmidt:** Conceptualization, Formal analysis, Investigation, Methodology, Project administration, Validation, Visualization, Writing – original draft, Writing – review & editing. **Andreas Wilden:** Conceptualization, Formal analysis, Investigation, Methodology, Project administration, Supervision, Validation, Visualization, Writing – original draft, Writing – review & editing. **Giuseppe Modolo:** Conceptualization, Funding acquisition, Project administration, Resources, Supervision, Writing – review & editing. **Dirk Bosbach:** Conceptualization, Funding acquisition, Resources, Supervision, Writing – review & editing. **Beatrix Santiago-Schübel:** Formal analysis, Investigation, Methodology, Resources, Validation, Writing – review & editing. **Michelle Hupert:** Formal analysis, Investigation, Methodology,

Validation, Writing – review & Editing. **Bruce J. Mincher**: Conceptualization, Formal analysis, Investigation, Methodology, Resources, Validation, Writing – review & Editing. **Stephen P. Mezyk**: Conceptualization, Formal analysis, Investigation, Methodology, Resources, Validation, Visualization, Writing – original draft, Writing – review & Editing. **Jaroslav Švehla**: Formal analysis, Investigation, Methodology, Validation, Writing – review & Editing. **Bohumir Grüner**: Formal analysis, Funding acquisition, Investigation, Methodology, Resources, Validation, Writing – review & Editing. **Christian Ekberg**: Funding acquisition, Methodology, Resources, Validation, Writing – review & Editing. All authors have read and agreed to the published version of the manuscript.

## Declaration of competing interest

The authors declare that they have no known competing financial interests or personal relationships that could have appeared to influence the work reported in this paper.

## Acknowledgements

Financial support for this research was provided by the German Federal Ministry of Education and Research (Contract No. 02NUK059D) and the European Commission from the European Atomic Energy Community's 7th Framework program project SACSESS – grant agreement No. FP7-Fission-2012-323-282 and by the H2020 Euratom Research and Innovation Programme under grant agreement n°755171 (project GENIORS). The research used resources of the Brookhaven National Laboratory Laser-Electron Accelerator Facility of the BNL Accelerator Center for Energy Research, also supported by the US-DOE Office of Basic Energy Sciences, Division of Chemical Sciences, Geosciences, and Biosciences under contract DE-SC0012704.

## Appendix A. Supplementary data

Supplementary data to this article can be found online at <https://doi.org/10.1016/j.radphyschem.2021.109696>.

## References

- Afsar, A., Distler, P., Harwood, L.M., John, J., Westwood, J., 2016. Synthesis and Screening of Modified 6,6'-Bis(5,5,8,8-tetramethyl-5,6,7,8-tetrahydrobenzo[e]1,2,4-triazin-3-yl)-2,2'-bipyridine Ligands for Actinide and Lanthanide Separation in Nuclear Waste Treatment. *J. Org. Chem.* 81 (21), 10517–10520. <https://doi.org/10.1021/acs.joc.6b01264>.
- Anheim, E., Ekberg, C., Fermvik, A., Foreman, M.R.S.J., Retegan, T., Skarnemark, G., 2010. A TBP/BTBP-based GANEX separation process. Part 1: feasibility. *Solvent Extr. Ion Exch.* 28 (4), 437–458. <https://doi.org/10.1080/07366299.2010.480930>.
- Anheim, E., Ekberg, C., Fermvik, A., Foreman, M.R.S.J., Grüner, B., Hájková, Z., Kvičalová, M., 2011. A TBP/BTBP-based GANEX separation process - Part 2: ageing, hydrolytic, and radiolytic stability. *Solvent Extr. Ion Exch.* 29 (2), 157–175. <https://doi.org/10.1080/07366299.2011.539462>.
- Anheim, E., Bauhn, L., Ekberg, C., Foreman, M., Löfström-Engdahl, E., 2012a. Extraction experiments after radiolysis of a proposed GANEX solvent - the effect of time. *Proc. Chem. J.* 123–129. <https://doi.org/10.1016/j.proche.2012.10.022>.
- Anheim, E., Ekberg, C., Foreman, M.R.S., Löfström-Engdahl, E., Mabile, N., 2012b. Studies of a solvent for GANEX applications containing CyMe<sub>4</sub>-BTBP and DEHBA in cyclohexanone. *Separ. Sci. Technol.* 47 (5), 663–669. <https://doi.org/10.1080/01496395.2011.627908>.
- Anheim, E., Ekberg, C., Foreman, M.R.S., 2013. A TBP/BTBP-Based GANEX separation process – Part 3: fission product handling. *Solvent Extr. Ion Exch.* 31 (3), 237–252. <https://doi.org/10.1080/07366299.2012.757158>.
- Authen, T.L., Wilden, A., Halleröd, J., Schneider, D., Kreft, F., Modolo, G., Ekberg, C., 2021. Batch tests for optimisation of solvent composition and process flexibility of the CHALMEX FS-13 process. *Solvent Extr. Ion Exch.* 39 (1), 1–17. <https://doi.org/10.1080/07366299.2020.1797988>.
- Berthon, L., Paquet, A., Saint-Louis, G., Guilbaud, P., 2021. How phase modifiers disrupt third-phase formation in solvent extraction solutions. *Solvent Extr. Ion Exch.* 39 (2), 204–232. <https://doi.org/10.1080/07366299.2020.1831782>.
- Bjergbakke, E., 1970. The ferrous-cupric dosimeter. In: Holm, N.W., Berry, R.J. (Eds.), *Manual on Radiation Dosimetry*. Marcel Dekker Inc., New York, pp. 319–321.
- Buxton, G.V., Greenstock, C.L., Helman, W.P., Ross, A.B., 1988. Critical review of rate constants for reactions of hydrated electrons, hydrogen atoms and hydroxyl radicals (OH•/O•) in aqueous solution. *J. Phys. Chem. Ref. Data* 17 (2), 513–886. <https://doi.org/10.1063/1.555805>.
- Distler, P., Kondé, J., John, J., Hájková, Z., Švehla, J., Grüner, B., 2015. Characterization of solvents containing CyMe<sub>4</sub>-BTBP in selected cyclohexanone-based diluents after irradiation by accelerated electrons. *Nukleonika* 60, 4 (Pt. II), 885–891. <https://doi.org/10.1515/nuka-2015-0123>.
- Ekberg, C., Fermvik, A., Retegan, T., Skarnemark, G., Foreman, M.R.S., Hudson, M.J., Englund, S., Nilsson, M., 2008. An overview and historical look back at the solvent extraction using nitrogen donor ligands to extract and separate An(III) from Ln(III). *Radiochim. Acta* 96 (4–5 EUROPART), 225–233. <https://doi.org/10.1524/ract.2008.1483>.
- Fermvik, A., 2011. Radiolytic Degradation of BTBP Type Molecules for Treatment of Used Nuclear Fuel by Solvent Extraction. Chalmers University, Gothenburg, Sweden.
- Fermvik, A., Berthon, L., Ekberg, C., Englund, S., Retegan, T., Zorz, N., 2009. Radiolysis of solvents containing C5-BTBP: identification of degradation products and their dependence on absorbed dose and dose rate. *Dalton Trans.* 32, 6421–6430. <https://doi.org/10.1039/b907084b>.
- Fermvik, A., Nilsson, M., Ekberg, C., 2010. Radiolytic degradation of heterocyclic nitrogen containing ligands from low dose-rate gamma sources. In: Wai, C.M., Mincher, B.J. (Eds.), *Nuclear Energy and the Environment*, vol. 1046. American Chemical Society, Washington, pp. 215–229.
- Fermvik, A., Grüner, B., Kvičalová, M., Ekberg, C., 2011. Semi-quantitative and quantitative studies on the gamma radiolysis of C5-BTBP. *Radiochim. Acta* 99 (2), 113–119. <https://doi.org/10.1524/ract.2011.1800>.
- Fermvik, A., Anheim, E., Grüner, B., Hájková, Z., Kvičalová, M., Ekberg, C., 2012. Radiolysis of C5-BTBP in cyclohexanone irradiated in the absence and presence of an aqueous phase. *Radiochim. Acta* 100 (4), 273–282. <https://doi.org/10.1524/ract.2012.1908>.
- Freeman, G.R., 1970. Radiolysis of alcohols. *Actions Chim. Biol. Radiat.* 14, 73–134.
- Geist, A., 2010. Extraction of nitric acid into alcohol: kerosene mixtures. *Solvent Extr. Ion Exch.* 28 (5), 596–607. <https://doi.org/10.1080/07366299.2010.49286>.
- Geist, A., Modolo, G., September, 2009. TODGA process development: an improved solvent formulation. In: Proceedings of GLOBAL (The Nuclear Fuel Cycle: Sustainable Options & Industrial Perspectives): Paris, 2009, vols. 6–11, pp. 1022–1026 paper 9193.
- Geist, A., Panak, P.J., 2021. Recent progress in trivalent actinide and lanthanide solvent extraction and coordination chemistry with triazinylpyridine N donor ligands. *Solvent Extr. Ion Exch.* 39 (2), 128–151. <https://doi.org/10.1080/07366299.2020.1831235>.
- Geist, A., Hill, C., Modolo, G., Foreman, M.R.S.J., Weigl, M., Gompper, K., Hudson, M.J., Madic, C., 2006. 6,6'-Bis(5,5,8,8-tetramethyl-5,6,7,8-tetrahydro-benzo[1,2,4] triazin-3-yl)-[2,2']bipyridine, an effective extracting agent for the separation of americium(III) and curium(III) from the lanthanides. *Solvent Extr. Ion Exch.* 24 (4), 463–483. <https://doi.org/10.1080/073662990600761936>.
- Geist, A., Adnet, J.-M., Bourg, S., Ekberg, C., Galán, H., Guilbaud, P., Miguiditchian, M., Modolo, G., Rhodes, C., Taylor, R., 2020. An overview of solvent extraction processes developed in Europe for advanced nuclear fuel recycling. Part 1 — heterogeneous recycling. *Separ. Sci. Technol.* <https://doi.org/10.1080/01496395.2020.1795680>.
- Halleröd, J., Ekberg, C., Löfström-Engdahl, E., Anheim, E., 2015. Development of the Chalmers grouped actinide extraction process. *Nukleonika* 60, 4 (Pt. II), 829–835. <https://doi.org/10.1515/nuka-2015-0115>.
- Hill, C., Guillauneux, D., Berthon, L., 2002. SANEX-BTP process development studies. In: Proceedings of 16<sup>th</sup> International Solvent Extraction Conference, ISEC2002, 17–21 March, 2002, pp. 1205–1209. Cape Town, South Africa.
- Hill, C., Berthon, L., Madic, C., October, 2005. Study of the stability of BTP extractants under radiolysis. In: Proceedings of GLOBAL: Tsukuba, Japan, 2005, 9–13, p. 283.
- Horne, G.P., Zarzana, C., Rae, C., Cook, A.R., Mezyk, S.P., Zalupski, P., Wilden, A., Mincher, B.J., 2020. Does addition of 1-octanol as a phase modifier provide radical scavenging radioprotection for N,N,N',N'-tetraoctyldiglycolamide (TODGA)? *Phys. Chem. Chem. Phys.* 22 (43), 24978–24985. <https://doi.org/10.1039/D0CP04310A>.
- Hudson, M.J., Boucher, C.E., Braekers, D., Desreux, J.F., Drew, M.G.B., Foreman, M.R.S., J., Harwood, L.M., Hill, C., Madic, C., Marken, F., Youngs, T.G.A., 2006. New bis (triazinyl) pyridines for selective extraction of americium(III). *New J. Chem.* 30 (8), 1171–1183. <https://doi.org/10.1039/b514108g>.
- Kolarik, Z., Mullich, U., Gassner, F., 1999. Selective extraction of Am(III) by Eu(III) by 2,6-di(triazolyl)- and 2,6-di(triazinyl)pyridines. *Solvent Extr. Ion Exch.* 17 (1), 23–32. <https://doi.org/10.1080/07366299909834598>.
- Kondé, J., Distler, P., John, J., Švehla, J., Grüner, B., Belčíková, Z., 2016. Radiation influencing of the extraction properties of the CyMe<sub>4</sub>-BTBP and CyMe<sub>4</sub>-BTPhen solvents with FS-13. *Procedia Chem.* 21, 174–181. <https://doi.org/10.1016/j.proche.2016.10.025>.
- Lang, B.E., 2012. Solubility of water in octan-1-ol from (275 to 369) K. *J. Chem. Eng. Data* 57 (8), 2221–2226. <https://doi.org/10.1021/jc3001427>.
- Lewis, F.W., Harwood, L.M., Hudson, M.J., Drew, M.G.B., Desreux, J.F., Vidick, G., Bouslimani, N., Modolo, G., Wilden, A., Sypula, M., Vu, T.-H., Simonin, J.-P., 2011. Highly efficient separation of actinides from lanthanides by a phenanthroline-derived bis-triazine ligand. *J. Am. Chem. Soc.* 133 (33), 13093–13102. <https://doi.org/10.1021/ja203378m>.
- Lewis, F.W., Harwood, L.M., Hudson, M.J., Drew, M.G.B., Wilden, A., Sypula, M., Modolo, G., Vu, T.-H., Simonin, J.-P., Vidick, G., Bouslimani, N., Desreux, J.F., 2012. From BTBPs to BTPhens: the effect of ligand pre-organization on the extraction properties of quadridentate bis-triazine ligands. *Proc. Chem.* 7, 231–238. <https://doi.org/10.1016/j.proche.2012.10.038>.
- Lewis, F.W., Harwood, L.M., Hudson, M.J., Drew, M.G.B., Hubscher-Bruder, V., Videva, V., Arnaud-Neu, F., Stambek, K., Vyas, S., 2013. BTBPs versus BTPhens:

- some reasons for their differences in properties concerning the partitioning of minor actinides and the advantages of BTPhens. *Inorg. Chem.* 52 (9), 4993–5005. <https://doi.org/10.1021/ic3026842>.
- Logunov, M.V., Voroshilov, Y.A., Starovoirov, N.P., Shadrin, A.Y., Smirnov, I.V., Kvasnitskiy, I.B., Tananaev, I.G., Myasoedov, B.F., Morgalyuk, V.P., Kamiya, M., Koma, I., Koyama, T., 2006. Radiation resistance of a series of organophosphorus extractants. *Radiochemistry* 48 (1), 55–61. <https://doi.org/10.1134/S1066362206010127>.
- Magnusson, D., Christiansen, B., Foreman, M.R.S., Geist, A., Glatz, J.P., Malmbeck, R., Modolo, G., Serrano-Purroy, D., Sorel, C., 2009a. Demonstration of a SANEX process in centrifugal contactors using the CyMe<sub>4</sub>-BTBP molecule on a genuine fuel solution. *Solvent Extr. Ion Exch.* 27 (2), 97–106. <https://doi.org/10.1080/07366290802672204>.
- Magnusson, D., Christiansen, B., Malmbeck, R., Glatz, J.P., 2009b. Investigation of the radiolytic stability of a CyMe<sub>4</sub>-BTBP based SANEX solvent. *Radiochim. Acta* 97 (9), 497–502. <https://doi.org/10.1524/ract.2009.1647>.
- Magnusson, D., Geist, A., Wilden, A., Modolo, G., 2013. Direct selective extraction of actinides (III) from PUREX raffinate using a mixture of CyMe<sub>4</sub>-BTBP and TODGA as 1-cycle SANEX solvent Part II: flow-sheet design for a counter-current centrifugal contactor demonstration process. *Solvent Extr. Ion Exch.* 31 (1), 1–11. <https://doi.org/10.1080/07366299.2012.700596>.
- Mezyk, S.P., Mincher, B.J., Dhiman, S.B., Layne, B., Wishart, J.F., 2016. The role of organic solvent radical cations in separations ligand degradation. *J. Radioanal. Nucl. Chem.* 307 (3), 2445–2449. <https://doi.org/10.1007/s10967-015-4582-7>.
- Mincher, B.J., Mezyk, S.P., 2009. Radiation chemical effects on radiochemistry: a review of examples important to nuclear power. *Radiochim. Acta* 97 (9), 519–534. <https://doi.org/10.1524/ract.2009.1646>.
- Mincher, B.J., Arbon, R.E., Knighton, W.B., Meikrantz, D.H., 1994. Gamma-ray-induced degradation of PCBs in neutral isopropanol using spent reactor-fuel. *Appl. Radiat. Isot.* 45 (8), 879–887. [https://doi.org/10.1016/0969-8043\(94\)90219-4](https://doi.org/10.1016/0969-8043(94)90219-4).
- Mincher, B.J., Modolo, G., Mezyk, S.P., 2009. Review article: the effects of radiation Chemistry on solvent extraction: 1. Conditions in acidic solution and a review of TBP radiolysis. *Solvent Extr. Ion Exch.* 27 (1), 1–25. <https://doi.org/10.1080/0736629080264767>.
- Mincher, B.J., 2010a. An overview of selected radiation chemical reactions affecting fuel cycle solvent extraction. Chap. 15. In: Wai, C.M., Mincher, B.J. (Eds.), *Nuclear Energy and the Environment*, vol. 1046. American Chemical Society, pp. 181–192.
- Mincher, B.J., Modolo, G., Mezyk, S.P., 2010b. Review: the effects of radiation Chemistry on solvent extraction 4: separation of the trivalent actinides and considerations for radiation-resistant solvent systems. *Solvent Extr. Ion Exch.* 28 (4), 415–436. <https://doi.org/10.1080/07366299.2010.485548>.
- Modolo, G., Wilden, A., Daniels, H., Geist, A., Magnusson, D., Malmbeck, R., 2013. Development and demonstration of a new SANEX partitioning process for selective actinide(III)/Lanthanide(III) separation using a mixture of CyMe<sub>4</sub>-BTBP and TODGA. *Radiochim. Acta* 101 (3), 155–162. <https://doi.org/10.1524/ract.2013.2016>.
- Modolo, G., Wilden, A., Kaufholz, P., Boshach, D., Geist, A., 2014. Development and demonstration of innovative partitioning processes (i-SANEX and 1-cycle SANEX) for actinide partitioning. *Prog. Nucl. Energy* 72, 107–114. <https://doi.org/10.1016/j.pnucene.2013.07.021>.
- Modolo, G., Geist, A., Miguiditchian, M., 2015. Minor actinide separations in the reprocessing of spent nuclear fuels: recent advances in Europe. Chap. 10. In: Taylor, R. (Ed.), *Reprocessing and Recycling of Spent Nuclear Fuel*. Woodhead Publishing, Oxford, pp. 245–287.
- Modolo, G., Sypula, M., Geist, A., Hill, C., Sorel, C., Malmbeck, R., Magnusson, D., Foreman, M.R.S.J., October, 2008. Development and demonstration of a new SANEX-process for actinide(III)/Lanthanide(III) separation using a mixture of CyMe<sub>4</sub>-BTBP and TODGA as selective extractant. In: *Proceedings of 10th Information Exchange Meeting on Actinide and Fission Product Partitioning and Transmutation: Mito, Japan, 2008*, vols. 6–10, pp. 235–241.
- Nicolas, G., Jankowski, C.K., Lucas-Lamoureaux, C., Bresson, C., 2011. Development of normal phase-high performance liquid chromatography-atmospherical pressure chemical ionization-mass spectrometry method for the study of 6,6'-bis-(5,5,8-tetramethyl-5,6,7,8-tetrahydro-benzo 1,2,4-triazin-3-yl)-2,2'-bipyridine hydrolytic degradation. *J. Chromatogr. A* 1218 (37), 6369–6378. <https://doi.org/10.1016/j.chroma.2011.07.003>.
- Nilsson, M., Andersson, S., Ekberg, C., Foreman, M.R.S., Hudson, M.J., Skarnemark, G., 2006. Inhibiting radiolysis of BTP molecules by addition of nitrobenzene. *Radiochim. Acta* 94 (2), 103–106. <https://doi.org/10.1524/ract.2006.94.2.103>.
- OECD-NEA Potential Benefits and Impacts of Advanced Nuclear Fuel Cycles with Actinide Partitioning and Transmutation, 2011. OECD, Nuclear Energy Agency (NEA).
- Panaj, P.J., Geist, A., 2013. Complexation and extraction of trivalent actinides and lanthanides by triazinylpyridine N-donor ligands. *Chem. Rev.* 113 (2), 1199–1236. <https://doi.org/10.1021/cr3003399>.
- Poinssot, C., Bourg, S., Boullis, B., 2016. Improving the nuclear energy sustainability by decreasing its environmental footprint. Guidelines from life cycle assessment simulations. *Prog. Nucl. Energy* 92, 234–241. <https://doi.org/10.1016/j.pnucene.2015.10.012>.
- Retegan, T., Ekberg, C., Englund, S., Fermvik, A., Foreman, M.R.S., Skarnemark, G., 2007. The behaviour of organic solvents containing C5-BTBP and CyMe<sub>4</sub>-BTBP at low irradiation doses. *Radiochim. Acta* 95 (11), 637–642. <https://doi.org/10.1524/ract.2007.95.11.637>.
- Schmidt, H., Wilden, A., Modolo, G., Švehla, J., Grüner, B., Ekberg, C., 2015. Gamma radiolytic stability of CyMe<sub>4</sub>-BTBP and effect of nitric acid. *Nukleonika* 60, 4 (Pt. II), 879–884. <https://doi.org/10.1515/nuka-2015-0156>.
- Schmidt, H., Wilden, A., Modolo, G., Boshach, D., Santiago-Schübel, B., Hupert, M., Švehla, J., Grüner, B., Ekberg, C., 2016. Gamma radiolysis of the highly selective ligands CyMe<sub>4</sub>-BTBP and CyMe<sub>4</sub>-BTPhen: qualitative and quantitative investigation of radiolysis products. *Procedia Chem.* 21, 32–37. <https://doi.org/10.1016/j.proche.2016.10.005>.
- Seidl, R., Flüeler, T., Krüti, P., 2021. Sharp discrepancies between nuclear and conventional toxic waste: technical analysis and public perception. *J. Hazard Mater.* 414, 125422. <https://doi.org/10.1016/j.jhazmat.2021.125422>.
- Serp, J., Poinssot, C., Bourg, S., 2017. Assessment of the anticipated environmental footprint of future nuclear energy systems. Evidence of the beneficial effect of extensive recycling. *Energies* 10 (9), 1445. <https://doi.org/10.3390/en10091445>.
- Sugo, Y., Sasaki, Y., Tachimori, S., 2002. Studies on hydrolysis and radiolysis of N,N,N',N'-tetraoctyl-3-oxapentane-1,5-diamide. *Radiochim. Acta* 90 (3), 161–165. <https://doi.org/10.1524/ract.2002.90.3.2002.161>.
- Sugo, Y., Izumi, Y., Yoshida, Y., Nishijima, S., Sasaki, Y., Kimura, T., Sekine, T., Kudo, H., 2007. Influence of diluent on radiolysis of amides in organic solution. *Radiat. Phys. Chem.* 76 (5), 794–800. <https://doi.org/10.1016/j.radphyschem.2006.05.008>.
- Sulich, A., Grodkowski, J., Mirkowski, J., Kocia, R., 2014. Reactions of ligands from BT (BP) family with solvated electrons and benzophenone ketyl radicals in 1-octanol solutions. Pulse radiolysis study. *J. Radioanal. Nucl. Chem.* 300 (1), 415–421. <https://doi.org/10.1007/s10967-014-3021-5>.
- Swallow, A.J., 1987. Radiation Chemistry of the liquid state: (2) organic liquids. Chap. 11. In: Farhatiaziz, Rodgers, Michael A.J. (Eds.), *Radiation Chemistry - Principles and Applications*. VCH Verlagsgesellschaft mbH, Weinheim, Germany, pp. 351–375.
- Symons, M.C.R., Eastland, G.W., 1977. Radiation mechanisms. Part 18. The radiolysis of alcohols: an electron spin resonance study. *J. Chem. Res.* (S) 254–255.
- Szreder, T., Schmidt, H., Modolo, G., 2019. Fast radiation-induced reactions in organic phase of SANEX system containing CyMe<sub>4</sub>-BTPhen extracting agent. *Radiat. Phys. Chem.* 164, 108356. <https://doi.org/10.1016/j.radphyschem.2019.108356>.
- Velisek-Carolan, J., 2016. Separation of actinides from spent nuclear fuel: a review. *J. Hazard Mater.* 318, 266–281. <https://doi.org/10.1016/j.jhazmat.2016.07.027>.
- Wilden, A., Schreinemachers, C., Sypula, M., Modolo, G., 2011. Direct selective extraction of actinides (III) from PUREX raffinate using a mixture of CyMe<sub>4</sub>-BTBP and TODGA as 1-cycle SANEX solvent. *Solvent Extr. Ion Exch.* 29 (2), 190–212. <https://doi.org/10.1080/07366299.2011.539122>.
- Wilden, A., Modolo, G., Schreinemachers, C., Sadowski, F., Lange, S., Sypula, M., Magnusson, D., Geist, A., Lewis, F.W., Harwood, L.M., Hudson, M.J., 2013. Direct selective extraction of actinides (III) from PUREX raffinate using a mixture of CyMe<sub>4</sub>-BTBP and TODGA as 1-cycle SANEX solvent Part III: demonstration of a laboratory-scale counter-current centrifugal contactor process. *Solvent Extr. Ion Exch.* 31 (5), 519–537. <https://doi.org/10.1080/07366299.2013.775890>.
- Wilden, A., Modolo, G., Hupert, M., Santiago-Schübel, B., Löfström-Engdahl, E., Halleröd, J., Ekberg, C., Mincher, B.J., Mezyk, S.P., 2016. Gamma-radiolytic stability of solvents containing C5-BP (2,6-Bis-(5-(2,2-dimethylpropyl)-1H-pyrazol-3-yl)pyridine) for actinide(III)/lanthanide(III) separation. *Solvent Extr. Ion Exch.* 34 (1), 1–12. <https://doi.org/10.1080/07366299.2015.1115694>.
- Wishart, J.F., Cook, A.R., Miller, J.R., 2004. The LEAF picosecond pulse radiolysis facility at brookhaven national laboratory. *Rev. Sci. Instrum.* 75 (11), 4359–4366. <https://doi.org/10.1063/1.1807004>.
- Woodhead, D., McLachlan, F., Taylor, R., Müllich, U., Geist, A., Wilden, A., Modolo, G., 2019. Nitric acid extraction into a TODGA solvent modified with octanol. *Solvent Extr. Ion Exch.* 37 (2), 173–190. <https://doi.org/10.1080/07366299.2019.1625201>.
- Yu, C.H., Zhang, J.W., Dai, J., Peng, J., Li, J.Q., Zhai, M.L., 2010. Radiation stability and analysis of radiolysis product of 1-octanol. *Acta Phys. - Chim. Sin.* 26 (4), 988–992. <https://doi.org/10.3866/pku.whxb20100434>.
- Zhou, H.Y., Ao, Y.Y., Yuan, J., Peng, J., Li, J.Q., Zhai, M.L., 2014. Extraction mechanism and γ-radiation effect on the removal of Eu<sup>3+</sup> by a novel BTPhen/[c<sub>6</sub>mim][NTf<sub>2</sub>] system in the presence of nitric acid. *RSC Adv.* 4 (85), 45612–45618. <https://doi.org/10.1039/c4ra07662a>.
- Zsabka, P., Van Hecke, K., Wilden, A., Modolo, G., Hupert, M., Jespers, V., Voorspoels, S., Verwerf, M., Binnemans, K., Cardinaels, T., 2020. Gamma radiolysis of TODGA and CyMe<sub>4</sub>-BTPhen in the ionic liquid tri-n-octylmethylammonium nitrate. *Solvent Extr. Ion Exch.* 38 (2), 212–235. <https://doi.org/10.1080/07366299.2019.1710918>.

## Paper 6<sup>[152]</sup>

Galán, H., Zarzana, C.A., Wilden, A., Núñez, A., Schmidt, H., Egberink, R.J.M., Leoncini, A., Cobos, J., Verboom, W., Modolo, G., Groenewold, G.S., Mincher, B.J. Gamma-Radiolytic Stability of New Methylated TODGA Derivatives for Minor Actinide Recycling. *Dalton Trans.* **2015**, 44 (41), 18049-18056.

DOI: 10.1039/c5dt02484f

### Contribution:

For this work, solvent extraction experiments, analysis (gamma-spectrometry, results of ICP-MS), as well as product identification of mass spectrometric experiments were conducted mainly by A. Wilden and me. Additionally, I participated in paper preparation.





Cite this: *Dalton Trans.*, 2015, **44**, 18049

## Gamma-radiolytic stability of new methylated TODGA derivatives for minor actinide recycling

Hitos Galán,<sup>a</sup> Christopher A. Zarzana,<sup>b</sup> Andreas Wilden,<sup>c</sup> Ana Núñez,<sup>a</sup> Holger Schmidt,<sup>c</sup> Richard J. M. Egberink,<sup>d</sup> Andrea Leoncini,<sup>d</sup> Joaquín Cobos,<sup>a</sup> Willem Verboom,<sup>d</sup> Giuseppe Modolo,<sup>c</sup> Gary S. Groenewold<sup>b</sup> and Bruce J. Mincher<sup>b</sup>

The stability against gamma radiation of MeTODGA (methyl tetraoctyldiglycolamide) and Me<sub>2</sub>TODGA (dimethyl tetraoctyldiglycolamide), derivatives from the well-known extractant TODGA (*N,N,N',N'*-tetraoctyldiglycolamide), were studied and compared. Solutions of MeTODGA and Me<sub>2</sub>TODGA in alkane diluents were subjected to <sup>60</sup>Co γ-irradiation in the presence and absence of nitric acid and analyzed using LC-MS to determine their rates of radiolytic concentration decrease, as well as to identify radiolysis products. The results of product identification from three different laboratories are compared and found to be in good agreement. The diglycolamide (DGA) concentrations decreased exponentially with increasing absorbed dose. The MeTODGA degradation rate constants (dose constants) were uninfluenced by the presence of nitric acid, but the acid increased the rate of degradation for Me<sub>2</sub>TODGA. The degradation products formed by irradiation are also initially produced in greater amounts in acid-contacted solution, but products may also be degraded by continued radiolysis. The identified radiolysis products suggest that the weakest bonds are those in the diglycolamide center of these molecules.

Received 30th June 2015,  
Accepted 15th September 2015  
DOI: 10.1039/c5dt02484f

www.rsc.org/dalton

## Introduction

Current nuclear reactors consume less than 1% of their natural uranium, which is obviously a low efficiency. In order to achieve long-term sustainability of nuclear energy from fission, new technological solutions which are able to use more than 80% of this natural uranium are being developed. The new technology is based on the combination of fast neutron systems with multi-recycling of the fuel in advanced fuel cycles. The advanced fuel cycles are being designed to reuse most of the uranium, plutonium, and the minor actinides (Am, Np, Cm).<sup>1</sup> To recover the minor actinides from used fuel it is necessary to develop suitable separation processes. Up to now, hydrometallurgical (*i.e.* solvent extraction) processes have been the reference technology for recycling the major actinides uranium and plutonium from used fuel. The recycling of minor actinides, particularly americium, is currently of high R&D interest due to its major contribution to waste radiotoxicity and heat generation. Several processes for americium

recovery are under development in national and international projects. Most proposals rely on the pre-separation of a major uranium and plutonium stream by a conventional PUREX (Plutonium Uranium Redox EXtraction) process with the minor actinides then consecutively separated by multi-step (DIAMEX-SANEX concept)<sup>2,3</sup> or single step processes (1-cycle SANEX,<sup>4</sup> innovative-SANEX,<sup>5</sup> ALSEP,<sup>6</sup> and/or EXAm<sup>7</sup>) from the PUREX raffinate, which still also contains lanthanides, activation products and other fission products.

The diglycolamides (DGAs) are alkyl-3-oxapentane-1,5-diamide derivatives, emerging as promising candidates for the separation of minor actinides which, unlike tributyl phosphate (TBP, extractant of the PUREX process), can extract actinide ions in the trivalent state.<sup>8</sup> Unfortunately, this ligand family, made up of CHON (carbon, hydrogen, oxygen and nitrogen) elements and therefore completely incinerable, cannot discriminate between trivalent actinides (An(III)) and lanthanides (Ln(III)). Nevertheless, the DGAs have many favorable properties, such as high actinide extraction affinity, fast mass transfer, high loading capacities and reasonable stability under relevant process conditions.

It is realized that the extraction and stripping of An(III) and Ln(III) ions strongly depends on the nature of the alkyl group attached to the DGA nitrogen atoms.<sup>9</sup> The *n* = 8 and 10 derivatives are soluble in alkane diluents, and these compounds complex and extract actinides and lanthanides with distribution ratios that increase with increasing aqueous nitric acid

<sup>a</sup>Centro de Investigaciones Energéticas, Medioambientales y Tecnológicas (CIEMAT), Madrid 28040, Spain. E-mail: hitos.galan@ciemat.es

<sup>b</sup>Idaho National Laboratory, Idaho Falls, ID, USA

<sup>c</sup>Forschungszentrum Jülich GmbH, Institut für Energie- und Klimaforschung -Nukleare Entsorgung und Reaktorsicherheit- (IEK 6), Jülich, Germany

<sup>d</sup>Laboratory of Molecular Nanofabrication, Mesa+ Institute for Nanotechnology, University of Twente, Enschede, The Netherlands

concentration, and that follow the order  $M(\text{III})/M(\text{IV}) > M(\text{VI}) > M(\text{V})$ . Particularly the octyl derivative,  $N,N,N',N'$ -tetraoctyldiglycolamide (TODGA, Fig. 1) has thus received detailed study for its potential applications at the back end of the nuclear fuel cycle for the extraction of lanthanides and actinides.<sup>10–13</sup> In continued European research within the FP 7 ACSEPT project, TODGA was modified by the addition of one or two methyl groups on the methylene carbon positions to produce MeTODGA and Me<sub>2</sub>TODGA, respectively (Fig. 1).<sup>14–16</sup> Extraction efficiency decreased with increasing methyl substitution, probably due to steric considerations. Among them, the most interesting extractant is MeTODGA, particularly for the GANEX (Group ActiNide Extraction) process, since it was found that the extraction efficiency of the undesired fission products decreased while the distribution ratios and loading capacity of the desired Ln(III) and An(III) remained acceptable under relevant conditions. Subsequent stripping at low nitric acid concentrations might also be improved.<sup>16</sup>

To evaluate the applicability of solvents based on DGAs for process development, it is necessary to prove not only their good extraction properties, but also their degradation resistance, since the organic phase is in contact with highly radioactive solutions and high nitric acid concentrations. Solvent degradation may lead to undesirable effects such as decreases in solvent extraction efficiency, decreases in selectivity, and/or third phase formation.

While the long-chain DGAs appear to be hydrolytically stable, radiolytic degradation of DGAs has been observed.<sup>17–26</sup> The decrease in ligand concentration is exponential with dose, and has been mainly attributed to electron-transfer reactions between radiolytically-produced diluent radical cations.<sup>17,19</sup> The presence of nitric acid during irradiation has been reported to have variable effects. For example, for irradiation experiments to absorbed doses as high as 400 kGy in *n*-dodecane, the presence of the acidic aqueous phase had little effect on the dose constants for the degradation of TODGA.<sup>19</sup> However, when Galán *et al.*<sup>18</sup> irradiated TODGA in the alkane diluent hydrogenated tetrapropene (TPH, used in AREVA's reprocessing plant) that had been pre-contacted with nitric acid to an absorbed dose of 1000 kGy, a slight protective effect was measured when taking into account the remaining concentration of TODGA. In that same work a clear protective effect was seen for irradiations in a diluent composed of TPH and 1-octanol. Thus nitric acid protection occurs depending

on the diluent. It has also been demonstrated that the major sites for degradation effects are the bonds within the diglycolamide functional group, specifically the C–O<sub>ether</sub> and N–C<sub>carbonyl</sub>.<sup>18,19</sup>

Recently, several studies have appeared regarding the effects of DGA irradiation on solvent extraction metal distribution ratios.<sup>20–24</sup> Initially, DGA degradation was inferred based on the decrease in distribution ratios.<sup>21–23</sup> However, studies of the main degradation products have since shown that the new species have extraction properties that markedly differ from those of the original ligands.<sup>18,24</sup> Thus distribution ratios cannot be used as a metric for ligand degradation.

Since the ether DGA linkage is especially susceptible to radiolytic attack, efforts to reduce degradation should naturally focus on protecting these bonds. In addition to their solvent extraction advantages, the new class of methyl TODGA derivatives (Fig. 1) may offer such stability. Herein we describe an investigation of the  $\gamma$ -radiolytic stability of methyl TODGA derivatives in both *n*-dodecane and TPH using LC-MS techniques. Stability was assessed based on the decrease in DGA concentration with absorbed dose and the generation of degradation products, as measured at three different laboratories as part of a collaborative effort. Irradiations were performed for the organic solutions in the presence and absence of an aqueous nitric acid phase and the results are compared to previous work with un-substituted TODGAs.

## Results and discussion

### Degradation of MeTODGA in TPH

The mono-substituted MeTODGA at 0.1 M was irradiated in TPH after acid preequilibration over a series of absorbed doses to a maximum of 1000 kGy. For comparison, similar MeTODGA solutions were stored at 25 °C for 56 days, to investigate the stability of unirradiated DGAs (ageing effects) and hydrolysis. Fig. 2 shows the exponential concentration decrease as measured by HPLC-DAD for these samples. The effects of ageing and hydrolysis were negligible for this length of exposure and temperature. Also shown in Fig. 2 is that a 50% reduction in MeTODGA concentration takes place by an absorbed dose of 250 kGy.

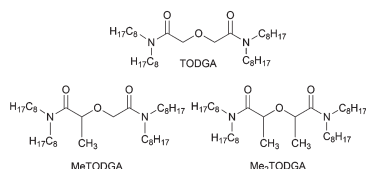


Fig. 1 Structures of TODGA, MeTODGA and Me<sub>2</sub>TODGA.

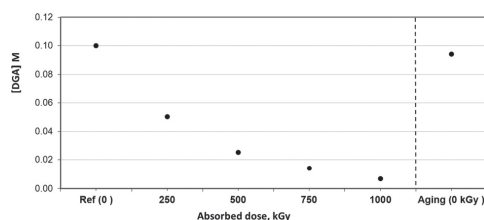


Fig. 2 Quantitative determination of the MeTODGA concentration of fresh (Ref), aged (aging, 0 kGy) and irradiated MeTODGA solutions (250–1000 kGy). Ligand concentration was initially 0.1 M in TPH diluent.



### Degradation of MeTODGA and Me<sub>2</sub>TODGA in *n*-dodecane

The two substituted DGAs, MeTODGA and Me<sub>2</sub>TODGA, were also irradiated in *n*-dodecane to facilitate a comparison to previous work with TODGA and T(EH)DGA (*N,N,N',N'*-tetra-2-ethyl-hexyldiglycolamide).<sup>19</sup> The change in the concentration of DGAs versus absorbed dose for samples irradiated as only the organic phase, or as the organic phase in contact with 2.5 M HNO<sub>3</sub> is shown in Fig. 3. The concentration change for each was exponential, suggesting pseudo-first-order kinetics, as has been previously shown for the other TODGAs.<sup>19</sup> Therefore, the radiolytic degradation as a function of absorbed dose can be described by a dose constant.<sup>27</sup>

Calculated dose constants for the systems studied here are given in Table 1. Dose constants for uncontacted and nitric acid contacted TODGA are reproduced from Zarzana *et al.*<sup>19</sup> for comparison.

It is well known that ether bonds are susceptible to scission under radiolysis. According to Belevskii *et al.*,<sup>28</sup> the electron deficiency in an ionized methylamide is most pronounced at the H-atoms of the methyl groups. The analogous situation for diglycolamides would suggest that electron deficiency is localized

on the methylene H-atoms, thus facilitating loss of the H-atom to produce a carbon-centered radical. This could favor C–O bond rupture as has been observed for DGAs<sup>15,18,19</sup> and bis-DGAs.<sup>24</sup> Substitution of a methylene H-atom by a methyl group, as in MeTODGA, might be expected to protect that bond, improving the radiolytic stability of the molecule. However, single methyl substitution here instead increased the degradation rate of MeTODGA in *n*-dodecane compared to TODGA. A second methyl substitution (Me<sub>2</sub>TODGA) does result in increased radiolytic stability in *n*-dodecane over TODGA.

Previously, we reported that the dose constants for unsubstituted TODGA and T(EH)DGA were unchanged in *n*-dodecane upon acid contact.<sup>19</sup> However, in this case, the presence of nitric acid definitely increased the degradation rate of MeTODGA and Me<sub>2</sub>TODGA. Nitric acid does not provide a protective effect for Me<sub>2</sub>TODGA, at least in nonpolar solvents where the extraction of nitric acid is low.<sup>29</sup> Thus, if methylation of the DGA protects the ether linkage, these results suggest that another bond is susceptible in the presence of the acid. Several reports have indicated that the amide C–N linkages are susceptible to radiolytic rupture in the presence of nitric acid.<sup>30,31</sup>

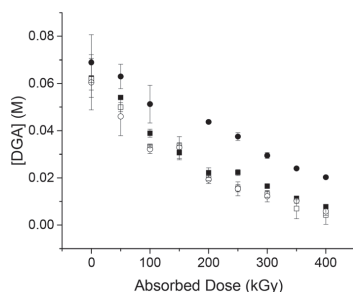


**Fig. 3** The change in initially nominal 0.05 M DGA concentration versus absorbed dose. MeTODGA (solid squares), Me<sub>2</sub>TODGA (solid circles) MeTODGA/HNO<sub>3</sub> (open squares) and Me<sub>2</sub>TODGA/HNO<sub>3</sub> (open circles). There were instrumental difficulties measuring the Me<sub>2</sub>TODGA sample at 150 kGy absorbed dose, so those data have been omitted.

**Table 1** Dose constants for the degradation of TODGA, MeTODGA and Me<sub>2</sub>TODGA (kGy<sup>−1</sup>) calculated as the exponential constants for fits to the plots of concentration versus absorbed dose. Uncertainties are at the 99% confidence interval. MeTODGA and Me<sub>2</sub>TODGA and MeTODGA/TPH from this work. TODGA/*n*-dodecane from previous work<sup>19</sup>

Sample	Dose constant (10 <sup>−3</sup> kGy <sup>−1</sup> )		
	0.05 M in <i>n</i> -dodecane	0.05 M in <i>n</i> -dodecane 2.5 M HNO <sub>3</sub>	0.1 M in TPH, 3 M HNO <sub>3</sub> pre-equilibration
TODGA	4.1 ± 0.3	3.8 ± 0.3	
MeTODGA	5.0 ± 0.3	5.8 ± 0.4	2.6 ± 0.3
Me <sub>2</sub> TODGA	3.0 ± 0.2	5.3 ± 0.4	

### Identification and behavior of MeTODGA radiolysis products

Previous TODGA stability studies revealed that the main ruptures take place in the C–O<sub>ether</sub> and C<sub>carbonyl</sub>–N bonds, giving rise to ten degradation compounds.<sup>18,19,23</sup> In solvent formulations containing 1-octanol, the formation of acids, amines or esters is favored, but the first two can also be observed in alkane diluents when nitric acid is present. As mentioned before, one of the challenges of this family of DGA compounds is to reduce the radiolytic degradation rates by protecting the ether bonds. Therefore, it was of interest to identify and quantify the degradation compounds formed when unsymmetrical MeTODGA was subjected to irradiation. Similar structures were identified both in *n*-dodecane and TPH, and the three mass spectrometric techniques employed at our laboratories produced very consistent results. Fig. 4 shows the structures assigned to the products found after the irradiation of MeTODGA in *n*-dodecane or TPH from the mass analysis spectra. Thirteen mass signals were identified as possible radiolysis products for MeTODGA for which we have assigned the structures 1–10 and 14–16 (Fig. 4). For most of these radiolytic degradation products, reasonable structures were inferred based on simple homolytic cleavage of the parent structure, followed by capping of the resultant radical. The exception to this is product 13 (*m/z* 256.3), which could be assigned to an oxidation of dioctylamine, since a simple cleavage and capping reaction could not produce a satisfactory structural hypothesis, and so the structure of this compound is at present not clear. The rupture of bonds on the carbonyl and alkyl sides of the amides gives rise to products 11–16. Rupture of the ether linkage in non-symmetrical MeTODGA also results in four possible products (1–4), depending on which side of



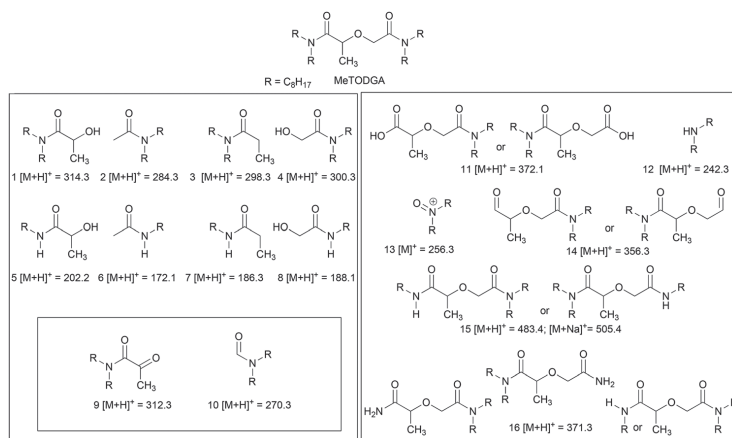


Fig. 4 Proposed structures of the products found in irradiated MeTODGA solution.

the linkage the break occurs. The ether linkage breaks are shown in Fig. 5.

If the ether break occurs on the side adjacent to the methyl group, the products have protonated masses 300.3 (compound 4 in Fig. 4 and 5) and 298.3 (compound 3 in Fig. 4 and 5). Compound 4 is the same product as for TODGA radiolysis, namely 2-hydroxy-*N,N*-dioctylacetamide. This compound grew in with absorbed dose slightly faster in the samples irradiated in the presence of the acidic aqueous phase. This is shown in Fig. 6, and is in good agreement with previous results on TODGA radiolysis.<sup>18,24</sup>

If the ether linkage ruptures on the side opposite the methyl group, products at protonated masses 314.3 (compound 1 in Fig. 4 and 5) and 284.3 (compound 2 in Fig. 4 and 5) occur. Signals at these masses were detected. Compound 1, with a methylated ether linkage, had a slightly higher signal intensity than the non-methylated hydroxyacetamide compound 4, possibly indicating that pathway in Fig. 5 is preferred. This would indicate that the methylated ether linkage was somewhat protected, assuming that the mass spectrometric response factors are the same for both fragments. This 2-hydroxy-*N,N*-dioctylpropanamide also grew in faster in

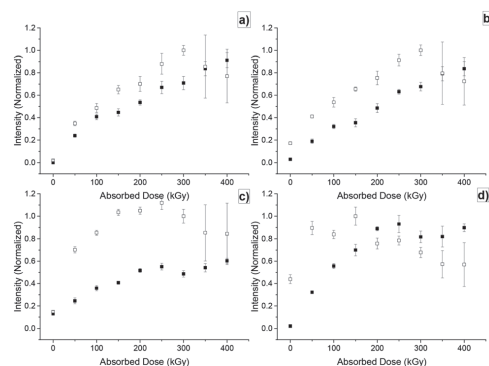


Fig. 6 Formation of compounds (a) 4, (b) 1, (c) 11 and (d) 15 (Fig. 4) versus absorbed dose for the irradiation of 0.05 M MeTODGA in *n*-dodecane (solid squares), for pure organic samples, and for samples irradiated in the presence of 2.5 M HNO<sub>3</sub> (open squares). Intensities are normalized to the maximum detected signal for each compound.

the presence of the acidic aqueous phase, as also shown in Fig. 6, in agreement with previous studies.<sup>18</sup> In the presence of nitric acid, compounds with a 2-hydroxyalkylamide structure are always the main products formed, and compound 1 was detected in all samples by all three laboratories. These results again support the hypothesis of different degradation pathways in presence of nitric acid.

Structural degradation analysis was also conducted for irradiated samples of MeTODGA in TPH that were pre-equilibrated with 3 M HNO<sub>3</sub>. In fact, an irradiation to 1000 kGy was carried out to maximize the concentrations of degradation products. The HPLC-MS chromatograms for MeTODGA, and also TODGA

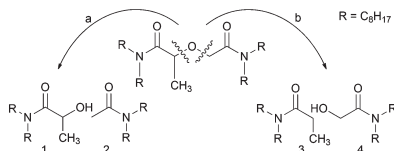


Fig. 5 The four possible products of ether linkage rupture for the unsymmetrical MeTODGA.

for comparison, irradiated under these conditions are shown in Fig. 7, where a higher number of signals corresponding to products were found for MeTODGA, as expected for a non-symmetric structure. However, it should be noted that this is not an indication that only these products were generated since the radiolysis products may also undergo radiolytic decomposition. The chromatograms in Fig. 7 also show the products of the rupture of the ether linkage, compounds 4 and 3, and 2 and 1, as the main products in TPH solution after 1000 kGy. The peak heights of these compounds are consistent with increased C–O bond stability on the substituted side of the ether.

Loss of a single alkyl chain also occurred for MeTODGA in both *n*-dodecane and TPH, in analogy with TODGA and T(EH)DGA in *n*-dodecane.<sup>18,19</sup> The single de-octylation (protonated mass 483.4, or sodiated mass 505.4, compound 15 in Fig. 4) was clearly favored by the presence of the acidic aqueous phase; as was previously shown for bis-DGAs.<sup>24</sup> This is shown

in Fig. 8. These results again support the hypothesis of different degradation pathways in presence of nitric acid.

The product corresponding to the loss of a single octyl group (compound 15, Fig. 4) was also detected for irradiations in TPH, but upon irradiation to 1000 kGy, it was present in only negligible amounts, probably indicating its own radiolytic decomposition. The products of a second de-alkylation were also detected in *n*-dodecane; however, they were present in unirradiated samples, and did not show a clear trend with absorbed dose, and thus may not be radiolysis products.

Rupture of the amide moiety to produce a carboxylic acid and the corresponding amine (protonated mass 372.1, compound 11, Fig. 4) was found in irradiated MeTODGA/*n*-dodecane samples, again with favored production in the presence of acidic aqueous phase, at least initially (Fig. 6). Following about 200 kGy absorbed dose, the carboxylic acid product concentration dropped below that found in the pure organic samples, for samples irradiated in the presence of the aqueous phase. The formation of the amine (protonated mass 242.3, compound 12, Fig. 4) was not measured in *n*-dodecane at INL due to the conditions of the mass detector selected for these experiments. It was found in the same samples using the parameters adopted at Jülich. The radiolytic generation of the amine was also observed in experiments performed in TPH pre-equilibrated with nitric acid at CIEMAT. Compounds corresponding to rupture of the methylene-carbonyl C–C bonds were also detected in irradiated MeTODGA/*n*-dodecane samples, but only at very low signal strength. Rupture of this bond is not preferred.

Previously, degradation of TODGA and T(EH)DGA was attributed to the electron transfer reaction with the *n*-dodecane radical cation.<sup>17,19</sup> However, perhaps unsurprisingly, the TPH results here suggest that *n*-dodecane is not a unique source of reactive species, and that the ionization of other alkanes also

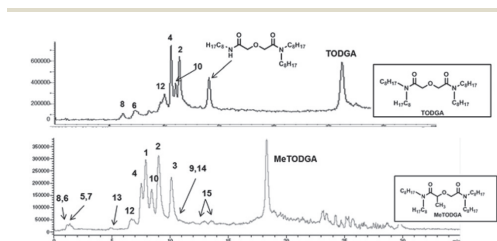


Fig. 7 HPLC-MS(APCI<sup>+</sup>) chromatograms for TODGA and MeTODGA irradiated to 1000 kGy in acid pre-equilibrated TPH. Peak numbers correspond to compounds in Fig. 4.

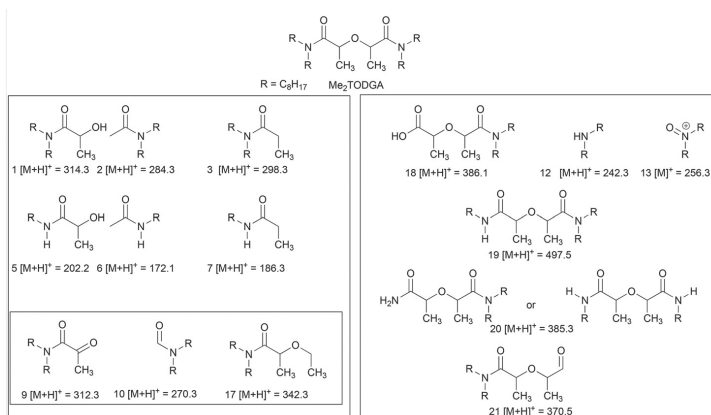


Fig. 8 Proposed structures of the products found in irradiated Me<sub>2</sub>TODGA solutions.

produces radical cations that are capable of participating in electron transfer reactions with the diglycolamides. The smaller dose constant reported in Table 1 for MeTODGA in TPH solution may reflect smaller rate constants for branched alkane radical cation electron transfer reactions, since branched alkane radicals are expected to have a lower ionization potential, resulting in a slower electron transfer reaction between solvent and the DGA molecule. The ionization potential of DGAs was calculated by the semiempirical AM1 method to be less than that of *n*-dodecane by a factor of 1.6 eV.<sup>32</sup> The difference in the ionization potentials supports the charge transfer from radical cations of *n*-dodecane to these amide molecules.

### Identification and behavior of Me<sub>2</sub>TODGA radiolysis products

The study of structural degradation of Me<sub>2</sub>TODGA was performed in the same way as for MeTODGA. In this case a lower number of degradation compounds were identified, shown in Fig. 8. The highest signal intensity product of Me<sub>2</sub>TODGA radiolysis occurred at mass 314.3, and corresponds to the product 2-hydroxy-*N,N*-dioctylpropanamide (compound 1, Fig. 8); the same as produced by MeTODGA irradiation (compound 1, Fig. 4). It was detected at all three laboratories. Since Me<sub>2</sub>TODGA is symmetrical, compound 1 is produced by rupture on either side of the ether. Although small amounts were detected in unirradiated samples, it is also clearly a radiolysis product for which the concentration increases with absorbed dose, until the highest absorbed dose applied of 400 kGy. As shown in Fig. 9, its generation was again enhanced by the presence of the acidic aqueous phase. Rupture of the ether linkage would also be expected to produce *N,N*-dioctylmethylacetamide from the balance of the initial molecule and this compound was indeed detected (mass 298.3, compound 3 in Fig. 8), although at fairly low signal intensity. Products gener-

ated by loss of alkyl substituents also occurred for Me<sub>2</sub>TODGA. Loss of a single octyl group (mass 497.5, compound 19 in Fig. 8) took place in both purely organic and acid contacted conditions, and was again favored by the presence of the acidic aqueous phase. It was detected at all three laboratories.

Fig. 9 shows as well the ingrowth of this signal for irradiation under both conditions. At higher absorbed doses a signal at mass 385.3 appeared (compound 20, Fig. 8), attributed to loss of a second octyl group. This species did not appear until sufficient absorbed dose had been accumulated, indicating that it is likely produced from the single dealkylation product. It continued to grow in with continued irradiation, and was favored by the presence of the acidic aqueous phase. This is also depicted in Fig. 9.

The other relatively abundant product was the expected carboxylic acid produced by rupture of the DGA C–N bond (mass 385.1, compound 18, Fig. 8). Initially, the presence of acid seems to have favored rupture of the amide bond to give the carboxylic acid, but the product appears to undergo radiolysis with a declining concentration above about 200 kGy, when irradiated in contact with nitric acid, similarly to that shown for the analogous carboxylic acid produced by MeTODGA radiolysis in Fig. 6. This is shown in Fig. 9.

## Conclusions

The results indicate that rupture of the ether linkage is a main pathway for the radiolytic decomposition of all the studied TODGAs in the two alkane diluents investigated. The introduction of a methyl group on only one methylene carbon atom of the ether linkage did not protect MeTODGA. In fact, MeTODGA degraded faster than non-substituted TODGAs, possibly because the unsubstituted C–O linkage was weakened by this structural change. This is supported by the fact that products of the ether linkage rupture are still very abundant for this compound, and that the products created by rupture on the non-substituted side of the molecule are the most abundant. The substitution of the industrial diluent TPH for *n*-dodecane did not affect this result, indicating that other radical cations besides that derived from *n*-dodecane are capable of electron transfer reactions with the DGAs, although presumably with different rate constants. Reactions of branched alkyl radicals might be expected to be slower, since branched carbon centered radicals are more stable. This is consistent with the slower dose constant found for MeTODGA degradation in TPH. The addition of a second methyl group on the second methylene carbon atom of the ether linkage did protect Me<sub>2</sub>TODGA, which had a much slower rate of radiolytic degradation than MeTODGA, and a lower rate than that measured for the unsubstituted TODGAs in our previous work, at least in the organic phase.

Other important degradation products included species produced by loss of an octyl group, and for Me<sub>2</sub>TODGA, loss of two octyl groups. Cleavage of the amide C–N bond also occurred to produce carboxylic acids, especially in the pres-

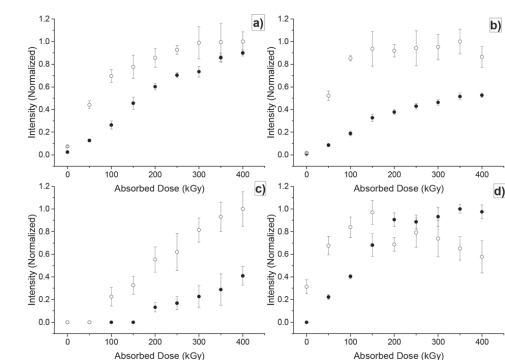


Fig. 9 Formation of compounds (a) 1, (b) 19, (c) 20, and (d) 18 (Fig. 8) versus absorbed dose for the irradiation of 0.05 M MeTODGA in *n*-dodecane (solid squares), for pure organic samples, and for samples irradiated in the presence of 2.5 M HNO<sub>3</sub> (open squares). Intensities are normalized to the maximum detected signal for each compound.

ence of nitric acid. This has also been reported for other amidic ligands, including other TODGAs. The presence of the acidic aqueous phase appears to have a greater adverse effect on the stability of MeTODGA and Me<sub>2</sub>TODGA than was found in previous work with the non-substituted TODGAs. Especially for Me<sub>2</sub>TODGA, the degradation rate of the DGA was much higher in the presence of the acidic aqueous phase. In each case the main degradation products, regardless of which bond was cleaved to produce them, occurred with higher yields for samples irradiated in the presence of the acidic aqueous phase. This suggests that methyl substitution, while possibly protecting the bond hosting the substitution, may activate other bonds in the molecule, especially toward reaction with reactive species produced by acid and water radiolysis. The most likely of these would be reactive  $\cdot\text{OH}$  and  $\cdot\text{NO}_3$  radicals, both probably reacting by  $\cdot\text{H}$ -atom abstraction from the susceptible sites on the DGA. The overall dose constants for MeTODGA and Me<sub>2</sub>TODGA for irradiation in the presence of the aqueous phase are comparable to those reported for the unsubstituted TODGAs.

## Experimental

### Ligand preparation

MeTODGA and Me<sub>2</sub>TODGA were synthesised following the methodology described before<sup>15</sup> or were purchased from TechnoComm Ltd, Wellbrae, Scotland.

### Gamma irradiation procedure

Gamma-irradiation was performed at either CIEMAT (Spain) or INL (USA). The CIEMAT irradiations were performed at the Náyade facility, which is a pool of 1.2 m<sup>2</sup> by 4.5 m deep. It consists of 60 <sup>60</sup>Co sources distributed in six lots with a total activity of  $1.1 \times 10^{14}$  Bq. The irradiation container used provides a homogeneous irradiation flux. Samples were prepared by dissolving ligands in TPH up to 0.1 M and were pre-equilibrated by contacting twice (15 min each) with 3 M HNO<sub>3</sub> at room temperature. The samples were irradiated up to 1000 kGy at a dose rate of 1.78 kGy h<sup>-1</sup>. No volume decrease was observed during irradiation, hence evaporation of the solvent is assumed to be negligible. The glass bottles were then stored in a freezer while awaiting further analyses. Reference samples for aging control were kept in the laboratory during the irradiation process.

The INL irradiations were performed using a Nordion (Ottawa, Canada) Gamma Cell 220 <sup>60</sup>Co irradiator, with a sample cell, center-line dose rate of 5.4 kGy h<sup>-1</sup> up to a maximum absorbed dose of 400 kGy. The ligands were prepared as 0.05 M solutions in *n*-dodecane, either as the pure organic phase, or in contact with an equal volume of 2.5 M HNO<sub>3</sub>. Mixed phase solutions were well-agitated prior to irradiation. It should be noted that sealed vessel irradiations should be considered to be deaerated due to rapid scavenging of dissolved oxygen by produced solvated electrons.

### DAD/MS measurement procedure

The chemical composition of the irradiated samples was characterised by LC-DAD/MS or LC-HRMS. The HPLC-DAD measurements were performed by using a reverse phase C-18 column and CH<sub>3</sub>CN/H<sub>2</sub>O as the mobile phase at 205 nm.

HPLC-MS measurements were performed using three methods. For TPH samples at CIEMAT an Agilent 1100 (Quadrupole detector 6120A) HPLC-MS with a Protosil C-8 column (50 × 2 mm, 5 μm) at 40 °C using a gradient of mobile phase [(A: 0.1% v/v CH<sub>3</sub>CN/HCOOH), (B: 0.1% v/v formic acid)] in the APCI<sup>+</sup> ionization mode (SCAN 100 a 1500 umas/SIM) was used. The mass spectrometer conditions were: capillary voltage: 2000 V; corona current: 5 μA; charging voltage: 2000 V; positive mode; dry temp.: 250 °C; vaporization temp 200 °C; nebulizer gas and dry gas were both N<sub>2</sub>; nebulizer pressure: 1.4 bar; dry gas flow rate: 5 L min<sup>-1</sup>. Samples were analysed without pre-evaporation and diluted up to 0.5 and 1.0 mM in a (90:10)% v/v MeOH/1-octanol mixture. All measurements were repeated twice.

For *n*-dodecane samples at INL, a Dionex (Sunnyvale, CA) ultra-high-performance liquid chromatograph (UHPLC) with an Ultimate 3000 RS pump, 3000 RS autosampler, 3000 RS column compartment and a 3000 RS diode-array detector, coupled to a Bruker (Billerica, MA) microTOFQ-II electrospray ionization quadrupole time-of-flight mass spectrometer with Hystar 3.2 software was used. The mass spectrometer conditions were: capillary: 4500 V; positive mode; temp.: 220 °C; nebulizer gas and dry gas were both N<sub>2</sub>; nebulizer pressure: 0.4 bar; dry gas flow rate: 9 L min<sup>-1</sup>. Samples were analysed without pre-evaporation and diluted up to 1:31 600 in 2-propanol prior to analysis. All experiments conducted on the Dionex UHPLC were carried out isocratically using a 30% aqueous, 70% organic mobile phase. The aqueous component was 0.1% v/v formic acid in NanoPure® water, and the organic component was 4% v/v 1-octanol in 2-propanol. The chromatographic separation was achieved using a 3 μL injection volume onto a C18 reverse-phase (RP-C18) column (Dionex Acclaim® RSCL 120 C18, 10 cm × 2.1 mm, 2.2 μm) with a flow rate of 200 μL min<sup>-1</sup>. The column was maintained at 50 °C. Each sample was injected 5 times. Standards were prepared by serial dilution of unirradiated, non-acid contacted samples with 2-propanol to final concentrations ranging from 0.5 μM to 5 μM.

Also for *n*-dodecane samples, LC-HRMS measurements were performed at Forschungszentrum Jülich using a hybrid linear ion trap FTICR mass spectrometer LTQFT Ultra™ (Thermo Fisher Scientific, Bremen, Germany) coupled with an Agilent 1200 system (Agilent, Waldbronn, Germany). A ZORBAX Eclipse Plus C18, 4.6 × 100 mm, 3.4 μm (Agilent, Waldbronn) column was used using a gradient of mobile phase [(A: 0.1% v/v CH<sub>3</sub>CN/HCOOH), (B: 0.1% v/v formic acid)]. The mass spectrometer was tuned and calibrated in the positive ion mode. Mass spectra were recorded in full scan from 100 to 1000 Da with a resolution of 100 000 at *m/z* 400. All data were processed using the Xcalibur software version 2.0.

## Acknowledgements

Financial support for this research was provided by the European Commission (project SACSESS – Contract no. FP7-Fission-2012-323-282), the German Federal Ministry of Education and Research (Contract no. 02NUK020E), and the U.S. Department of Energy, Assistant Secretary for Nuclear Energy, under the Fuel Cycle R&D Program; DOE Idaho Operations Office contract DE-AC07-05ID14517. We would like to thank Dr Beatriz Santiago-Schübel and Michelle Hupert from Forschungszentrum Jülich GmbH, Zentralinstitut für Engineering, Elektronik und Analytik (ZEA-3).

## Notes and references

- 1 C. Poinssot, S. Bourg, N. Ouvrier, N. Combernoux, C. Rostaing, M. Vargas-Gonzales and J. Bruno, *Energy*, 2014, **69**, 199.
- 2 P. Baron, X. Hérès, M. Lecomte and M. Masson, Proceedings of International Conference on Future Nuclear Systems, (GLOBAL'01), Paris, 2001.
- 3 G. Modolo, A. Wilden, A. Geist, D. Magnusson and R. Malmbeck, *Radiochim. Acta*, 2012, **100**, 715.
- 4 A. Wilden, G. Modolo, C. Schreinemachers, F. Sadowski, S. Lange, M. Sypula, D. Magnusson, A. Geist, F. W. Lewis, L. M. Harwood and M. J. Hudson, *Solvent Extr. Ion Exch.*, 2013, **31**, 519.
- 5 A. Wilden, G. Modolo, P. Kaufholz, P. Sadowski, S. Lange, M. Sypula, D. Magnusson, U. Müllich, A. Geist and D. Bosbach, *Solvent Extr. Ion Exch.*, 2015, **33**, 91.
- 6 G. J. Lumetta, A. V. Gelis, J. C. Carter, C. M. Niver and M. R. Smoot, *Solvent Extr. Ion Exch.*, 2014, **32**, 333.
- 7 M. J. Bollseteros, J. M. Calor, S. Costenoble, M. Montuיר, V. Pacary, C. Sorel, F. Burdet, D. Espinoux, X. Hérès and C. Eysseric, *Proc. Chem.*, 2012, **7**, 178.
- 8 S. A. Ansari, P. Pathak, P. K. Mohapatra and V. K. Manchanda, *Chem. Rev.*, 2012, **112**, 1751.
- 9 Y. Sasaki, Y. Sugo, S. Suzuki and S. Tachimori, *Solvent Extr. Ion Exch.*, 2001, **19**, 91.
- 10 D. Magnusson, B. Christiansen, J. P. Glatz, R. Malmbeck, G. Modolo, D. Serrano-Purroy and C. Sorel, *Solvent Extr. Ion Exch.*, 2009, **27**, 26.
- 11 G. Modolo, A. Wilden, A. Geist, D. Magnusson and R. Malmbeck, *Radiochim. Acta*, 2012, **100**, 715.
- 12 J. Brown, F. McLachlan, M. J. Sarsfield, R. J. Taylor, G. Modolo and A. Wilden, *Solvent Extr. Ion Exch.*, 2012, **30**, 127.
- 13 M. Carrott, K. Bell, J. Brown, A. Geist, C. Gregson, X. Hérès, C. Maher, R. Malmbeck, C. Mason, G. Modolo, U. Müllich, M. Sarsfield, A. Wilden and R. Taylor, *Solvent Extr. Ion Exch.*, 2014, **32**, 447.
- 14 S. Bourg, C. Hill, C. Caravaca, C. Rhodes, C. Ekberg, R. Taylor, A. Geist, G. Modolo, L. Casayre, R. Malmbeck, M. Harrison, G. De Angelis, A. Espartero, S. Bouvet and N. Ouvrier, *Nucl. Eng. Des.*, 2011, **241**, 3427.
- 15 M. Iqbal, J. Huskens, W. Verboom, M. Sypula and G. Modolo, *Supramol. Chem.*, 2010, **22**, 827.
- 16 A. Wilden, G. Modolo, S. Lange, F. Sadowski, B. B. Beele, A. Skerencak-Frech, P. J. Panak, M. Iqbal, W. Verboom, A. Geist and D. Bosbach, *Solvent Extr. Ion Exch.*, 2014, **32**, 119.
- 17 Y. Sugo, Y. Izumi, Y. Yoshida, S. Nishijima, Y. Sasaki, T. Kimura, T. Sekine and H. Kudo, *Radiat. Phys. Chem.*, 2007, **76**, 794.
- 18 H. Galán, A. Núñez, A. González-Espartero, R. Sedano, A. Durana and J. de Mendoza, *Proc. Chem.*, 2012, **7**, 195.
- 19 C. A. Zarzana, G. S. Groenewold, B. J. Mincher, S. P. Mezyk, A. Wilden, H. Schmidt, G. Modolo, J. F. Wishart and A. R. Cook, *Solvent Extr. Ion Exch.*, 2015, **33**, 431.
- 20 B. J. Mincher, G. Modolo and S. P. Mezyk, *Solvent Extr. Ion Exch.*, 2010, **28**, 415.
- 21 R. B. Gujar, S. A. Ansari, M. S. Murali, P. K. Mohapatra and V. K. Manchanda, *J. Radioanal. Nucl. Chem.*, 2010, **284**, 377.
- 22 G. Modolo, H. Asp, C. Schreinemachers and H. Vijgen, *Solvent Extr. Ion Exch.*, 2007, **25**, 703.
- 23 Y. Sugo, Y. Sasaki and S. Tachimori, *Radiochim. Acta*, 2002, **90**, 161.
- 24 H. Galán, M. T. Murillo, R. Sedano, A. Núñez, J. de Mendoza, A. González-Espartero and P. Prados, *Eur. J. Org. Chem.*, 2011, 3959.
- 25 R. Ruhela, J. N. Sharma, B. S. Tomar, K. K. Singh, M. Kumar, P. N. Bajaj, R. C. Hubli and A. K. Suri, *Radiochim. Acta*, 2012, **100**, 37.
- 26 R. B. Gujar, S. A. Ansari, A. Bhattacharyya, A. S. Kanekar, P. N. Pathak, P. K. Mohapatra and V. K. Manchanda, *Solvent Extr. Ion Exch.*, 2012, **30**, 278.
- 27 B. J. Mincher and R. D. Curry, *Appl. Radiat. Isot.*, 2000, **52**, 189.
- 28 V. N. Belevskii, D. A. Tyurin and N. D. Chuvylkin, *High Energy Chem.*, 1998, **32**, 305.
- 29 A. Geist, *Solvent Extr. Ion Exch.*, 2010, **28**, 596.
- 30 B. J. Mincher, S. P. Mezyk, G. Elias, G. S. Groenewold and L. G. Olson, *Solvent Extr. Ion Exch.*, 2013, **31**, 715.
- 31 L. Berthon, J. M. Morel, N. Zorz, C. Nicol, H. Virelizier and C. Madic, *Sep. Sci. Technol.*, 2001, **36**, 709.
- 32 M. J. S. Dewar, E. G. Zoebisch, E. F. Healy and J. J. P. Stewart, *J. Am. Chem. Soc.*, 1985, **107**, 3902.

## Paper 7<sup>[147]</sup>

Zarzana, C.A.; Groenewold, G.S.; Mincher, B.J.; Mezyk, S.P.; Wilden, A.; Schmidt, H.; Modolo, G.; Wishart, J.F.; Cook, A.R. A Comparison of the  $\gamma$ -Radiolysis of TODGA and T(EH)DGA Using UHPLC-ESI-MS Analysis. *Solvent Extr. Ion Exch.* **2015**, *33* (5), 431-447.

DOI: 10.1080/07366299.2015.1012885

### Contribution:

For this work, solvent extraction experiments analysis (gamma-spectrometry, results of ICP-MS), as well as product identification of mass spectrometric experiments were conducted mainly by A. Wilden and me. Additionally, I participated in paper preparation.



## A COMPARISON OF THE $\gamma$ -RADIOLYSIS OF TODGA AND T(EH)DGA USING UHPLC-ESI-MS ANALYSIS

Christopher A. Zarzana<sup>1</sup>, Gary S. Groenewold<sup>1</sup>, Bruce J. Mincher<sup>1</sup>, Stephen P. Mezyk<sup>2</sup>, Andreas Wilden<sup>3</sup>, Holger Schmidt<sup>3</sup>, Giuseppe Modolo<sup>3</sup>, James F. Wishart<sup>4</sup>, and Andrew R. Cook<sup>4</sup>

<sup>1</sup>Idaho National Laboratory, Idaho Falls, ID, USA

<sup>2</sup>California State University at Long Beach, Long Beach, CA, USA

<sup>3</sup>Forschungszentrum Jülich GmbH, Institut für Energie- und Klimaforschung-Nukleare Entsorgung und Reaktorsicherheit (IEK-6), Jülich, Germany

<sup>4</sup>Chemistry Department, Brookhaven National Laboratory, Upton, NY, USA

*Solutions of TODGA and T(EH)DGA in n-dodecane were subjected to  $\gamma$ -irradiation in the presence and absence of an aqueous nitric acid phase and analyzed using UHPLC-ESI-MS to determine the rates of radiolytic decay of the two extractants, as well as to identify radiolysis products. The DGA concentrations decreased exponentially with increasing dose, and the measured degradation rate constants were uninfluenced by the presence or absence of an acidic aqueous phase, or by chemical variations in the alkyl side-chains. The DGA degradation was attributed to reactions of the dodecane radical cation, whose kinetics were measured for TODGA using picosecond electron pulse radiolysis to be  $k_2 = (9.72 \pm 1.10) \times 10^9 \text{ M}^{-1} \text{ s}^{-1}$ . The identified radiolysis products suggest that the bonds most vulnerable to radiolytic attack are those in the diglycolamide center of these molecules and not on the side-chains.*

## INTRODUCTION

The diglycolamides are finding increasing attention for potential applications in rare earth and actinide separations.<sup>[1]</sup> Sasaki et al. investigated a series of related diglycolamides that varied in their *N*-alkyl substituents (Fig. 1), and reported that derivatives with 4, 5, or 6 *N*-alkyl carbons were barely soluble in aliphatic hydrocarbon diluents such as *n*-dodecane, the commonly used diluent in actinide solvent extraction.<sup>[2]</sup> However, the *n* = 8 and 10 derivatives were soluble in *n*-dodecane, and these compounds complexed and extracted actinides and lanthanides with distribution ratios that increased with increasing aqueous nitric acid acidity, and that followed the order  $\text{M}^{\text{III}}/\text{M}^{\text{IV}} > \text{M}^{\text{VI}} > \text{M}^{\text{V}}$ . In experiments designed to separate trivalent lanthanides from trivalent actinides such as Am, separation factors ( $\alpha_{\text{Eu}/\text{Am}}$ ) as high as 9 were achieved using the octyl derivative *N,N,N',N'*-tetraoctyldiglycolamide (TODGA, Fig. 1a) although the diglycolamides are

Address correspondence to Bruce J. Mincher, Aqueous Separations and Radiochemistry Department, Idaho National Laboratory, PO Box 1625, Idaho Falls, ID 83415-4107, USA. E-mail: [bruce.mincher@inl.gov](mailto:bruce.mincher@inl.gov)



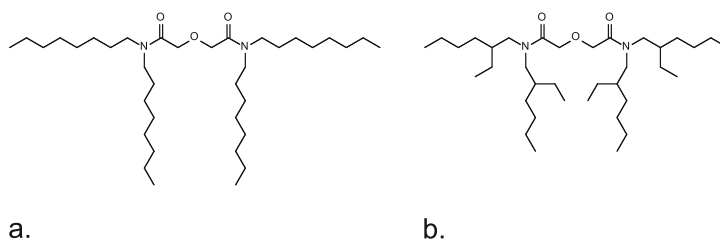


**Figure 1** Structures of the two diglycolamides studied here: a. *N,N,N',N'*-tetraoctyldiglycolamide (TODGA) and b. *N,N,N',N'*-tetra-2-ethylhexyldiglycolamide (T(EH)DGA).

generally considered to be group 4*f*- and 5*f*-element extraction reagents. TODGA has thus received detailed study for its potential applications at the back end of the nuclear fuel cycle. Modolo et al.,<sup>[3]</sup> for example, reported that 0.2 M TODGA, modified with 0.5 M tri-*n*-butyl phosphate (TBP) in hydrogenated tetrapropene (TPH), an industrial alkane diluent, successfully extracted Eu<sup>III</sup>, Am<sup>III</sup>, Cm<sup>III</sup>, Cf<sup>III</sup>, and Th<sup>IV</sup> across the nitric acid concentration range 1–3 M. However, it was such a good complexing agent that holdback reagents were required to mitigate Zr, Mo, and Pd extraction, and Sr extraction was regarded as a problem for separations from a simulated first-cycle PUREX raffinate aqueous phase.

The branched-chain TODGA derivative *N,N,N',N'*-tetra-2-ethylhexyldiglycolamide (T(EH)DGA, Fig. 1b) has been promoted as a cheaper alternative with less affinity for fission product complexation.<sup>[4]</sup> The weaker complexing ability of T(EH)DGA was used to advantage by Lumetta et al.<sup>[5]</sup> in the design of the ALSEP (Actinide Lanthanide Separation) solvent, where, in combination with the acidic soft-donor ligand diethylenetriamine pentaacetic acid (DTPA), it was used to give a single extraction/strip cycle separation of the actinides from the lanthanides.<sup>[5,6]</sup> A loaded organic phase consisting of 0.05 M T(EH)DGA and 0.75 M 2-ethylhexylphosphonic acid mono-2-ethylhexyl ester (HEH[EHP]) in *n*-dodecane, when stripped with an aqueous phase consisting of 0.01 M DTPA and 0.2 M citric acid, provided  $\alpha_{\text{Nd/Am}}$  values in the range 10–30.<sup>[5]</sup> Higher separation factors were obtained in the TODGA/HEH[EHP] system with TODGA concentrations < 0.1 M, with values in the range 50–90 for  $\alpha_{\text{Eu/Am}}$ .<sup>[6]</sup>

In continued European research within the FP 7 ACSEPT project, TODGA was modified by the addition of one or two methyl groups on the methylene carbon positions to produce Me-TODGA and Me<sub>2</sub>-TODGA, respectively.<sup>[7–9]</sup> These derivatives were then used as 0.1 M solutions in the TPH alkane diluent to measure the distribution ratios of Am<sup>III</sup> and Eu<sup>III</sup> across a wide range of nitric acid concentration. Extraction efficiency decreased with increasing methyl substitution, probably due to steric considerations. However, adequate extraction of both the actinides and lanthanides occurred at the higher nitric acid concentrations typical of fuel cycle solvent extraction processes. Importantly, the undesirable co-extraction of strontium that occurs with unsubstituted TODGA was mitigated.

Short-chain derivatives of the diglycolamides have also found applications in metal separations processes. Tetrabutyl diglycolamide (TBDGA) has been proposed for inter-group lanthanide separations by solvent extraction, both in the conventional molecular diluent octanol, and in ionic liquid diluents.<sup>[10]</sup> Tetrabutyl diglycolamide is not soluble in the longer chain alkanes used to dissolve TODGA and T(EH)DGA. It was reported

that the lanthanides were conveniently separated into heavy, intermediate, and light groups using 7 mM TBDGA in octanol. Furthermore,  $\text{Eu}^{\text{III}}$  was better extracted than  $\text{Am}^{\text{III}}$ , with a separation factor of about 10 across a wide range of nitric acid concentrations. Upon decreasing the alkane chain length further, the diglycolamides even become water soluble. The aqueous diglycolamides have been used to strip lanthanides and actinides from loaded TODGA organic phases.<sup>[11–13]</sup> Tetraethyldiglycolamide (TEDGA) at 0.25 M in 1 M  $\text{HNO}_3$  has been used as a lanthanide stripping agent for the loaded T(EH)DGA/HEH[EHP] solvent used in the ALSEP process above, following initial back extraction of the actinides into buffered DTPA solution.<sup>[5]</sup> Given the success of the cited studies, it seems likely that the diglycolamides will receive continued study as potential actinide and lanthanide complexing agents. However, the acid hydrolysis of TEDGA may be of concern, and Lumetta et al. made fresh solutions daily prior to use, although hydrolysis rates were not specifically investigated in that work.<sup>[5]</sup>

For application to highly acidic media, or in media exposed to ionizing radiation, hydrolytic and radiolytic stability of the diglycolamides is of obvious potential concern. Only a few such studies have been performed to date. Sugo et al. examined the hydrolytic and  $\gamma$ -radiolytic decomposition of TODGA, concluding that there was no evidence of hydrolysis after 4 weeks of continuous stirring of 0.1 M TODGA in *n*-dodecane with 3 M  $\text{HNO}_3$  at room temperature.<sup>[14]</sup> Modolo et al.<sup>[3]</sup> also found no changes in extraction performance for 0.2 M TODGA in TPH after 60 days of contact with 3 M  $\text{HNO}_3$ , and Sharma et al.<sup>[15]</sup> found no degradation products in 0.2 M T(EH)DGA/30% isodecanol/*n*-dodecane in contact with 0.5 M  $\text{HNO}_3$  at room temperature for 20 days. Thus, hydrolytic degradation does not seem to be a serious issue, at least for long-chain DGAs at moderate temperature. While these DGAs appear to be hydrolytically stable, radiolytic degradation of DGAs has been observed. The decrease in TODGA concentration is exponential with dose, but slower for neat TODGA than for TODGA in *n*-dodecane.<sup>[14]</sup> The presence of nitric acid during irradiation has little effect on the rate of TODGA radiolysis. Similar results have been reported for T(EH)DGA.<sup>[15]</sup> The so-called “sensitization effect,” in which the presence of *n*-dodecane increased the rate of decomposition of TODGA, was attributed to electron-transfer reactions between TODGA and radiolytically-produced *n*-dodecane radical cations.<sup>[16]</sup>

Several studies have appeared in recent years regarding the effects of DGA irradiation on solvent extraction metal distribution ratios ( $D_M$ ). For  $\gamma$ -irradiation in TPH, or in TPH with tributylphosphate (TBP) as a phase modifier, only a slight decrease in the distribution ratios for  $\text{Am}^{\text{III}}$  or  $\text{Eu}^{\text{III}}$  was found for doses as high as 1 MGy.<sup>[3]</sup> However, Gujar et al. irradiated TODGA in *n*-dodecane in the presence of several phase modifiers, including TBP, and found large decreases in the americium distribution ratio ( $D_{\text{Am}}$ ) at the same absorbed dose, accompanied by decreases in  $D_{\text{Sr}}$  and increases in  $D_{\text{Mo}}$ .<sup>[17]</sup> Stripping distribution ratios for americium were not affected. In continued work, Gujar et al. compared TODGA to T(EH)DGA, finding that the changes in solvent extraction behavior caused by  $\gamma$ -radiolysis were analogous, and similar to those reported for TODGA above.<sup>[17]</sup> In contrast, Sharma et al. reported decreased metal distribution ratios for Mo, as well as significant increases in stripping distribution ratios for Eu and Am for irradiated T(EH)DGA/isodecanol/*n*-dodecane solution.<sup>[15]</sup> In further study of the radiolysis of T(EH)DGA, Deepika et al. found that  $D_{\text{Am}}$  values decreased more for T(EH)DGA when irradiated in the presence of the *n*-dodecane and  $\text{HNO}_3$ .<sup>[4]</sup> However, these authors did not attempt to separate the effects of the diluent and the aqueous phase and erroneously concluded that nitric acid enhanced T(EH)DGA decomposition, rather than to electron transfer

reactions with the *n*-dodecane radical cation. Thus, contradictory reports have appeared in the literature, possibly confounded by the use of the various phase modifiers.

Recently a study was published concerning the  $\gamma$ -radiolysis of an additional diglycolamide, didodecylldioctyldiglycolamide (D<sup>3</sup>DODGA), which was evaluated by changes in  $D_{Am}$  with absorbed dose.<sup>[18]</sup> This unsymmetrical diglycolamide was designed to minimize third phase formation during extractions with high metal loading, and to minimize Sr extraction.<sup>[19]</sup> The presence of *n*-dodecane increased decomposition rates for D<sup>3</sup>DODGA in a manner similar to TODGA and T(EH)DGA, and the authors reported little effect due to the presence or absence of 4 M HNO<sub>3</sub>. Like some reports for the other diglycolamides,  $D_{Am}$  and  $D_{Sr}$  decreased with increasing absorbed dose, but stripping was unaffected.<sup>[18]</sup>

The products of TODGA radiolysis reported by Sugo et al. indicated that the most susceptible bonds were the ether linkage (yielding dioctylacetamide and dioctylglycolamide), the methylene-carbonyl bond (forming dioctylformamide), and the amide C–N bond (producing dioctylamine), as measured by gas chromatography with a mass spectrometer detector (GC-MS).<sup>[14]</sup> The presence of nitric acid favored C–N bond rupture. The Modolo group<sup>[20]</sup> also reported the generation of dioctylacetamide and dioctylglycolamide for irradiations in the absence of an aqueous phase, using HPLC-MS, as well as products corresponding to loss of octyl groups. Products of the  $\gamma$ -radiolysis of neat T(EH)DGA, detected by GC-MS included the diglycolamide resulting from loss of an ethylhexyl group, and the formamide produced by rupture of the methylene-carbonyl C–C bond, analogous to the products identified in TODGA radiolysis. T(EH)DGA degradation products reported were also those caused by cleavage of ether and amide linkages, to produce formamide, acetamide, and glycolamide derivatives analogous to those reported above for TODGA, except that the carboxylic acid associated with the amine product was also detected for samples irradiated in the presence of acid.<sup>[15]</sup> It is commonly reported that rupture of the N–C bond to produce an amine and a carboxylic acid is favored by the presence of HNO<sub>3</sub>.<sup>[20]</sup>

To date, most studies of TODGA and T(EH)DGA have used GC-MS for quantification of DGA degradation, and for identification of radiolysis products. Because GC separates analytes in the gas phase, those analytes must be volatile, or be rendered volatile through chemical derivatization. For quantitative work, derivatization is undesirable, since the derivatization reaction adds a source of uncertainty. Furthermore, derivatization reactions on an irradiated sample could produce unanticipated products, complicating the identification of true radiolysis products. Ultra-high pressure liquid chromatography with electrospray ionization mass spectrometry detection (UHPLC-ESI-MS) is an alternative quantification and identification method that offers some advantages for studying DGA systems. As these DGA systems are liquids, UHPLC is a natural method for separating their components. Positive-mode electrospray produces gas-phase ions from solution-phase analytes through either addition of a cation (usually a proton, but sometimes a sodium cation) to the analyte molecule, which must have a functional group that will protonate. Negative-mode electrospray ionization produces gas-phase ions through removal of a proton. The diglycolamide functional group, in particular the two carbonyl groups, should readily accept protons, so the DGAs will ionize efficiently. In addition, the expected radiolysis products of the DGAs should retain basic functional groups that will also ionize efficiently by protonation. In particular, radiolysis products containing a carboxylic acid functional group will ionize readily by both positive and negative-mode ESI, while analysis of carboxylic acid containing molecules by GC-MS is difficult, due to their elevated boiling points. Therefore, UHPLC-ESI-MS analysis of these DGA systems should

offer complimentary information to GC-MS analysis, with the potential for identifying nonvolatile compounds that might not be detectable using GC-MS.

In this article we present an investigation of the  $\gamma$ -radiolytic stability of TODGA and T(EH)DGA in *n*-dodecane using UHPLC-ESI-MS based on their decrease in concentration with absorbed dose and the generation of products, as part of a larger study of symmetric diglycolamides. Each was irradiated at the same concentration to allow for appropriate comparison of their *G*-values, and irradiations were performed for the organic solution in the presence and absence of an aqueous nitric acid phase. Additionally, the kinetics of the reaction of the *n*-dodecane radical cation with TODGA were measured using pico-second (ps) electron pulse radiolysis.

## EXPERIMENTAL

### Gamma-Ray Irradiation of Diglycolamide Solutions

TODGA and T(EH)DGA (Eichrome Industries, Darien, IL) were irradiated as 0.05 M solutions in *n*-dodecane. Aliquots of these solutions were irradiated as the pure organic phase, or in contact with an equal volume of either 0.1 M HNO<sub>3</sub> or 2.5 M HNO<sub>3</sub>. The mixed-phase solutions were well agitated by hand prior to irradiation. The samples were sealed in screw-capped glass liquid scintillation vials and therefore must be considered deaerated after the deposition of a small absorbed dose. The irradiations were performed using a <sup>60</sup>Co Gamma Cell source (Nordion, Ottawa, Canada), with a center-line sample chamber dose-rate of 5.4 kGy h<sup>-1</sup>, as determined by decay-corrected Fricke dosimetry. Irradiations were conducted at room temperature (20–23°C); the sample temperature was not controlled externally and was likely elevated above this range due to the absorbed radiation.

### UHPLC-ESI-MS

Irradiated DGA samples in *n*-dodecane were diluted 1:30,000 in HPLC grade 2-propanol (Fisher Scientific, Pittsburg, PA) prior to analysis in order to generate a concentration in the low micromolar ( $\mu$ M) range (i.e., in the middle of the response versus concentration curve). The diluted samples were analyzed using a Dionex (Sunnyvale, CA) ultra-high-performance liquid chromatograph (UHPLC) with an Ultimate 3000 RS pump, 3000 RS autosampler, 3000 RS column compartment and a 3000 RS diode array detector, coupled to a Bruker (Billerica, MA) micrOTOF-II electrospray-ionization-quadrupole-time-of-flight mass spectrometer with Hystar 3.2 software. All experiments with the UHPLC were carried out isocratically using a 30% aqueous/70% organic mobile phase. The aqueous component was 0.1% v/v formic acid in NanoPure<sup>®</sup> water, and the organic component was 4% v/v 1-octanol in 2-propanol (all HPLC grade). The chromatographic separation was achieved using a 3  $\mu$ L injection volume onto a C18 reverse-phase (RP-C<sub>18</sub>) column (Dionex Acclaim<sup>®</sup> RSCL 120 C18, 10 cm x 2.1 mm, 2.2  $\mu$ m) with a flow rate of 200  $\mu$ L/min. The column was maintained at 50°C. The mass spectrometer conditions were: capillary: 4.5 kV, positive mode; temperature: 220°C; nebulizer gas and dry gas were both N<sub>2</sub>, nebulizer pressure: 0.4 bar; dry gas flow rate: 9 L/min. The mass spectrometer was operated using standard Bruker tuning parameters, specifically “tune high” (Table S1, Supplementary Information). Each sample was injected 5 times.

### Standard Preparation

Standards for TODGA and T(EH)DGA were prepared by serial dilution of unirradiated, non-acid contacted 0.05 M DGA solutions in *n*-dodecane with 2-propanol, to final concentrations ranging from 0.5  $\mu\text{M}$  to 5  $\mu\text{M}$ . These standards were used to construct a calibration curve using the integrated chromatographic peak areas for the diglycolamides using the UHPLC-ESI-MS analytical method (see Fig. S1). Each sample result was the mean of five measurements, and the error bars shown represent 99% confidence intervals.

### Picosecond Electron Pulse Radiolysis

Pulse radiolysis based transient absorption experiments were performed at the Brookhaven LEAF facility, as described previously.<sup>[21]</sup> Samples were irradiated in 1.0 cm pathlength NSG ES Quartz semimicro cuvettes sealed with Teflon stoppers. The doses per pulse for various experiments were in the range 20–40 Gy. Time-resolved kinetics were obtained using a Hamamatsu R1328-03 biplanar tube (rise time 60 ps) amplified using a B&H AC4020H20L1 amplifier (4 GHz) and digitized using a LeCroy WaveRunner 640Zi oscilloscope (4GHz). Ten nm bandpass interference filters were used for wavelength selection of the analyzing light.

## RESULTS AND DISCUSSION

### Degradation of TODGA and T(EH)DGA as a Function of Absorbed Dose

The change in TODGA concentration versus absorbed  $\gamma$ -dose for samples irradiated as the organic phase or in contact with either 0.1 M or 2.5 M  $\text{HNO}_3$  is shown in Fig. 2. Results for T(EH)DGA irradiated as the organic phase or in contact with 0.1 M  $\text{HNO}_3$  are also shown. The concentration change versus absorbed dose data may be well fit with an exponential curve, suggesting pseudo-first-order kinetics, probably by reaction with a direct radiolysis product of the diluent. Dose constants ( $d$ ) for each system are shown in Table 1, with the mean value for all conditions being  $(4.1 \pm 0.3) \times 10^{-3} \text{ kGy}^{-1}$ . Sugo et al. reported a similar value of  $4.5 \times 10^{-3} \text{ kGy}^{-1}$ , with increasing dose constants at lower TODGA concentrations.<sup>[16]</sup> Since the decompositions of TODGA and T(EH)DGA occur exponentially, the  $G$ -value is not an appropriate metric; as a rate rather than a rate constant, the  $G$ -value changes with concentration under these conditions.<sup>[22]</sup> Since  $G$ -values have historically been reported in studies of systems undergoing radiolysis, they are reported here to aid in comparison to previous work. Initial  $G$ -values ( $G_o$ , in  $\mu\text{mol J}^{-1}$ ) may be calculated based on the initial DGA concentration and the dose constant, according to Eq. (1):

$$G_o = d [\text{DGA}] (1.3 \times 10^3) \quad (1)$$

where  $d$  is the dose constant, [DGA] is the initial DGA concentration, and the factor  $1.3 \times 10^3$  includes appropriate unit conversions and density corrections. Calculated  $G_o$  values for each system are given in Table 1.

The presence of the acidic aqueous phase, whether dilute or concentrated  $\text{HNO}_3$ , has no obvious effect on the degradation rate, in agreement with the findings of Sugo et al.,<sup>[14]</sup> Ravi et al.,<sup>[19]</sup> Sharma et al.,<sup>[15]</sup> and the solvent extraction results of Modolo et al.<sup>[13]</sup> This

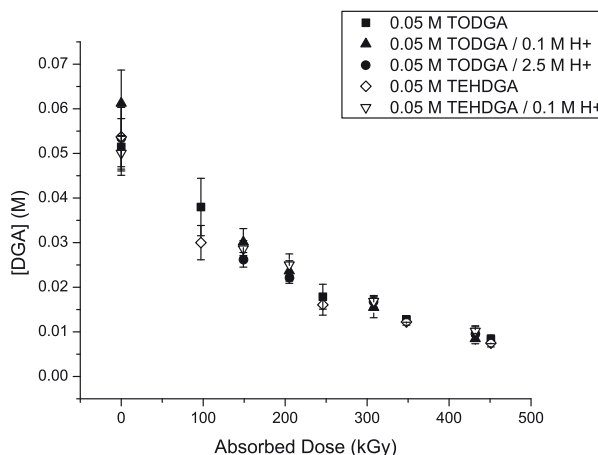


**Figure 2** DGA concentration vs. absorbed dose. The solid squares are 0.05 M TODGA; the open diamonds are 0.05 M T(EH)DGA; the solid upward-facing triangles are 0.05 M TODGA contacted with 0.1 M HNO<sub>3</sub>; the open inverted triangles are 0.05 M T(EH)DGA contacted with 0.1 M HNO<sub>3</sub>; and the solid circles are 0.05 M TODGA contacted with 2.5 M HNO<sub>3</sub>. Each point is the mean of five measurements, and the error bars represent 99% confidence intervals.

**Table 1** Measured dose constants and  $G_0$  values for the degradation of TODGA and T(EH)DGA in the three systems studied. The dose constants were calculated from linear fits of plots of  $\ln[\text{DGA}]$  vs. absorbed dose, and the  $G_0$  values were calculated according to Eq. (1). The uncertainty in the dose constants are 99% confidence intervals.

Sample	$G_0$ ( $\mu\text{mol J}^{-1}$ )	Dose constant $d$ ( $\text{kGy}^{-1}$ )
0.05 M TODGA	0.27	$(4.1 \pm 0.3) \times 10^{-3}$
0.05 M T(EH)DGA	0.29	$(4.3 \pm 0.3) \times 10^{-3}$
0.05 M TODGA/0.1 M HNO <sub>3</sub>	0.30	$(4.5 \pm 0.2) \times 10^{-3}$
0.05 M T(EH)DGA/0.1 M HNO <sub>3</sub>	0.25	$(3.7 \pm 0.2) \times 10^{-3}$
0.05 M TODGA/2.5 M HNO <sub>3</sub>	0.25	$(3.8 \pm 0.3) \times 10^{-3}$

indicates that free radicals generated during irradiation of the aqueous phase are not important for TODGA degradation. Given the low starting concentration of DGAs (0.05 M), the likely mechanism for radiological degradation would be by reaction of a direct radiolysis product of the diluent, *n*-dodecane, as postulated by Sugo et al.<sup>[16]</sup> It must be noted that this is in contrast to the results of Galán et al.,<sup>[23]</sup> who reported a protective effect for TODGA solutions pre-equilibrated with 3 M HNO<sub>3</sub>.

There does not appear to be any difference in the degradation rates between TODGA and T(EH)DGA. This is somewhat surprising, as it was expected that the branched carbon on the side-chains of T(EH)DGA would provide an additional site for bond cleavage or addition. Branched alkanes typically decompose with higher  $G$ -values than do *n*-alkanes.<sup>[24]</sup> However, the similarity in the degradation rates between TODGA and T(EH)DGA, along with the identified radiolysis products, discussed below, strongly suggest that the diglycolamide center of these molecules, not the side-chains, is most vulnerable to radiolytic degradation.

### Identification and Behavior of TODGA and T(EH)DGA Radiolysis Products

A number of radiolysis products of TODGA and T(EH)DGA were identified by UHPLC with positive-mode ESI-MS detection. A superposition of representative ion chromatograms for the compounds detected in 0.05 M TODGA/*n*-dodecane contacted with 2.5 M HNO<sub>3</sub> after absorbing 432 kGy is shown in Fig. 3. The total-ion chromatogram contains several other peaks that were identified as nonradiolytically-produced contaminants, based on their detection in the mobile phase and their signal invariance with absorbed dose, and so have been omitted for clarity. Radiolysis products were identified both by examining the masses of the noncontaminant peaks, and by explicitly searching for ion signals that would correspond to structures that could possibly be formed from the parent DGA through bond cleavage, followed by capping with various radicals (H•, CH<sub>3</sub>•, •OH, etc.). Proposed structures for the identified compounds, based on a logical bond cleavage followed by capping that would result in the protonated and sodiated measured masses, along with the bond cleavages that would result in their formation are shown in Fig. 4. The same kinds of radiolysis products were identified for both TODGA and T(EH)DGA, with the differences in the proposed structure being octyl side-chains for TODGA-derived products and ethylhexyl side-chains for T(EH)DGA derived species. Curiously, no compounds that would result from bond cleavage within either the octyl or the ethylhexyl side-chains were

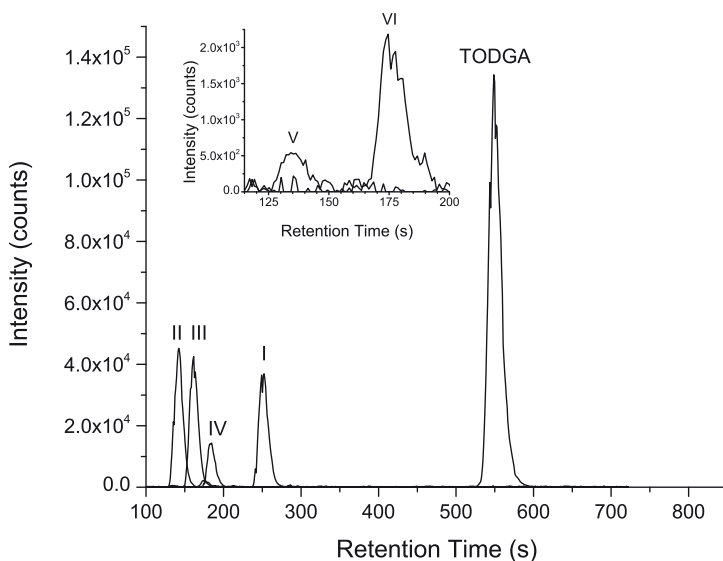


**Figure 3** Overlaid ion chromatograms of TODGA and its detected degradation products for irradiation to 432 kGy absorbed dose in contact with 2.5 M HNO<sub>3</sub>. The inset shows Compounds V and VI only. The compound I chromatogram  $m/z = 469.4$  (the protonated species); the compound II chromatogram  $m/z = 380.3$  (the sodiated species); the compound III ion chromatogram  $m/z = 300.3$  (the sodiated species); the compound IV ion chromatogram  $m/z = 284.3$  (the protonated species); the compound V ion chromatogram  $m/z = 314.3$  (the protonated species); the compound VI ion chromatogram  $m/z = 270.3$  (the protonated species); and the TODGA ion chromatogram  $m/z = 581.5$  (the protonated species).

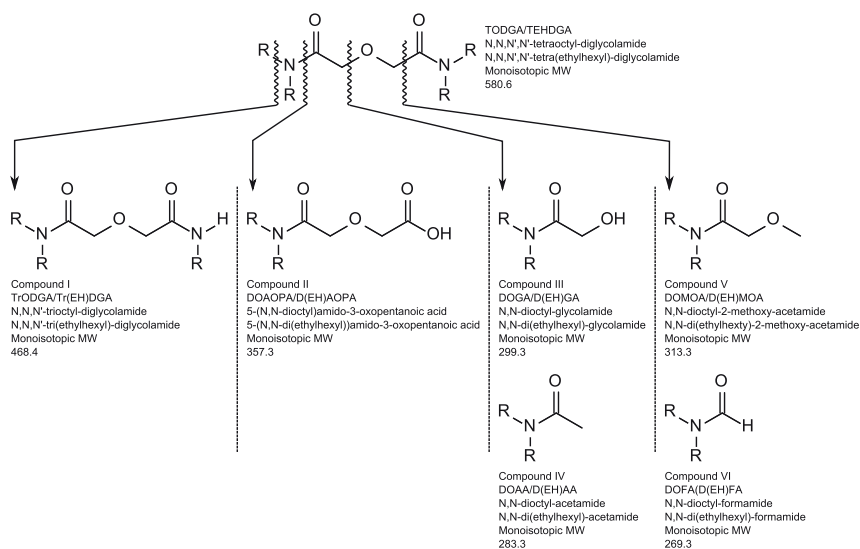


**Figure 4** Proposed structures for radiolysis products observed for both DGAs with positive-mode ESI-MS, where R is octyl for TODGA and ethylhexyl for T(EH)DGA.

detected (see Fig. S2 for a list of potential radiolysis products that were explicitly searched for but not detected). This lack of products due to side-chain fragmentation supports the conclusion that, from a radiological degradation perspective, TODGA and T(EH)DGA are identical.

Compound I produced a peak at  $m/z$  469, assigned to  $M+H^+$ , and an accompanying peak 22 mass units higher, assigned to  $M+Na^+$  (see Fig. 5b). This indicates the monoisotopic molecular mass of compound I is 468, a loss of 112 mass units from the parent molecule. The side-chain for both DGAs has the formula  $C_8H_{17}$ , with a mass of 113. Therefore, a loss of 112 would correspond to loss of a side-chain and replacement with a hydrogen atom, giving *N,N,N'*-trioctyldiglycolamide (TrODGA) from TODGA and *N,N,N'*-tri(ethylhexyl)diglycolamide (Tr(EH)DGA) from T(EH)DGA, as indicated in the proposed structure for compound I in Fig. 4. Compound II produced peaks at  $m/z$  358 and 380, suggesting a monoisotopic molecular mass of 357. Since this mass is odd, the nitrogen rule indicates this species must have an odd number of nitrogen atoms. Cleavage of the  $N-C_{\text{carbonyl}}$  bond followed by addition of an OH group gives 5-(*N,N*-dioctyl)amido-3-oxopentanoic acid (DOAOPA) from TODGA and 5-(*N,N*-di(ethylhexyl)amido-3-oxopentanoic acid (D(EH)AOPA) from T(EH)DGA, as indicated in Fig. 4. A peak at the expected mass of deprotonated DOAOPA ( $m/z$  356) was detected using negative-mode ESI-MS (data not shown), further supporting this structural assignment. Compounds III-VI have even protonated peaks, so they all have odd monoisotopic masses, indicating odd numbers of nitrogen atoms. The proposed structure for each of these compounds was obtained by cleaving the  $C-O_{\text{ether}}$  bond (compounds III and IV) or the  $C-C_{\text{carbonyl}}$  bond (compounds V and VI), followed by addition of a hydrogen atom.

The radiolysis products DOAOPA and D(EH)AOPA are different than the other detected compounds, in that these products are formed by bond cleavage followed by



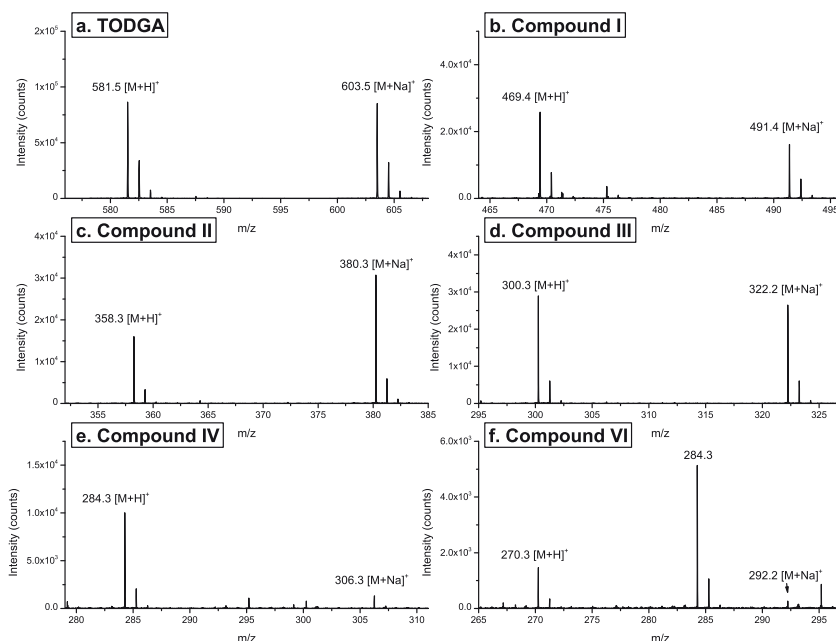


**Figure 5** Mass spectra of TODGA and its detected degradation products showing the ratio of the sodiated peak to the protonated peak. Compound V is omitted due to its low signal intensity.

capping with an OH group, rather than with a hydrogen atom as in all the others. A possible source of  $\bullet\text{OH}$  radical could be entrained water in the organic phase. What is also interesting is that since DOAOPA and D(EH)AOPA are detected, one might expect the analogous products resulting from cleavage of other bonds followed by capping with OH, but no evidence for any of these other compounds was detected (see Fig. S1).

Additional support for the proposed structures comes from examination of the ratios of peaks for the protonated and sodiated molecule, shown in Fig. 5. Sodium is a ubiquitous, adventitious contaminant frequently seen in the electrospray experiments, which nevertheless is useful for confirming the molecular weight of the compound in question, and in this case is indicative of the compound structure. The ratio of the sodiated to protonated peak for intact TODGA (Fig. 5a) is approximately one, as is the peak ratio for TrODGA (compound I, Fig. 5b). Both molecules have an intact diglycolamide functional group that can form a sodium adduct. In the proposed structure for DOAOPA (compound II) one of the amide groups has been modified to a carboxylic acid, but the molecule still has the ability to bind in a similar tridentate fashion. Here, the ratio of the sodiated to protonated peaks is even higher (approximately 2, Fig. 5c), which suggests that DOAOPA has the ability to bind even more strongly with  $\text{Na}^+$ . *N,N*-dioctyl-glycolamide (DOGA) (compound III) also displays a high intensity ratio for the sodiated and protonated peaks (Fig. 5d); here, tridentate bonding cannot occur; however, bidentate bonding involving two O atoms does occur, accounting for the higher ratio observed.

The high sodiated/protonated ion intensity ratios seen for the above compounds contrast sharply with the ratios recorded for the two amide products *N,N*-dioctylacetamide

and *N,N*-dioctylformamide (compounds IV and VI), which have very small sodiated peaks compared to their protonated peaks (Fig. 5e and Fig. 5f). This observation is consistent with the assignment of structures that cannot bind in a multidentate fashion to  $\text{Na}^+$  and hence do not form abundant sodiated peaks.

How these degradation products will affect  $D_M$  depends on the efficiency with which the products are able to complex metal ions and the solubilities of those complexes in the aqueous and organic phases. Additionally, subsequent aqueous stripping could be impaired if a radiolysis product holds the metal in the organic phase during back extraction. Organic-soluble acidic degradation products (like DOGA and D(EH)GA) are the most common degradation products known to impair stripping. Of the previous studies that have investigated  $D_M$  versus absorbed dose for irradiated DGAs, those performed in the presence of organic phase modifiers [3,15,25] are not strictly comparable to the products studied here, since phase modifiers may perturb reaction chemistry with the ligand by radical scavenging reactions. Of those which examined post-irradiation  $D_M$  for DGAs in *n*-dodecane, each examined americium extraction and found approximately exponential changes in  $D_{Am}$  with absorbed dose.[4,18–19] Although it is tempting to attempt to correlate this with the exponential decrease in DGA concentration, extraction of americium by a changing mixture of complexing agents could produce the same effect. Additional studies examining the effect of DGA radiolysis products on  $D_M$  would be valuable in this regard.

The concentration changes of the detected radiolysis products as a function of absorbed dose (Fig. 6) can be examined based on the proposed structures. The signal for each compound is normalized to the maximum signal detected in a given solution (for example, the signal for compound I in the 0.05 M TODGA solution is normalized to the maximum detected compound I signal for all the exposed 0.05 M TODGA samples, found at 348 kGy total absorbed dose) because, due to the lack of intensity calibration standards and internal standards, it is difficult to directly compare the measured signal intensities. Compounds I and II (Fig. 6a and Fig. 6b, respectively) are present in the zero absorbed-dose samples, possibly as byproducts or precursors from synthesis of TODGA and T(EH)DGA, but grow in as dose increases, indicating they are also readily formed by radiolysis. The signal for compound II peaks at around 250 kGy absorbed dose and then begins to decrease, indicating this radiolysis product is itself susceptible to radiolysis. Given the proposed structures, DOAOPA from TODGA and D(EH)AOPA from T(EH)DGA, this is not surprising, since these structures still have the  $\text{C}-\text{O}_{\text{ether}}$ ,  $\text{C}-\text{C}_{\text{carbonyl}}$ , and  $\text{N}-\text{C}_{\text{carbonyl}}$  bonds whose rupture is proposed to lead to the other detected radiolysis products. The signal for compound I could be beginning to decrease at maximum absorbed dose, but there is too much scatter in the data to be sure. That the intensity of compound II peaks before that of compound I suggests that compound II is more susceptible to radiolysis than compound I, possibly due to enhanced reactivity of the carboxylic acid in DOAOPA and D(EH)AOPA. Compounds III and IV (Fig. 6c and Fig. 6d, respectively) are not detected in the zero absorbed-dose samples and grow in as absorbed dose increases, consistent with their structural assignments as small radiolysis products.

### Comparison to Previous Work

The identified radiolysis products agree with those reported by Sugo et al. for TODGA,[14] and those reported by Sharma et al. for T(EH)DGA,[15] with two exceptions. A product detected here that was not reported previously was compound I,

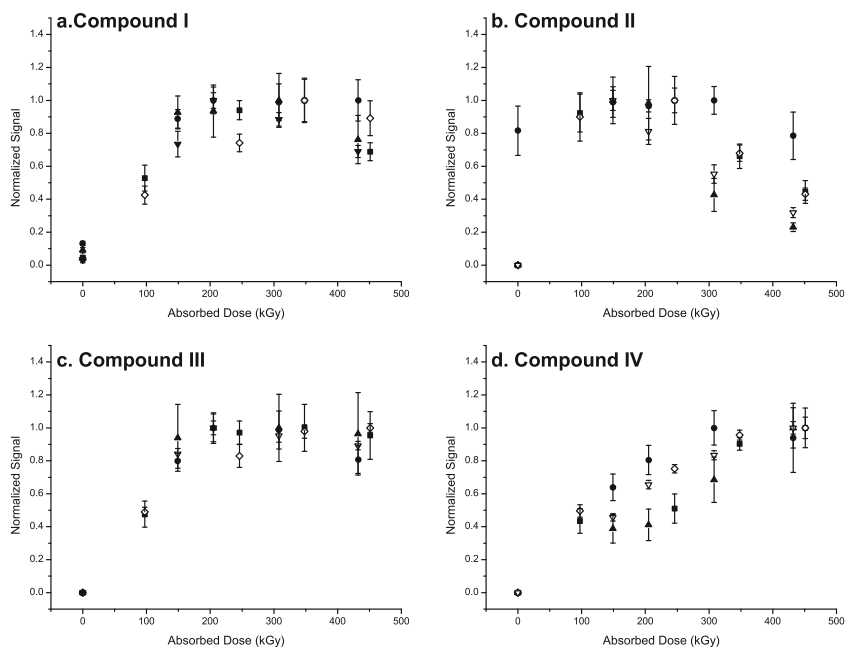


**Figure 6** Normalized signal vs absorbed dose for a. Compound I, b. Compound II, c. Compound III, d. Compound IV. The solid squares are 0.05 M TODGA; the open diamonds are 0.05 M T(EH)DGA; the solid upward-facing triangles are 0.05 M TODGA contacted with 0.1 M  $\text{HNO}_3$ ; the open inverted triangles are 0.05 M T(EH)DGA contacted with 0.1 M  $\text{HNO}_3$ ; and the solid circles are 0.05 M TODGA contacted with 2.5 M  $\text{HNO}_3$ . Each point is the mean of five measurements, and the error bars represent 99% confidence intervals.

identified as *N,N,N'*-trioctyldiglycolamide (TrODGA) in TODGA solutions and *N,N,N'*-tri(ethylhexyl)diglycolamide (Tr(EH)DGA) in T(EH)DGA solutions, which result from loss of a single side-chain followed by replacement with a hydrogen atom. However, Galán et al.<sup>[23]</sup> did detect the de-alkylation product for irradiated TODGA. Curiously, the analogous radiolysis products, loss of two side-chains, were not detected in this or the previous work. This may be due to its expected low abundance, since it must be formed from already existing TrODGA or Tr(EH)DGA. The product formed from H-capping the *N*-alkyl group ( $\text{C}_8\text{H}_{18}$ ) will not ionize by electrospray since it does not contain protonatable functional groups, and so is not detected.

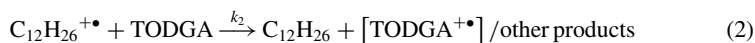
Amines, which would be produced by cleavage of the amide bond, were not detected for either irradiated TODGA or T(EH)DGA samples here. However, both Sugo et al.<sup>[14]</sup> and Galán et al.<sup>[23]</sup> identified dioctylamine (DOA) in irradiated TODGA. Sharma et al.<sup>[15]</sup> identified the corresponding amine di(ethylhexyl)amine (D(EH)A), in the T(EH)DGA system. The product formed from the other side of this cleavage, compound II, DOAOPA in TODGA solutions, and D(EH)AOPA in T(EH)DGA solutions, was detected here, suggesting that there is appreciable cleavage of the amide bond. Additionally, the mass spectrometer tuning parameters, “tune high,” suffers from a substantial drop in transmission efficiency around the expected  $m/z$  of the amines ( $m/z$  242). Therefore, it is likely DOA and D(EH)A are formed but not detected efficiently by the mass spectrometer due to the tuning parameters used in this study.

For the systems studied, the highest signals were for compounds I through IV, with compounds V and VI having much lower signals (Fig. 3 is representative). This is in general agreement with Galán et al.,<sup>[23]</sup> who found abundant production of the compounds labelled here as I, III, and IV in TODGA samples. Because there were no standards for these radiolysis products, the magnitudes of their signal intensities cannot be directly related to concentrations. However, the signals for compounds V and VI are substantially lower than for the other detected compounds. Positive-mode electrospray is expected to produce ions from these compounds through proton attachment to the carbonyl oxygen. Examining these structures, the proton affinity for compounds V and VI would not be expected to be substantially lower than the others, nor should their mass-transmission efficiencies be substantially different than that of compounds III and IV. Therefore, based on the lower signals for compounds V and VI in all systems studied, it is likely that these are minor radiolysis products, and the cleavage of the C—C<sub>carbonyl</sub> bond is less likely to occur than cleavage of the other bonds in the diglycolamide portion of these molecules. This agrees with Sugo et al.<sup>[14]</sup> who reported the reactivity of cleavage of the C—C<sub>carbonyl</sub> bond in TODGA was lower than the cleavage of the C—O<sub>ether</sub> bond and the amide-bond (N—C<sub>carbonyl</sub> bond).

Galán et al.<sup>[23]</sup> reported the same radiolysis products for dry and acid-contacted TODGA solutions, although their abundances varied. In that work, acidity apparently favored rupture of the ether bond, to generate compound III; that effect was not detected here. In this work, rupture of the amide C<sub>carbonyl</sub>—N bond may have been favored by acidity, especially at higher absorbed doses, but the scatter in the data (Fig. 6b) precludes a definitive statement in this regard. However, it is noted that the presence of nitric acid was shown to favor amine bond rupture for TODGA by Sugo et al.<sup>[14]</sup> for the malonamide dimethyl dioctyl hexylethoxymalonamide (DMDOHEMA) by Berthon et al.<sup>[26]</sup> and for octylphenyl-*N,N*-diisobutylcarbamoyl phosphine oxide by Mincher et al.<sup>[27]</sup>

### Radical Cation Kinetics

The  $\gamma$ -radiolysis of an organic diluent such as *n*-dodecane results in a mixture of radical ( $H^\bullet$ ,  $C_xH_y^\bullet$ ) and ionic ( $e^-_{solv}$ ,  $R^{+\bullet}$ ) species formed by bond breakage and ionization. Under aerated conditions, the most important species that will react with added extractants such as DGAs is expected to be the solvent radical cation,  $R^{+\bullet}$ . The *n*-dodecane radical cation has been previously identified<sup>[16]</sup> using UV- visible absorption spectroscopy, and its reaction with TODGA qualitatively established. However, no kinetics for this reaction



have been reported.

Therefore, in this study, the importance of this degradation pathway was elucidated by measurement of the absolute second-order rate constant,  $k_2$  utilizing electron pulse radiolysis which generates the same radical and ionic species as gamma radiolysis.<sup>[24]</sup> Figure 7a shows the measured kinetic data for TODGA concentrations in the range 0–50 mM. Based on the previously reported *n*-dodecane radical cation absorbance enhancement<sup>[16]</sup> when  $CH_2Cl_2$  was used as a solvent, our irradiations were performed in solutions consisting of 0.10 M  $CH_2Cl_2$  in aerated *n*-dodecane. These kinetic measurements were performed at 650 nm, which gave the best signal-to-noise ratio for this system. Within experimental error, the same kinetic data were obtained at the peak absorbance of 800 nm (Fig. 7b, Inset).

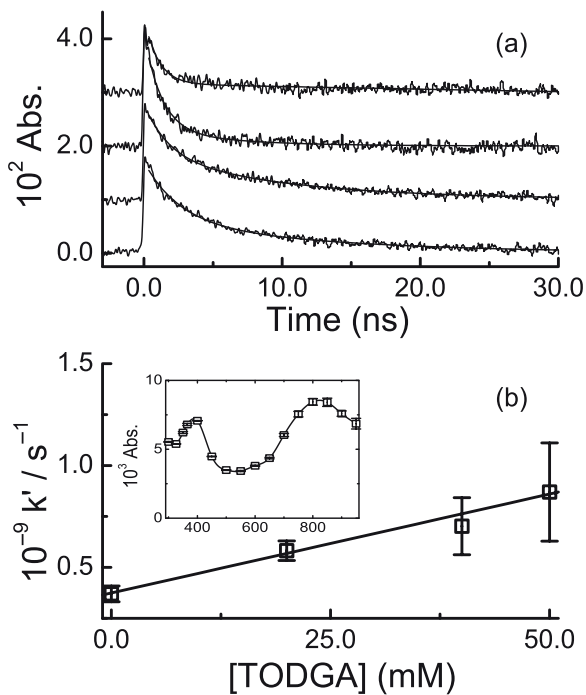


**Figure 7** a) Kinetic traces obtained for ps electron-pulse radiolysis of *n*-dodecane/0.10 M  $\text{CH}_2\text{Cl}_2$  aerated solutions containing zero (bottom), 20 mM (second bottom), 40 mM (second top), and 50 mM (top) TODGA at 650 nm. Data offset for clarity. Solid lines are double-exponential decays, with initial decay rate constants of  $(4.0 \pm 0.1) \times 10^8 \text{ s}^{-1}$ ,  $(5.8 \pm 0.2) \times 10^8 \text{ s}^{-1}$ ,  $(8.0 \pm 0.3) \times 10^8 \text{ s}^{-1}$ , and  $(1.04 \pm 0.05) \times 10^9 \text{ s}^{-1}$ , respectively. b) Inset: Zero-time extrapolated, transient absorption spectra obtained for pulse irradiated aerated 0.10 M TODGA/0.10 M  $\text{CH}_2\text{Cl}_2$ /dodecane. The x-axis is wavelength in nm. Main: Second-order rate constant determination from kinetic data of part a). Individual data points and corresponding error bars are the average of 2–3 individual measurements for each TODGA concentration. Solid line is weighted linear fit, corresponding to a slope of  $k_2 = (9.7 \pm 1.1) \times 10^9 \text{ M}^{-1} \text{ s}^{-1}$ , and an intercept of  $(3.7 \pm 0.4) \times 10^8 \text{ s}^{-1}$  ( $R^2 = 0.974$ ).

The kinetic data were fitted to a double-exponential decay function, with the faster rate constant assumed to correspond to the radical cation reaction, and the second exponential used to correct for any baseline drift. The concentration dependence of the fitted pseudo-first-order rate constants ( $k'$ ) is shown in Fig. 7b, and from the slope of this plot, a value of  $k_2 = (9.72 \pm 1.10) \times 10^9 \text{ M}^{-1} \text{ s}^{-1}$  is obtained. To our knowledge, this is the first absolute rate-constant measurement of the *n*-dodecane radical cation reported. This rate constant is of the order of the normal diffusion rate constant in this alkane<sup>[28]</sup> and considerably slower than that reported for *n*-dodecane excited radical cation ( $\text{R}^{+*}$ , formed by geminate recombination of radical cations with solvated electrons) with triethylamine of  $3.3 \times 10^{11} \text{ M}^{-1} \text{ s}^{-1}$ .<sup>[28]</sup> However, this fast reaction suggests that the radical cation reaction will be a major degradation pathway for species such as these DGAs that have relatively low ionization potentials. This is consistent with previous measurements performed in this diluent, where no radical cation scavenging was observed for decalin ( $\text{C}_{10}\text{H}_{18}$ ).<sup>[29]</sup> Degradation was also observed for  $\gamma$ -irradiated CMPO (which contains a phosphoryl moiety) in *n*-dodecane;

however, in this case the degradation was mitigated by the presence of nitric acid, suggesting a slower rate constant for the reaction of the *n*-dodecane radical with CMPO than was measured here for TODGA.<sup>[27]</sup>

## CONCLUSIONS

The results of this study suggest that there is no difference in the  $\gamma$ -radiolysis of TODGA and T(EH)DGA in *n*-dodecane, nor is there a difference in chemistry that depends on the acidity of an aqueous phase in contact with the DGAs in *n*-dodecane. In both molecules, the major sites for radiolytic attack are the bonds within the diglycolamide functional group, specifically the C–O<sub>ether</sub>, N–C<sub>carbonyl</sub>, and the N–C<sub>side-chain</sub> bonds, and to a lesser extent the C–C<sub>carbonyl</sub> bond, while the bonds in the N–alkyl side-chains do not participate. This suggests that modification of the alkane side-chains to produce an extractant with desired solubility and complexation behavior resulting from steric considerations will not have an effect on the  $\gamma$ -radiation stability of the new extractant compared to TODGA and T(EH)DGA. Furthermore, this suggests that efforts to reduce the radiolytic decay of diglycolamide extractants should focus on protecting the bonds in the diglycolamide functional group, specifically the C–O<sub>ether</sub> and N–C<sub>carbonyl</sub>. The new class of methylated TODGA derivatives may offer such stability, and their radiation chemistry will be investigated in future work. Direct measurement of the *n*-dodecane radical cation charge-transfer kinetics shows that this reaction is very fast,  $k_2 = (9.7 \pm 1.1) \times 10^9 \text{ M}^{-1} \text{ s}^{-1}$  for TODGA, indicating that this could be a major degradation pathway. Finally, comparison of the radiolysis products of TODGA and T(EH)DGA detected here using UHPLC-ESI-MS with those previously detected with GC-MS suggests that UHPLC-ESI-MS is a powerful new technique for analyzing these extraction systems.

## FUNDING

The gamma-ray irradiation and UHPLC-ESI-MS experiments performed at Idaho National Laboratory were supported by the US Department of Energy (US-DOE), Assistant Secretary for Nuclear Energy, under the Fuel Cycle R&D Program, Idaho Operations Office Contract DE-AC07-05ID14517. Additional financial support for this research was provided by the European Commission (projects SACSESS – Contract No. FP7-Fission-2012-323-282). The radiolysis experiments performed at Brookhaven National Laboratory (BNL) and use of the LEAF Facility of the BNL Accelerator Center for Energy Research were supported by the US-DOE Office of Science, Division of Chemical Sciences, Geosciences and Biosciences under contract DE-AC02-98CH10886.

## SUPPLEMENTAL MATERIAL

Supplemental material for this article can be found on the [publisher's website](#).

## REFERENCES

1. Ansari, S. A.; Pathak, P.; Mohapatra, P. K.; Manchanda, V. K. Chemistry of diglycolamides: Promising extractants for actinide partitioning. *Chem. Rev.* **2011**, *112*, 1751–1772.

2. Sasaki, Y.; Sugo, Y.; Suzuki, S.; Tachimori, S. The novel extractants, diglycolamides, for the extraction of lanthanides and actinides in  $\text{HNO}_3$ -*n*-dodecane system. *Solvent Extr. Ion Exch.* **2001**, *19*, 91–103.
3. Modolo, G.; Asp, H.; Schreinemachers, C.; Vijgen, H. Development of a TODGA based process for partitioning of actinides from a PUREX raffinate part 1: Batch extraction optimization studies and stability tests. *Solvent Extr. Ion Exch.* **2007**, *25*, 703–721.
4. Deepika, P.; Sabharwal, K. N.; Srinivasan, T. G.; Vasudeva Rao, P. R. Studies on the use of N,N,N',N'-tetra(2-ethylhexyl)diglycolamide (TEHDGA) for actinide partitioning II: Investigation on radiolytic stability. *Solvent Extr. Ion Exch.* **2011**, *29*, 230–246.
5. Lumetta, G. L.; Gelis, A. V.; Carter, J. C.; Niver, C. M.; Smoot, M. R. The actinide-lanthanide separation concept. *Solvent Extr. Ion Exch.* **2014**, *32*, 333–347.
6. Gelis, A. V.; Lumetta, G. J. Actinide Lanthanide Separation Process – ALSEP. *Ind. Eng. Chem.* **2014**, *53*, 1624–1631.
7. Bourg, S.; Hill, C.; Caravaca, C.; Rhodes, C.; Ekberg, C.; Taylor, R.; Geist, A.; Modolo, G.; Casayre, L.; Malmbeck, R.; Harrison, M.; De Angelis, G.; Espartero, A.; Bouvet, S.; Ouvrier, N. ACSEPT-Partitioning technologies and actinide science: Towards pilot plant facilities in Europe. *Nucl. Eng. Des.* **2011**, *241*, 3427–3435.
8. Wilden, A.; Modolo, G.; Lange, S.; Sadowski, F.; Beele, B. B.; Skerencak-Frech, A.; Panak, P. J.; Iqbal, M.; Verboom, W.; Geist, A.; Bosbach, D. Modified diglycolamides for the An(III) + Ln(III) co-separation: evaluation by solvent extraction and time-resolved laser fluorescence spectroscopy. *Solvent Extr. Ion Exch.* **2014**, *32*, 119–137.
9. Iqbal, M.; Huskens, J.; Verboom, W.; Sypula, M.; Modolo, G. Synthesis and Am/Eu extraction of novel TODGA derivatives. *Supramol. Chem.* **2010**, *11–12*, 827–837.
10. Mincher, M. E.; Quach, D. L.; Liao, Y. J.; Mincher, B. J.; Wai, C. M. The partitioning of americium and the lanthanides using tetrabutyl diglycolamide (TBDGA) in octanol and ionic liquid solution. *Solvent Extr. Ion Exch.* **2012**, *30*, 735–747.
11. Sasaki, Y.; Sugo, Y.; Kitatsujii, Y.; Kirishima, A.; Kimura, T.; Choppin, G. R. Complexation and back extraction of various metals by water-soluble diglycolamide. *Anal. Sci.* **2007**, *23*, 727–731.
12. Miguirditchian, M.; Chareyre, L.; Hérès, X.; Hill, C.; Baron, P.; Masson, M. In *GANEX: Adaptation of the DIAMEX-SANEX process for the group actinide separation*, Proc. Internat. Conf. Global (Advanced Nuclear Fuel Cycles and Systems), Boise, ID, USA, 2007.
13. Rostaing, C.; Poinssot, C.; Warin, D.; Baron, P.; Lorrain, B. Development and validation of the EXAm separations process for single Am recycling. *Procedia Chem.* **2012**, *7*, 367–373.
14. Sugo, Y.; Sasaki, Y.; Tachimori, S. Studies on hydrolysis and radiolysis of N,N,N',N'-tetraoctyl-3-oxapentane-1,5-diamide. *Radiochim. Acta.* **2002**, *90*, 161–165.
15. Sharma, J. N.; Ruhela, R.; Singh, K. K.; Kumar, M.; Janardhanan, C.; Achutan, P. V.; Monaoahar, S.; Wattal, P. K.; Suri, A. K. Studies on hydrolysis and radiolysis of tetra(2-ethylhexyl)diglycolamide (TEHDGA)/isodecyl alcohol/*n*-dodecane solvent system. *Radiochim. Acta.* **2010**, *98*, 485–491.
16. Sugo, Y.; Izumi, Y.; Yoshida, Y.; Nishijima, S.; Sasaki, Y.; Kimura, T.; Sekine, T.; Kudo, H. Influence of diluent on radiolysis of amides in organic solution. *Radiat. Phys. Chem.* **2007**, *76*, 794–800.
17. Gujar, R. B.; Ansari, S. A.; Murali, M. S.; Mohapatra, P. K.; Manchanda, V. K. Comparative evaluation of two substituted diglycolamide extractants for “actinide partitioning.” *J. Radioanal. Nucl. Chem.* **2010**, *284*, 377–385.
18. Ravi, J.; Selvan, B. R.; Venkatesan, K. A.; Antony, M. P.; Srinivasan, T. G.; Vasudeva Rao, P. R. Evaluation of radiation stability of N,N-didodecyl N',N'-di-octyl diglycolamide: a promising reagent for actinide partitioning. *J. Radioanal. Nucl. Chem.* **2014**, *299*, 879–885.
19. Ravi, J.; Venkatesan, K. A.; Antony, M. P.; Srinivasan, T. G.; Vasudeva Rao, P. R. Feasibility of using di-dodecyl-di-octyl diglycolamide for partitioning of minor actinides from fast reactor high-level waste. *Solvent Extr. Ion Exch.* **2014**, *32*, 424–436.

20. Mincher, B. J.; Modolo, G.; Mezyk, S. P. Review article: The effects of radiation chemistry on solvent extraction 3: A review of actinide and lanthanide extraction. *Solvent Extr. Ion Exch.* **2009**, *27*, 579–606.
21. Wishart, J. F.; Cook, A. R.; Miller, J. R. The LEAF Picosecond Pulse Radiolysis Facility at Brookhaven National Laboratory. *Rev. Sci. Instrum.* **2004**, *75*, 4359–4366.
22. Mincher, B. J.; Curry, R. D. Considerations for choice of a kinetic fig. of merit in process radiation chemistry for waste treatment. *Appl. Radiat. Isotopes* **2000**, *52*, 189–193.
23. Galán, H.; Núñez, A.; Espartero, A.; Sedano, R.; Durana, A.; de Mendoza, J. Radiolytic stability of TODGA: Characterization of degraded samples under different experimental conditions. *Procedia Chem.* **2012**, *7*, 195–201.
24. Spinks, J. W. T.; Woods, R. J. *An Introduction to Radiation Chemistry*, 3rd ed.; Wiley-Interscience: NY, 1990.
25. Gujar, R. B.; Ansari, S. A.; Bhattacharyya, A.; Kanekar, A. S.; Pathak, P. N.; Mohapatra, P. K.; Manchanda, V. K. Radiolysis of N,N,N',N'-tetraoctyl diglycolamide (TODGA) in the presence of phase modifiers dissolved in *n*-dodecane. *Solvent Extr. Ion Exch.* **2012**, *30*, 278–290.
26. Berthon, L.; Morel, J. M.; Zorz, N.; Nicol, C.; Virelizier, H.; Madic, C. DIAMEX process for minor actinide partitioning: Hydrolytic and radiolytic degradations of malonamide extractants. *Sep. Sci. Technol.* **2001**, *36*, 709–728.
27. Mincher, B. J.; Mezyk, S. P.; Elias, G.; Groenewold, G. S.; Riddle, C. L.; Olson, L. G. The radiation chemistry of CMPO: Part 1. Gamma radiolysis. *Solvent Extr. Ion Exch.* **2013**, *31*, 715–730.
28. Kondoh, T.; Yang, J.; Norizawa, K.; Kan, K.; Yoshida, Y. Femtosecond pulse radiolysis study on geminate ion recombination in *n*-dodecane. *Radiat. Phys. Chem.* **2011**, *80*(2), 286–290.
29. Izumi, Y.; Kojima, T.; Okawa, H.; Yamamoto, T.; Yoshida, Y.; Mizutani, Y.; Kozawa, T. M.; Miyako; Tagawa, S. *Pulse Radiolysis Studies on the Radiation Resistance of Liquid N-Alkane in the Presence of Additives*; Technology Reports of the Osaka University Osaka University: **1998**; pp 317–324.





## Paper 8<sup>[153]</sup>

Roscioli-Johnson, K.M.; Zarzana, C.A.; Groenewold, G.S.; Mincher, B.J.; Wilden, A.; Schmidt, H.; Modolo, G.; Santiago-Schübel, B. A Study of the  $\gamma$ -Radiolysis of N,N-Didodecyl-N',N'-Dioctyldiglycolamide Using UHPLC-ESI-MS Analysis. *Solvent Extr. Ion Exch.* **2016**, *34* (5), 439-453.






DOI: 10.1080/07366299.2016.1212540

### Contribution:

For this work, solvent extraction experiments, analysis (gamma-spectrometry, results of ICP-MS) as well as product identification of mass spectrometric experiments were conducted mainly by A. Wilden and me. Additionally, I participated in paper preparation.



## A Study of the $\gamma$ -Radiolysis of *N,N*-Didodecyl-*N'*, *N'*-Dioctyldiglycolamide Using UHPLC-ESI-MS Analysis

Kristyn M. Roscioli-Johnson<sup>a</sup>, Christopher A. Zarzana <sup>a</sup>, Gary S. Groenewold<sup>a</sup>, Bruce J. Mincher <sup>a</sup>,  
Andreas Wilden <sup>b</sup>, Holger Schmidt <sup>b</sup>, Giuseppe Modolo <sup>b</sup>, and Beatrix Santiago-Schübel<sup>c</sup>

<sup>a</sup>Idaho National Laboratory, Idaho Falls, ID, USA; <sup>b</sup>Forschungszentrum Jülich GmbH, Institut für Energie- und Klimaforschung- Nukleare Entsorgung und Reaktorsicherheit (IEK-6), Jülich, Germany; <sup>c</sup>Forschungszentrum Jülich GmbH, Zentralinstitut für Engineering, Elektronik und Analytik (ZEA-3), Jülich, Germany

### ABSTRACT

Solutions of *N,N*-didodecyl-*N'*,*N'*-dioctyldiglycolamide in *n*-dodecane were subjected to  $\gamma$ -irradiation in the presence and absence of both an aqueous nitric acid phase and air sparging. The solutions were analyzed using ultra-high-performance liquid chromatography-electrospray ionization-mass spectrometry (UHPLC-ESI-MS) to determine the rates of radiolytic decay of the extractant as well as to identify radiolysis products. The DGA concentration decreased exponentially with increasing dose, and the measured degradation rate constants were uninfluenced by the presence or absence of acidic aqueous phase, or by air sparging. The identified radiolysis products suggest that the bonds most vulnerable to radiolytic attack are those in the diglycolamide center of these molecules and not in the side chains.

### KEYWORDS


Diglycolamide; UHPLC-MS; radiolysis; D3DODGA; radiation chemistry

### Introduction

The safe processing and disposal of used nuclear fuel is a major step required for the widespread use of nuclear power. However, the radiotoxicity of untreated used fuel requires several hundred thousand years to decay to the level of natural uranium ore, presenting a significant challenge for secure, long-term disposal. Long-lived radioisotopes of plutonium, and the minor actinides neptunium, americium and curium make up the bulk of nuclides responsible for the thermal heat load and radiotoxicity past several hundred years.<sup>[1–4]</sup> Thus, separation of these constituents from the rest of the fission products (partitioning) followed by burning in a fast nuclear reactor (transmutation) can dramatically reduce the storage requirements for the remaining high-level waste (HLW). In fact, by reducing waste heat production, a more efficient utilization of the repository is likely. These are important issues to ensure the future sustainability of nuclear power.

One class of molecules that has received much attention in the last decade as candidate extractants for lanthanides and actinides is the diglycolamides (DGAs).<sup>[5]</sup> These molecules are of interest because they exhibit higher Am(III) affinity than extractants such as octyl-(phenyl)-*N,N*-diisobutyl carbamoyl methyl phosphine oxide (CMPO) from solutions with nitric acid concentrations in the range found in HLW.<sup>[6]</sup> Additionally, because DGAs contain only carbon, hydrogen, oxygen, and nitrogen (CHON), they can be easily incinerated, reducing the volume of secondary waste generated from reprocessing used nuclear fuel. Sasaki et al.<sup>[7]</sup> synthesized a series of diglycolamides, varying their *N*-alkyl substituents (alkyl =  $C_nH_{2n+1}$  with  $n = 3, 4, 5, 6, 8$ , and 10) and found that as  $n$  increased, solubility in water decreased, solubility in aliphatic hydrocarbon diluents such as *n*-dodecane increased, and the americium distribution ratio (extraction from 1 M  $HNO_3$  by 0.1 M

**CONTACT** Christopher A. Zarzana  christopher.zarzana@inl.gov  Idaho National Laboratory, 775 University Boulevard, Idaho Falls, ID 83415-3531, USA.

 Supplemental data for this article can be accessed at <http://dx.doi.org/10.1080/07366299.2016.1212540>.

© 2016 Taylor & Francis

DGA) decreased. Mowafy and Aly<sup>[8]</sup> synthesized a series of DGAs with straight and branched *N*-alkyl substituents and obtained similar results. These studies indicate that the *N*-alkyl substituents play a significant role in the hydrophilicity, lipophilicity, and extraction behavior of DGAs.

Of the DGAs, *N,N,N',N'*-tetraoctyldiglycolamide (TODGA) has received the most attention for actinide partitioning within the back end of the nuclear fuel cycle, as it is freely soluble in *n*-dodecane with high americium distribution ratios from strong nitric acid. The branched DGA *N,N,N',N'*-tetra(2-ethylhexyl)diglycolamide (T(EH)DGA) has also been investigated as an alternative to TODGA, with lower affinity toward trivalent actinides and for some undesirable fission products. Because of the high concentrations of metal ions and HNO<sub>3</sub> acidity in HLW, candidate separation processes must be robust against third-phase formation. Third-phase formation occurs when the organic phase splits into two distinct phases (a metal-rich phase and a diluent-rich phase), an undesirable condition for industrial-scale solvent extraction. The limiting organic concentration (LOC) is the maximum concentration of metal ions that can be loaded into the organic phase without third-phase formation. Unfortunately, TODGA and T(EH)DGA form third phases in paraffinic diluents at low (millimolar) metal concentrations and thus will suffer from third-phase formation when used with HLW. Studies of third-phase formation of DGA/*n*-dodecane organic phases have found that the LOC for Nd increased with temperature, DGA concentration, and *N*-alkyl chain length.<sup>[9–11]</sup> However, an increase in TODGA concentration also increased the extraction of HNO<sub>3</sub> which would impede back extraction. Addition of *N,N*-dihexyloctanamide (DHOA) as a phase modifier increased the LOC. Thus, all processes using DGAs that have been tested with simulated or actual HLW have used phase modifiers. For example, a process developed at Forschungszentrum Jülich used 0.2 M TODGA modified with 0.5 M tri-*n*-butyl phosphate (TBP) in the industrial alkane diluent hydrogenated tetrapropene (TPH) to extract Eu<sup>III</sup>, Am<sup>III</sup>, Cm<sup>III</sup>, Cf<sup>II</sup>, and Th<sup>IV</sup> from simulated high-level raffinates with nitric acid concentrations from 1 to 3 M.<sup>[12–14]</sup> The TBP acted as an extractant and a phase modifier, mitigating third-phase formation. However, oxalic acid and *N*-(2-hydroxyethyl)-ethylenediamine-triacetic acid (HEDTA) were required to mitigate the co-extraction of zirconium, molybdenum, and palladium.

While phase modifiers can successfully suppress third-phase formation, their use can increase the overall cost and complexity of a separation process; therefore, it is desirable to develop alternative extractants that are resilient to third-phase formation without the use of phase modifiers. For symmetric DGAs (all four *N*-alkyl groups are the same), extraction strength decreases and resistance to third-phase formation increases as the alkyl chain length increases. Ravi et al.<sup>[15]</sup> suggested that a DGA with side groups with two different lengths would result in a DGA that had a combination of the properties of the two associated symmetric DGAs. Using this idea, researchers at the Indira Gandhi Center for Atomic Research, Kalpakkam, developed the new unsymmetrical 2-(2-(didodecylamino)-2-oxoethoxy)-*N,N*-dioctylacetamide (trivially *N,N*-didodecyl-*N',N'*-dioctyldiglycolamide, D<sup>3</sup>DODGA, Fig. 1) as a potential modifier-free actinide extractant.<sup>[16–19]</sup> They found that D<sup>3</sup>DODGA had high distribution ratios for trivalent lanthanides and actinides ( $D_M > 300$  for 3–8 M HNO<sub>3</sub>), low distribution ratios for strontium, and no third-phase formation was observed in 3–4 M HNO<sub>3</sub> solutions. Systematic variation of the non-*n*-didodecyl side chains suggested the presence of the didodecyl side chains was sufficient to prevent third-phase formation.<sup>[20]</sup> Extraction experiments using simulated fast-reactor high-level liquid waste showed 0.1 M D<sup>3</sup>DODGA in *n*-dodecane had similar performance to TODGA-based systems without requiring a phase modifier.<sup>[17]</sup> Addition of trans-1,2-diaminocyclohexane-*N,N,N',N'*-tetraacetic acid (CDTA) helped prevent the co-extraction of zirconium and palladium.<sup>[21]</sup>

Solvent extraction systems for partitioning of used nuclear fuel will be exposed to high radiation fields and highly acidic conditions; therefore, the radiolytic and hydrolytic stability of extractant molecules is of interest for the development of robust separation processes. Prior research indicates that the long-chain DGAs are hydrolytically stable but vulnerable to radiolytic degradation.<sup>[12,22–31]</sup> Investigation of DGA radiolysis in *n*-dodecane suggests that the most vulnerable bonds are those within the diglycolamide functional group, specifically the C–O<sub>ether</sub>, N–C<sub>carbonyl</sub>, and the N–C<sub>side-chain</sub>

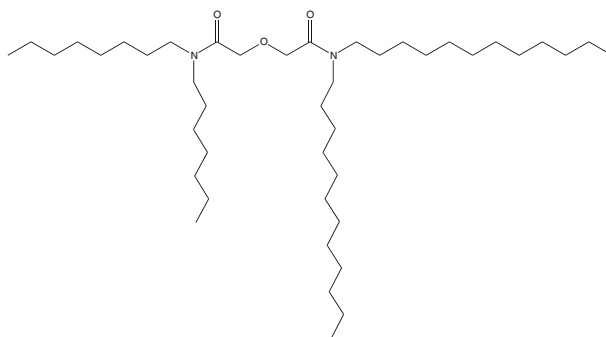


**Figure 1.** Structure of the diglycolamide studied here: *N,N*-didodecyl-*N',N'*-dioctyldiglycolamide ( $D^3DODGA$ ).

bonds, and to a lesser extent the C–C<sub>carbonyl</sub> bond.<sup>[22,24–26]</sup> Neither Zarzana et al.<sup>[25]</sup> nor Sugo et al.<sup>[22]</sup> observed any influence from nitric acid contact on the radiolysis of TODGA and T(EH)DGA; however, Galán et al.<sup>[24]</sup> did report a protective effect due to nitric acid contact for TODGA. Additionally, compounds with one (MeTODGA) or two (Me<sub>2</sub>TODGA) methyl groups added to the DGA backbone appeared to be more sensitive to radiolysis when contacted with nitric acid.<sup>[26]</sup>

At present, the only study of the radiolysis of  $D^3DODGA$  used changes in metal distribution ratios as a measure of DGA degradation.<sup>[30]</sup> However, prior studies of DGA degradation products indicated that radiolytically produced species can have significantly different extraction properties than the parent DGA;<sup>[24,28]</sup> thus, distribution ratios are an inappropriate measure of DGA degradation. In this article, we present an investigation of the  $\gamma$ -radiolytic stability of  $D^3DODGA$  in *n*-dodecane using ultra-high-performance liquid chromatography–electrospray ionization–mass spectrometry (UHPLC-ESI-MS) and high-performance liquid chromatography/mass spectrometry (HPLC-HRMS) to directly monitor the decrease in DGA concentration with absorbed dose and the generation of products. The irradiations were performed on the organic phase in the presence and absence of an aqueous nitric acid phase and with or without air sparging. While previous studies have examined the effect of an acidic aqueous phase on DGA radiolysis,<sup>[25,26]</sup> as a scavenger of many radiolytically produced reactive species, dissolved oxygen is also important in radiation chemistry. However,  $\gamma$ -radiolysis studies are usually conducted in sealed vessels in which dissolved oxygen is depleted in the first few Gy of absorbed dose, while the processes under which solvent extraction ligands are used are likely to be in contact with air.<sup>[27]</sup> Therefore, some  $D^3DODGA$  samples were also irradiated with continuous air sparging to ensure that dissolved oxygen was not depleted during the experiment.

## Experimental

$D^3DODGA$  was purchased from TechnoComm Ltd. (Wellbrae, Scotland). All chemicals were of analytical grade and were used without further purification. Aqueous dilutions were done using ultrapure water (18.2 M $\Omega$ cm).

### Gamma-Ray Irradiation

$D^3DODGA$  was irradiated as nominally 0.05 M solutions in dodecane. Aliquots of these solutions were irradiated as the pure organic phase or in contact with 2.5 M HNO<sub>3</sub>. Samples with and without the presence of the aqueous phase were irradiated both with and without air sparging to ensure the presence of dissolved oxygen in the sparged samples. Sparging was conducted at an air flow rate of 1 mL/min, using a needle inserted through the septum of the sample container, with a second needle

inserted to release the air flow to atmosphere. Flow was controlled by a mass-flow controller with the flow rate selected to ensure no evaporation losses in the sample volume but sufficient to provide a reasonable expectation of air saturation in the 5 mL samples. Irradiations were conducted using a Nordion GammaCell 220E (Ottawa, Canada)  $^{60}\text{Co}$  source, with a center-line sample chamber dose rate of 4.5 kGy/h, as determined by decay-corrected Fricke dosimetry. Irradiation of the samples did not result in an elevated temperature.

### UHPLC-ESI-TOF-MS

Irradiated  $\text{D}^3\text{DODGA}$  samples in *n*-dodecane were diluted in Optima® LC/MS 2-propanol (Fisher Scientific, Pittsburgh, PA, USA) prior to analysis in order to generate a concentration in the low micromolar ( $\mu\text{M}$ ) range (i.e., in the middle of the response vs. concentration curve). At this point, 2.5  $\mu\text{L}$  of a 100  $\mu\text{M}$  solution of TODGA was added; TODGA served as an internal standard. Calibration standards were constructed from the analyses of solutions of reagent-grade  $\text{D}^3\text{DODGA}$  solutions; the primary standard was generated gravimetrically and secondary standards by serial dilution. Prior to analysis, each serial standard was spiked with the TODGA internal standard, as described above. For each calibration standard, the ratios of the intensities of the  $\text{D}^3\text{DODGA}$  and TODGA protonated ions ( $I_{\text{D}^3\text{DODGA}}/I_{\text{TODGA}}$ ) were multiplied by the TODGA concentration, and this value was plotted versus the  $\text{D}^3\text{DODGA}$  concentration; the slope of the line of this plot was then used to calculate the  $\text{D}^3\text{DODGA}$  concentration in the experiments. All of the diluted samples and calibration solutions were analyzed using a Dionex (Sunnyvale, CA, USA) ultra-high-performance liquid chromatograph (UHPLC) with an Ultimate 3000 RS pump, 3000 RS autosampler, 3000 RS column compartment and a 3000 RS diode array detector, coupled to a Bruker (Billerica, MA, USA) microTOFQ-II electrospray ionization quadrupole time-of-flight mass spectrometer with Hystar 3.2 software.

The chromatographic separation was achieved using 5  $\mu\text{L}$  injections on a Kinetex 1.3  $\mu\text{m}$  particle size, C18 stationary phase, 50 mm  $\times$  2.1 mm column (Phenomenex, Torrance, CA, USA) held at 50°C. The aqueous component was Optima® LC/MS water with 0.1% v/v formic acid (Fisher Scientific, Hampton, NH, USA), and the organic component was 3% v/v 1-octanol in Optima® LC/MS 2-propanol. A gradient mobile-phase profile was used with a flow rate of 200  $\mu\text{L}/\text{min}$ . The profile started at 50% organic for 5 min, followed by a 10 min ramp from 50% organic to 75% organic, followed by a hold at 75% organic for 10 min, and ending with a 1 min ramp back to 50% organic. The column was pre-equilibrated for 3 min at 50% organic before each injection. The mass-spectrometer conditions were capillary, 4.5 kV, positive mode; temperature, 220°C; nebulizer gas and dry gas, both  $\text{N}_2$ ; nebulizer pressure, 0.4 bar; dry gas flow rate, 9 L/min. The mass spectrometer was operated using standard Bruker tuning parameters, specifically “tune low” (Table S1, Supplementary Information). Each sample was injected five times.

### HPLC-APCI-FT-MS

HPLC-APCI-FT-MS measurements were performed at Forschungszentrum Jülich using a hybrid linear ion trap FTICR mass spectrometer LTQFT Ultra™ (Thermo Fisher Scientific, Bremen, Germany) coupled with an Agilent 1200 system (Agilent, Waldbronn, Germany). A ZORBAX Eclipse Plus C18, 4.6  $\times$  100 mm, 3.4  $\mu\text{m}$  (Agilent) column was used with the following gradient: the gradient started with 60% *B* for 2 min, followed by a 8 min ramp from 60% *B* to 98% *B*, followed by a hold of 98% *B* for 10 min, and a re-equilibration of 10 min with 60% *B* (*A*: 0.1% v/v formic acid in  $\text{H}_2\text{O}$ , *B*: 0.1% v/v formic acid in ACN).

The mass spectrometer was used in the positive APCI mode. The MS conditions were capillary temperature, 275°C; APCI vaporizer temperature, 400°C; sheath gas flow, 50; auxiliary gas flow, 5. The source voltage was 6 kV, the capillary voltage 34 V, and the tube lens 80 V. Mass spectra were recorded in full scan from 100 to 1000 mass units with a resolution of 100,000 at  $m/z$  400. All data were processed using the Xcalibur software, version 2.0.

## Results and Discussion

### Degradation of D<sup>3</sup>DODGA as a Function of Absorbed Dose

The change in D<sup>3</sup>DODGA concentration versus absorbed  $\gamma$ -dose for samples irradiated as the organic phase or in contact with 2.5 M HNO<sub>3</sub> both with and without sparging is shown in Fig. 2. The concentration change versus absorbed dose data may be well fitted with an exponential curve, suggesting pseudo-first-order kinetics, probably a reaction with a direct radiolysis product of the diluent.<sup>[23]</sup> Dose constants ( $d$ ) for each system are shown in Table 1, with the mean value for all conditions of  $(3.9 \pm 0.3) \times 10^{-3} \text{ kGy}^{-1}$ . This is comparable to the dose constants reported by Zarzana et al. for TODGA and TEHDGA of  $(4.1 \pm 0.3) \times 10^{-3} \text{ kGy}^{-1}$ ,<sup>[25]</sup> and slightly lower than the dose constants reported by Galán et al. for methylated TODGA derivatives of  $\sim 5 \times 10^{-3} \text{ kGy}^{-1}$ .<sup>[26]</sup> As stated in previous work,<sup>[25]</sup> the  $G$ -value is not an appropriate metric because the decomposition of D<sup>3</sup>DODGA occurs exponentially.

Neither contact with the acidic aqueous phase nor the presence of sparged air had a significant effect on the radiolytic degradation rate of D<sup>3</sup>DODGA. This is in agreement with the work of Zarzana et al.<sup>[25]</sup> and others,<sup>[23,24]</sup> where it was found for two similar DGA compounds (TODGA and T(EH)DGA) that the free radicals generated during irradiation of both mildly acidic and highly acidic aqueous phases, such as  $\cdot\text{OH}$ ,  $\cdot\text{NO}_3$ , and/or  $\cdot\text{NO}_2$  radicals, were apparently not important for the degradation of the DGA species. Further, the lack of a dissolved-oxygen effect indicates that  $\cdot\text{H}$

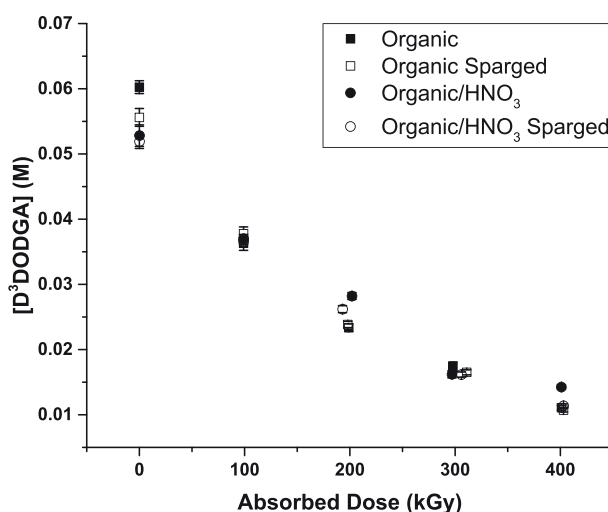


**Figure 2.** D<sup>3</sup>DODGA concentration versus absorbed dose. The unirradiated solutions are nominally 0.05 M D<sup>3</sup>DODGA in *n*-dodecane. Solid squares correspond to D<sup>3</sup>DODGA organic phase; open squares, D<sup>3</sup>DODGA air-sparged organic phase; solid circles, the D<sup>3</sup>DODGA organic phase contacted with 2.5 M HNO<sub>3</sub>; open circles, the D<sup>3</sup>DODGA air-sparged organic phase contacted with 2.5 M HNO<sub>3</sub>. Each point is the mean of five measurements and the error bars represent 99% confidence intervals.

**Table 1.** Measured dose constants for the degradation of D<sup>3</sup>DODGA in the four systems studied.

Sample	Dose constant $d$ (kGy <sup>-1</sup> )
0.05 D <sup>3</sup> DODGA organic	$(4.1 \pm 0.3) \times 10^{-3}$
0.05 D <sup>3</sup> DODGA/2.5 M HNO <sub>3</sub>	$(3.4 \pm 0.4) \times 10^{-3}$
Air-sparged 0.05 D <sup>3</sup> DODGA organic	$(4.1 \pm 0.3) \times 10^{-3}$
Air-sparged 0.05 D <sup>3</sup> DODGA/2.5 M HNO <sub>3</sub>	$(3.9 \pm 0.2) \times 10^{-3}$
Mean value	$(3.9 \pm 0.3) \times 10^{-3}$

The dose constants were calculated from linear fits of plots of  $\ln[\text{D}^3\text{DODGA}]$  versus absorbed dose. The uncertainty in the dose constants are 99% confidence intervals.



atom and/or solvated electrons are not important reactive species in this system, because these would be quenched in the presence of oxygen, resulting in different radiolysis rates and pathways. Given the low starting concentration of the DGA (0.05 M), direct radiolytic decomposition is also not likely significant; therefore, based on the process of elimination, the most likely mechanism for radiological degradation would be by reaction with a direct radiolysis product of the diluent, *n*-dodecane. This was previously postulated by Sugo et al.<sup>[23]</sup> and Zarzana et al.<sup>[25]</sup> and called the sensitization effect.

### Identification of D<sup>3</sup>DODGA Radiolysis Products

A number of radiolysis products of D<sup>3</sup>DODGA were identified by UHPLC with positive-mode ESI-MS detection. A superposition of representative ion chromatograms for the compounds detected in 0.05 M D<sup>3</sup>DODGA/*n*-dodecane after absorbing 401 kGy is shown in Fig. 3. Radiolysis products were identified by examining variation in compound signal as a function of dose and by explicitly searching for ion signals that would correspond to structures that could be formed from the parent DGA through bond cleavage, followed by capping with various radicals (<sup>•</sup>H, <sup>•</sup>CH<sub>3</sub>, <sup>•</sup>OH, etc.). Identification of radiolysis products was also guided by compounds identified in radiolysis studies of other DGA molecules.<sup>[25,26]</sup> Additionally, HRMS after chemical separation of the radiolysis products using HPLC in the Jülich laboratories was used to calculate molecular formulas based on measured exact mass. The measured *m/z* ratios and calculated *m/z* ratios of each compound based on the most abundant isotopes agreed well (Supplementary Information, Table S2); deviations of the measured from the calculated *m/z* ratio were smaller than 1 ppm. The compounds detected by both laboratories using ESI and APCI were in good agreement. Proposed structures for the identified compounds, based on logical bond cleavage followed by capping that would result in the protonated and sodiated measured masses, along with the bond cleavages that would result in their formation are shown in Fig. 4. Additional support for these structural assignments comes from collision-induced dissociation (CID) measurements.

Ionization using ESI and APCI generally produces intact protonated species, and while HRMS can yield an unambiguous molecular formula, there is no structural information contained in the mass spectrum. CID measurements can be used to obtain some structural information by fragmenting precursor ions in the gas phase and examining the ions that are produced. Briefly, the precursor

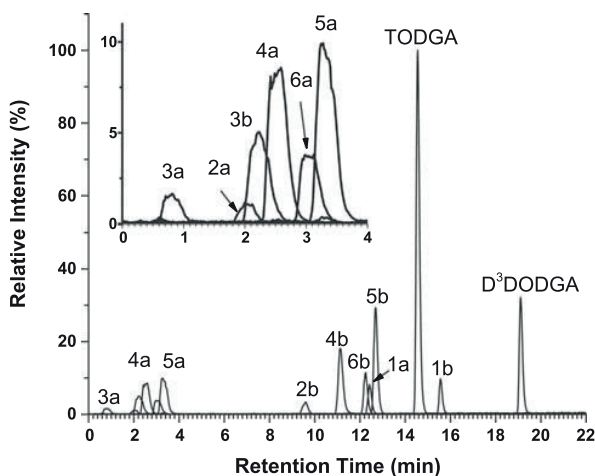


**Figure 3.** Overlaid ion chromatograms of 0.05 M D<sup>3</sup>DODGA and its detected degradation products for irradiation of the D<sup>3</sup>DODGA organic (no sparging or acid contact) to 401 kGy absorbed dose. The inset shows compounds 2a, 3a, 3b, 4a, 5a, and 6a only. The *m/z* values for D<sup>3</sup>DODGA and the degradation products all correspond to the respective protonated molecules: 1a chromatogram *m/z* = 525.5; 1b, 581.6; 2a, 358.3; 2b, 470.4; 3a, 242.3; 3b, 354.4; 4a, 300.3; 4b, 412.4; 5a, 284.3; 5b, 396.4; 6a, 270.3; 6b, 382.4; TODGA, 581.6; D<sup>3</sup>DODGA, 693.7.

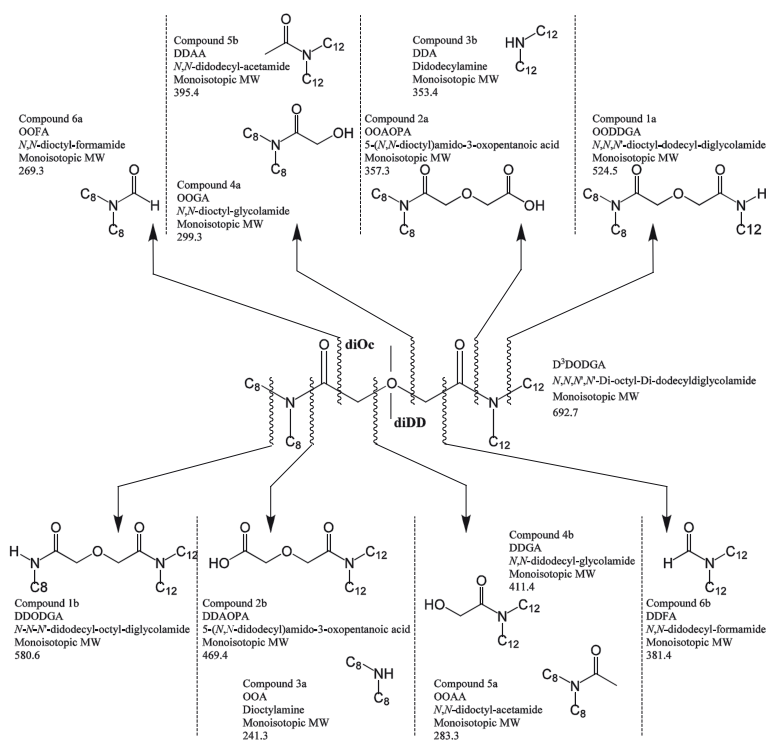


**Figure 4.** Proposed structures for radiolysis products observed for  $D^3DODGA$  with positive-mode ESI-MS, where  $C_8$  is  $C_8H_{17}$  and  $C_{12}$  is  $C_{12}H_{25}$ .

ions are isolated using a mass analyzer after the ionization source (so no other ions are present) and then directed into a collision cell with a low pressure of neutral gas. The isolated precursor ions are activated through low-energy collisions with the neutral gas, adding internal energy to the ions. The added energy is rapidly (on the order of femtoseconds) redistributed throughout all the vibrational modes of the precursor ion, causing the precursor ion to fragment into secondary ions that are then analyzed by mass spectrometry. The mass difference between the precursor and the detected secondary ions corresponds to neutral fragments lost by the precursor ion during fragmentation. These fragment ions and neutral losses can provide clues about the structure of the precursor.

$D^3DODGA$  is expected to undergo radiolytic bond cleavage at every position along the DGA core:  $C_{alkyl}-N$ ,  $N-C_{carbonyl}$ ,  $C_{carbonyl}-CH_2$ , and  $CH_2-O_{ether}$ . Since  $D^3DODGA$  is unsymmetrical (one side, designated  $diOc$ , contains two  $N$ -octyl moieties, while the other, designated  $diDD$ , contains two  $N$ -dodecyl moieties), there are two variants for each of the bond-cleavage reactions. The naming scheme used in Fig. 4 has been designed so that all the labels that include the letter “a” contain the  $N$ -octyl moieties and all the labels that contain the letter “b” contain the  $N$ -didecyl moieties.

Examination of the CID spectrum of the protonated parent DGA reveals fragmentation patterns that can be used to identify the structure of radiolysis products. The CID spectrum of  $D^3DODGA$  (Fig. 5a) is dominated by two pairs of peaks at  $m/z = 452.4$  and  $424.4$ , and  $340.3$  and  $312.3$ . These two groups can be explained as arising from similar fragmentation mechanisms on each side of the unsymmetrical DGA molecule. Scheme 1 illustrates proposed fragmentation mechanisms and ion and neutral fragment structures for fragmentations occurring on the dioctyl side of  $D^3DODGA$  that would result in peaks at  $m/z = 452.4$  and  $424.4$ . Cleavage of the  $N-C_{carbonyl}$  bond on the dioctyl side of  $D^3DODGA$  followed by a hydrogen transfer to the nitrogen (Scheme 1a) results in loss of neutral

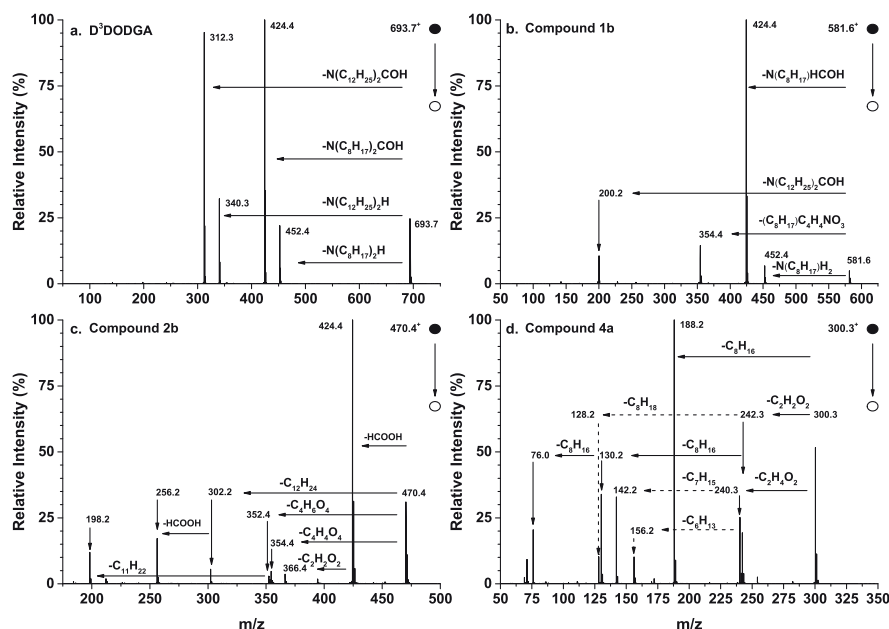
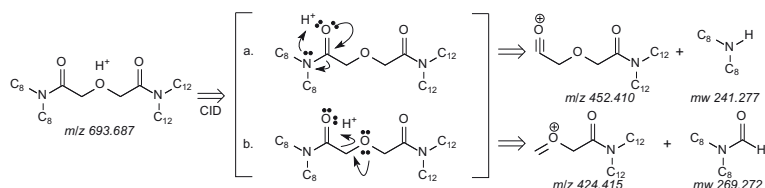


**Figure 5.** Collision-induced dissociation (CID) mass spectra of (a) D<sup>3</sup>DODGA, (b) Compound 1a, (c) Compound 2b, and (d) Compound 4a. Horizontal arrows with neutral loss formulae represent proposed ion-fragmentation pathways.

dioctyl amine and the formation of the ion at  $m/z = 452.4$ . Cleavage of the  $C_{\text{carbonyl}}-\text{CH}_2$  bond followed by a hydrogen transfer (Scheme 1b) would result in elimination of neutral dioctyl formamide and the formation of the ion at  $m/z = 424.4$ . Similar cleavages on the didodecyl side of D<sup>3</sup>DODGA would form ions with  $m/z = 340.3$  and  $312.3$ .

The CID spectra of compounds 1a and 1b are consistent with structures resulting from the radiolytic elimination of the dodecyl and octyl side chains, respectively. The CID reactions of Compound 1b (Fig. 4) are described in detail here, and we note that the CID reactions of Compound 1a are directly analogous. The mass spectrum of Compound 1b has a base peak at  $m/z = 581.5$ , assigned as  $[M+H]^+$  and a secondary peak, 22 mass units higher, at  $603.5$ , assigned to  $[M+Na]^+$ . The monoisotopic molecular weight of 1a is thus  $580.5$  g/mol, which is  $112.1$  g/mol less than D<sup>3</sup>DODGA, consistent with radiolytic cleavage of a  $C_{\text{octyl}}-\text{N}$  bond on the diOc side of D<sup>3</sup>DODGA followed by hydrogen capping. This strongly suggests that 1b is *N,N,N'*-didodecyloctyldiglycolamide (DDOGA). The other product of this cleavage would be octane, but this compound lacks the ability to accept a proton and so will not be observed in the UHPLC-ESI-MS analysis.

The CID spectrum of Compound 1b (Fig. 5b) supports this structural assignment. This spectrum contains three peaks ( $m/z = 452.4$ ,  $424.4$ , and  $200.2$ ) that would be formed from

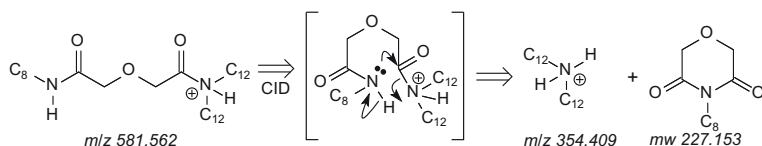


**Scheme 1.** Proposed structures and fragmentation mechanisms for the ions at  $m/z = 452.4$  and  $424.4$  in the CID spectrum of D<sup>3</sup>DODGA.

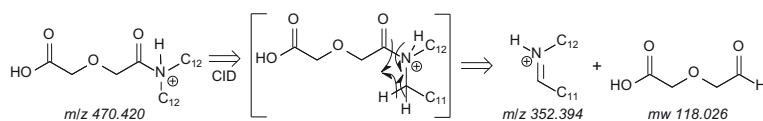
fragmentation mechanisms similar to those in Scheme 1:  $m/z = 452.4$  and  $424.4$  from cleavage of the  $\text{N-C}_{\text{carbonyl}}$  and  $\text{C}_{\text{carbonyl}}\text{-CH}_2$  bonds, respectively, on the now mono- $\text{Oc}$  side of the molecule, forming the same ions seen in the  $\text{D}^3\text{DODGA}$  CID spectrum, and  $m/z = 200.2$  from cleavage of the  $\text{C}_{\text{carbonyl}}\text{-CH}_2$  bond on the diDD side of the molecule, forming an ion 112.2 mass units lighter than the ion at  $m/z = 312.3$  in the  $\text{D}^3\text{DODGA}$  CID spectrum. Interestingly, there is no peak at  $m/z = 228.2$ , which would arise from cleavage of  $\text{N-C}_{\text{carbonyl}}$  bond on the diDD side of  $\text{D}^3\text{DODGA}$  and loss of the neutral didodecyl amine. There is, however, a peak at  $m/z = 354.4$ , which would correspond to the protonated didodecylamine and elimination of a neutral molecule with a molecular weight of 227.1. We hypothesize the protonated amines arise from a molecular rearrangement mechanism, shown in Scheme 2. There is no direct evidence for the structure of either the detected ion or the eliminated neutral, but the hypothetical structures shown in Scheme 2 would be expected to be stable. Protonated dioctylamine and protonated didodecylamine are observed in the CID spectra of the de-alkylated compounds 1a (peak at  $m/z = 242.2$  in Supplementary Information, Fig. S1a) and 1b, respectively (peak at  $m/z = 354.4$  in Fig. 5b). Protonated didodecylamine is also seen in the CID spectrum of the acidic Compound 2b ( $m/z = 354.4$  in Fig. 5c). Curiously, the protonated amines are not seen in the CID spectrum of protonated  $\text{D}^3\text{DODGA}$ . The difference may lie in the fact that the intact DGA lacks a second mobile proton, which is available in the aforementioned degradation products 1a, 1b, and 2b. We hypothesize that the fragmentation mechanism proposed in Scheme 2 is kinetically much faster than the cleavage of the  $\text{N-C}_{\text{carbonyl}}$  bond depicted in Scheme 1 when there is a second mobile proton on the opposite side of the molecule from the  $\text{N-C}_{\text{carbonyl}}$  bond.

Cleavage of the  $\text{N-C}_{\text{carbonyl}}$  (amide) bond on the diOc side with H-atom capping of the dangling bonds would be expected to form dioctylamine and the corresponding aldehyde 5-(*N,N*-di(dodecyl)amido)-3-oxopentanal. The aldehyde derivative would have a high proton affinity and should readily produce abundant protonated and sodiated ions at  $m/z$  of 454.4 and 476.4, respectively, but these are not observed; therefore, we conclude that the aldehyde is not formed. Instead, a chromatographic peak, Compound 2b, with a mass spectrum characterized by  $m/z$  of 470.4 and 492.4 is observed: separated by 22 mass units, these probably represent protonated and sodiated versions of the same molecule. This suggests that in this cleavage, the dangling bond at the carbonyl is capped by a hydroxyl radical, forming 5-(*N,N*-di(dodecyl)amido)-3-oxopentanoic acid, which would have a molecular weight of 469.4 g/mol, and would furnish the protonated and sodiated ions seen.

The CID spectrum of Compound 2b (Fig. 5c) has a base peak at 424.4, which is a loss of 46.0 mass units, or  $\text{HCOOH}$ , from the precursor ion ( $m/z = 470.4$ ). This would correspond to gas-phase cleavage of the  $\text{C}_{\text{carbonyl}}\text{-CH}_2$  bond followed by H capping on the diOc side of the proposed structure of Compound 2b, with elimination of neutral formic acid. The peak at  $m/z = 354.4$  corresponds to the protonated didodecylamine, which could be formed by a mechanism hypothesized to be similar to that depicted in Scheme 2. Elimination of a  $\text{C}_{12}\text{H}_{24}$  group (loss of 168.1 mass units) would yield the ion at  $m/z = 302.2$ , and a subsequent loss of formic acid (via the same mechanism that produced  $m/z = 424.4$ ) would yield the ion at  $m/z = 256.2$ . The peak at  $m/z = 352.4$  represents a new fragmentation pattern, namely formation of an ion at 2 mass units below the protonated amine. We hypothesize this ion is the *N*-dodecyldodecanimine cation, formed by the mechanism proposed in Scheme 3.



**Scheme 2.** Proposed structures and fragmentation mechanism for the ion at  $m/z = 354.4$  in the CID spectrum of Compound 1b.

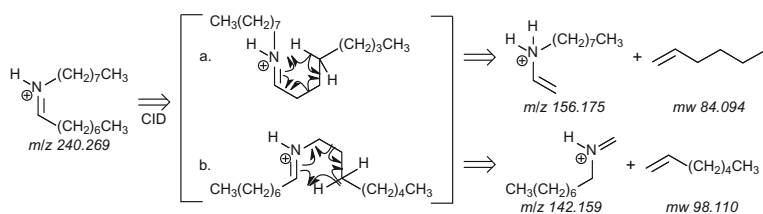


**Scheme 3.** Proposed structures and fragmentation mechanism for the ion at  $m/z = 352.4$  in the CID spectrum of Compound 2b.

The other product of radiolytic cleavage of the N- $C_{\text{carbonyl}}$  (amide) bond on the diOc side would be dioctylamine, with a molecular weight of 241.2. A chromatographic peak (Compound 3a) is observed with a mass spectrum with a dominant ion at  $m/z$  of 242.2 ( $[M+H]^+$ ), indicating a monoisotopic molecular mass of 241.2. The odd value for the monoisotopic molecular weight is consistent with a composition containing an odd number of nitrogen atoms, in accordance with the nitrogen rule. The CID spectrum of Compound 3a (Supplementary Information, Fig. S2a) shows a peak corresponding to the loss of a  $C_8H_{16}$  group, consistent with the structural assignment of dioctylamine. The elemental composition of the compound was identified by accurate mass measurement using HRMS.

The third type of expected radiolytic cleavage involves the  $C_{\text{carbonyl}}-CH_2$  bonds. Rupture on the diOc side followed by H-atom capping would be expected to generate two products: *N,N*-dioctylformamide (OOFA), and *N,N*-didodecyl-2-methoxyacetamide. Dioctylformamide has a molecular weight of 269 g/mol, and should generate protonated and sodiated ions at  $m/z$  of 270 and 292, which are observed in the mass spectrum of Compound 6a eluting at 3.5 min. Radiolytic cleavage of the  $C_{\text{carbonyl}}-CH_2$  bond on the diDD side should generate didodecylformamide (DDFA), with a molecular weight of 381, and protonated and sodiated ions at  $m/z$  of 382 and 404 seen in the mass spectrum of Compound 6b eluting at 12.3 min. The CID spectrum of Compound 6b (Supplementary Information, Fig. S2e) shows loss of  $C_{12}H_{24}$ , which would be expected from the fragmentation of didodecylformamide. The other product would be *N,N*-dioctyl-2-methoxyacetamide; however, neither of the methoxyacetamide derivatives are observed. Peaks with very low signal intensity were assigned as *N,N*-dioctyl-2-methoxyacetamide and *N,N*-di(2-ethylhexyl)-2-methoxyacetamide in the analysis of TODGA and T(EH)DGA,<sup>[25]</sup> but no methoxyacetamide products were observed for the methylated TODGA derivatives.<sup>[26]</sup> Because the formamide products are observed for all five DGAs we have studied (TODGA, T(EH)DGA, MeTODGA, Me<sub>2</sub>TODGA, and D<sup>3</sup>DODGA), it is likely this bond cleavage occurs. Therefore, it is unclear if the methoxyacetamide products are formed as a result of this cleavage, but at levels below the detection limit, or if the cleavage leads to formation of an alternative compound instead.

Finally, cleavage of the C- $O_{\text{ether}}$  bond on the diDD side followed by H-atom capping of the dangling bonds would produce two compounds: *N,N*-dioctyl glycolamide, with a monoisotopic molecular mass of 299.3 g/mol, and *N,N*-di(dodecyl)acetamide, with a monoisotopic molecular mass of 395.4 g/mol. The CID spectrum of Compound 4a ( $[M+H]^+ = 299.3$ , Fig. 5d) has a base peak at  $m/z = 188.2$ , which would arise from elimination of a  $C_8$  olefin from one of the octyl side chains of *N,N*-dioctyl glycolamide. The fragment ions at  $m/z = 242.3$  and  $m/z = 240.3$  are hypothesized to correspond to the protonated dioctylamine and the octyloctanimine cations, formed from protonated *N,N*-dioctyl glycolamide by mechanisms similar to those depicted in Scheme 2 and Scheme 3, respectively. Additionally, each of these ions could fragment to form other peaks found in the CID spectrum. For example, the peaks at  $m/z = 156.2$  and  $142.2$  could come from two different McLafferty rearrangements<sup>[32]</sup> of the octyloctanimine cation depicted in Scheme 4, further supporting this structural assignment. The other expected radiolytic product of the cleavage of the C- $O_{\text{ether}}$  bond on the diDD side of D<sup>3</sup>DODGA would be didodecylacetamide, which would have a monoisotopic molecular mass of 395.4, the same as Compound 5b. The CID spectrum of Compound 5b (Supplementary Information, Fig. S2d) shows a peak corresponding to protonated didodecyl amine ( $m/z = 354.4$ ) and a peak corresponding to loss of a  $C_{12}H_{24}$  side chain ( $m/z = 228.2$ ),



**Scheme 4.** Proposed structures and fragmentation mechanisms for the ions at  $m/z = 156.2$  and  $142.2$  in the CID spectrum of Compound 4a.

suggesting Compound 5b is didodecylacetamide. The proposed structures for Compounds 1a, 3b, and 5a are based on the above arguments using logical cleavages and capping, monoisotopic molecular weight, and CID data (SI, Figs. S1 and S2).

Several other compounds were detected that appear to be related to the  $D^3DODGA$  radiolysis (their signal increases with absorbed dose), but are unlikely to be primary radiolysis products. The first compound (Compound 2c, Supplementary Information, Fig. S3) has a chromatographic peak with ions at  $m/z = 526$  and  $548$  (indicating a protonated–sodiated pair), so the neutral molecular mass is likely 525, with a formula of  $C_{32}H_{65}NO_4$  (Supplementary Information, Table S2). The dodecyl ester of Compound 2a would have a molecular formula matching this. The CID fragmentation spectrum (Supplementary information, Fig. S4a) shows loss of 168 ( $C_{12}H_{24}$ ), which is consistent with cleavage of the ester– $C_{12}H_{25}$  bond. The ion at  $m/z = 312$  in the CID spectrum could be formed from cleavage of the DGA  $C-O_{ether}$  bond. This ion is seen in the CID spectra of  $D^3DODGA$  and several degradation products with proposed structures with the  $C_8$  side of the molecule intact. The ion at  $m/z = 312$  could lose  $C_8H_{16}$  to form the ion at  $m/z = 200$ . Another compound, 2d ( $m/z = 386$ , Supplementary Information, Table S2, Figs. S3 and S4b), has an exact formula and CID spectrum consistent with the ethyl-ester of Compound 2a. Both of these esters could be formed from a reaction between Compound 2a and the appropriate alcohol; however, the source of the alcohols is unknown. The signals from both of these compounds are extremely low, so they could be the result of reactions of Compound 2a with alcohols present as contaminants in the diluent.

Two other detected compounds, Unknown 1 ( $m/z = 256$ ) and Unknown 2 ( $m/z = 368$ ), also have signals that increase with absorbed dose, especially for the acid contacted samples. Each has a peak 22 mass units higher with the same chromatographic profile when ionized using ESI, suggesting neutral formulas of  $C_{16}H_{33}NO$  and  $C_{24}H_{49}NO$ , respectively. The CID spectra of these two compounds show loss of  $C_8H_{16}$  (Unknown 1) and  $C_{16}H_{24}$  (Unknown 2), suggesting they are related to  $D^3DODGA$ , but the carbon/hydrogen ratio suggests part of each molecule is unsaturated. Unknown 1 is present in the unirradiated samples, so it could be a synthesis impurity that is also produced by radiolysis or hydrolysis. However, there is not enough information to draw conclusions about the identity of these compounds.

### Behavior of $D^3DODGA$ Radiolysis Products as a Function of Absorbed Dose

The effects on solvent extraction separations due to these degradation products have not been thoroughly investigated. Núñez et al.<sup>[33]</sup> reported on properties of selected TODGA degradation compounds and their effects on solvent extraction systems. Acidic degradation compounds were found to possibly interfere with a selective back-extraction step in solvent extraction processes. Other degradation compounds showed increased co-extraction of fission products. Degradation compounds with 2-hydroxyacetamide structure showed increased Mo extraction, and other degradation compounds showed higher co-extraction of Zr and Pd. It was concluded that the degradation of TODGA would lead to an overall increased co-extraction of undesired fission products. However, based on analogy with TODGA and the solvent extraction ligand CMPO, the production of acidic

degradation products (such as DDAOPA and OOAOPA, Fig. 4) may adversely affect stripping of the metal-loaded organic phase.<sup>[34,35]</sup> The concentration changes of the detected radiolysis products as a function of absorbed dose (Fig. 6) can be examined based on the proposed structures. Compounds 1b and 2b (Fig. 6a and 6b, respectively) grow in as dose increases, indicating they are directly formed by radiolysis. The signal for Compound 1b peaks at about 300 kGy and the signal for Compound 2b peaks at about 200 kGy at which point the signal begins to decrease, indicating these radiolysis products themselves are susceptible to radiolysis. Given the proposed structures, DDODGA and DDAOPA, this is not surprising, since these structures still have the C–O<sub>ether</sub>, C–C<sub>carbonyl</sub>, and N–C<sub>carbonyl</sub> bonds whose rupture is proposed to lead the other detected radiolysis products. The same behavior was observed by Galán et al.<sup>[26]</sup> for structurally comparable degradation compounds, which are believed to be formed through the same radiolysis mechanism. The acidic compound 2-((1-(dioctylamino)-1-oxopropan-2-yl)oxy)acetic acid (comparable to Compound 2a) and the single dealkylation compound (comparable to Compound 1a) showed the same increase in dose up to 200–300 kGy, after which the normalized intensity decreased. Compounds 5b and 6b (Fig. 6c and 6d, respectively) grow in as absorbed dose increases, consistent with their structural assignments as small radiolysis products.

The course of the radiolysis does appear to be affected, however, in the acid-contacted experiment compared with the non-acid-contacted experiment. After 100 kGy, more of the de-alkylated, and de-aminated products are formed in the acid contacted experiments, and conversely, there is comparatively less of the products arising from radiolytic cleavage of the C<sub>carbonyl</sub>–C and C–O<sub>ether</sub> bonds. Acid contact clearly tends to favor cleavage at the nitrogen atoms, though this preference does not seem to affect the overall degradation rate. We hypothesize that the presence of acid results in amide functional groups that are at least partially protonated, resulting in weakening of the N–C<sub>alkyl</sub> and N–C<sub>carbonyl</sub> bonds relative to the C–C<sub>carbonyl</sub> and C–O<sub>ether</sub> bonds. The primary degradation products

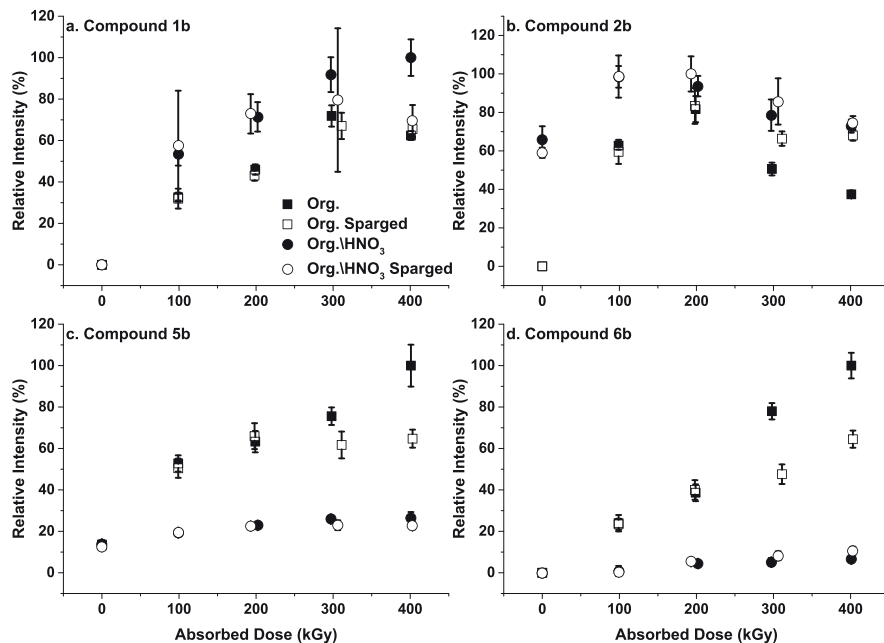


**Figure 6.** Normalized signal versus absorbed dose for degradation products 1b, 2b, 5b, and 6b. Solid squares correspond to 0.05 M D<sup>3</sup>DODGA organic phase; open squares, 0.05 M D<sup>3</sup>DODGA air-sparged organic phase; solid circles, 0.05 M D<sup>3</sup>DODGA organic phase contacted with 2.5 M HNO<sub>3</sub>; open circles, 0.05 M D<sup>3</sup>DODGA air-sparged organic phase contacted with 2.5 M HNO<sub>3</sub>. Each point is the mean of five measurements and the error bars represent 99% confidence intervals.



formed in the presence of the acidic aqueous phase will have high metal-coordination-complex formation constants. These degradation products could decrease the distribution ratios if they have aqueous solubility and could impede stripping if they remain in the organic phase. In contrast, in the non-acid-contacted experiments there is a greater rate of formation of products in which the DGA core is broken, which would not be expected to be effective extractants.

## Conclusions

The results of this study suggest that there is no difference between the rate of  $\gamma$ -radiolysis of D<sup>3</sup>DODGA and those of TODGA and T(EH)DGA. Additionally, the rate appears to be unaffected by contact with nitric acid and air sparging, providing additional evidence that radical cations produced in the alkane diluent are the reactive species initiating decomposition. There does seem to be a difference in degradation chemistry that depends on whether the organic phase is in contact with acid; in the presence of an acidic aqueous phase, the preferred site for radiolytic attack appears to be at the amide nitrogen atoms, which produces a higher fraction of products generated from rupture of the N–C<sub>carbonyl</sub> and the N–C<sub>alkyl</sub> bonds. The C–O<sub>ether</sub> and C–C<sub>carbonyl</sub> bonds are also broken, but these reactions account for a greater fraction of the overall reactivity in the non-acid-contacted experiments. Thus, a study of the effect of the potentially more deleterious radiolysis products generated in the presence of the acidic aqueous phase on solvent extraction performance is warranted.

There is also a striking similarity in the degradation pathway of D<sup>3</sup>DODGA when compared with the degradation of TODGA, T(EH)DGA, MeTODGA, and Me<sub>2</sub>TODGA.<sup>[24,25]</sup> The similarity in degradation rates of these DGA compounds, along with the identified radiolysis products discussed above, strongly suggests that the diglycolamide center of these molecules, not the side chains, is most vulnerable to radiolytic degradation, apparently all by reaction with a common species produced by radiolysis of the diluent.

## Funding

The gamma irradiation and UHPLC-ESI-MS experiments performed at Idaho National Laboratory were supported by the US Department of Energy (US-DOE), Office of Nuclear Energy, under the Fuel Cycle R&D Program, Idaho Operations Office Contract DE-AC07-05ID14517. Additional financial support for this research was provided by the European Commission (projects SACSESS – contract number FP7-Fission-2012-323-282).

## ORCID

Christopher A. Zarzana  <http://www.orcid.org/0000-0001-9617-7123>

Bruce J. Mincher  <http://www.orcid.org/0000-0003-3108-2590>

Andreas Wilden  <http://www.orcid.org/0000-0001-5681-3009>

Holger Schmidt  <http://www.orcid.org/0000-0002-3448-3579>

Giuseppe Modolo  <http://www.orcid.org/0000-0001-6490-5595>

## References

1. Todd, T.A. Separation research for advanced nuclear fuel cycles. In *Nuclear Energy and the Environment*; Wai, C.M., Mincher, B.J., Eds.; American Chemical Society: Washington, D.C., 2010; pp 13–18.
2. Hudson, M.J.; Harwood, L.M.; Laventine, D.M.; Lewis, F.W. Use of soft heterocyclic N-donor ligands to separate actinides and lanthanides. *Inorg. Chem.* 2013, 52(7), 3414–3428.
3. Madic, C.; Lecomte, M.; Baron, P.; Boullis, B. Separation of long-lived radionuclides from high active nuclear waste. *C. R. Phys.* 2002, 3(7–8), 797–811.
4. Magill, J.; Berthou, V.; Haas, D.; Galy, J.; Schenkel, R.; Wiese, H.-W.; Heusener, G.; Tommasi, J.; Youinou, G. Impact limits of partitioning and transmutation scenarios on the radiotoxicity of actinides in radioactive waste. *Nucl. Energy* 2003, 42(5), 263–277.



5. Ansari, S.A.; Pathak, P.; Mohapatra, P.K.; Manchanda, V.K. Chemistry of diglycolamides: Promising extractants for actinide partitioning. *Chem. Rev.* 2012, *112*(3), 1751–1772.
6. Ansari, S.A.; Pathak, P.; Mohapatra, P.K.; Manchanda, V.K. Aqueous partitioning of minor actinides by different processes. *Sep. Purif. Rev.* 2011, *40*(1), 43–76.
7. Sasaki, Y.; Sugo, Y.; Suzuki, S.; Tachimori, S. The novel extractants, diglycolamides, for the extraction of lanthanides and actinides in  $\text{HNO}_3$ -*n*-Dodecane system. *Solvent Extr. Ion Exch.* 2001, *19*(1), 91–103.
8. Mowafy, E.A.; Aly, H.F. Synthesis of some *N, N, N', N'*-tetraalkyl-3-oxa-pentane-1,5-diamide and their applications in solvent extraction. *Solvent Extr. Ion Exch.* 2007, *25*(2), 205–224.
9. Tachimori, S.; Sasaki, Y.; Suzuki, S. Modification of TODGA-*N*-dodecane solvent with a monoamide for high loading of lanthanides(III) and actinides(III). *Solvent Extr. Ion Exch.* 2002, *20*(6), 687–699.
10. Sasaki, Y.; Sugo, Y.; Suzuki, S.; Kimura, T. A method for the determination of extraction capacity and its application to *N, N, N', N'*-tetraalkyl derivatives of diglycolamide-monoamide/*n*-dodecane media. *Anal. Chim. Acta* 2005, *543*(1–2), 31–37.
11. Sasaki, Y.; Zhu, Z.-X.; Sugo, Y.; Suzuki, H.; Kimura, T. Extraction capacity of diglycolamide derivatives for Ca (II), Nd(III) and Zr(IV) from nitric acid to *n*-dodecane containing a solvent modifier. *Anal. Sci.* 2005, *21*(10), 1171–1175.
12. Modolo, G.; Asp, H.; Schreinemachers, C.; Vijgen, H. Development of a TODGA based process for partitioning of actinides from a PUREX raffinate. Part I: Batch extraction optimization studies and stability tests. *Solvent Extr. Ion Exch.* 2007, *25*(6), 703–721.
13. Modolo, G.; Asp, H.; Vijgen, H.; Malmbeck, R.; Magnusson, D.; Sorel, C. Demonstration of a TODGA-based continuous counter-current extraction process for the partitioning of actinides from a simulated PUREX raffinate. Part II: Centrifugal contactor runs. *Solvent Extr. Ion Exch.* 2007, *26*(1), 62–76.
14. Magnusson, D.; Christiansen, B.; Glatz, J.; Malmbeck, R.; Modolo, G.; Serrano-Purroy, D.; Sorel, C. Demonstration of a TODGA based extraction process for the partitioning of minor actinides from a PUREX raffinate. *Solvent Extr. Ion Exch.* 2009, *27*(1), 26–35.
15. Ravi, J.; Suneesh, A.S.; Prathibha, T.; Venkatesan, K.A.; Antony, M.P.; Srinivasan, T.G.; Vasudeva Rao, P.R. Extraction behavior of some actinides and fission products from nitric acid medium by a new unsymmetrical diglycolamide. *Solvent Extr. Ion Exch.* 2011, *29*(1), 86–105.
16. Ravi, J.; Venkatesan, K.A.; Antony, M.P.; Srinivasan, T.G.; Vasudeva Rao, P.R. Tuning the diglycolamides for modifier-free minor actinide partitioning. *J. Radioanal. Nucl. Chem.* 2013, *295*(2), 1283–1292.
17. Ravi, J.; Venkatesan, K.A.; Antony, M.P.; Srinivasan, T.G.; Vasudeva Rao, P.R. Feasibility of using di-dodecyl-di-octyl diglycolamide for partitioning of minor actinides from fast reactor high-level liquid waste. *Solvent Extr. Ion Exch.* 2014, *32*(4), 424–436.
18. Nayak, P.K.; Kumaresan, R.; Shivkumar, C.; Venkatesan, K.A.; Subramanian, G.G.S.; Prathibha, T.; Syamala, K. V.; Selvan, B.R.; Rajeswari, S.; Antony, M.P.; et al. Studies on the feasibility of using completely incinerable reagents for the single-cycle separation of Americium(III) from simulated high-level liquid waste. *Radiochim. Acta* 2014, *103*(4), 265.
19. Nayak, P.K.; Kumaresan, R.; Shivkumar, C.; Venkatesan, K.A.; Subramanian, G.G.S.; Rajeswari, S.; Antony, M. P.; Vasudeva Rao, P.R.; Bhanage, B.M. Demonstration of trivalent actinide partitioning from simulated high-level liquid waste using modifier-free unsymmetrical diglycolamide in *N*-dodecane. *Radiochim. Acta* 2015, *103* (5), 359.
20. Jammu, R.; Venkatesan, K.A.; Antony, M.P.; Srinivasan, T.G.; Vasudeva Rao, P.R. New unsymmetrical diglycolamide ligands for trivalent actinide separation. *Radiochim. Acta* 2014, *102*(7), 609.
21. Sypula, M.; Wilden, A.; Schreinemachers, C.; Malmbeck, R.; Geist, A.; Taylor, R.; Modolo, G. Use of poly-aminocarboxylic acids as hydrophilic masking agents for fission products in actinide partitioning processes. *Solvent Extr. Ion Exch.* 2012, *30*(7), 748–764.
22. Sugo, Y.; Sasaki, Y.; Tachimori, S. Studies on hydrolysis and radiolysis of *N, N, N', N'*-tetraoctyl-3-oxapentane-1,5-diamide. *Radiochim. Acta* 2002, *90*, 161–165.
23. Sugo, Y.; Izumi, Y.; Yoshida, Y.; Nishijima, S.; Sasaki, Y.; Kimura, T.; Sekine, T.; Kudo, H. Influence of diluent on radiolysis of amides in organic solution. *Radiat. Phys. Chem.* 2007, *76*, 794–800.
24. Galán, H.; Núñez, A.; Espartero, A.G.; Sedano, R.; Durana, A.; Mendoza, J. de. Radiolytic stability of TODGA: Characterization of degraded samples under different experimental conditions. *Procedia Chem.* 2012, *7*(0), 195–201.
25. Zarzana, C.A.; Groenewold, G.S.; Mincher, B.J.; Mezyk, S.P.; Wilden, A.; Schmidt, H.; Modolo, G.; Wishart, J.F.; Cook, A.R. A comparison of the  $\gamma$ -radiolysis of TODGA and T(EH)DGA using UHPLC-ESI-MS analysis. *Solvent Extr. Ion Exch.* 2015, *33*(5), 431–447.
26. Galán, H.; Zarzana, C.A.; Wilden, A.; Nunez, A.; Schmidt, H.; Egberink, R.J.M.; Leoncini, A.; Cobos, J.; Verboom, W.; Modolo, G.; et al. Gamma-radiolytic stability of new methylated TODGA derivatives for minor actinide recycling. *Dalton Trans.* 2015, *44*(41), 18049–18056.
27. Mincher, B.J.; Modolo, G.; Mezyk, S.P. Review article: The effects of radiation chemistry on solvent extraction 3: a review of actinide and lanthanide extraction. *Solvent Extr. Ion Exch.* 2009, *27*(5–6), 579–606.

28. Galán, H.; Murillo, M.T.; Sedano, R.; Núñez, A.; de Mendoza, J.; González-Espartero, A.; Prados, P. Hydrolysis and radiation stability of M-xylene bis-diglycolamide: Synthesis and quantitative study of degradation products by HPLC–APCI+. *Eur. J. Org. Chem.* **2011**, 2011(20–21), 3959–3969.
29. Jammu, R.; Robert, S.B.; Venkatesan, K.A.; Antony, M.P.; Srinivasan, T.G.; Vasudeva Rao P.R. Radiolytic stability of di-2-ethylhexyl-dioctyl diglycolamide. *Radiochim. Acta* **2014**, *102*(5), 451.
30. Ravi, J.; Robert Selvan, B.; Venkatesan, K.A.; Antony, M.P.; Srinivasan, T.G.; Vasudeva Rao, P.R. Evaluation of radiation stability of *N, N*-didodecyl *N', N'*-di-octyl diglycolamide: A promising reagent for actinide partitioning. *J. Radioanal. Nucl. Chem.* **2014**, *299*(1), 879–885.
31. Gujar, R.B.; Ansari, S.A.; Bhattacharyya, A.; Kanekar, A.S.; Pathak, P.N.; Mohapatra, P.K.; Manchanda, V.K. Radiolytic stability of *N, N, N', N'*-Tetraoctyl Diglycolamide (TODGA) in the presence of phase modifiers dissolved in N-dodecane. *Solvent Extr. Ion Exch.* **2012**, *30*(3), 278–290.
32. McLafferty, F.W. 6.8 Amines. In *Interpretation of Mass Spectra*; W. A. Benjamin, Inc.: London, 1973; pp 156–163.
33. Núñez, A.; Galán, H.; Cobos, J. TODGA degradation compounds: Properties and effects on extraction systems. In *Proceedings of GLOBAL 2015 Nuclear Fuel Cycle for a Low-Carbon Future*; Paris, France, 2015; p 1623–1630, Paper 5400.
34. Nash, K.L.; Gatrone, R.C.; Clark, G.A.; Rickert, P.G.; Horwitz, E.P. Hydrolytic and radiolytic degradation of O<sub>o</sub>d(iB)Cmpo: Continuing studies. *Sep. Sci. Technol.* **1988**, *23*(12–13), 1355–1372.
35. Mincher, B.J.; Mezyk, S.P.; Elias, G.; Groenewold, G.S.; Riddle, C.L.; Olson, L.G. The radiation chemistry of CMPO: Part 1. gamma radiolysis. *Solvent Extr. Ion Exch.* **2013**, *31*(7), 715–730.



## Paper 9<sup>[154]</sup>

Hubscher-Bruder, V.; Mogilireddy, V.; Michel, S.; Leoncini, A.; Huskens, J.; Verboom, W.; Galan, H.; Núñez, A.; Cobos Sabate, J.; Modolo, G.; Wilden, A.; Schmidt, H.; Charbonnel, M.-C.; Guilbaud, P.; Boubals, N. Behaviour of the Extractant Me-TODGA Upon Gamma Irradiation: Quantification of the Degradation Compounds and Individual Influences on Complexation and Extraction. *New J. Chem.* **2017**, *41*, 13700-13711.

DOI: 10.1039/C7NJ02136D

### Contribution:

For this work, solvent extraction experiments as well as their analysis (gamma-spectrometry, results of ICP-MS) using the synthesized degradation products of TODGA and Me-TODGA were conducted mainly by A. Wilden and me. Additionally, I participated in paper preparation.





Cite this: *New J. Chem.*, 2017, 41, 13700

# Behaviour of the extractant Me-TODGA upon gamma irradiation: quantification of degradation compounds and individual influences on complexation and extraction

V. Hubscher-Bruder,<sup>a</sup> V. Mogilireddy,<sup>a</sup> S. Michel,<sup>a</sup> A. Leoncini,<sup>b</sup> J. Huskens,<sup>b</sup> W. Verboom,<sup>b</sup> H. Galán,<sup>c</sup> A. Núñez,<sup>c</sup> J. Cobos,<sup>c</sup> G. Modolo,<sup>d</sup> A. Wilden,<sup>d</sup> H. Schmidt,<sup>d</sup> M.-C. Charbonnel,<sup>e</sup> P. Guilbaud<sup>e</sup> and N. Boubals<sup>e</sup>

Diglycolamides (DGAs), and in particular *N,N,N',N'*-tetraoctyl diglycolamide (TODGA), are well-known candidates for the co-extraction of trivalent actinides (An(III)) and lanthanides (Ln(III)) from highly acidic aqueous solutions of nuclear waste. A derivative of TODGA, the so-called Me-TODGA with the addition of a methyl-substituent on the central part of the TODGA molecule, has been proposed to improve its stability properties and extraction behaviour. This work describes the stability and viability of Me-TODGA by studying the properties of its degradation compounds formed upon gamma irradiation. The main degradation products have been synthesised and studied individually. Particular attention has been paid to their quantification, as well as their complexation and extraction properties, for a better understanding of the degradation pathways and the behaviour of the solvents upon gamma irradiation. The extraction behaviour of irradiated Me-TODGA solvents and their degradation compounds have been studied toward the fission products and lanthanides present in a highly active raffinate (HAR) solution. Binding properties of parent molecules (TODGA and Me-TODGA) and their main degradation compounds with Ln(III) have also been determined in a homogeneous phase. All the results obtained on degradation compounds are compared with those of the parent molecules in order to assess the effects of these compounds on the separation process. Among the radiolytic compounds, 2-hydroxyoctylamides are the most problematic compounds not only because of their high affinity for lanthanides but also for other fission products.

Received 14th June 2017,  
Accepted 28th September 2017

DOI: 10.1039/c7nj02136d

rsc.li/njc

## Introduction

For many years, efforts have been made to develop partitioning and recycling processes for used nuclear fuel in order to reduce the long-term radiotoxicity and heat load of nuclear waste. The current industrial Plutonium Uranium Reduction Extraction (PUREX) process, which allows the recovery of uranium and plutonium, could be followed by different processes (DIAMEX, SANEX, i-SANEX) proposed to separate long-lived trivalent minor

actinides from the highly active raffinate.<sup>1–6</sup> Among the molecules designed and tested, tridentate diglycolamides (DGAs) and in particular *N,N,N',N'*-tetraoctyl diglycolamide (TODGA) (Fig. 1) showed good extraction abilities for the first step which is co-separation of trivalent actinides (An(III)) and lanthanides (Ln(III)) from highly concentrated nitric acid solutions.<sup>7–13</sup> Recently, TODGA derivatives with additional methyl-substituents on the DGA backbone were studied and found to be interesting alternatives to TODGA, especially methyl-TODGA (Me-TODGA in Fig. 1).<sup>14,15</sup> The objective of such a modification (introduction of a methyl group between the ether and an amide moiety) is the increase of its radiolytic stability and the improvement of the stripping behaviour.

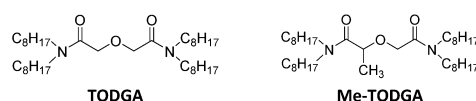


Fig. 1 Chemical structures of TODGA and Me-TODGA.

<sup>a</sup> Université de Strasbourg, CNRS, IPHC UMR 7178, F-67000 Strasbourg, France. E-mail: veronique.hubscher@unistra.fr; Tel: +33 3 68 85 26 09

<sup>b</sup> Laboratory of Molecular Nanofabrication, MESA+ Institute for Nanotechnology, University of Twente, P.O. Box 217, 7500 AE Enschede, The Netherlands

<sup>c</sup> Centro de Investigaciones Energéticas, Medioambientales y Tecnológicas (CIEMAT), Madrid 28040, Spain

<sup>d</sup> Forschungszentrum Jülich GmbH (FZJ), Institut für Energie- und Klimaforschung, Nukleare Entsorgung und Reaktorsicherheit (IEK-6), 52428 Jülich, Germany

<sup>e</sup> CEA, Nuclear Energy Division, Marcoule, Research Department on Processes for Mining and Fuel Recycling, LLL Laboratory, 30207 Bagnols sur Cèze, France

To evaluate the applicability of new solvents for process development in the nuclear field, the important properties to check are not only their good extraction abilities, but also their hydrolytic and radiolytic stability since the extracting systems will be in contact with highly radioactive aqueous solutions and high nitric acid concentrations. The presence of degradation products may lead to undesirable effects such as a decrease of performance (extraction efficiency and selectivity), or deterioration of physical properties (third phase formation). The addition of a regeneration process to avoid (or limit) such behaviour could increase the volume of the secondary waste and the process cost. Most often, the new species generated have extraction properties that markedly differ from those of the original ligands and can have an impact on the long-live radioactive waste management and safety.

A methodology for studying the stability of DGAs as selective extractants of An(III) and Ln(III) was previously set up, involving complete characterization by HPLC-MS of irradiated samples.<sup>16</sup> This methodology allowed exploring the degradation process with identification and quantification of the degradation products formed during irradiation. It has been applied to TODGA solvents to get a complete set of data, to assess how and why the experimental conditions can affect the proportions and amounts of degradation products.<sup>17</sup> Among others, these studies have shown a double protective role of nitric acid in the stability of diglycolamide-based ligands. The acid medium (H<sup>+</sup>) provides a protective effect on the O<sub>ether</sub>-C bond, which was found to be the weakest bond of the molecule and on the other hand, nitrate ions would act as scavengers of reactive species formed during gamma irradiation as described in related work.<sup>18,19</sup> Recently, the radiolytic stability of TODGA, Me-TODGA and Me<sub>2</sub>-TODGA has also been published pointing out the effect of additional methyl group(s) on the diglycolamide structure.<sup>20</sup> The addition of one methyl group seems to increase the degradation rate constant of DGAs, favoring the rupture of one of the O<sub>ether</sub>-C bonds over the other. Analytical methods based on LC-MS and especially Atmospheric Pressure Chemical Ionization (APCI<sup>+</sup>), a generally weak ionization method, have been used to identify and quantify the degradation products formed during the irradiation process for TODGA and Me-TODGA degraded samples in TPH as a diluent.<sup>17,20</sup> Considering the main chromatographic peaks and assigned structures, Me-TODGA samples gave rise to ten degradation compounds due to radiation damage and hydrolytic degradation of amide groups. Based on the intensities of the peaks corresponding to compounds 1, 2, 3 and 4 (the main degradation compounds), the rupture of the ether linkage was proposed *via* paths 'a' and 'b' as shown in Fig. 2. The rupture path 'a' with the formation of 1 and 2 compounds was found to be preferred. Koubský *et al.* studied the radical degradation of TODGA and the methylated analogues using quantum chemistry. Although their findings for the degradation of Me-TODGA were ambiguous taking into account DFT energy levels, calculation at the Hartree-Fock level of theory gave a clear preference for degradation path 'a'.<sup>21</sup>

The present work, which should be noticed as a continuation of Galán *et al.*,<sup>20</sup> delves into a complete characterization of

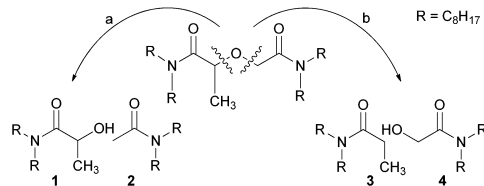


Fig. 2 Main ruptures of Me-TODGA after gamma irradiation.<sup>20</sup>

Me-TODGA degraded solvents, irradiated by an external <sup>60</sup>Co source under different irradiation conditions. In the previous publication, only the parent molecule was well quantified, while the quantity of degradation products was only evaluated from the intensities observed in the LC-MS analysis. Therefore, in this study, particular attention is paid to the quantification of the degradation products formed during the irradiation process. The second part of this paper is focused on the extraction properties of the irradiated Me-TODGA. To better understand the variation of extraction of Am(III), Ln(III) and some fission products (FPs), the synthesis of various identified radiolysis fragments was performed and the extraction behaviour of such individual degradation product solutions was followed. Microcalorimetric studies were also carried out to better describe the thermodynamic properties related to the extraction, but also the complexation of lanthanides with the parent molecules (TODGA and Me-TODGA) and some of their degradation compounds.

## Experimental

### Reagents and chemicals

Reagents and chemicals for the synthesis of compounds and intermediates were purchased from commercially available sources without further purification. Solvents were distilled and dried before use by standard methods. CH<sub>3</sub>CN and HCOOH were of HPLC-MS quality grade. The diluent TPH (hydrogenated tetrapropene) was supplied by CEA, Marcoule. Nitric acid was purified by the Quartz sub-boiling distillation system (MLS-Milestone), whose solutions were prepared by diluting the concentrated nitric acid obtained with ultrapure water (18 MΩ cm). Methanol, 1-octanol, and *n*-dodecane used for microcalorimetry were bought from Sigma Aldrich and were of 99.9% purity. The metal salts La(NO<sub>3</sub>)<sub>3</sub>·6H<sub>2</sub>O, Eu(NO<sub>3</sub>)<sub>3</sub>·6H<sub>2</sub>O and Yb(NO<sub>3</sub>)<sub>3</sub>·xH<sub>2</sub>O (Alfa Aesar, 99.99%) were dried under vacuum before use, and the concentration of lanthanides in solutions was determined by complexometric titrations with Titrplex III and Xylenol orange as indicators. The titrplex complexing agent was bought from Merck and color indicator Xylenol orange from Riedel-de-Haen.<sup>22</sup>

The radiotracers <sup>241</sup>Am and <sup>152</sup>Eu were supplied by Isotope Products Laboratories, California (USA) and by Isotopendienst M. Blaseg GmbH, Walldburg, Germany and Eckert and Ziegler Nuclitec GmbH, Braunschweig, Germany. For the selectivity study the aqueous solutions were prepared with a 10 vol% dilution of simulated HAR solution in 3 or 4 mol L<sup>-1</sup> HNO<sub>3</sub>. The synthetic

HAR solution used corresponds to a PUREX raffinate with a volume of 5000 L t<sup>-1</sup> UOX fuel with an initial <sup>235</sup>U enrichment of 3.5%, a thermal burn-up of 40 GWd<sub>tHM</sub><sup>-1</sup> and cooling for 3 years.<sup>23–25</sup> The synthetic PUREX raffinate was prepared by a specific dissolving strategy, mainly based on the use of metal nitrate salts. Its composition was described in previous work.<sup>26</sup>

### Gamma irradiation

Organic solutions of TODGA and Me-TODGA were prepared by dissolving appropriate amounts of each of them, up to 0.1 mol L<sup>-1</sup> in TPH at 23 ± 2 °C. Before use, the organic solutions were pre-equilibrated twice with nitric acid solutions by vigorous stirring for 5 min (600 µL of organic solution and the same volume of 3 mol L<sup>-1</sup> nitric acid). The phases were separated by centrifugation at 5000 rpm and sent to the Náyade, which is the gamma-irradiation facility at CIEMAT. It consists of a pool of area 1.2 m<sup>2</sup> and depth of 4.5 m with <sup>60</sup>Co sources distributed in six lots with a total activity of 1.1 × 10<sup>14</sup> Bq. The irradiation container used provides a homogeneous irradiation flux. The samples were irradiated up to 250, 500, 750 and 1000 kGy at dose rates of 1.78 and 6.32 kGy h<sup>-1</sup>. No volume decrease was observed during irradiation, hence evaporation of the solvent is assumed to be negligible. The glass bottles were then stored in a freezer while awaiting further analyses. Reference samples for aging control were kept in the laboratory during the irradiation process.

### HPLC-DAD/MS measurements

The chemical composition of the irradiated samples was characterized by HPLC-DAD/MS (Agilent 1100, Quadrupole detector 6120A at CIEMAT). The measurements were performed by using a Prontosil C-8 column (50 × 2 mm, 5 µm) at 40 °C using a gradient of mobile phase [(A: 0.1% v/v CH<sub>3</sub>CN/HCOOH), (B: 0.1% v/v H<sub>2</sub>O/HCOOH)] in the APCI<sup>+</sup> ionization mode (SCAN 100 a 1500 umas/SIM). The mass spectrometer conditions were: capillary voltage: 2000 V; corona current: 5 µA; charging voltage: 2000 V; positive mode; dry temp.: 250 °C; vaporization temp 200 °C; nebulizer gas and dry gas were both N<sub>2</sub>; nebulizer pressure: 1.4 bar; dry gas flow rate: 5 L min<sup>-1</sup>. Samples were analyzed without pre-evaporation and diluted up to 0.5 and 1.0 mmol L<sup>-1</sup> in a (90:10 v/v) MeOH/1-octanol mixture. All measurements were repeated twice.

### Synthesis of the compounds and intermediates

<sup>1</sup>H- and <sup>13</sup>C-NMR spectra were recorded on a Bruker 400 MHz NMR spectrometer. ESI mass spectra were recorded on a WATERS LCT mass spectrometer.

***N,N*-Diocetyl propionamide (3).** To a solution of sodium hydroxide (1.04 g, 26 mmol, 10 equiv.) in water (25 mL) was added dioctylamine (0.62 g, 2.6 mmol) at 0 °C under vigorous stirring. Subsequently, a solution of propionyl chloride (0.96 g, 10.4 mmol, 4 equiv.) in ethyl acetate (30 mL) was added dropwise at that temperature, whereupon it was reacted for 3 h at room temperature. After separation of the layers, the organic layer was washed with 5% NaHCO<sub>3</sub> solution (3 × 50 mL) and water (2 × 50 mL), and dried with MgSO<sub>4</sub>. Removal of the solvent gave the pure compound as oil in 93% yield. <sup>1</sup>H NMR

(400 MHz, CDCl<sub>3</sub>) δ 3.25–3.19 (m, 2H), 3.15–3.09 (m, 2H), 2.24 (q, *J* = 7.4 Hz, 2H), 1.51–1.39 (m, 4H), 1.28–1.13 (m, 20H), 1.07 (t, *J* = 7.4 Hz, 3H), 0.81 (q, *J* = 6.8 Hz, 6H). <sup>13</sup>C NMR (101 MHz, CDCl<sub>3</sub>) δ 173.3, 48.0, 46.0, 31.9 (2×), 29.5, 29.4 (2×), 29.3, 29.2, 27.9, 27.2, 27.0, 26.4, 22.7 (2×), 14.2 (2×), 9.8. ESI-MS: *m/z* 298.2 [M + H]<sup>+</sup>; ESI-HRMS: *m/z* 298.3046 [M + H]<sup>+</sup>; calculated 298.3110 for C<sub>19</sub>H<sub>40</sub>NO.

***N*-Octyl propionamide (7).** *N*-Octyl propionamide (7) was prepared in a similar way to compound 3 starting from sodium hydroxide (2.10 g, 52.6 mmol), octylamine (0.68 g, 5.3 mmol) and propionyl chloride (1.95 g, 21.0 mmol) as an oil in 96% yield. <sup>1</sup>H NMR (400 MHz, CDCl<sub>3</sub>) δ 5.40 (br s, 1H), 3.24 and 3.23 (t, *J* = 7.2 Hz, 2H), 2.19 (q, *J* = 7.6 Hz, 2H), 1.53–1.44 (m, 2H), 1.33–1.23 (m, 10H), 1.15 (t, *J* = 7.6 Hz, 3H), 0.87 (t, *J* = 6.9 Hz, 3H). <sup>13</sup>C NMR (101 MHz, CDCl<sub>3</sub>) δ 173.8, 39.7, 31.9, 30.0, 29.8, 29.4, 29.3, 27.1, 22.8, 14.2, 10.1; ESI-MS: *m/z* 186.2 [M + H]<sup>+</sup>; ESI-HRMS: *m/z* 186.1689 [M + H]<sup>+</sup>; calculated 186.1858 for C<sub>11</sub>H<sub>24</sub>NO.

**2-Bromo-*N,N*-dioctylpropanamide (11).** A solution of Et<sub>3</sub>N (3.3 g, 33 mmol, 1.3 equiv.) and dioctylamine (5.9 g, 24.5 mmol, 0.98 equiv.) in Et<sub>2</sub>O (150 mL) was added dropwise to a solution of 2-bromopropionyl bromide (10; 5.4 g, 25 mmol, 1 equiv.) and Et<sub>3</sub>N (0.5 g, 4.9 mmol, 0.2 equiv.) in dry Et<sub>2</sub>O (200 mL) at 0 °C. After stirring for 2 h at room temperature, the solid was filtered off and the liquid phase was evaporated. The residue was dissolved in Et<sub>2</sub>O (100 mL) and washed with 10% HCl (3 × 100 mL). After filtration, the solution was dried with MgSO<sub>4</sub> and the solvent evaporated under reduced pressure to give the product (1.82 g, 99%) as an oil. <sup>1</sup>H NMR (400 MHz, CDCl<sub>3</sub>) δ 4.52 (q, *J* = 6.6 Hz, 1H), 3.61–3.39 (m, 2H), 3.17–3.01 (m, 2H), 1.81 (d, *J* = 6.6 Hz, 3H), 1.74–1.61 (m, 1H), 1.61–1.45 (m, 3H), 1.36–1.17 (m, 20H), 0.88 (q, *J* = 6.8 Hz, 6H). <sup>13</sup>C NMR (101 MHz, CDCl<sub>3</sub>) δ 168.9, 77.2, 48.2, 46.6, 38.7, 31.8, 31.75, 29.6, 29.4, 29.3, 29.2 (2×), 27.2, 26.9, 22.7, 22.6, 21.8, 14.1 (2×). ESI-MS: *m/z* 376.3 [M + H]<sup>+</sup>; ESI-HRMS: *m/z* 376.2627 [M + H]<sup>+</sup>; calculated 376.2137 for C<sub>19</sub>H<sub>39</sub>BrNO.

**2-Acetoxy-*N,N*-dioctylpropanamide (12).** A suspension of 2-bromo-*N,N*-dioctylpropanamide (11; 0.48 g, 1.26 mmol, 1 equiv.), potassium acetate (0.5 g, 5.05 mmol, 4 equiv.) and 18-crown-6 (10 mg, 0.04 mmol, 0.03 equiv.) in dry acetonitrile (10 mL) was refluxed for 5 h. The reaction mixture was filtered through celite and the solvent was evaporated. The solid residue was dissolved in Et<sub>2</sub>O (30 mL) and washed with water (3 × 20 mL). The organic solution was dried with MgSO<sub>4</sub> and the solvent evaporated to afford pure 12 (0.47 g, 94%) as an oil. <sup>1</sup>H NMR (400 MHz, CDCl<sub>3</sub>) δ 5.30 (q, *J* = 6.7 Hz, 1H), 3.48–3.38 (m, 1H), 3.32–3.12 (m, 3H), 2.11 (s, 3H), 1.76–1.62 (m, 1H), 1.63–1.46 (m, 3H), 1.43 (d, *J* = 6.7 Hz, 3H), 1.38–1.19 (m, 20H), 0.94–0.82 (m, 6H). <sup>13</sup>C NMR (101 MHz, CDCl<sub>3</sub>) δ 170.7, 169.9, 77.2, 67.0, 47.6, 46.3, 31.8 (2x), 29.3 (2x), 29.25, 29.2, 29.0, 27.5, 26.9 (2x), 22.7, 22.6, 20.9, 17.3, 14.1. ESI-MS: *m/z* 356.3 [M + H]<sup>+</sup>; ESI-HRMS: *m/z* 356.3131 [M + H]<sup>+</sup>; calculated 356.3086 for C<sub>21</sub>H<sub>42</sub>NO<sub>3</sub>.

**2-Methoxy-*N,N*-dioctylpropanamide (13).** A solution of 2-hydroxy-*N,N*-dioctylpropanamide (1; 500 mg, 1.6 mmol, 1 equiv.) in dry THF (15 mL) was added dropwise to a suspension of NaH (96 mg, 2.4 mmol, 1.5 equiv.) in dry THF (20 mL) at



0 °C, whereupon the suspension was stirred at room temperature for 1 h. Subsequently, MeI (150  $\mu$ L, 335 mg, 2.4 mmol, 1.5 equiv.) was added and the mixture was stirred overnight. After evaporation of the solvent, the residue was dissolved in Et<sub>2</sub>O (30 mL), and the resulting solution washed with saturated NH<sub>4</sub>Cl (3  $\times$  30 mL), dried with MgSO<sub>4</sub>, whereupon the solvent was evaporated under reduced pressure. The residue was passed through a short plug of silica (hexane:ethyl acetate = 3:1) to afford the product (420 mg, 80%) as an oil. <sup>1</sup>H NMR (400 MHz, CDCl<sub>3</sub>)  $\delta$  4.14 (q,  $J$  = 6.6 Hz, 1H), 3.42–3.20 (m, 4H), 3.31 (s, 3H), 1.64–1.47 (m, 4H), 1.36 (d,  $J$  = 6.6 Hz, 3H), 1.34–1.20 (m, 20H), 0.96–0.80 (m, 6H). <sup>13</sup>C NMR (101 MHz, CDCl<sub>3</sub>)  $\delta$  171.4, 77.2, 75.1, 56.4, 47.0, 45.95, 31.8 (2 $\times$ ), 29.4, 29.3 (3 $\times$ ), 29.2, 27.5, 27.1, 26.9, 22.6, 17.8, 14.1. ESI-MS:  $m/z$  328.3 [M + H]<sup>+</sup>; ESI-HRMS:  $m/z$  328.3190 [M + H]<sup>+</sup>; calculated: 328.3137 for C<sub>20</sub>H<sub>42</sub>NO<sub>2</sub>.

### Solvent extraction studies

Organic solutions of degradation compounds were prepared by dissolving the appropriate amount of each of them, up to 0.1 mol L<sup>-1</sup> in TPH. The extraction experiments were performed by mixing 500  $\mu$ L of both, the organic phase and the aqueous phase at room temperature (22  $\pm$  2 °C) for 15 or 60 min, respectively. After centrifugation (2500 or 5000 rpm), the phases were separated and aliquots of each phase (300  $\mu$ L) were taken for analysis. Used HPGe detectors were supplied by Canberra electronics or EG&G Ortec, equipped with the Genie-2000 or Gamma Vision software, respectively. The gamma lines at 59.5 keV (35.9%) and 121.8 keV (28.4%) were analyzed for <sup>241</sup>Am and <sup>152</sup>Eu, respectively. The results are reported as distribution ratios  $D$  ( $D_M = [M^{3+}]_{org}/[M^{3+}]_{aq}$ ), which have an uncertainty of  $\pm 5\%$ , and detection limits are  $500 > D > 0.002$ . Non-radioactive elements present in the samples were analyzed using a Sector Field Inductively Coupled Plasma Mass Spectrometer (Thermo Scientific™ iCAP™ Q ICP-MS) or a Quadrupole Perkin Elmer Sciex ELAN 6100 DRC ICP-MS. The aqueous phases were measured directly after adequate dilution; the organic phase was mixed with a matrix of 1% HNO<sub>3</sub> containing the non-ionic surfactant TRITON-X-100 and diluted to an adequate concentration.

### Microcalorimetry and van't Hoff studies

Microcalorimetric titrations were performed at 25.00  $\pm$  0.05 °C using a 2277 thermal activity monitor microcalorimeter (TA instruments).

Liquid–liquid extraction of metals (Nd<sup>3+</sup> and Yb<sup>3+</sup>) from an aqueous phase to an organic phase containing the ligand was performed as follows: 500  $\mu$ L of an aqueous phase (0.06 mol L<sup>-1</sup> of metal nitrate in a solution containing 0.1 mol L<sup>-1</sup> HNO<sub>3</sub> and 0.9 mol L<sup>-1</sup> LiNO<sub>3</sub> ( $I$  = 1 mol L<sup>-1</sup>)) and 300  $\mu$ L of an organic phase (0.1 mol L<sup>-1</sup> TODGA or Me-TODGA in a mixture of *n*-dodecane/1-octanol (95/5)) were introduced in a calorimetric cell. Each titration experiment consisted of 10 injections of 15  $\mu$ L of the organic phase containing 0.1 mol L<sup>-1</sup> of the ligand. Prior to microcalorimetry titration, organic phases were pre-equilibrated with an identical aqueous phase without the metal cation. In order to respect the equilibrium kinetics, the time of

the measurement was set to 90 minutes between each addition. The aqueous phase was sampled after the calorimetric run and analyzed by ICP-AES to determine the amount of metal cations transferred into the organic phase. The global heat of reaction has to take into account the multiple reactions that occur in the cell during the extraction process, and especially the dilution of both phases during the extraction process. These additional heats have to be identified, measured, and subtracted from the titration heat thermogram in order to assess the extraction heat. The measurement of the heat released during the extraction led to the determination of the enthalpy change  $\Delta H'$ . Knowing the  $\Delta G'$  value, it is possible to calculate the entropy change  $\Delta S'$ .

The van't Hoff method was used by contacting and shaking equal volumes (500  $\mu$ L) of aqueous and organic solutions for 30 minutes in a thermostatic cell at different temperatures (from 288 to 311 K). The temperature was measured precisely and the concentration of neodymium in each phase was determined using ICP-AES in order to obtain the cation distribution coefficient variation as a function of temperature.

The heat of formation of complexes was measured after the addition of seventeen aliquots (15  $\mu$ L each) of about 10<sup>-2</sup> mol L<sup>-1</sup> of the lanthanide cation solution, in a microcalorimetric cell containing 2.5 mL of the ligand solution. All the solutions were prepared in methanol. Titrations were carried out at 25 °C. Changes in enthalpies also include the heat of dilutions. Hence, a blank experiment with the addition of metal solution into 2.5 mL of pure solvent (methanol in this case) was performed in order to obtain the enthalpy values related to the complexation reaction. The overall stability constants ( $\beta'$ ) and the enthalpies of complexation ( $\Delta H'$ ) were refined simultaneously from the recorded data using the ligand binding analysis program DIGITAM version 4.1.<sup>27</sup> The corresponding overall entropies of complexation ( $\Delta S'$ ) were calculated from the expression  $\Delta G' = \Delta H' - T\Delta S'$ , knowing that  $\Delta G' = -RT \ln \beta'$ . Chemical calibration was made by determination of the complexation enthalpy of Ba<sup>2+</sup> with 18C6 in water or of Rb<sup>+</sup> with 18C6 in methanol, as recommended.<sup>28</sup>

## Results and discussion

To study the Me-TODGA degradation products, irradiation experiments as described in ref. 20 were intensified and were carried out at the Náyade facility at 23  $\pm$  2 °C, with an integrated dose of up to 250, 500, 750 and 1000 kGy, at 1.78 and 6.32 kGy h<sup>-1</sup> dose rates. After irradiation, no precipitate was observed, but the samples got a slightly yellow color when the integrated dose increased. This effect was especially observed for samples irradiated at a low dose rate, since more time was necessary to get an integrated dose of 1000 kGy.

Fig. 3 shows the qualitative HPLC-DAD analysis of Me-TODGA samples irradiated with 6.32 kGy h<sup>-1</sup>. At 250 kGy the chromatogram shows the presence of at least ten new peaks corresponding to the degradation compounds formed. The intensity of these new signals increase with the integrated dose

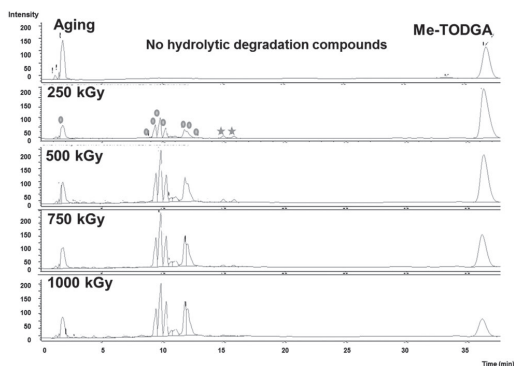


Fig. 3 HPLC-DAD chromatograms of aging and irradiated Me-TODGA samples, irradiated at  $6.32 \text{ kGy h}^{-1}$  in 100% TPH pre-equilibrated with  $3 \text{ mol L}^{-1} \text{ HNO}_3$  (circles indicate compounds with increasing intensity, stars indicate compounds with decreasing intensity).

(marked as circles in Fig. 3), while the Me-TODGA signal decreases, a result in agreement with previous work on *m*-xylene bisdiglycolamide.<sup>16</sup> However, it is important to mention that the minor degradation compounds observed at 250 kGy, marked as stars in Fig. 3, disappear as the integrated dose increases. This behaviour indicates that the initial compounds are sensitive to irradiation, which was not observed with irradiated TODGA samples. These results are in good agreement with our previous work.<sup>20</sup>

### Synthesis of the studied compounds

Among all the Me-TODGA degradation compounds identified, nine molecules (**1** to **9** Fig. 4) were synthesized to verify their structures, quantify them in irradiated solutions and study their influence in a liquid–liquid extraction process. The extraction properties, third phase formation and behaviour during the stripping step were followed. To compare the TODGA and Me-TODGA radiolytic behaviour, the degradation compound **I** (the TODGA degradation product obtained by the loss of one

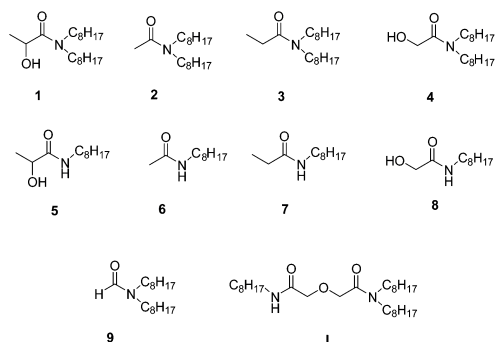


Fig. 4 Structures of the degradation products of Me-TODGA (**1** to **9**) and TODGA (**I**).

octyl group) was also synthesized. Similar degradation was identified with Me-TODGA,<sup>20</sup> however, the related chromatographic peaks (at 14.9 and 15.7 min in Fig. 3) disappear as the integrated dose increases. The structures of the synthesized and individually studied degradation products are summarized in Fig. 4.

TODGA was synthesized *via* a modified route compared to the published one, working under an air atmosphere and without drying solvents and glassware.<sup>17,29</sup> Me-TODGA was synthesized following the methodology described before.<sup>14</sup> Compounds **1**, **2**, **4**, **5**, **6**, **8** and **9** were prepared according to the procedure described in previous studies.<sup>16,17,30–32</sup>

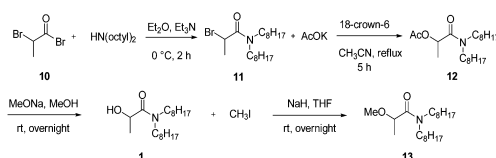
*N,N*-Diocetyl (**3**) and *N*-octyl propionamide (**7**) were prepared by reaction of propionyl chloride and the proper amine using Schotten–Baumann conditions in 93 and 96% yields, respectively.

To better study the possible influence of the hydroxyl group in propanamide **1**, 2-acetoxy-**(12)** and 2-methoxy-*N,N*-dioctylpropanamide (**13**) were also prepared as summarized in Scheme 1. 2-Bromopropionyl bromide **10** was reacted with dioctylamine to give propanamide **11** in 99% yield. A subsequent reaction of **11** with potassium acetate in the presence of 18-crown-6 gave the target compound **12** in 94% yield. In its  $^1\text{H}$  NMR spectrum the  $\text{CH}_3\text{C}(\text{O})$  peak is at  $\delta$  2.11, while the  $\text{CHC}(\text{O})$  signal shifted from  $\delta$  4.52 (q) in **11** to  $\delta$  5.30 (q) in **12** and the  $\text{CHCH}_3$  methyl absorption band shifted from  $\delta$  1.81 (d) to  $\delta$  1.43 (d). Saponification of the ester moiety in **12** with sodium methoxide afforded **1** in 93% yield, which was reacted with methyl iodide in the presence of NaH as a base to afford **13** in 80% yield. The  $^1\text{H}$  NMR spectrum exhibits a characteristic singlet for the methoxy group at  $\delta$  3.31, while in this case the  $\text{CHCH}_3$  resonates at  $\delta$  4.14 (q) and  $\delta$  1.36 (d).

### Quantification of Me-TODGA degradation products

The new results obtained with these synthesized degradation compounds confirmed the main bond ruptures (Fig. 2) as well as the structure of the identified compounds due to both degradation pathways, hydrolytic degradation of amide groups and radiation damage.<sup>20</sup>

Fig. 5 shows the results obtained from quantitative HPLC-MS analysis of a  $0.1 \text{ mol L}^{-1}$  solution of Me-TODGA in TPH after 1000 kGy irradiation with two different dose-rates ( $1.78$  and  $6.32 \text{ kGy h}^{-1}$ ). The concentration of the degradation compounds confirms the preference of degradation path 'a' in Fig. 2, since the amounts of **1** and **2** are higher than those of **3** and **4**. These findings support the assumption that the introduction of an additional methyl group in the diglycolamide backbone increases the radiolytic resistance of the substituted C–O linkage.



Scheme 1 Synthesis of 2-acetoxy (**12**) and 2-methoxy-*N,N*-dioctylpropanamide (**13**).

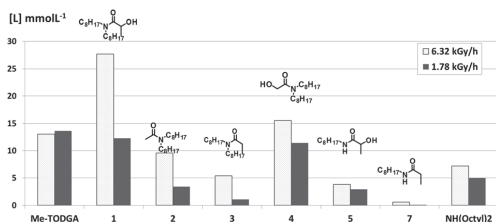


Fig. 5 Quantitative determination of the remaining Me-TODGA concentration and the most relevant degradation products present in an irradiated Me-TODGA sample by HPLC-MS (APCI<sup>+</sup>) (initial Me-TODGA concentration: 0.1 mol L<sup>-1</sup> in TPH pre-equilibrated with 3 mol L<sup>-1</sup> HNO<sub>3</sub>, 1000 kGy).

## Solvent extraction behaviour

### Extraction of Ln and fission products by degradation products.

The extraction of Am(III) and Eu(III) using an irradiated Me-TODGA solvent was assessed by contacting the solvent with <sup>241</sup>Am and <sup>152</sup>Eu spiked tracer solutions. The distribution ratios obtained with reference, aging and irradiated Me-TODGA samples are represented in Fig. 6. The low influence of dose rate could be explained by the low hydrolytic degradation in an apolar diluent such as TPH, where hydrolysis reaction is not favoured. The radiolytic degradation effect can be observed from 250 kGy where the *D*<sub>M(III)</sub> values decrease progressively for Am(III) and Eu(III) at both dose rates (1.78 and 6.32 kGy h<sup>-1</sup>). Previous studies estimated that after around 1–2 years of operation of the DIAMEX process (which is also a first step after PUREX), the organic phases will be exposed to around 800 kGy.<sup>33</sup> Me-TODGA (as TODGA) systems show a sufficient extraction capability (1 < *D* < 10) for Am(III) and Eu(III) even after 750 kGy of the absorbed dose. When both systems are compared under the same experimental conditions (Fig. 6), the TODGA system looks more resistant. Even if the initial extraction is higher with TODGA, the sensitivity of Me-TODGA upon irradiation is more important as indicated by the reduction of the concentration by 50% after 250 kGy.<sup>20</sup> Moreover, the extraction behaviour of degradation compounds may be different. As described previously, only compounds **1** and **4** showed extraction properties for Ln(III), especially compound **1**, which still has a diglycolamide structure and may play a role in retaining the original performance of TODGA samples.<sup>17</sup> A similar degradation compound to **1** was

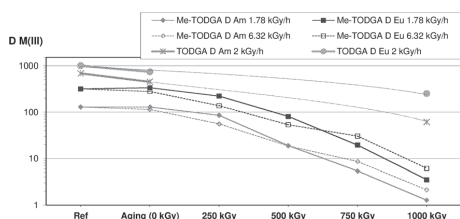


Fig. 6 Am(III) and Eu(III) distribution ratios obtained by extraction with reference, aging and irradiated Me-TODGA and TODGA samples at different integrated doses and dose rates. Organic phase: 0.1 mol L<sup>-1</sup> TODGA or Me-TODGA in TPH. Aqueous phase: <sup>241</sup>Am and <sup>152</sup>Eu in 3 mol L<sup>-1</sup> HNO<sub>3</sub>. TODGA data are taken from ref. 17.

also identified for Me-TODGA, however, as we mentioned before this compound disappears as the dose increases, being eligible after 750 kGy (Fig. 3, 14.9–15.7 min). Therefore compound **1** seems to be more sensitive to irradiation.

To better evaluate the performance of irradiated Me-TODGA solvents, for example as substitutes for TODGA in a GANEX (Grouped Actinide Extraction) process,<sup>34,35</sup> the extraction of Ln and FPs by Me-TODGA and the main degradation compounds was assessed. In order to compare the affinity of degradation compounds toward Ln and FPs, similar compositions were selected, although the concentrations of each degradation compound differ in irradiated solvents as presented in Fig. 5: the concentration of each molecule of 0.1 mol L<sup>-1</sup> in TPH or kerosene and 3 and 4 mol L<sup>-1</sup> HNO<sub>3</sub>. The *D* values obtained previously showed that among compounds **2**, **4**, **6** and **8**, only **4** is able to extract Ln(III) as well as <sup>241</sup>Am(III) with a *D* value around 1 (*D*<sub>Am</sub> = 1.5; *D*<sub>Eu</sub> = 1.6) from an aqueous solution at 3 mol L<sup>-1</sup> HNO<sub>3</sub>.<sup>17</sup> The extraction studies of Me-TODGA and the fragments **1**, **3**, **5** and **7** were carried out simultaneously at Jülich and CIEMAT and the data are in good agreement. It turned out that none of the tested compounds showed comparable distribution ratios as Me-TODGA under these conditions. Distribution ratios measured at lower nitric acid concentrations (not shown) were even lower, in line with literature data.<sup>15</sup> These data explain why upon degradation of Me-TODGA a significant decrease of Am(III) and Eu(III) extraction is observed, its degradation products not being able to retain the extraction ability in contrast to bis-DGAs<sup>16</sup> and TODGA degradation compounds<sup>17,36</sup> (in particular **1** (Fig. 4)) which showed significant *D* values (*D*<sub>Am</sub> = 3.5; *D*<sub>Eu</sub> = 30).<sup>13</sup>

To check the presence of possible higher distribution ratios under the conditions used in the GANEX process, the extraction of Ln(III), Am and FPs from the synthetic HAR solution<sup>26</sup> by Me-TODGA and its degradation compounds was assessed at a higher nitric acid concentration (4 mol L<sup>-1</sup> HNO<sub>3</sub>). The *D* values presented in Fig. 7 showed that under these conditions, compounds **1** and **4** are able to extract Ln(III) and <sup>241</sup>Am effectively (especially compound **4** which shows *D*<sub>Ln(III)</sub> values > 1).

Regarding the FPs and the rest of the Ln elements, metals such as Zr, Mo and Pd were co-extracted mainly due to the presence of compounds **1**, **2**, **4** and **5**, which have also shown solubility problems in apolar diluents as TPH or kerosene at a concentration of 0.1 mol L<sup>-1</sup>.<sup>36</sup> At high nitric acid concentrations, the distribution ratios of all other FPs are < 0.1 except for Cu (*D* around 0.3–6.2).

To study the possible influence of the hydroxyl group on the extraction ability of compounds **1** and **4**, the hydroxyl group of **1** was protected as methoxy and acetoxy groups, *i.e.* compounds **12** and **13** (Scheme 1). These compounds were tested with a similar concentration (0.1 mol L<sup>-1</sup> in TPH) and with different nitric acid concentrations (from 0.01 to 4.1 mol L<sup>-1</sup>). Distribution ratios for both nuclides, <sup>241</sup>Am and <sup>152</sup>Eu, were very low (*D* < 0.002) and therefore are not shown here. These results indicate that the presence of the –OH functional group in compounds **1** and **4** contributes to the extraction.

Since 2-hydroxypropionamide (**1**) is one of the major degradation compounds and one of the few compounds able to extract Ln(III), further experiments were conducted using higher

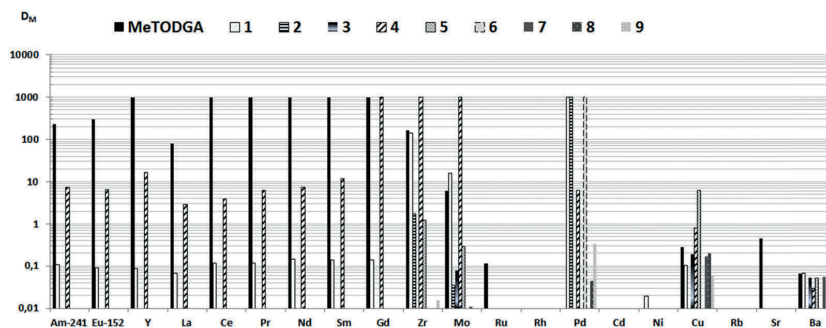


Fig. 7 Extraction studies of Am(III), Ln(III) and selected FPs (from the synthetic HAR solution – ref. 26) by Me-TODGA and the main degradation compounds. Organic phase: 0.1 mol L<sup>-1</sup> Me-TODGA in kerosene. Aqueous phase: 4 mol L<sup>-1</sup> HNO<sub>3</sub> containing given elements including the <sup>241</sup>Am/<sup>152</sup>Eu tracer (*T* = 23 °C). Me-TODGA *D*<sub>Pd</sub> was removed due to problems with the measurement.

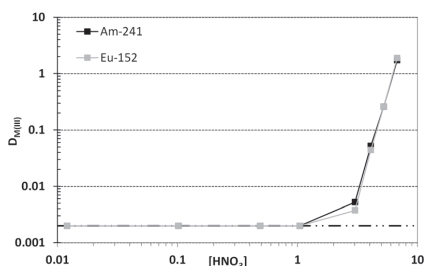


Fig. 8 Distribution ratios of Am and Eu by 2-hydroxypropionamide (**1**) for different nitric acid concentrations. Organic phase: 0.1 mol L<sup>-1</sup> of **1** in TPH. Aqueous phase: HNO<sub>3</sub> with <sup>241</sup>Am/<sup>152</sup>Eu tracers. Contact time 60 minutes at 22 °C.

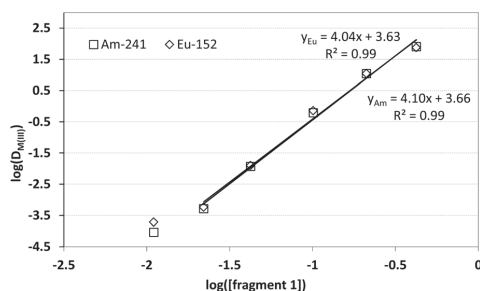


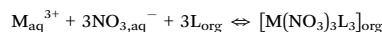
Fig. 9 Slope analysis for 2-hydroxypropionamide (**1**). Organic phase: varying concentrations of **1** in TPH. Aqueous phase: constant nitric acid concentration of 6.8 mol L<sup>-1</sup>, containing the <sup>241</sup>Am/<sup>152</sup>Eu tracer. Extraction for 60 minutes at 22 °C.

nitric acid concentrations. Experiments up to 6.8 mol L<sup>-1</sup> HNO<sub>3</sub> provided distribution ratios of *D*<sub>Am</sub> = 1.7, and *D*<sub>Eu</sub> = 1.9 (Fig. 8).

Hence, the concentration of degradation product **1** was varied and a slope analysis was conducted from the log-log plot shown in Fig. 9 to obtain information about the complex stoichiometry. Therefore, the concentration of **1** was increased, while the nitric acid concentration was kept constant at 6.8 mol L<sup>-1</sup>. The slope of the linear fit of the logarithmic distribution ratio as a function of the logarithmic ligand concentration provides a slope of 4.04 and 4.10 for <sup>152</sup>Eu and <sup>241</sup>Am, respectively. Therefore, it is concluded that degradation product **1** forms 1:4 complexes with americium(III) as well as europium(III), assuming that 2-hydroxypropionamide is not consumed by co-extraction of nitric acid and is a monomer in TPH.

**Thermodynamic properties related to the extraction of lanthanides.** To better understand the driving force of extraction, thermodynamic properties related to lanthanide extraction by TODGA and Me-TODGA were measured mainly by microcalorimetry. Even if a few studies<sup>37,38</sup> are available, microcalorimetry remains the reference method to obtain enthalpic extraction data. Two lanthanides in the series were selected: Yb<sup>3+</sup> and Nd<sup>3+</sup> (comprehensive information is given in the Experimental section).

The extraction equilibrium considered in this study corresponds to the formation of [M(NO<sub>3</sub>)<sub>3</sub>L<sub>3</sub>] (*L* = TODGA or Me-TODGA and *M* = Yb<sup>3+</sup> or Nd<sup>3+</sup>) as previously described for lanthanides.<sup>15,39,40</sup>



with *K*<sub>ext</sub>', the extraction constant, defined as

$$K_{ext}' = \frac{[M(NO_3)_3L_3]_{(org)}}{[M^{3+}][NO_3^{-}]^3[L]_{(org)}^3}$$

The different concentrations were calculated as follows: [M(NO<sub>3</sub>)<sub>3</sub>L<sub>3</sub>]<sub>(org)</sub> = *C*<sub>M</sub><sup>org</sup>, [M<sup>3+</sup>] = *C*<sub>M</sub><sup>aq</sup> (the complexation by nitrate is negligible under these conditions), [NO<sub>3</sub><sup>-</sup>] = *C*<sub>NO<sub>3</sub></sub><sup>init</sup> – 3*C*<sub>M</sub><sup>org</sup>. [*L*] = *C*<sub>L</sub><sup>org</sup> – 3*C*<sub>M</sub><sup>org</sup>. The activity coefficients were not considered since the ionic force in the aqueous phase was similar and constant in all experiments. Gibbs energy modification and entropy modification, Δ<sub>ext</sub>*G*' and Δ<sub>ext</sub>*S*', respectively, were calculated from the following equations:

$$\Delta_{ext}G' = RT \ln K_{ext}'$$

$$\Delta_{ext}G' = \Delta_{ext}H' - T\Delta_{ext}S'$$

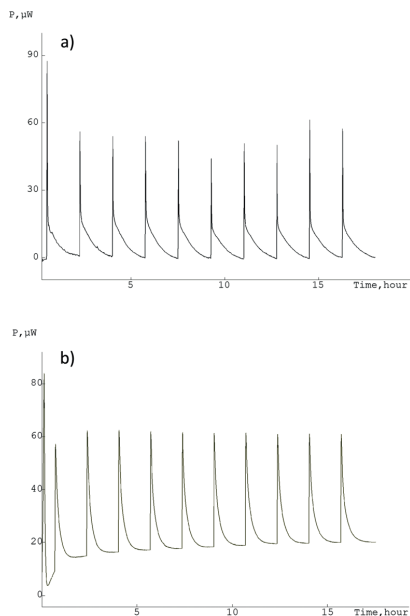


Fig. 10 Thermograms of the extraction by TODGA of  $\text{Yb}^{3+}$  (a) and of  $\text{Nd}^{3+}$  (b);  $T = 25^\circ\text{C}$ . Initial conditions: 500  $\mu\text{L}$  of aqueous phase,  $C_{\text{Nd or Yb}} = 0.06 \text{ mol L}^{-1}$  in  $0.1 \text{ mol L}^{-1} \text{HNO}_3 - 0.9 \text{ mol L}^{-1} \text{LiNO}_3$  and 300  $\mu\text{L}$  of organic phase,  $0.1 \text{ mol L}^{-1}$  TODGA in  $n$ -dodecane/1-octanol (95/5) pre-equilibrated. Addition of  $10 \times 15 \mu\text{L}$  organic phase, stirring with gold propeller (120 rpm).

with  $R$  being the gas constant and  $T$  the temperature in Kelvin.

Thermograms obtained by the extraction of  $\text{Yb}^{3+}$  and  $\text{Nd}^{3+}$  by TODGA are shown in Fig. 10. Among all dilution experiments performed, only the dilution of the organic phase showed significant heat effects. These experimental data allowed the determination of  $\Delta_{\text{ext}}H$ , the enthalpy change during the extraction process. The heat released during the extraction of  $\text{Yb}^{3+}$  and  $\text{Nd}^{3+}$  by Me-TODGA was very low and no reliable results were obtained.

In order to compare the extraction data obtained with TODGA and Me-TODGA, the Nd extraction enthalpies were also determined using the van't Hoff method under similar chemical conditions. The variation of the distribution ratio with temperature was measured and the variation of  $K_{\text{ext}}'$  is presented in Fig. 11.

According to this approach, the enthalpy variation for the investigated extraction reaction ( $\Delta_{\text{ext}}H'$ ) can be deduced from the temperature dependence of the extraction equilibrium constant:

$$\ln(K_{\text{ext}}') = -\frac{\Delta_{\text{ext}}H'}{RT} + \frac{\Delta_{\text{ext}}S'}{R}$$

Thermodynamic parameters related to the extraction of  $\text{Yb}^{3+}$  and  $\text{Nd}^{3+}$  by TODGA and Me-TODGA using microcalorimetry and the van't Hoff method are reported in Table 1.

In the case of TODGA the enthalpy variations obtained using both the van't Hoff method and microcalorimetry are in very

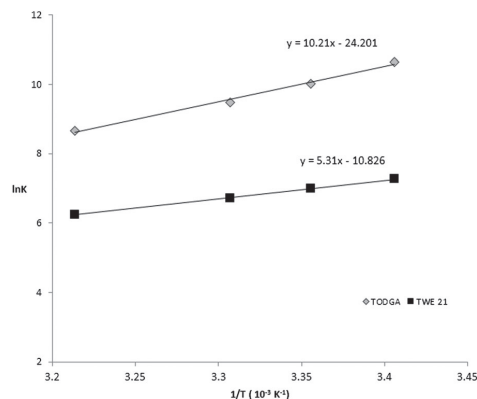


Fig. 11 Variation of the extraction constant of  $\text{Nd}(\text{NO}_3)_3$  by  $0.1 \text{ mol L}^{-1}$  TODGA and  $0.1 \text{ mol L}^{-1}$  Me-TODGA in  $n$ -dodecane/1-octanol (95/5) as a function of the reverse of the temperature (conditions:  $C_{\text{Nd}} = 0.06 \text{ mol L}^{-1}$  in  $0.1 \text{ mol L}^{-1} \text{HNO}_3 - 0.9 \text{ mol L}^{-1} \text{LiNO}_3$  – organic phase:  $0.1 \text{ mol L}^{-1}$   $C_{\text{ligand}}$  in  $n$ -dodecane/1-octanol (95/5) pre-equilibrated).

good agreement. The Gibbs energy modifications ( $-\Delta G$ ) are similar for both cations  $\text{Nd}^{3+}$  and  $\text{Yb}^{3+}$  and are consistent with the values obtained with  $\text{Eu}^{3+}$  studied by Arisaka and Kimura.<sup>39</sup> The thermodynamic data reported in Table 1 indicate that the reaction is exothermic ( $\Delta H < 0$ ) and enthalpy-driven, as often observed with extraction by solvation. This feature could be explained by a strong interaction between the ligand and the cation.

The extraction of  $\text{Nd}^{3+}$  and  $\text{Yb}^{3+}$  by Me-TODGA led to less important values than in the case of TODGA ( $\Delta\Delta G_{\text{TODGA-Me-TODGA}}' = -8 \text{ kJ mol}^{-1}$  and  $-19 \text{ kJ mol}^{-1}$  for  $\text{Nd}^{3+}$  and  $\text{Yb}^{3+}$ , respectively), which is consistent with the  $D$  values obtained for both ligands with lanthanides.

Due to these low values and considering the even lower values expected for degradation products of Me-TODGA, it was decided to obtain information on the affinity between some lanthanides and a selection of degradation compounds by dedicated complexation studies in homogeneous phases. This methodology is logical if we consider that binding is often the principal contribution, compared with transfer contributions and by modification of the solvation.

**Thermodynamic properties related to the complexation with lanthanides.** The complexation of three representative lanthanides ( $\text{La}^{3+}$ ,  $\text{Eu}^{3+}$  and  $\text{Yb}^{3+}$ ) with the extractants (TODGA and Me-TODGA) and six of their main degradation compounds (1, an exclusive TODGA degradation product, 1, 3, 4, 5 and 7 presented in Fig. 4) was studied in methanol using microcalorimetric titrations.

TODGA and Me-TODGA exhibited a similar behaviour in the presence of the three lanthanides. In all cases, thermograms obtained during complexation showed more important heat effects than those related to dilution of the salts. With  $\text{La}^{3+}$  and  $\text{Eu}^{3+}$ , exothermic signals were observed and after a ratio  $C_{\text{M}}/C_{\text{L}}$  of 0.5, the intensity of the peaks decreased and overlapped with that of dilution, indicating the end of complexation (Fig. 12).

**Table 1** Thermodynamic parameters related to the extraction of Yb<sup>3+</sup> and Nd<sup>3+</sup> by TODGA and Me-TODGA (*TAS* is given for *T* = 298 K).<sup>a</sup>

Ligand	Cations	<i>D<sub>M</sub></i> (25 °C)	−Δ <sub>ext</sub> <i>G</i> ' (kJ mol <sup>−1</sup> )	−Δ <sub>ext</sub> <i>H</i> ' (kJ mol <sup>−1</sup> )	microcalorimetry	van't Hoff	<i>T</i> Δ <sub>ext</sub> <i>S</i> ' (kJ mol <sup>−1</sup> )	Δ <sub>ext</sub> <i>S</i> ' (J mol <sup>−1</sup> K <sup>−1</sup> )
TODGA	Nd <sup>3+</sup>	0.61	25 (1)	82 (10)	84 (10)	−57 (2)	−200 (4)	−271
	Eu <sup>3+</sup> 39		34.7	116				
	Yb <sup>3+</sup>	0.85	32 (2)	119 (8)			−86 (9)	−291 (30)
Me-TODGA	Nd <sup>3+</sup>	0.21	17 (2)	n.d.	44 (3)	−28 (1)	−94 (2)	n.d.
	Yb <sup>3+</sup>	0.15	13 (1)	n.d.				

Conditions: *C*<sub>Nd</sub> = 0.06 mol L<sup>−1</sup> in 0.1 mol L<sup>−1</sup> HNO<sub>3</sub> – 0.9 mol L<sup>−1</sup> LiNO<sub>3</sub>, organic phase: *C*<sub>ligand</sub> = 0.1 mol L<sup>−1</sup> in *n*-dodecane/1-octanol (95/5) pre-equilibrated.<sup>a</sup> Values in parentheses are standard deviations (*σ*<sub>*n*−1</sub>). n.d. = not determined.

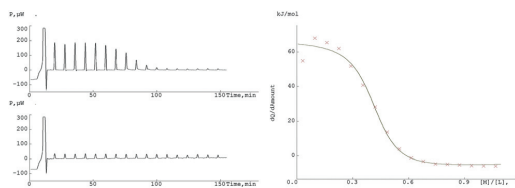


**Fig. 12** Microcalorimetric titration of TODGA with La<sup>3+</sup> in methanol (*T* = 25 °C). Left: Thermogram corresponding to the heat evolved during each addition of 17 × 15 μL of La(NO<sub>3</sub>)<sub>3</sub> in 2.5 mL of TODGA solution (*C*<sub>TODGA</sub> = 10<sup>−3</sup> mol L<sup>−1</sup>) – 0 ≤ *R* ≤ 1 – the lower thermogram corresponds to the dilution of the metal salt into the solvent. Right: Experimental and calculated values for the derivative curve *dQ/d*(amount) vs. *C<sub>M</sub>/C<sub>L</sub>*.

With Yb<sup>3+</sup>, at least two phenomena were observed: the first one is strongly exothermic, while the second one is weakly endothermic, showing clearly the formation of more than one species. At the end of the experiments, the intensity of the peaks resembled that of dilution after a ratio *C<sub>M</sub>/C<sub>L</sub>* > 1.

The results were fitted with the complexation reactions: Ln<sup>3+</sup> + *n*TODGA ↔ Ln(TODGA)<sub>*n*</sub><sup>3+</sup>. The weak complexation with NO<sub>3</sub><sup>−</sup> in methanol was neglected. Then, the related calculated values are apparent stability constants β<sub>*n*</sub>. With La<sup>3+</sup> and Eu<sup>3+</sup>, the derivative curve *dQ/d*(amount) vs. *C<sub>M</sub>/C<sub>L</sub>* obtained with the two ligands exhibited an inflexion point for *C<sub>M</sub>/C<sub>L</sub>* = 0.5 (Fig. 12 right for TODGA) corresponding to the formation of a ML<sub>2</sub> species in methanol with these cations. In contrast with Me-TODGA, this inflexion appeared at *C<sub>M</sub>/C<sub>L</sub>* = 0.3 corresponding to the formation of a ML<sub>3</sub> complex. For both ligands, the best interpretation of these data was obtained considering two species: ML<sub>2</sub> and ML<sub>3</sub>. These results are consistent with those determined in a mixture of water and ethanol (40/60%) by luminescence for TODGA.<sup>41</sup> The complexation of TODGA, Me-TODGA and Me<sub>2</sub>-TODGA (addition of two methyl groups to the central methylene carbon atoms of the TODGA) studied comparatively by solvent extraction and TRLFS showed the formation of ML and ML<sub>3</sub> complexes in ethanol solution for Cm<sup>3+</sup> and Eu<sup>3+</sup> and the conditional stability constants have been calculated.<sup>15</sup> In other studies, it was shown that the extraction of europium involves 1:2 and 1:2 and 1:3 (metal:TODGA) species, in polar and non-polar solvents, respectively.<sup>40,42</sup>

With Yb<sup>3+</sup>, the derivative curve showed an inflexion near *C<sub>M</sub>/C<sub>L</sub>* = 0.3, corresponding to the formation of an ML<sub>3</sub> complex. Taking into account a second ML species, deduced from the heat effects, the fit is slightly improved.

The speciation deduced from the thermograms is similar for the two ligands (Table 2); the presence of the methyl group does not influence the nature of the complexes. Thermodynamic parameters (log β', Δ*H*' and *T*Δ*S*') related to the formation of these species also revealed a similar behaviour for the two ligands, but with lower values for Me-TODGA, a trend which was observed previously with Eu<sup>3+</sup>.<sup>15</sup> The stabilization of these complexes is mainly enthalpy-driven, with the entropy contribution being slightly favorable or near zero. Therefore, the strength of the interaction between cations and ligands is the main factor governing the stability of the complexes. Nevertheless, differences appear for the entropic contribution in ML<sub>3</sub> species formation in the case of Eu<sup>3+</sup> and Yb<sup>3+</sup>. For Me-TODGA, the entropy is near zero, whereas for TODGA, negative values were found, suggesting a possible high order, assumed by the molecule in the final complex.

The complexation properties of six degradation products of TODGA and Me-TODGA (1, 3, 4, 5 and 7) towards the same three lanthanides were studied using the same experimental conditions as those used for the parent molecules. The stability constants and the thermodynamic parameters are presented in Table 2.

With TODGA degradation compound 1, significant exothermic peaks were observed during the titration of La<sup>3+</sup> and Eu<sup>3+</sup> at the beginning of the experiment and the intensity gradually decreased to reach the values of peaks related to dilution for a ratio *R* = *C<sub>M</sub>/C<sub>L</sub>*, close to 1. On the other hand, the *dQ/d*(amount) vs. *C<sub>M</sub>/C<sub>L</sub>* curve showed an inflexion at the ratio *R* = 0.5, as the TODGA parent molecule. These observations are in agreement with the formation of both ML and ML<sub>2</sub> species, a model which perfectly fits the experimental data (line in Fig. 13). With Yb<sup>3+</sup>, the thermogram presented similar phenomena as for TODGA: the first part is classical for a strongly exothermic reaction, while the second one, after a ratio of about 0.5, indicates weakly endothermic phenomena. At a ratio *R* = 1, the intensity of the peaks indicates an exothermic reaction. The derivative curve showed an inflexion near 0.3 corresponding to the formation of a ML<sub>3</sub> complex. Taking into account a second ML species the fit improved. In the presence of La<sup>3+</sup>, two species were determined with 1 (ML and ML<sub>2</sub>), whereas the formation of only one ML<sub>2</sub> species was observed with TODGA. The ML<sub>2</sub> species is less stable with 1 than with TODGA, the interaction seems to be weaker regarding the lower value of the enthalpy (−Δ*H* = 34 kJ mol<sup>−1</sup> for 1 and −Δ*H* = 48 kJ mol<sup>−1</sup> for TODGA). The entropy is near zero as for TODGA.



**Table 2** Stoichiometries (M:L), overall stability constants ( $\log \beta$ ) and thermodynamic parameters (in  $\text{kJ mol}^{-1}$ ) for lanthanide complexes with TODGA, Me-TODGA and degradation products **1**, **1** and **5** in methanol ( $T = 25\text{ }^{\circ}\text{C}$ )<sup>a</sup>

Chemical system	1:1 complexes				1:2 complexes				1:3 complexes			
	$\log \beta'$	$-\Delta G'$	$-\Delta H'$	$T\Delta S'$	$\log \beta'$	$-\Delta G'$	$-\Delta H'$	$T\Delta S'$	$\log \beta'$	$-\Delta G'$	$-\Delta H'$	$T\Delta S'$
La-TODGA					8.5 (3)	48 (2)	48 (2)	0.5 (4)				
La- <b>1</b>	3.20 (4)	18.2 (2)	9 (2)	9 (2)	6.30 (6)	35.9 (3)	34 (2)	2 (2)				
La-Me-TODGA					8.1 (1)	46.1 (2)	41 (1)	5 (1)				
La- <b>1</b>	2.67 (3)	15.2 (2)	17.0 (9)	-2 (1)								
La- <b>5</b>	2.9 (6)	17 (3)	4 (2)	13 (5)								
Eu-TODGA					8.58 (4)	48.9 (2)	48 (3)	0.9 (3)	12.2 (3)	69 (2)	87 (3)	-17 (5)
Eu- <b>1</b>					7 (1)	40 (6)	33.7 (1)	6 (6)	10 (1)	57 (6)	43 (9)	14 (15)
Eu-Me-TODGA					7.7 (3)	44 (2)	42 (5)	2 (7)	11.2 (4)	64 (2)	58 (7)	6 (9)
Eu- <b>1</b>	2.64 (5)	15.1 (3)	17.4 (9)	-2 (1)								
Eu- <b>5</b>	2.4 (2)	14 (1)	6 (1)	8 (2)								
Yb-TODGA	4.4 (3)	25 (2)	16 (1)	9 (3)					12.3 (4)	70 (2)	96 (1)	-26 (3)
Yb- <b>1</b>	3.0 (2)	17 (1)	-2 (6)	19 (7)					9 (1)	51 (6)	63 (2)	-12 (8)
Yb-Me-TODGA	4.00 (7)	22.8 (4)	15 (4)	8 (4)					11.9 (2)	68 (1)	67 (1)	1 (2)
Yb- <b>1</b>	3.2 (4)	18 (2)	18 (5)	0 (5)								
Yb- <b>5</b>	3.2 (4)	18 (2)	8 (1)	10 (3)								

<sup>a</sup> Values in parentheses are standard deviations ( $\sigma_{n-1}$ ) in the last significant digit.

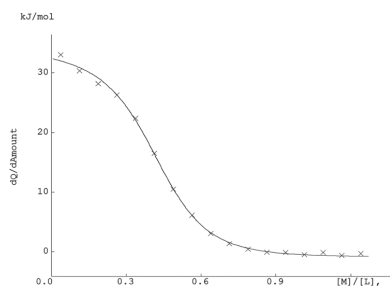


**Fig. 13** Microcalorimetric titration of **1** by  $\text{La}^{3+}$  in methanol ( $T = 25\text{ }^{\circ}\text{C}$ ). Experimental and calculated values for the derivative curve  $dQ/d(\text{amount})$  vs.  $C_M/C_L$ .

In the case of  $\text{Eu}^{3+}$  and  $\text{Yb}^{3+}$ , the experimental data were interpreted with the same complexes as for TODGA ( $\text{ML}_2$  and  $\text{ML}_3$  for  $\text{Eu}^{3+}$  and  $\text{ML}$  and  $\text{ML}_3$  for  $\text{Yb}^{3+}$ ), but with lower stability constants and with less negative enthalpies suggesting lower interactions. Differences appear for the entropic contribution to the formation of the  $\text{ML}_3$  species in the case of  $\text{Eu}^{3+}$ : near to the zero value for **1**, whereas for TODGA, negative values were found. Regarding the thermodynamic parameters for the  $\text{ML}$  complex in the  $\text{Yb}^{3+}/\text{I}$  system, the near to zero value of the enthalpy is compensated by a high value of the entropic term. For the  $\text{ML}_3$  species, enthalpy and entropy follow the same trends as for TODGA. They are characterized by a favourable enthalpic contribution and an unfavourable entropic term.

Concerning the complexation of 2-hydroxyacetamide **4** with lanthanides, studies conducted with similar ligand concentrations as performed with TODGA and Me-TODGA gave thermograms with slightly higher peaks for titration than for dilution. The increase in ligand concentration (8 times) in order to force complexation, led to significant heat effects, but no enthalpy value could be deduced because of non-reproducible data. Nevertheless, these results reveal

the interaction of **4** with  $\text{Ln}(\text{III})$  as also shown from the extraction results (Fig. 7).

The experiments performed with *N,N*-dioctylpropionamide (**3**) and *N*-octylpropionamide (**7**) with the three lanthanides, led to identical titration and dilution thermograms, even at high metal to ligand concentration ratios ( $R = C_M/C_L$  near 20) suggesting no complexation. These results are in agreement with the extraction studies (Fig. 7).

With compounds **1** and **5**, bearing one hydroxyl group, the profiles of the thermograms with the three lanthanides were very similar, showing exothermic peaks being significantly higher than those obtained for dilution, suggesting the occurrence of complexation with these cations. For both ligands, the best interpretation for the three lanthanides was obtained considering only one  $\text{ML}$  species with low stability ( $\log \beta$  between 2.4 and 3.2). This can be explained by the small size of these molecules containing less donor atoms compared to TODGA and Me-TODGA. The stability constants determined for **1** and **5** (Table 2) are in the same order of magnitude for each cation and no selectivity is observed along the lanthanide series. This stoichiometry is not consistent with that determined with slope analysis (Fig. 9) and this feature should be deepened. In the case of **1**, the stabilization is enthalpy-driven ( $\Delta H$  around  $-17.5\text{ kJ mol}^{-1}$  with the three lanthanides), suggesting a strong interaction which could be provided from the formation of a 6-membered chelate. A major enthalpic contribution was also observed during solvent extraction; the entropic contribution remains low or negative.

## Conclusions

We investigated the effect of  $^{60}\text{Co}$   $\gamma$ -irradiation on the extraction behaviour of Me-TODGA. Upon irradiation ten degradation compounds were identified. Among them the products originating from the rupture of the ether linkage are most abundant. 2-Hydroxypropionamide (**1**) and *N,N*-dioctylacetamide (**2**) are formed by preferred rupture on the non-substituted side of the

molecule. Despite previous results revealing that the degradation rate constant of the ligand Me-TODGA is higher than TODGA, the introduction of a methyl group in the diglycolamide backbone increases the radiolytic resistance of the substituted C–O linkage over the unsubstituted C–O bond. At high acidity, the main degradation products impacting the extraction of lanthanides,  $^{241}\text{Am}$  and some fission products are 2-hydroxyalkylamides. Dedicated extraction studies performed with degradation products **1** and **4** alone support their affinity towards Zr, Mo and Pd. When the hydroxyl group is replaced by a methoxy or acetoxy group, the extraction of Eu(III) and Am(III) decreases. During the process, the compounds that should be monitored are 2-hydroxyalkylamides.

To better understand the driving force of lanthanide extraction and to study the interactions between lanthanides and ligands, thermodynamic studies were performed not only in biphasic systems, but also in homogeneous solution (methanol). The extraction and complexation with TODGA and Me-TODGA are always enthalpy driven. Among the TODGA and Me-TODGA degradation products studied by microcalorimetry, the compounds **1**, **4** and **5** showed significant heat effects, which were related to a strong interaction with the three lanthanides. Unlike the initial diglycolamides TODGA and Me-TODGA, which give 1 : 1, 1 : 2 and 1 : 3 (metal : ligand) complexes with lanthanides, the 2-hydroxyalkylamides produced upon radiolysis, only form 1 : 1 complexes, consistent with the formation of chelates. This study shows the importance of a detailed analysis of complexation in solution to understand extraction processes.

## Conflicts of interest

There are no conflicts to declare.

## Acknowledgements

Financial support was provided by two European projects ACSEPT (contract No. FP7-CP-2007-211267) and SACSESS (Contract No. FP7-Fission-2012-323-282).

## Notes and references

- C. Madic, M. Lecomte, P. Baron and B. Boullis, *C. R. Phys.*, 2002, **3**, 797–811.
- D. Serrano-Purroy, P. Baron, B. Christiansen, C. Sorel and J.-P. Glatz, *Radiochim. Acta*, 2005, **93**, 351–355.
- M. Miguiditchian, L. Chareyre, X. Hérès, C. Hill, P. Baron and M. Masson, *Proc. GLOBAL 2007, Advanced Nuclear Fuel Cycles and Systems*, American Nuclear Society, Boise, Idaho, 2007, pp. 550–552.
- M. Miguiditchian, X. Heres, M. Masson and C. Poinssot, *Abstracts of Papers, 247th ACS National Meeting & Exposition*, Dallas, TX, United States, March 16–20, 2014, NUCL-43.
- A. Wilden, G. Modolo, P. Kaufholz, F. Sadowski, S. Lange, M. Sypula, D. Magnusson, U. Muellich, A. Geist and D. Bosbach, *Solvent Extr. Ion Exch.*, 2015, **33**, 91–108.
- Reprocessing and Recycling of Spent Nuclear Fuel*, ed. R. Taylor, Woodhead Publishing, Oxford, 2015.
- Y. Sasaki, Y. Sugo, S. Suzuki and S. Tachimori, *Solvent Extr. Ion Exch.*, 2001, **19**, 91–103.
- S. A. Ansari, P. N. Pathak, V. K. Manchanda, M. Husain, A. K. Prasad and V. S. Parmar, *Solvent Extr. Ion Exch.*, 2005, **23**, 463–479.
- D. Magnusson, B. Christiansen, J.-P. Glatz, R. Malmbeck, G. Modolo, D. Serrano-Purroy and C. Sorel, *Solvent Extr. Ion Exch.*, 2009, **27**, 26–35.
- G. Modolo, A. Wilden, A. Geist, D. Magnusson and R. Malmbeck, *Radiochim. Acta*, 2012, **100**, 715–725.
- J. Brown, F. McLachlan, M. J. Sarsfield, R. J. Taylor, G. Modolo and A. Wilden, *Solvent Extr. Ion Exch.*, 2012, **30**, 127–141.
- S. A. Ansari, P. Pathak, P. K. Mohapatra and V. K. Manchanda, *Chem. Rev.*, 2012, **112**, 1751–1772.
- G. Modolo, A. Wilden, P. Kaufholz, D. Bosbach and A. Geist, *Prog. Nucl. Energy*, 2014, **72**, 107–114.
- M. Iqbal, J. Huskens, W. Verboom, M. Sypula and G. Modolo, *Supramol. Chem.*, 2010, **22**, 827–837.
- A. Wilden, G. Modolo, S. Lange, F. Sadowski, B. B. Beele, A. Skerencak-Frech, P. J. Panak, M. Iqbal, W. Verboom, A. Geist and D. Bosbach, *Solvent Extr. Ion Exch.*, 2014, **32**, 119–137.
- H. Galán, M. T. Murillo, R. Sedano, A. Núñez, J. de Mendoza, A. Gonzalez-Espartero and P. Prados, *Eur. J. Org. Chem.*, 2011, 3959–3969.
- H. Galán, A. Núñez, A. Gonzalez-Espartero, R. Sedano, A. Durana and J. de Mendoza, *Procedia Chem.*, 2012, **7**, 195–201.
- B. J. Mincher, G. Modolo and S. P. Mezyk, *Solvent Extr. Ion Exch.*, 2009, **27**, 1–25.
- Y. Katsumura, *The Chemistry of Free Radicals: N-Centered Radicals*, ed. Z. B. Alfassi, Wiley, Weinheim, 1998, ch. 12, pp. 393–412.
- H. Galán, C. A. Zarzana, A. Wilden, A. Núñez, H. Schmidt, R. J. M. Egberink, A. Leoncini, J. Cobos, W. Verboom, G. Modolo, G. S. Groenewold and B. J. Mincher, *Dalton Trans.*, 2015, **44**, 18049–18056.
- T. Koubský, J. Fojtikova and L. Kalvoda, *Prog. Nucl. Energy*, 2017, **94**, 208–215.
- Méthodes d'Analyses Complexométriques par les Titriplex*, ed. E. Merck, AG, Darmstadt, Germany, 3rd edn, 1992.
- B. Heits, *Zusammensetzung und Herstellung von HAW/HAWC-Simulaten gemäß den Planungsgrundlagen der DWK und den Erfahrungen der WAK*, Deutsche Gesellschaft für Wiederaufarbeitung von Kernbrennstoffen mbH, Karlsruhe, 1982.
- L. Cecille, D. Landat and F. Mannone, *Radiochem. Radioanal. Lett.*, 1977, **31**, 19–28.
- L. Cecille, M. Lestang and F. Mannone, *Radiochem. Radioanal. Lett.*, 1977, **31**, 29–37.
- G. Modolo, H. Asp, C. Schreinemachers and H. Vijgen, *Solvent Extr. Ion Exch.*, 2007, **25**, 703–721.
- D. Hallen, *Pure Appl. Chem.*, 1993, **65**, 1527–1532.
- From: Thermometric, Experimental and Technical note EN 014b, 2002.
- E. P. Horwitz, D. R. McAlister, A. H. Bond and R. E. Barrans, Jr., *Solvent Extr. Ion Exch.*, 2005, **23**, 319–344.



- 30 H. Narita, M. Tanaka, K. Morisaku and T. Abe, *Hydrometallurgy*, 2006, **81**, 153–158.
- 31 W. P. Ratchford and C. H. Fisher, *J. Org. Chem.*, 1950, **15**, 317–325.
- 32 M. L. Fein and E. M. Filachione, *J. Am. Chem. Soc.*, 1953, **75**, 2097–2099.
- 33 J. M. Mincher, G. Modolo and S. P. Mezyk, *Solvent Extr. Ion Exch.*, 2009, **27**, 579–606.
- 34 M. Carrott, K. Bell, J. Brown, A. Geist, C. Gregson, X. Hères, C. Maher, R. Malmbeck, C. Mason, G. Modolo, U. Müllich, M. Sarsfield, A. Wilden and R. Taylor, *Solvent Extr. Ion Exch.*, 2014, **32**, 447–467.
- 35 M. Carrott, A. Geist, X. Hères, S. Lange, R. Malmbeck, M. Miguirditchian, G. Modolo, A. Wilden and R. Taylor, *Hydrometallurgy*, 2015, **152**, 139–148.
- 36 A. Núñez, H. Galán and J. Cobos, *Proceedings of Global 2015*, September 20–24, 2015, Paris (France).
- 37 P. R. Zalupski and K. L. Nash, *Solvent Extr. Ion Exch.*, 2008, **26**, 514–533.
- 38 F. Rodrigues, N. Boubals, M.-C. Charbonnel and N. Morel-Desrosiers, *Procedia Chem.*, 2012, **7**, 59–65.
- 39 M. Arisaka and T. Kimura, *Solvent Extr. Ion Exch.*, 2011, **29**, 72–85.
- 40 M. R. Antonio, D. R. McAlister and E. P. Horwitz, *Dalton Trans.*, 2015, **44**, 515–521.
- 41 P. N. Pathak, S. A. Ansari, S. V. Godbole and V. K. Manchanda, *Spectrochim. Acta, Part A*, 2009, **73**, 348–352.
- 42 Y. Sasaki, P. Rapold, M. Arisaka, M. Hirata, T. Kimura, C. Hill and G. Cote, *Solvent Extr. Ion Exch.*, 2007, **25**, 187–204.

## Paper 10<sup>[158]</sup>

Wilden, A.; Lumetta, G.J.; Sadowski, F.; Schmidt, H.; Schneider, D.; Gerdes, M.; Law, J.D.; Geist, A.; Bosbach, D.; Modolo, G. An Advanced TALSPEAK Concept for Separating Minor Actinides. Part 2. Flowsheet Test with Actinide-Spiked Simulant. *Solvent Extr. Ion Exch.* **2017**, *35* (6), 396-407.

DOI: 10.1080/07366299.2017.1368901





### Contribution:

For this work, solvent extraction experiments as well as their analysis (gamma-spectrometry, results of ICP-MS) were conducted in the IEK-6, Forschungszentrum Jülich, in which I was involved.





## An Advanced TALSPEAK Concept for Separating Minor Actinides. Part 2. Flowsheet Test with Actinide-spiked Simulant

Andreas Wilden <sup>a</sup>, Gregg J. Lumetta <sup>b</sup>, Fabian Sadowski<sup>a</sup>, Holger Schmidt <sup>a</sup>,  
Dimitri Schneider<sup>a</sup>, Markus Gerdes<sup>a</sup>, Jack D. Law<sup>c</sup>, Andreas Geist<sup>d</sup>, Dirk Bosbach<sup>a</sup>,  
and Giuseppe Modolo <sup>a</sup>

<sup>a</sup>Forschungszentrum Jülich GmbH, Institut für Energie – und Klimaforschung – Nukleare Entsorgung und Reaktorsicherheit (IEK-6), Jülich, Germany; <sup>b</sup>Nuclear Science and Engineering Group, Pacific Northwest National Laboratory, Richland, DC, USA; <sup>c</sup>Aqueous Separations and Radiochemistry Department, Idaho National Laboratory, Idaho Falls, ID, USA; <sup>d</sup>Karlsruhe Institute of Technology (KIT), Institute for Nuclear Waste Disposal (INE), Karlsruhe, Germany

### ABSTRACT

An Advanced TALSPEAK (trivalent actinide–lanthanide separations by phosphorus-reagent extraction from aqueous complexes) counter-current flowsheet test was demonstrated using a simulated feed spiked with radionuclides in annular centrifugal contactors. A solvent comprising 2-ethylhexylphosphonic acid mono-2-ethylhexyl ester (HEH[EHP] or PC88A) in *n*-dodecane was used to extract trivalent lanthanides away from the trivalent actinides Am<sup>3+</sup> and Cm<sup>3+</sup>, which were preferentially complexed in a citrate-buffered aqueous phase with *N*-(2-hydroxyethyl)ethylenediamine-*N,N',N'*-triacetic acid (HEDTA). In a 24-stage demonstration test, the trivalent actinides were efficiently separated from the trivalent lanthanides with decontamination factors >1000, demonstrating the excellent performance of the chemical system. Clean actinide and lanthanide product fractions and spent solvent with very low contaminations were obtained. The results of the process test are presented and discussed.

### KEYWORDS

Actinide separation;  
HEH[EHP]; lanthanide  
separation; PC88A;  
TALSPEAK

## Introduction

Fractionation of used nuclear fuel constituents into different parts based on radiological and chemical considerations is an important research field in view of the nuclear fuel cycle and ultimate waste handling strategy.<sup>[1,2]</sup> Therefore, a large number of different strategies have been developed worldwide and are still under consideration.<sup>[3–7]</sup> Recent developments aim at the separation of the minor actinides (MA: Np, Am, Cm) as they are main contributors to the long-term radiotoxicity and repository heat-load.

A partitioning strategy investigated in the United States is based on the separation of the major actinides uranium and plutonium by the PUREX (plutonium uranium reduction extraction) process, followed by the TRUEX (transuranic extraction)<sup>[8–10]</sup> and TALSPEAK (trivalent actinide–lanthanide separations by phosphorus-reagent extraction from aqueous complexes) processes.<sup>[4,11]</sup> Advanced PUREX processes also aim at the separation of Np, together with U and Pu.<sup>[12]</sup> The TRUEX process separates the trivalent lanthanides (Ln(III)) together with Am and Cm as a group from the rest of the fission products. Subsequently, Am and Cm are separated from the lanthanides in the TALSPEAK process. This separation of Ln(III) and trivalent actinides (An(III)) is required for the partitioning and transmutation strategy, as many lanthanide isotopes have large neutron-capture cross-sections and

**CONTACT** Andreas Wilden  [a.wilden@fz-juelich.de](mailto:a.wilden@fz-juelich.de)  Forschungszentrum Jülich GmbH, Institut für Energie- und Klimaforschung - Nukleare Entsorgung und Reaktorsicherheit (IEK-6), 52428 Jülich, Germany

Color versions of one or more of the figures in the article can be found online at [www.tandfonline.com/lsei](http://www.tandfonline.com/lsei).

This article was originally published with errors. This version has been corrected. Please see erratum (<https://doi.org/10.1080/07366299.2017.1377421>)

© 2017 Taylor & Francis Group, LLC

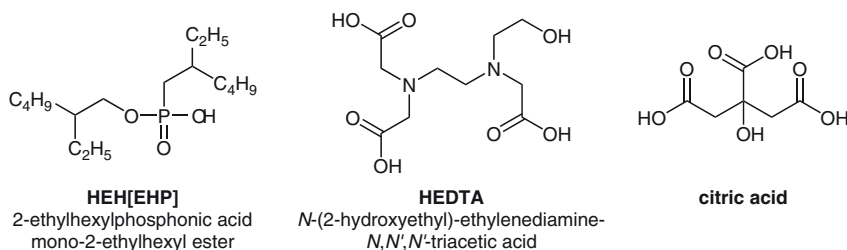


Figure 1. Chemical structures of HEH[EHP] (left), HEDTA (middle), and citric acid (right).

would therefore hinder an efficient re-use of the material. The TALSPEAK process has been investigated since the 1960s, and a substantial amount of scientific work has been gathered on this subject.<sup>[13,14]</sup> However, the chemistry of the original TALSPEAK process is complex, and its successful implementation requires tight control of the pH, which has hindered its industrial development. An alternative was sought to overcome these limitations of TALSPEAK.<sup>[15–21]</sup>

A new chemical system was investigated in depth based on the use of a combination of 2-ethylhexylphosphonic acid mono-2-ethylhexyl ester (HEH[EHP] or PC88A) and *N*-(2-hydroxyethyl) ethylenediamine-*N,N',N'*-triacetic acid (HEDTA) in a citrate-buffered system (Fig. 1). Optimal process conditions were found for 1.0 mol/L HEH[EHP] in *n*-dodecane as the solvent, and a feed solution containing the metal ions and 0.125 mol/L HEDTA and 0.6 mol/L citrate at pH 2.6.

This article is the second part of a series describing the development of the Advanced TALSPEAK concept. In the first article of the series, the optimization of the chemical system and single-stage centrifugal contactor experiments performed to identify the kinetics in the actual devices to be used and to allow the development of a flowsheet for the actual centrifugal-contactor demonstration test using computer-code calculations are described.<sup>[22]</sup> This second article reports the results of a flowsheet test that was performed with an actinide-spiked simulant solution.

## Experimental

### Materials

HEH[EHP] (95%) was purchased from BOC Sciences (Shirley, NY, USA), *n*-dodecane ( $\geq 99\%$ , ReagentPlus) was purchased from Sigma-Aldrich (Taufkirchen, Germany), HEDTA (99%) was purchased from Acros Organics (Geel, Belgium), and citric acid ( $\geq 99\%$ ) and concentrated nitric acid (65%, analytical grade) were purchased from Merck (Darmstadt, Germany). All chemicals were used as received without further purification. The organic and aqueous solutions were prepared by dissolving weighed quantities of the desired substance in the desired solvent. For aqueous dilutions, demineralized water (18.2 M $\Omega$ cm) was used. The radiotracers <sup>241</sup>Am, <sup>244</sup>Cm, and <sup>152</sup>Eu were purchased from Isotopendienst M. Blaseg GmbH, Waldburg, Germany, Oak Ridge National Laboratory, Oak Ridge, TN, USA, and Eckert & Ziegler Nuclitec GmbH, Braunschweig, Germany. Ln nitrate salts were obtained from a variety of commercial sources, and were used as received.

A feed solution with the same Ln in concentrations as expected in a feed for the Advanced TALSPEAK process was used, which was spiked with the radiotracers <sup>241</sup>Am, <sup>244</sup>Cm, and <sup>152</sup>Eu. The feed solution was prepared by dissolving Ln nitrates, citric acid, and HEDTA in water. Then, the pH was set to the desired pH value using a 10 mol/L NaOH solution in water and finally adding the radiotracers. The final concentrations and the pH value of the feed solution are given in Table 1.

**Table 1.** Composition of the Advanced TALSPEAK feed solution.

Component	Concentration	Component	Concentration	Component	Concentration
La	260.0 mg/L	Eu	39.5 mg/L	Citrate	0.6 mol/L
Ce	570.2 mg/L	Gd	98.4 mg/L	HEDTA	0.125 mol/L
Pr	213.5 mg/L	<sup>241</sup> Am	3.6 MBq/L	pH	2.6
Nd	1029 mg/L	<sup>244</sup> Cm	3.6 MBq/L		
Sm	171.4 mg/L	<sup>152</sup> Eu	10.2 MBq/L		

### Procedures and analytical methods of the process demonstration

The demonstration of the process was carried out using 1 cm annular miniature centrifugal contactors produced by Institute of Nuclear Energy Technology, Tsinghua University, Beijing, China, with the rotors made of titanium and the stator housings made of stainless steel.<sup>[23,24]</sup> The process was run in counter-current mode with a rotator speed of 4500 rpm, and the speed was checked with a stroboscope tachometer regularly during the experiment. The contactor battery setup consists of 4 batteries with 4 stages each, resulting in a total available number of 16 stages. As the calculated flowsheet comprises 24 stages, the test was split into two parts as described below. Calibrated syringe pumps were used to deliver the different organic and aqueous flows.

The following analyses were carried out on all samples collected from all stages (aqueous and organic), including the samples taken to determine the steady state:  $\gamma$ -spectroscopy for <sup>241</sup>Am and <sup>152</sup>Eu using a high-purity Ge-detector system,  $\alpha$ -spectroscopy for <sup>241</sup>Am and <sup>244</sup>Cm, and ICP-MS for all inactive elements. The aqueous phases were directly measured after appropriate dilution. The organic phases were also directly measured after mixture with the non-ionic surfactant TRITON-X-100 and dilution to an appropriate concentration. The acidity profiles were determined for the aqueous phase by potentiometric titration with NaOH or pH measurement using a Metrohm 691 pH meter. Details of the equipment, procedure, and analytics are described elsewhere.<sup>[25–27]</sup>

Distribution ratios were calculated as the radioactivity or concentration of the metal ion in the organic phase divided by the respective radioactivity or concentration in the aqueous phase. Distribution ratios between 0.01 and 100 exhibit an uncertainty of  $\pm 5\%$ , while lower/higher values exhibit larger uncertainties.

The process decontamination factor,  $DF_{\text{feed}/\text{An product}}$ , was calculated according to Eq. (1), where  $Q$  is the volumetric flow rate and  $C$  is the metal ion concentration. The An/Ln decontamination factors were calculated according to Eq. (2).

$$DF_{\text{feed}/\text{An product}} = \frac{Q_{\text{feed}} C_{\text{feed}}}{Q_{\text{An product}} C_{\text{An product}}} \quad (1)$$

$$DF_{\text{An/Ln}} = \frac{C(\text{Ln})_{\text{feed}} C(\text{An})_{\text{prod}}}{C(\text{Ln})_{\text{prod}} C(\text{An})_{\text{feed}}} \quad (2)$$

### Results and discussion

This article describes a laboratory-scale spiked demonstration of the Advanced TALSPEAK process. Part 1 of this series of publication describes the optimization of the chemical system which found a combination of 1.0 mol/L HEH[EHP] in *n*-dodecane and 0.125 mol/L HEDTA in a citric acid (0.6 mol/L) buffered aqueous phase at pH 2.6 to be most effective for the desired separation of An(III) from Ln(III). Further batch distribution measurements and single-stage kinetics tests using different types of centrifugal contactors are presented.<sup>[22]</sup> Based on these findings, a flowsheet was designed and simulated using the Argonne Model for Universal Solvent Extraction (AMUSE) code,<sup>[28]</sup> which is shown in Fig. 2. The flowsheet consists of three phases: extraction, scrubbing, and stripping. In the extraction section, Ln(III) are extracted into the organic phase. An aqueous-to-organic phase ratio of 2:1 is used. In the scrubbing section, a 1:1 phase ratio is applied. The scrubbing section is used to back-extract An(III), which are co-extracted in minor amounts. The stripping section is used to strip

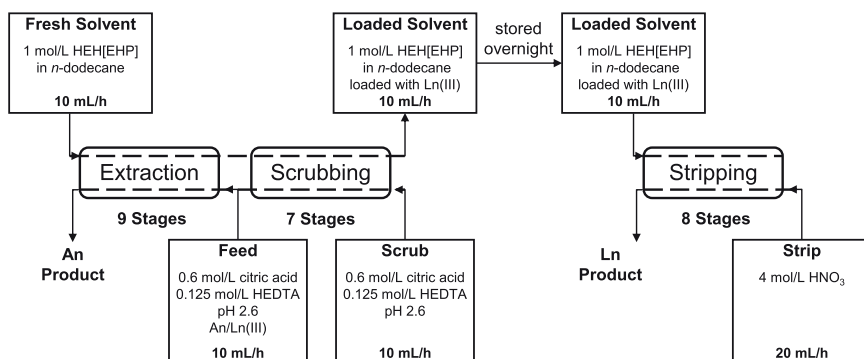


Figure 2. Flowsheet of the Advanced TALSPEAK process demonstration test.

Table 2. Average residence time of the phases in the mixing chambers of the centrifugal contactors (approximately 6 mL volume) for each part of the flowsheet (see Fig. 2).

Section	Total flow rate (organic + aqueous) (mL/h)	Residence time (min)
Extraction	30	12
Scrubbing	20	18
Stripping	30	12

Ln(III) back into an aqueous phase, and again a 2:1 phase ratio is used. The organic solvent could then be recycled. The average residence time of the phases in the mixing chamber of the centrifugal contactors for each part of the flowsheet is given in Table 2. The residence time is relatively long compared with other processes run in these centrifugal contactors, for example, for An(III)/Ln(III) co-extraction,<sup>[25]</sup> but comparable to processes for the selective separation of An(III) from Ln(III).<sup>[26,29]</sup>

Due to the limitation of the available number of 16 centrifugal contactors, it was not possible to run the complete process in a single run. Therefore, the extraction + scrubbing parts were tested first and enough loaded solvent was collected and stored overnight to be used on the consecutive day for the stripping part.

For the actual process test, the centrifugal contactors were first filled with scrub solution through the inlets for scrub and feed, as it had an identical composition as the feed except for metal ions. After the first drops of aqueous phase left the contactor rig through the aqueous outlet, the solvent was fed into the rig until the first organic phase left the rig through the organic outlet, with the aqueous flows set in the correct ratios to the organic flow. After the centrifugal contactors were completely filled with both phases, the active feed was introduced, and the process test was started using the flow rates given in Fig. 2. During the process test, samples of the organic and aqueous effluents were taken to follow the evolution of the steady state. Gamma spectroscopy was used to monitor the <sup>241</sup>Am and <sup>152</sup>Eu concentrations in the effluents at run time, while alpha spectroscopy and ICP-MS measurements were performed later. Figure 3 shows the concentrations of all metal ions in the organic phase outlet and those of the radioactive tracers in the aqueous phase outlet as a function of the experiment run-time. The organic profiles show that steady state was reached after 3 h, as the <sup>152</sup>Eu concentration reached a plateau. This result from gamma spectroscopy was confirmed by ICP-MS measurements. Europium and the other Ln metal ions were routed to the organic phase outlet and the steady state was reached in the same time for all Ln. The Ln concentrations in the aqueous phase outlet were very low (close to or below the detection limits) and therefore only the results from <sup>152</sup>Eu are shown here. Am and Cm were routed to the aqueous-phase outlet. The <sup>241</sup>Am and <sup>244</sup>Cm concentrations, however, increased more slowly, and it took 10 h to reach the steady state. The selectivity of the Advanced TALSPEAK system for An/Ln separation was very good, as concentrations of Am and Cm close to or below the detection limits were found in the loaded organic phase, and similarly low concentrations of Ln were found in the aqueous An product phase.

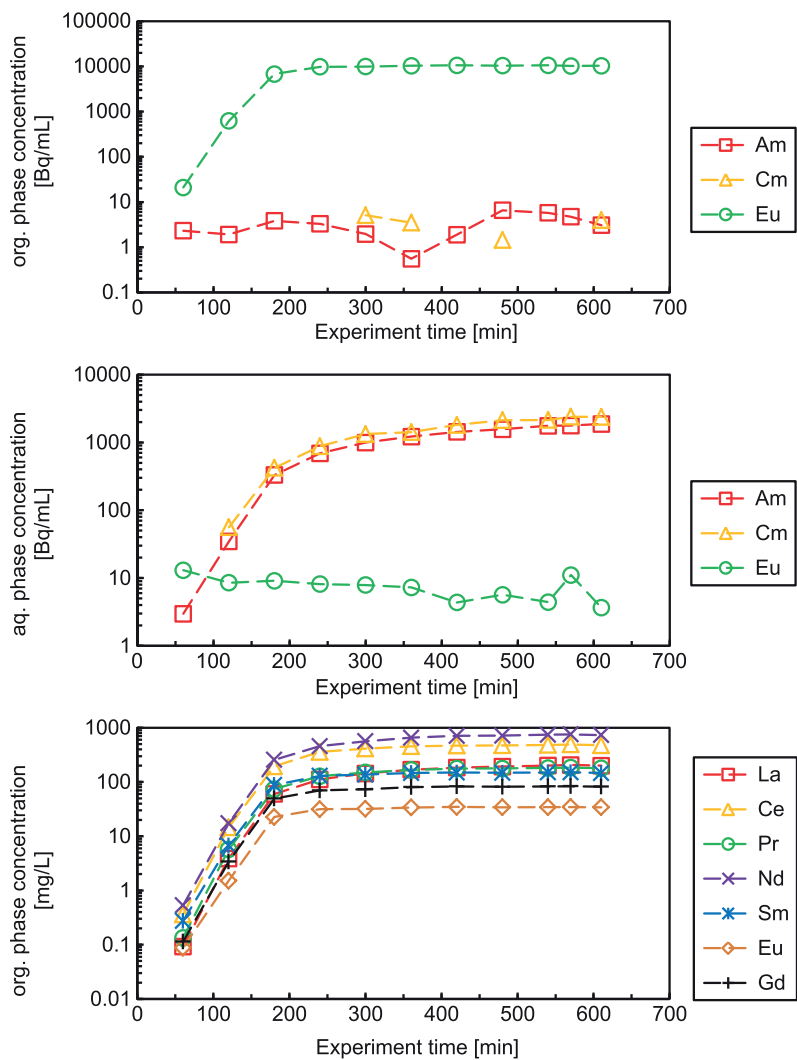


**Figure 3.**  $^{241}\text{Am}$ ,  $^{244}\text{Cm}$ , and  $^{152}\text{Eu}$  concentrations in the organic (top) and aqueous (middle) outlets and the other Ln metal ions in the organic outlet (bottom) of the centrifugal-contactor battery as a function of the experiment run time of the extraction/scrubbing part of the test.  $^{241}\text{Am}$  and  $^{152}\text{Eu}$  data points show results from gamma-spectroscopy;  $^{244}\text{Cm}$  data points show results from alpha-spectroscopy. The Ln metal ion concentrations were determined by ICP-MS. Missing data points were below the detection limit.

**Table 3.** Mass balances, recoveries, process, and An/Ln decontamination factors obtained during the Advanced TALSPeAK test.

Element	Percentage in An product	Percentage in loaded solvent	Percentage in Ln product	Percentage in spent solvent	$DF_{\text{feed}/\text{An product}}$	$DF_{\text{An}/\text{Ln}}$
$^{241}\text{Am}$	99.9	0.1	0.1	<0.1	1	–
$^{244}\text{Cm}$	>99.9	<0.1	<0.1	<0.1	1	–
La	0.002	>99.9	>99.9	0.017	$3.0 \times 10^4$	$1.5 \times 10^4$
Ce	<0.001	>99.9	>99.9	0.020	$1.2 \times 10^5$	$6.2 \times 10^4$
Pr	<0.001	>99.9	>99.9	0.023	$1.1 \times 10^5$	$5.4 \times 10^4$
Nd	0.003	>99.9	>99.9	0.023	$1.6 \times 10^4$	$8.2 \times 10^3$
Sm	<0.001	>99.9	>99.9	0.033	$>1.0 \times 10^{4a}$	$>1.0 \times 10^{4a}$
$^{152}\text{Eu}$	0.1	99.9	99.9	<0.1	$8.0 \times 10^{2a}$	$>1.0 \times 10^{3a}$
Eu	0.001	>99.9	>99.9	0.032	$5.9 \times 10^4$	$3.0 \times 10^4$
Gd	0.001	>99.9	>99.9	0.029	$4.9 \times 10^4$	$2.5 \times 10^4$

<sup>a</sup>Concentration in the An product was close to or below the detection limit.



All organic samples collected after 240 min were combined and stored overnight. The concentrations of  $^{241}\text{Am}$  and  $^{244}\text{Cm}$  in the loaded solvent were close to or below the detection limits. The Ln were quantitatively extracted, which is also confirmed by the Ln concentration profiles (Figs. 5 and 6) and the fact that the concentrations of Ln in the An product fraction were extremely low (Table 3). The Ln-loaded solvent was clear and free of precipitates or phase entrainment and was directly used the next day.

On the next day, the stripping part of the flowsheet was tested with eight centrifugal contactors. The contactors used in stages 9–16 were used after flushing with 4 mol/L  $\text{HNO}_3$  and *n*-dodecane in counter-current mode. For the stripping test, the contactors were prepared using 4 mol/L  $\text{HNO}_3$  and fresh solvent. Then, the organic phase was switched to the loaded organic phase of the first day, and the test was run for just under 6 h.

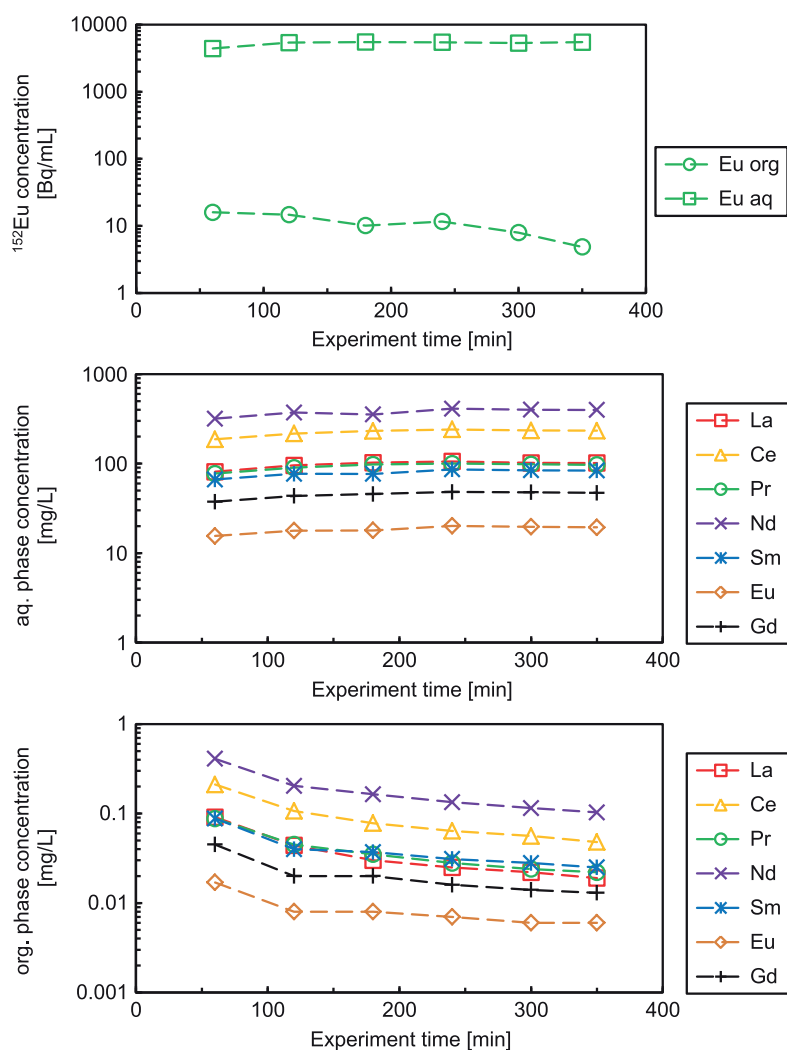


**Figure 4.**  $^{152}\text{Eu}$  concentrations in the organic and aqueous outlets (top) and the other Ln metal ions in the aqueous (middle) and organic outlet (bottom) of the centrifugal-contactor battery as a function of the experiment run time of the stripping part of the test.  $^{152}\text{Eu}$  data points show results from gamma-spectroscopy,  $^{241}\text{Am}$  and  $^{244}\text{Cm}$  data are not shown, as the measured concentrations were very low and close or below the detection limits. The Ln metal ion concentrations were determined by ICP-MS.

Figure 4 shows the  $^{152}\text{Eu}$  concentrations measured by gamma spectroscopy and the concentrations of all Ln measured by ICP-MS in the aqueous and organic outlets as a function of the stripping test run-time. Again, a plateau was reached very fast, indicating a quick evolution of the steady state. All Ln metal ions were stripped efficiently and routed to the aqueous Ln product stream. Am and Cm results are not shown in Fig. 4 as the concentrations determined by alpha and gamma spectroscopy were below or close to the detection limits.

The mass balances, recoveries, and decontamination factors obtained during the Advanced TALSPEAK test are shown in Table 3. The mass balances of the Ln elements measured by ICP-MS in the aqueous Ln product were in the range 97–115%. This large uncertainty is due to the accumulation of uncertainties in the ICP-MS measurements and the process flow rates. The concentrations of Ln in the other process streams (An product and spent solvent) were extremely low and <0.1% of the feed concentrations. Therefore, nearly quantitative recovery of Ln in the aqueous Ln product is assumed, and the mass balances were given as >99.9% in the table. The decontamination factors were calculated according to Eqs. (1) and (2) and were found to be excellent with the lowest process DF-value of 800 found for  $^{152}\text{Eu}$ . The An/Ln decontamination factors were all >1000, proving the high selectivity of the Advanced TALSPEAK system.

The concentration profiles were determined by sampling the content of the contactor mixing chambers after steady state was reached and the process was stopped. Samples taken from each mixing chamber were analyzed using alpha and gamma spectroscopy as well as ICP-MS. The  $^{241}\text{Am}$ ,  $^{244}\text{Cm}$ , and  $^{152}\text{Eu}$  profiles are shown in Fig. 5 and the profiles of the other Ln elements is shown in Fig. 6. The Am and Cm profiles clearly show the routing of those two elements to the aqueous raffinate and a steep profile in the scrubbing section. Distribution ratios of 0.6 and 0.4 were measured for both Am and Cm in the extraction and scrubbing sections, respectively (Table 4); these values were consistent with previously measured batch distribution ratios.<sup>[22]</sup> Only low concentrations have been measured in the stripping section. However, in stages 19 and 20, increased concentrations were observed. They were presumably caused by impurities of Am and Cm left over from insufficient rinsing of the contactors when set up for the stripping test. The contactors used here as stages 19 and 20 have been used as stages 11 and 12 on the first day, where high concentrations of An(III) were still present in the stages.

The Ln showed a steep profile in the extraction and stripping sections and were routed first to the loaded solvent and then to the aqueous Ln product. In the scrubbing section of the flowsheet a flat profile was obtained, indicating constant distribution ratios and no recycling of any of the elements. Stripping with 4 mol/L  $\text{HNO}_3$  was very efficient; the Ln were stripped efficiently in the

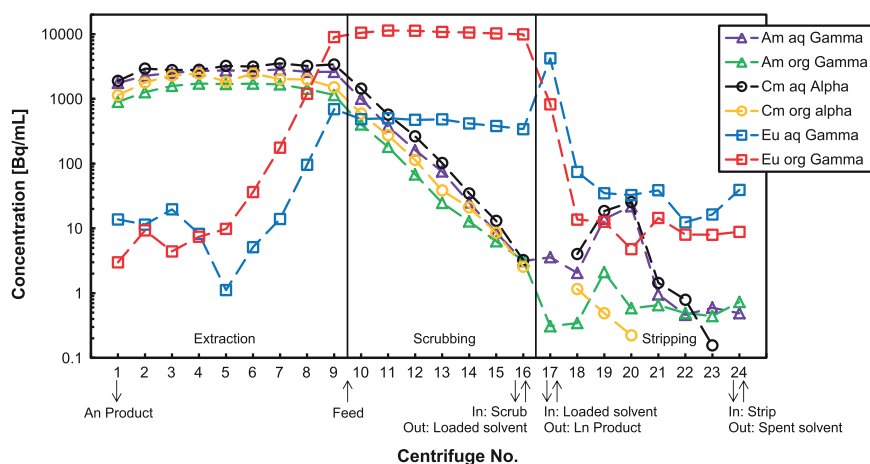


Figure 5. Experimental aqueous and organic concentration profiles of  $^{241}\text{Am}$ ,  $^{244}\text{Cm}$ , and  $^{152}\text{Eu}$  for the whole test. Stage numbering and section labeling are given according to the flowsheet given in Fig. 2.

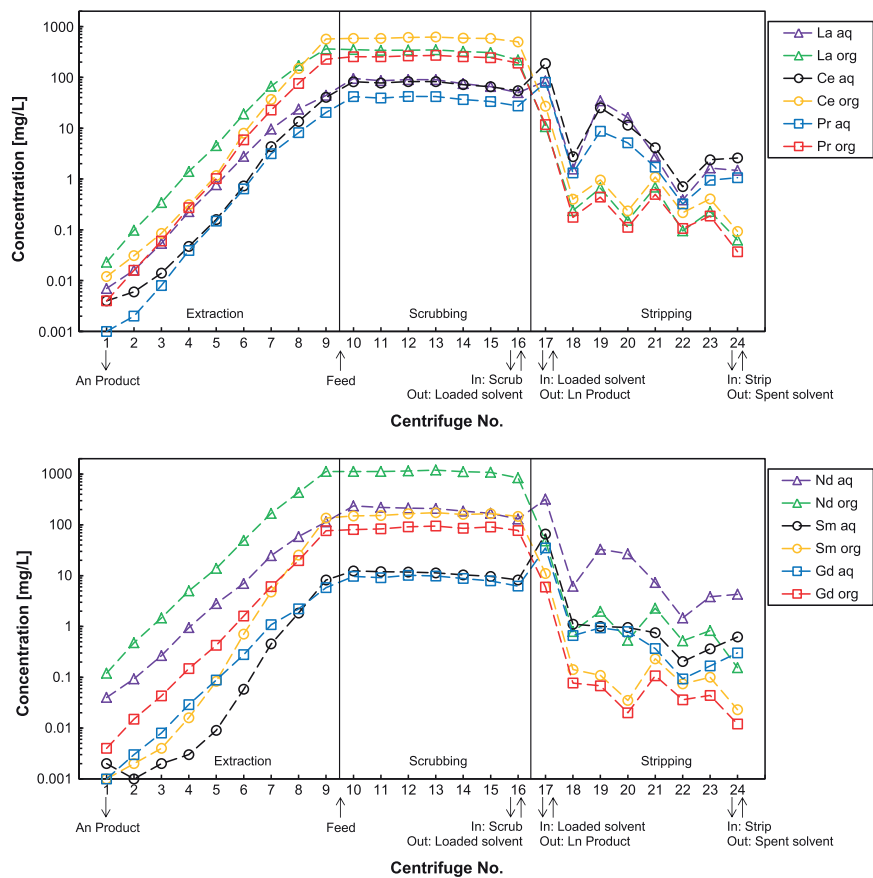


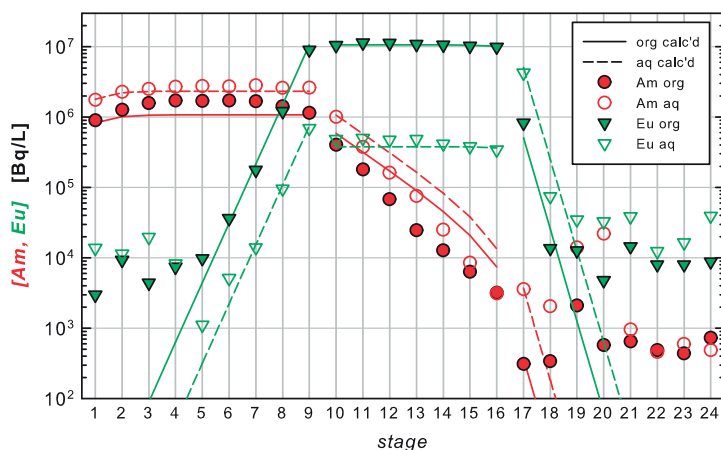
Figure 6. Experimental aqueous and organic concentration profiles of the Ln elements for the whole test. Eu profiles are not shown here, as they are comparable to those shown for <sup>152</sup>Eu in Fig. 5. Stage numbering and section labeling are given according to the flowsheet given in Fig. 2.

Table 4. Distribution ratios in the different process sections at steady state.

Element	Extraction Stage 7	Scrubbing Stage 12	Stripping Stage 17
<sup>241</sup> Am	0.6	0.4	0.1
<sup>244</sup> Cm	0.6	0.4	DL
La	7.0	3.8	0.1
Ce	8.5	7.4	0.1
Pr	7.2	6.3	0.2
Nd	6.8	5.4	0.2
Sm	10.5	14.1	0.2
<sup>152</sup> Eu	12.7	23.7	0.2
Eu	17.2	21.7	0.2
Gd	5.6	9.0	0.2

DL, at least one measured concentration below the detection limit.

first two stripping stages (stages 17–18). The distribution ratios of all metal ions were low (Table 4) at the stripping conditions, resulting in steep concentration profiles. However, the relatively high



**Figure 7.** Experimental (data points) and calculated (lines) concentration profiles for  $^{241}\text{Am}$  (circles) and  $^{152}\text{Eu}$  (triangles) using the stage efficiencies determined from single-stage centrifugal-contactor experiments.<sup>[22]</sup> Organic phase: filled symbols, solid lines; aqueous phase: open symbols, dashed lines.

concentrations of Ln measured in stages 20–24 were presumably also caused by insufficient rinsing of the contactors when set up for the stripping test as described above.

The concentration profiles were calculated using a computer-code model using batch extraction and single-stage centrifugal contactor kinetics data.<sup>[22,30,31]</sup> Figure 7 shows the experimental and calculated concentration profiles for  $^{241}\text{Am}$  and  $^{152}\text{Eu}$  using distribution data as reported in Part 1 of this series of articles. Since the single-stage centrifugal-contactor kinetics data had been measured only for the experimental conditions prevailing in the extraction section of the flowsheet, assumptions had to be made for the scrubbing and stripping sections: equilibrium distribution ratios were used in the scrubbing section, and distribution ratios of 0.1 were arbitrarily used in the stripping section. Agreement between experimental and calculated concentration profiles was relatively good in the extraction section, but deviations were observed especially for Am(III) in the scrubbing section. This is presumably due to the assumptions made for the scrubbing section and the lack of experimental single-stage data for this section. Small deviations of the pH or unknown species, which were co-extracted in the extraction section and facilitate the back-extraction of Am in the scrubbing section, could be other explanations.

Therefore, the Am stage efficiency for the scrubbing section was adjusted to fit the experimental profiles by using a distribution ratio of 0.4 (cf. Table 4). As shown in Fig. 8, this results in good agreement also for the scrubbing section. The discrepancy in the Am concentrations in stage 17 may be due to contamination, as discussed above.

## Conclusions

The presented Advanced TALSPEAK process is based on a chemical system using HEH[EHP] in *n*-dodecane to extract the trivalent lanthanides away from the trivalent actinides Am(III) and Cm(III). The An(III) elements are kept in the aqueous phase by preferential complexation with HEDTA in a citrate-buffered solution at pH 2.6. A 24-stage flowsheet was tested in counter-current mode using 1 cm centrifugal contactors. An excellent performance was observed, as clean An(III) and Ln(III) product fractions were obtained with high decontamination factors (>1000). The spent solvent was also very clean, enabling an easy recycling of the solvent. No hydrodynamic problems

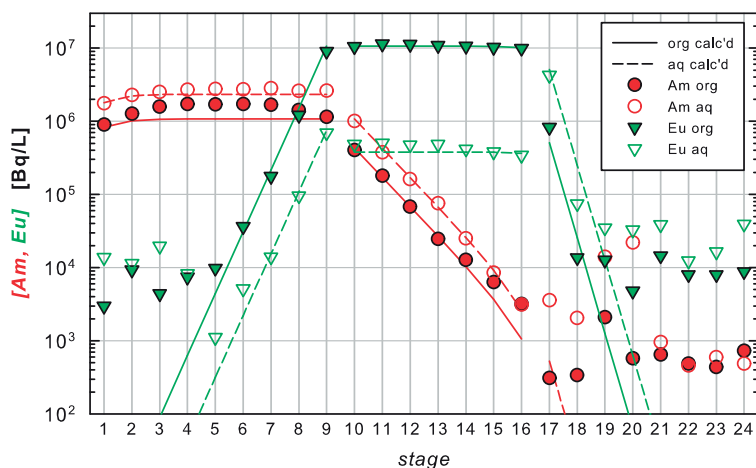


**Figure 8.** Experimental (data points) and calculated (lines) concentration profiles for  $^{241}\text{Am}$  (circles) and  $^{152}\text{Eu}$  (triangles) using the stage efficiencies determined from single-stage centrifugal-contactor experiments<sup>[22]</sup> except for Am in the scrubbing section. Organic phase: filled symbols, solid lines; aqueous phase: open symbols, dashed lines.

were observed during the test. The measured metal ion concentration profiles were described very well by a slightly modified computer-code model. The small adjustment of the Am stage efficiency in the scrubbing stages was needed as experimental data were only available for the extraction section of the flowsheet. In summary, the process performance was better than expected based on the initial AMUSE simulation; that is, a reduced number of stages could be used in further process development. The presented Advanced TALSPEAK process would be an excellent choice following a TRUEX process by separating the An(III) from Ln(III).

## Funding

Financial support for this research was provided by the European Commission (project SACSESS – contract number FP7-Fission-2012-323-282) and the U.S. Department of Energy, Office of Nuclear Energy, through the Fuel Cycle Research and Development Program. Pacific Northwest National Laboratory is operated by Battelle Memorial Institute for the U.S. Department of Energy under contract DE-AC05-76RL01830.

## ORCID

Andreas Wilden <http://orcid.org/0000-0001-5681-3009>  
 Gregg J. Lumetta <http://orcid.org/0000-0002-0216-8515>  
 Holger Schmidt <http://orcid.org/0000-0002-3448-3579>  
 Giuseppe Modolo <http://orcid.org/0000-0001-6490-5595>

## References

- González-Romero, E. M. Impact of Partitioning and Transmutation on the High Level Waste Management. *Nucl. Eng. Des.* 2011, 241(9), 3436–3444. [10.1016/j.nucengdes.2011.03.030](https://doi.org/10.1016/j.nucengdes.2011.03.030).
- Mathur, J. N.; Murali, M. S.; Nash, K. L. Actinide Partitioning: A Review. *Solvent Extr. Ion Exch.* 2001, 19(3), 357–390. [10.1081/SEI-100103276](https://doi.org/10.1081/SEI-100103276).
- Modolo, G.; Geist, A.; Miguiditchian, M. Minor Actinide Separations in the Reprocessing of Spent Nuclear Fuels: Recent Advances in Europe. Chap. 10 In *Reprocessing and Recycling of Spent Nuclear Fuel*; Taylor R., Ed.; Woodhead Publishing: Oxford, 2015; 245–287.

4. Moyer, B. A.; Lumetta, G. J.; Mincher, B. J. Minor Actinide Separation in the Reprocessing of Spent Nuclear Fuels: Recent Advances in the United States. Chap. 11 In *Reprocessing and Recycling of Spent Nuclear Fuel*; Taylor R., Ed.; Woodhead Publishing: Oxford, 2015; 289–312.
5. Poinssot, C.; Rostaing, C.; Baron, P.; Warin, D.; Boullis, B. Main Results of the French Program on Partitioning of Minor Actinides, a Significant Improvement Towards Nuclear Waste Reduction. *Proc. Chem.* 2012, 7, 358–366. [10.1016/j.proche.2012.10.056](https://doi.org/10.1016/j.proche.2012.10.056).
6. Taylor, R.; Bourg, S.; Glatz, J.-P.; Modolo, G. Development of Actinide Separation Processes for Future Nuclear Fuel Cycles in Europe. *Nucl. Future.* 2015, 11(4), 38–43.
7. Paiva, A. P.; Malik, P. Recent Advances on the Chemistry of Solvent Extraction Applied to the Reprocessing of Spent Nuclear Fuels and Radioactive Wastes. *J. Radioanal. Nucl. Chem.* 2004, 261(2), 485–496. [10.1023/B:JRNC.0000034890.23325.b5](https://doi.org/10.1023/B:JRNC.0000034890.23325.b5).
8. Horwitz, E. P.; Kalina, D. G.; Diamond, H.; Vandegrift, G. F.; Schulz, W. W. The TRUEX Process: A Process for the Extraction of the Transuranic Elements from Nitric-Acid Wastes Utilizing Modified Purex Solvent. *Solvent Extr. Ion Exch.* 1985, 3(1–2), 75–109. [10.1080/07366298508918504](https://doi.org/10.1080/07366298508918504).
9. Schulz, W. W.; Horwitz, E. P. The TRUEX Process and the Management of Liquid TRU Waste. *Separ. Sci. Technol.* 1988, 23(12–13), 1191–1210. [10.1080/01496398808075625](https://doi.org/10.1080/01496398808075625).
10. Horwitz, E. P.; Schulz, W. W., The TRUEX Process: A Vital Tool for Disposal of U.S. Defense Nuclear Waste, Proceedings of New Separation Chemistry for Radioactive Waste and Other Specific Application, Rome, Italy, 1990. May 16–18, 1990. pp. 16–18.
11. Weaver, B.; Kappellmann, F. A. TALSPEAK: A New Method of Separating Americium and Curium from the Lanthanides by Extraction from an Aqueous Solution of an Aminopolyacetic Acid Complex with A Monoacetic Organophosphate or Phosphonate; ORNL-3559; Oak Ridge National Laboratory: Oak Ridge, 1964.
12. Taylor, R. J.; Gregson, C. R.; Carrott, M. J.; Mason, C.; Sarsfield, M. J. Progress Towards the Full Recovery of Neptunium in an Advanced PUREX Process. *Solvent Extr. Ion Exch.* 2013, 31(4), 442–462. [10.1080/07366299.2013.800438](https://doi.org/10.1080/07366299.2013.800438).
13. Nash, K. L. The Chemistry of TALSPEAK: A Review of the Science. *Solvent Extr. Ion Exch.* 2015, 33(1), 1–55. [10.1080/07366299.2014.985912](https://doi.org/10.1080/07366299.2014.985912).
14. Nilsson, M.; Nash, K. L. Review Article: A Review of the Development and Operational Characteristics of the TALSPEAK Process. *Solvent Extr. Ion Exch.* 2007, 25(6), 665–701. [10.1080/07366290701634636](https://doi.org/10.1080/07366290701634636).
15. Lumetta, G. J.; Gelis, A. V.; Braley, J. C.; Carter, J. C.; Pittman, J. W.; Warner, M. G.; Vandegrift, G. F. The TRUSPEAK Concept: Combining CMPO and HDEHP for Separating Trivalent Lanthanides from the Transuranic Elements. *Solvent Extr. Ion Exch.* 2013, 31(3), 223–236. [10.1080/07366299.2012.670595](https://doi.org/10.1080/07366299.2012.670595).
16. Lumetta, G. J.; Casella, A. J.; Rapko, B. M.; Levitskaia, T. G.; Pence, N. K.; Carter, J. C.; Niver, C. M.; Smoot, M. R. An Advanced TALSPEAK Concept Using 2-Ethylhexylphosphonic Acid Mono-2-Ethylhexyl Ester as the Extractant. *Solvent Extr. Ion Exch.* 2015, 33(3), 211–223. [10.1080/07366299.2014.985920](https://doi.org/10.1080/07366299.2014.985920).
17. Lumetta, G. J.; Gelis, A. V.; Vandegrift, G. F. Review: Solvent Systems Combining Neutral and Acidic Extractants for Separating Trivalent Lanthanides from the Transuranic Elements. *Solvent Extr. Ion Exch.* 2010, 28(3), 287–312. [10.1080/07366291003684253](https://doi.org/10.1080/07366291003684253).
18. Braley, J. C.; Carter, J. C.; Sinkov, S. I.; Nash, K. L.; Lumetta, G. J. The Role of Carboxylic Acids in TALSQuEAK Separations. *J. Coord. Chem.* 2012, 65(16), 2862–2876. [10.1080/00958972.2012.704551](https://doi.org/10.1080/00958972.2012.704551).
19. Braley, J. C.; Grimes, T. S.; Nash, K. L. Alternatives to HDEHP and DTPA for Simplified TALSPEAK Separations. *Ind. Eng. Chem. Res.* 2012, 51(2), 629–638. [10.1021/ie200285r](https://doi.org/10.1021/ie200285r).
20. Braley, J. C.; Lumetta, G. J.; Carter, J. C. Combining CMPO and HEH[EHP] for Separating Trivalent Lanthanides from the Transuranic Elements. *Solvent Extr. Ion Exch.* 2013, 31(6), 567–577. [10.1080/07366299.2013.785912](https://doi.org/10.1080/07366299.2013.785912).
21. Lapka, J. L.; Nash, K. L. Advanced TALSPEAK Separations Using a Malonate Buffer System. *Solvent Extr. Ion Exch.* 2015, 33(4), 346–361. [10.1080/07366299.2015.1012878](https://doi.org/10.1080/07366299.2015.1012878).
22. Lumetta, G. J.; Levitskaia, T. G.; Wilden, A.; Casella, A. J.; Hall, G. B.; Lin, L.; Sinkov, S. I.; Law, J.; Modolo, G. An Advanced TALSPEAK Concept for Separating Minor Actinides. Part 1. Process Optimization and Flowsheet Development. *Solvent Extr. Ion Exch.* 2017. [10.1080/07366299.2017.1368901](https://doi.org/10.1080/07366299.2017.1368901).
23. Duan, W.; Zhao, M.; Wang, C.; Cao, S. Recent Advances in the Development and Application of Annular Centrifugal Contactors in the Nuclear Industry. *Solvent Extr. Ion Exch.* 2014, 32(1), 1–26. [10.1080/07366299.2013.833741](https://doi.org/10.1080/07366299.2013.833741).
24. Leonard, R. A. Design Principles and Applications of Centrifugal Contactors for Solvent Extraction. Chap. 10 In *Ion Exchange and Solvent Extraction, A Series of Advances*; Moyer B. A., Ed.; CRC Taylor and Francis: 2009; Vol. 19, 563–616.
25. Modolo, G.; Asp, H.; Vijgen, H.; Malmbeck, R.; Magnusson, D.; Sorel, C. Demonstration of a TODGA-Based Continuous Counter-Current Extraction Process for the Partitioning of Actinides from a Simulated PUREX Raffinate, Part II: Centrifugal Contactor Runs. *Solvent Extr. Ion Exch.* 2008, 26(1), 62–76. [10.1080/07366290701784175](https://doi.org/10.1080/07366290701784175).

26. Wilden, A.; Modolo, G.; Schreinemachers, C.; Sadowski, F.; Lange, S.; Sypula, M.; Magnusson, D.; Geist, A.; Lewis, F. W.; Harwood, L. M.; Hudson, M. J. Direct Selective Extraction of Actinides (III) from PUREX Raffinate Using a Mixture of CyMe<sub>4</sub>BTBP and TODGA as 1-Cycle SANEX Solvent Part III: Demonstration of a Laboratory-Scale Counter-Current Centrifugal Contactor Process. *Solvent Extr. Ion Exch.* 2013, 31(5), 519–537. [10.1080/07366299.2013.775890](https://doi.org/10.1080/07366299.2013.775890).
27. Kaufholz, P.; Modolo, G.; Wilden, A.; Sadowski, F.; Bosbach, D.; Wagner, C.; Geist, A.; Panak, P. J.; Lewis, F. W.; Harwood, L. M. Solvent Extraction and Fluorescence Spectroscopic Investigation of the Selective Am(III) Complexation with TS-BTPhen. *Solvent Extr. Ion Exch.* 2016, 34(2), 126–140. [10.1080/07366299.2016.1151308](https://doi.org/10.1080/07366299.2016.1151308).
28. Frey, K.; Krebs, J. F.; Pereira, C. Time-Dependent Implementation of Argonne's Model for Universal Solvent Extraction. *Ind. Eng. Chem. Res.* 2012, 51, 13219–13226. [10.1021/ie301421d](https://doi.org/10.1021/ie301421d).
29. Wilden, A.; Modolo, G.; Kaufholz, P.; Sadowski, F.; Lange, S.; Munzel, D.; Geist, A. Process Development and Laboratory-Scale Demonstration of a regular-SANEX Process Using C5-BPP. *Sep. Sci. Technol.* 2015, 50(16), 2467–2475. [10.1080/01496395.2015.1061008](https://doi.org/10.1080/01496395.2015.1061008).
30. Modolo, G.; Kluxen, P.; Geist, A. Demonstration of the LUCA Process for the Separation of americium(III) from curium(III), californium(III), and lanthanides(III) in Acidic Solution Using a Synergistic Mixture of Bis (Chlorophenyl)Dithiophosphinic Acid and Tris(2-Ethylhexyl)Phosphate. *Radiochim. Acta.* 2010, 98(4), 193–201. [10.1524/ract.2010.1708](https://doi.org/10.1524/ract.2010.1708).
31. Magnusson, D.; Geist, A.; Malmbeck, R. SX process-A Code for Solvent Extraction Processes in Centrifugal Contactors Simulation. *Chem. Eng. Sci.* 2013, 99, 292–297. [10.1016/j.ces.2013.06.008](https://doi.org/10.1016/j.ces.2013.06.008).

Band / Volume 603

**Development of components based on Ti<sub>2</sub>AlC/fiber composites for aggressive environmental conditions**

S. Badie (2023), x, 161 pp

ISBN: 978-3-95806-680-9

Band / Volume 604

**Multiregionales Energiesystemmodell mit Fokus auf Infrastrukturen**

T. M. Groß (2023), xx, 235 pp

ISBN: 978-3-95806-681-6

Band / Volume 605

**Temporal Aggregation Methods for Energy System Modeling**

M. A. C. Hoffmann (2023), XXVI, 341 pp

ISBN: 978-3-95806-683-0

Band / Volume 606

**Examining transport in the Upper Troposphere – Lower Stratosphere with the infrared limb imager GLORIA**

L. Krasauskas (2023), v, 107 pp

ISBN: 978-3-95806-691-5

Band / Volume 607

**Sustainable Fabrication of Ceramic Solid Electrolytes for Solid-State Lithium Batteries**

R. Ye (2023), vi, 119 pp

ISBN: 978-3-95806-694-6

Band / Volume 608

**Improving Nitrogen Retention in Soils Treated with Pig and Cattle Slurry Through the Use of Organic Soil Amendments**

X. Cao (2023), XVI, 119 pp

ISBN: 978-3-95806-696-0

Band / Volume 609

**Mechanisches Verhalten von Polymer-Elektrolyt-Membran-Elektrolysezellen und -Stacks**

S. Holtwerth (2023), x, 251 pp

ISBN: 978-3-95806-697-7

Band / Volume 610

**Membrane Reactor Concepts for Power-to-Fuel Processes**

H. Huang (2023), VI, 197 pp

ISBN: 978-3-95806-703-5



Band / Volume 611

**Deployment of Fuel Cell Vehicles in Road Transport and the Expansion of the Hydrogen Refueling Station Network: 2023 Update**

R. C. Samsun, M. Rex (2023), i, 39 pp

ISBN: 978-3-95806-704-2

Band / Volume 612

**Behavior/performance of tungsten as a wall material for fusion reactors**

M. Gago (2023), X, 120 pp

ISBN: 978-3-95806-707-3

Band / Volume 613

**Strategieentwicklung zur Umsetzung der Klimaschutzziele im Verkehrssektor mit dem Fokus Kraftstoffe**

M. Decker (2023), ix, 243 pp

ISBN: 978-3-95806-714-1

Band / Volume 614

**Joining of tungsten and steel for the first wall of a future fusion reactor**

V. Ganesh (2023), xxx, 142, a-v pp

ISBN: 978-3-95806-715-8

Band / Volume 615

**Polluter group specific emission optimisation for regional air quality analyses using four-dimensional variational data assimilation**

P. M. Backes (2023), xxi, 115 pp

ISBN: 978-3-95806-717-2

Band / Volume 616

**Effect of organic soil amendments on increasing soil N retention and reducing N losses from agricultural soils**

Z. Li (2023), XI, 134 pp

ISBN: 978-3-95806-721-9

Band / Volume 617

**Radiolytic Stability of BTBP-, BTPPhen- and DGA-based Ligands for the Selective Actinide Separation by Solvent Extraction**

H. Schmidt (2023), ca. 200 pp

ISBN: 978-3-95806-723-3

Weitere **Schriften des Verlags im Forschungszentrum Jülich** unter  
<http://www.zwb1.fz-juelich.de/verlagextern1/index.asp>



Energie & Umwelt / Energy & Environment  
Band / Volume 617  
ISBN 978-3-95806-723-3